

Faculty of Engineering and Science

**Development of a Novel Green Surfactant - Low Salinity Nanofluid for
Enhanced Oil Recovery Application**

Li Yisong

0000-0003-2901-4361

**This Thesis is presented for the Degree of
Doctor of Philosophy
of
Curtin University**

February 2022

Declaration

To the best of my knowledge and belief, this thesis contains no material previously published by any other person except where due acknowledgment has been made.

This thesis contains no material which has been accepted for the award of any other degree or diploma in any university.

Signature:

Date:28/02/2022.....

Acknowledgment

First of all, I would like to express my deepest appreciation to Professor Dr. Raoof Gholami (associate supervisor) for his continuous support and motivation during my Ph.D. study. Working with him always inspires me to think critically and gain original initiatives.

I would also like to thank Associate Professor Dr. Wee Siaw Khur (my supervisor), Dr. Mehdi Safari (associate supervisor), and Professor Dr. R.Nagarajan (thesis committee chair), who have provided insightful comments for improving the quality of my research.

I gratefully acknowledge all the people from the Geology, Petroleum, and Chemical Departments of Curtin University Malaysia, especially the lab technicians. Without their kind assistance in the laboratory, I couldn't make this research possible. Also, I would like to thank Professor Dr. Agus Saptoro (Director of Curtin Malaysia Graduate School and Deputy Dean of R&D), Ms. Florence, and Ms. Daisy from the Graduate School. Their kind support and guidance have made my study smoother and more productive.

My deepest gratitude goes to all my beloved family and friends – Li Jinsheng, Liu Cuili, Dr. Michelle Tiong, etc. Without their love, encouragement, and sacrifices, I cannot reach half of the research carried out so far.

Last but not least, I sincerely acknowledge the financial support from the Curtin Malaysia Research Institute (CMRI).

List of Publications

Journal papers:

1. Safari, M., Wong, J.J.J., Rahimi, A., Gholami, R., Li, Y., Wee, S.K. 2022. Salinity adjustment to improve the efficiency of nano glass flakes (NGFs) in interfacial tension reduction. Journal of Petroleum Science and Engineering, 212, 109874.

<https://doi.org/10.1016/j.petrol.2021.109874>.

2. Li, Y., Gholami, R., Safari, M., Rahimi, A., Wee, S.K. 2022. On surface interactions of environmental friendly surfactant/oil/rock/low salinity system: IFT, wettability, and foamability. Journal of Petroleum Science and Engineering, 208, 109370.

<https://doi.org/10.1016/j.petrol.2021.109370>

Conference proceedings:

1. Tiong, M, Raoof Gholami, Li, Y. A Novel Portland Cement for CO₂ Sequestration by Nanoparticles. International Petroleum Technology Conference, Riyadh, Saudi Arabia, February 21-23, 2022.

<https://doi.org/10.2523/IPTC-22392-MS>

Abstract

Energy is still a global demand while conventional resources, such as hydrocarbon reservoirs are depleted. To revive these reservoirs, enhanced oil recovery (EOR) techniques have been proposed. However, due to the complex formation environment, poor wettability condition, low sweep efficiency, pore-throat blockage, and surfactant adsorption, only a few of successful EOR applications reported on the field scale. Thus, it is crucial to develop an EOR approach that possesses: 1) a good wettability alteration and desirable interfacial tension (IFT) reduction, 2) good stability under different temperature conditions, 3) environmentally friendly, and 4) economic efficiency. Natural surfactants have been investigated as part of EOR processes due to their non-toxic and environmentally benign character. However, low stability, high adsorption rate, and poor wettability alteration highly restrict their application. Although low salinity water (LSW) and nanoparticles are excellent additives in these instances, the interaction of LSW and nanoparticles with natural surfactants to affect foamability, IFT, and wettability has not been deeply understood. This project attempts to develop a high-performance novel green surfactant - low salinity nanofluid, which can be used to improve oil recovery from matured reservoirs.

This thesis attempted to extract and characterize the natural surfactants that might be employed in conjunction with LSW for EOR applications. This was accomplished by extracting the natural surfactants from Soapnut and *Camellia oleifera*, then evaluating their physicochemical properties such as the pH, density, conductivity, critical micelle concentration (CMC), zeta-potential, and thermal stability. Moreover, the foamability, foam stability, IFT reduction, and wettability alteration were examined in the presence of saponins, salts, nanoparticles, and their combination. On the other hand, scanning electron microscope (SEM) and transmission electron microscopy (TEM) were applied to investigate bonding behavior and multi-particle interactions. The results indicated that water is the most appropriate solvent for extracting saponins. The extracted saponins have excellent thermal stability and can function at up to 100°C.

Both saponins possess a weak acidic character, and the average density of Soapnut saponin is 0.89957 g/cm³ and 0.92567 g/cm³ for Camellia oleifera saponin.

Based on zeta potential result, Soapnut saponin is considered a nonionic surfactant while Camellia oleifera saponin is considered an anionic surfactant. Thermogravimetry analysis (TGA) revealed that the natural surfactants possess great thermal stability. Both saponins have good foamability and foam stability, whereas the foam stability is reduced at high saponin concentrations. The increasing concentration of nanoparticles and salts increase the foam length and stability until it reaches the optimum concentration (20000ppm for salts and 0.003wt% for nanoparticles). The presence of crude oil accelerates the foam collapse, reduces the foam stability, and affects foamability. It was observed that the extracted saponins could significantly decrease the IFT and contact angle. The additional salts and nanoparticles enhanced the IFT reduction and wettability alteration further until the threshold concentration was reached. Specifically, the lowest IFT value was determined to be 3.8mN/m with 4.5wt% for Soapnut saponin and 3.72mN/m with 4wt% for Camellia oleifera saponin. On the other hand, the lowest contact angle of Soapnut saponin was observed in Malaysia sandstone (Miri formation) at 21.2° with 6wt%. Camellia oleifera saponin's lowest contact angle was observed in Malaysia sandstone at 19.93° with 5wt%. The optimum salinity was 3500ppm. The optimum concentrations of saponins and nanoparticles were varied in different situations. In terms of cost aspects, based on the extraction efficiency achieved (81% for Soapnut saponin and 79% for Camellia oleifera saponin), the prices of extracted saponin from Soapnut and Camellia oleifera were roughly located at 0.80 US\$/kg and 1.46 US\$/kg. Therefore, based on the 4 US\$/kg synthetic surfactant price, it approximately can reduce the cost by 80% with Soapnut saponin and 63.5% with Camellia oleifera saponin as surfactant alternatives.

Keywords: EOR, nanoparticles, low salinity water, green surfactants, CMC, foamability, IFT reduction, wettability alteration

Table of Contents

DECLARATION	II
ACKNOWLEDGMENT	III
LIST OF PUBLICATIONS	IV
ABSTRACT	V
TABLE OF CONTENTS	VII
LIST OF FIGURES	X
LIST OF TABLES	XIV
LIST OF SYMBOLS AND ABBREVIATIONS	XIVI
CHAPTER 1: INTRODUCTION AND FUNDAMENTALS	1
1.1 Introduction	1
1.2 Background	2
1.2.1 Low Salinity Water Injection (LSWI)	2
1.2.2 Nanoparticle Flooding	3
1.2.3 Green Surfactant	4
1.3 Problem Statement	5
1.4 Research Questions	5
1.5 Research Objectives	6
1.6 Research Significance	6
CHAPTER 2: LITERATURE REVIEW	7
2.1 Introduction	7
2.2 Reservoir Properties Related to EOR Techniques	8
2.2.1 Wettability	8
2.2.2 Interfacial Tension	9
2.2.3 Capillary Pressure	10
2.2.4 Saturation	10
2.2.5 Permeability	11
2.2.6 Porosity	12
2.3 Low Salinity Water Injection	13
2.3.1 Fines Migration	15
2.3.2 Multicomponent Ionic Exchange	16
2.3.3 Electrical Double Layer Expansion	17
2.3.4 pH Effect	19
2.4 Nanoparticle Flooding	20
2.4.1 Classification of nanoparticles	21
2.4.2 Wettability Alteration	23
2.4.3 Structure Disjoining Pressure	25
2.5 Surfactants Flooding	26
2.5.1 Surfactant Classification	26
2.5.2 Surfactant lost behavior	28
2.5.3 Application of Surfactant in Petroleum Industry	29
2.5.4 Limitations of Synthetic Surfactants	30
2.5.5 Green Surfactants	31
2.5.6 Synthetic Surfactants versus Green Surfactants in Cost Aspect	32
2.5.7 Surfactants Application in LSWI	35

2.6 Foamability and Foam Stability	37
2.6.1 Introduction	37
2.6.2 Foam formation	38
2.6.3 Foam application in EOR	39
2.6.4 Properties of Foamability and Foam Stability	40
2.7 Conclusion	46
CHAPTER 3: GREEN SURFACTANT EXTRACTION	49
3.1 Introduction	49
3.2 Methodology	52
3.2.1 Experimental Apparatus	52
3.2.2 Chemical Additives	53
3.2.3 Plant Materials Pretreatment	53
3.2.4 Green Surfactant Selection	54
3.2.5 Saponin Extraction	57
3.2.6 Isolation, Purification, and Dehydration of Saponin	59
3.3 Results and Discussion	62
3.4 Conclusions	63
CHAPTER 4: SAPONIN CHARACTERIZATION	65
4.1 Introduction	65
4.2 Methodology	65
4.2.1 Experimental Apparatus	65
4.2.2 Experimental Materials	66
4.2.3 Preparation of Surfactant Solutions	67
4.2.4 Density, pH, and Conductivity Determination	68
4.2.5 Critical Micelle Concentration (CMC)	69
4.2.6 Temperature	70
4.2.7 Particle Size Distribution	70
4.2.8 Zeta Potential	71
4.2.9 Thermogravimetric Analysis	72
4.2.10 SEM Analysis	72
4.2.11 UV-Vis Analysis	73
4.2.12 FTIR Analysis	74
4.3 Result and Discussion	74
4.3.1 Density	74
4.3.2 pH	75
4.3.3 Conductivity and Solubility	77
4.3.4 CMC Point Identification	78
4.3.5 Temperature Effect and CMC Variation	79
4.3.6 Particle Size Distribution and Zeta Potential	82
4.3.7 TGA	84
4.3.8 SEM	86
4.3.9 UV-Vis	87
4.3.10 FTIR	88
4.4 Conclusions	90
CHAPTER 5: FOAMABILITY AND FOAM STABILITY	93
5.1 Introduction	93
5.2 Methodology	93
5.2.1 Experimental Apparatus	93
5.2.2 Experimental Materials	94
5.2.3 Preparation of Green Surfactants Solutions	94

5.3 Results and Discussions	98
5.3.1 Salinity Effect	98
5.3.2 Foamability and Stability Test	84
5.4 Conclusion	107
CHAPTER 6: INTERFACIAL TENSION STUDY IN LOW SALINITY GREEN SURFACTANT NANOFLUID EOR SOLUTIONS	113
6.1 Introduction	113
6.2 Methodology	114
6.2.1 Experimental Apparatus	114
6.2.2 Experimental Materials	115
6.2.3 Test Fluids Preparation	117
6.2.4 IFT Measurements	120
6.2.5 Transmission Electron Microscopy (TEM) Characterization	123
6.3 Results and Discussions	124
6.3.1 IFT Measurements	124
6.3.2 TEM	142
6.4 Conclusion	144
CHAPTER 7: WETTABILITY STUDY IN LOW SALINITY GREEN SURFACTANT NANOFLUID EOE SOLUTIONS	147
7.1 Introduction	147
7.2 Methodology	148
7.2.1 Experimental Apparatus	148
7.2.2 Experimental Materials	149
7.2.3 Test Fluids Preparation	151
7.2.4 Formation Core Slices Cutting, Cleaning, and Aging	151
7.2.5 Contact Angle Measurements (Wettability)	152
7.2.6 SEM Characterization	154
7.3 Results and Discussions	156
7.3.1 Three-phase Contact Angle Measurements	156
7.3.2 SEM Observation	178
7.4 Conclusion	181
CHAPTER 8: CONCLUSIONS AND RECOMMENDATIONS	185
8.1 Conclusions	185
8.1.1 Characterization of Soapnut Saponin and Camellia oleifera saponin	186
8.1.2 Salinity Effect, Foamability, Foam Stability, and Bubble Structure	187
8.1.3 Investigation of IFT Reduction by Combined Low Salinity Green Surfactant Nanofluid and TEM Observation	189
8.1.4 Investigation of Wettability Alteration by Combined Low Salinity Green Surfactant Nanofluid and SEM Observation	191
8.1.5 Related Mechanisms Fundamental Explanations	193
8.2 Recommendations	196
REFERENCE	200

List of Figures

Figure 1.1: An overview of enhanced oil recovery techniques	2
Figure 2.1: Interpretation of wettability by various fluids.....	8
Figure 2.2: Interfacial tension that is acting on the surface of two immiscible phases ...	9
Figure 2.3: The illustration of bulk, grain, and pore volume	12
Figure 2.4: Illustration of low salinity water injection	14
Figure 2.5: Fines migration mechanism during LSWI	16
Figure 2.6: MIE mechanisms during LSWI	17
Figure 2.7: Adsorption mechanisms taking place on the clay surface	17
Figure 2.8: Illustration of electric double layer	18
Figure 2.9: Electrical double layer expansion and overlapping	19
Figure 2.10: pH effect of LSWI	20
Figure 2.11: Illustration of the structure of various nanoparticles	23
Figure 2.12: Mechanisms of wettability alteration of nano-flooding	24
Figure 2.13: Contact angle of different nanoparticles and their related emulsion state	25
Figure 2.14: Mechanism of the structure disjoining pressure	26
Figure 2.15: Structure of a surfactant molecule	27
Figure 2.16: Mechanism of surfactant-assisted water-flooding	30
Figure 2.17: Oil recovery by LS flooding and LSS flooding	36
Figure 2.18: IFT reduction induced by addition of surfactant in saline water	37
Figure 2.19: Two-dimensional foam structure	38
Figure 2.20: Marangoni Flows' foam structure and internal molecular film repair mechanism	39
Figure 2.21: The influence of gravity on foam drainage	42
Figure 2.22: A diagram illustrating the Gibbs-Marangoni effect... ..	43
Figure 3.1: Green surfactants. Top: <i>Camellia oleifera</i> ; a) Fruit diameters around 4cm; b) Seed opening; c) Fruit structure; d) <i>Camellia oleifera</i> -oil extracted from seeds, Bottom: e) Soapnut fruit; f) Soapnut kernel; g) Soapnut pericarp.....	50
Figure 3.2: The chemical structure of saponin extracted from Soapnut	52
Figure 3.3: The chemical structure of saponin extracted from <i>Camellia Oleifera</i>	52
Figure 3.4: Flow chart of saponin extraction	52
Figure 3.5: Potential green surfactant plants. a) Mulberry lea, b) <i>Glycyrrhiza</i> , c) <i>Tribulus Terrestris</i> , d) <i>Camellia oleifera</i> seed, e) <i>Sapindus mukorossi</i> (Soapnut)	53
Figure 3.6: The equipment for the DSA test. A) glass box, b) oil injection syringe, c) J-shape needle, d) IFT measurement	56
Figure 3.7: Extraction process. Extraction process. a) Maceration process of Soapnut powder and b) Ultrasonic homogenizer	58
Figure 3.8: Diagram of the surfactant separation technique	60
Figure 3.9: Purification and dehydration of Saponin. 1) Saponin solution; 2) Centrifuge tube assembling; 3) Centrifuge under 4000rpm for 20 minutes; 4) The filtered Saponin	

solution; 5) 600ml Freeze-dryer beaker; 6) Freeze-drying process; 7) Extracted Saponin powder	61
Figure 4.1: pH variation of the saponin extract vs. concentration. a) Soapnut saponin; b) Camellia oleifera saponin. The error bars were the standard deviation of the three independent measurements	76
Figure 4.2: The conductivity of saponin extract with increasing concentration. a) Soapnut saponin; b) Camellia oleifera saponin. The error bars were the standard deviation of the three independent measurements	78
Figure 4.3: CMC point of a) Soapnut saponin extract solution; b) Camellia oleifera saponin extract solution	78
Figure 4.4: Conductivity of the saponin solutions various concentrations under different temperatures. a) Soapnut saponin and b) Camellia oleifera saponin. The error bars were the standard deviation of the three independent measurements	80
Figure 4.5: Temperature effect on the CMC of Soapnut saponin with varying concentrations. a) 40°C; b) 50°C; c) 60°C; d) 70°C; e) 80°C; f) 100°C	81
Figure 4.6: Temperature effect on the CMC of Camellia oleifera saponin with varying concentrations. g) 40°C; h) 50°C; i) 60°C; j) 70°C; k) 80°C; l) 100°C	82
Figure 4.7: TGA results of a) Soapnut saponin and b) Camellia oleifera saponin	85
Figure 4.8: SEM images of extracted Soapnut saponin and Camellia oleifera saponin under drying powder status. a) an overall image of Soapnut saponin; b) Soapnut saponin particle; c) an overall image of Camellia oleifera saponin; d) Camellia oleifera saponin particle	87
Figure 4.9: UV-Vis of saponins. a) Soapnut saponin and b) Camellia oleifera saponin with increasing concentrations	88
Figure 4.10: FTIR absorption spectral data of saponin	89
Figure 4.11: FTIR absorption spectral data of Camellia oleifera saponin	89
Figure 5.1: The foamability and bubble structure of 2 wt% Soap-nut Saponin solution at 25°C.....	98
Figure 5.2: Foam height vs concentration of Soapnut saponin: a) 0.1wt%-3.5wt%, and b) 4wt%-8wt%	87
Figure 5.3: Foam height vs concentration of Camellia oleifera saponin. a) 0.1wt%-3.5wt%, and b) 4wt%-8wt%	87
Figure 5.4: Average foam size of saponins. a) Soapnut saponin, and b) Camellia oleifera saponin with various concentrations	88
Figure 5.5: Average bubble size at the Soapnut saponin of 0.3wt% (top), 3wt% (middle), and 5.5wt% (bottom)	90
Figure 5.6: The saponin foam height vs. time under increasing NGF concentration. a) Soapnut saponin, and b) Camellia oleifera saponin	98
Figure 5.7: Soapnut saponin foam height vs. Time with NGF under increasing salinity (above: 1000ppm-10000ppm, below: 20000ppm-100000ppm)	102
Figure 5.8: Camellia oleifera saponin foam height vs. Time with NGF under increasing salinity (above: 1000ppm-10000ppm, below: 20000ppm-100000ppm)	103
Figure 5.9: Soapnut saponin foam length vs. time in the absence and presence of crude oil. a) Soapnut saponin and b) Camellia oleifera saponin	106

Figure 6.1: IFT measurement equipments. a) 3ml syringe, b) 0.5mm J-shape stainless needle, c) glass box for IFT measurement.....	115
Figure 6.2: Additives applied in this study. a) Nano-galss flakes (NGF) , b) Soapnut saponin, and c) Camellia oleifera saponin	116
Figure 6.3: Salt used in this study. a) NaCl, and b) CaCl ₂	116
Figure 6.4: TEM image of NGF	116
Figure 6.5: Crude oil sample after filtration	117
Figure 6.6: Schematic diagram of DSA-100B apparatus used to IFT measurement	121
Figure 6.7: IFT measurement in DSA-100B	122
Figure 6.8: TEM image of Soapnut saponin in the designed solution that contains NaCl and NGF	124
Figure 6.9: IFT results for both saponins against concentration	127
Figure 6.10: Formation of membranous flocculate substance against saponin concentration	128
Figure 6.11: IFT results for both saponins against NGF concentration in saponin solution	131
Figure 6.12: IFT results for Soapnut saponins against salt type and concentration in saponin solution	133
Figure 6.13: IFT results for Camellia oleifera saponins against salt type and concentration in saponin solution	133
Figure 6.14: IFT results for the combination of saponin and NGF. a) 4.5wt% Soapnut saponin and 0.003wt NGF, and b) 4% Camellia oleifera saponin and 0.003wt% NGF, in increasing salinity	137
Figure 6.15: The summary of IFT reduction ability of Soapnut saponin in the presence of different additives and combinations	141
Figure 6.16: The summary of IFT reduction ability of Camellia oleifera saponin in the presence of different additives and combinations	141
Figure 6.17: TEM images of the Fern-like crystal structure formed by the combination of saponin, NGF and NaCl. a) self-assembled structures with Camellia oleifera saponin, b) self-assembled structures with Soapnut saponin, c) aggregated multi-particles of Camellia oleifera saponin, d) aggregated multi-particles of Soapnut saponin	142
Figure 7.1: Contact angle measurement equipment. a) DSA-100B, and b) Glass box for contact angle measurement.....	148
Figure 7.2: Shaw portable core drill	149
Figure 7.3: Formation cores used in wettability test. a) Berea sandstone core, b) Shale core, and c) Malaysia sandstone core	150
Figure 7.4: Core slice and polishing	151
Figure 7.5: Berea sandstone core slice. a) before aging, b) after aging, c) contact angle before aging: 83.9°, d) contact angle after aging: 161.8°	152
Figure 7.6: Schematic image of DSA-100B apparatus used to contact angle measurement	153
Figure 7.7: Quattro-S ESEM	155
Figure 7.8: SEM image of Berea sandstone core slice (before aging)	156

Figure 7.9: Contact angle of the various rock slices under increasing concentrations of a) Soapnut saponin; and b) <i>Camellia oleifera</i> saponin	160
Figure 7.10: Contact angle of the various rock slices under increasing NGF concentration in a) Soapnut saponin solution; and b) <i>Camellia oleifera</i> saponin solution	164
Figure 7.11: Contact angle of the various rock slices under increasing salinity of NaCl in a) Soapnut saponin solution; and b) <i>Camellia oleifera</i> saponin solution	166
Figure 7.12: Contact angle of the various rock slices under increasing salinity of CaCl_2 in a) Soapnut saponin solution; and b) <i>Camellia oleifera</i> saponin solution	167
Figure 7.13: Contact angle of the various rock slices under 3500ppm salinity of NaCl and CaCl_2 in Soapnut saponin solution	170
Figure 7.14: Contact angle of the various rock slices under 3500ppm salinity of NaCl and CaCl_2 in <i>Camellia oleifera</i> saponin solution	170
Figure 7.15: Contact angle of the various rock slices under increasing salinity of a) NaCl; and b) CaCl_2 , respectively, in the solution containing Soapnut saponin and NGF	174
Figure 7.16: Contact angle of the various rock slices under increasing salinity of a) NaCl; and b) CaCl_2 , respectively, in the solution containing <i>Camellia oleifera</i> saponin and NGF	175
Figure 7.17: The difference between contact angles achieved by optimum salinity and highest salinity in Soapnut saponin	177
Figure 7.18: The difference between contact angles achieved by optimum salinity and highest salinity in <i>Camellia oleifera</i> saponin	177
Figure 7. 19: SEM images of core slices before and after oil aging and immersed into low salinity NGF saponin fluid.	179

List of Tables

Table 2.1: Some of the typical surfactants used in the industry	28
Table 2.2: Natural surfactants summary and comparison	32
Table 2.3: Research on the use of synthetic surfactants and green surfactants in EOR .	32
Table 3.1: The composition, characteristics ratio, and properties of reservoir crude oil	56
Table 3.2: Fundamental IFT results of green surfactant plants selection	56
Table 3.3: Summary of yield percentages of the different solvent system	63
Table 4.1: Mixture ratio of different green surfactant solutions.....	68
Table 4.2: Molar conductivity of common anions and cations	69
Table 4.3: Density of the Soapnut saponin and Camellia oleifera saponin solutions	75
Table 4.4: Average particle size of saponin surfactant extracted from the Soapnut	82
Table 6.1: Effect of Soapnut saponin concentration on the IFT at oil/water interface	140
Table 6.2: Effect of Soapnut saponin concentration on the IFT at oil/water interface	122
Table 6.3: Summary of benchmark IFT for each batch test	125
Table 7.1: The mineralogy of Berea sandstone, Mancos shale, and Malaysia sandstone	150
Table 7.2: Contact angle images for crude oil droplet on Mancos shale slice in the Camellia oleifera saponin solution	154
Table 7.3: Reference values of contact angle under variable additives	158
Table 7.4: The optimum contact angle and related concentration achieved by saponins in various core slices	161
Table 7.5: The lowest contact angle and related optimum salinity achieved by saponins in various core slices	171
Table 7.6: The composition ratios of the immersed low salinity NGF saponin fluid	180

List of Symbols and Abbreviations

Symbol/Abbreviation	Designation	Units
CMC	Critical micelle concentration	-
EDL	Electrical double layer	-
EDX	Energy Dispersive X-Ray Analysis	-
EOR	Enhanced oil recovery	-
IFT	Interfacial tension	-
IOR	Improved oil recovery	-
LSWI	Low Salinity Water Injection	-
LVD	Low vacuum detector	-
MIE	Multicomponent ionic exchange	-
NGF	Nano-glass flakes	-
OOIP	Original oil in place	-
TEM	Transmission electron microscope	-
SEM	Scanning electron microscope	-
σ_{gw}	Interfacial tension of the gas-water phase	mN/m
σ_{ow}	interfacial tension of the oil-water phase	mN/m
r	Radius	m
h	Height of the liquid	m
ρ	Density of the solution	g/cm ³
ρ_w	Water density	g/cm ³
ρ_o	Oil density	g/cm ³
g	Gravity acceleration	m/s ²
θ	Contact angle	degree
P _c	Capillary pressure	psi
P _w	Pressure of the wetting phase	psi
P _o	Pressure in the oil phase	psi
P _g	Gas phase's pressure	psi
P _{nw}	Pressure of the non-wetting phase	psi
P _{cow}	Capillary pressure between oil and water phases	psi
P _{cgo}	Capillary pressure on the gas-oil system	psi
P _{cgw}	Capillary pressure on the gas-water system	psi
V _p	Pore volume	g/cm ³
V _g	Volumes of gas	cm ³
V _o	Volumes of oil	cm ³
V _w	Volumes of water	cm ³
S _g	Saturation of gas	%
S _o	Saturation of oil	%
S _w	Saturation of water	%
v	Velocity of the fluid	m/s

q	Volumetric flow rate	m^3/s
A	Overall area of rock formation	m^2
k	Rock formation permeability	d
μ	Dynamic fluid viscosity	$\text{N.m}^2\text{s}^{-1}$
dp/dx	Pressure variation over a distance	psi
ϕ_a	Absolute porosity	%
ϕ	Effective porosity	%
P_G	Gas pressure	psi
P_L	Liquid pressure	psi
γ	Surface tension	N/m
R	Radius	m
W_{filled}	Weight after pycnometer filled by solution	g
W_{empty}	Weight of the empty pycnometer	g
V	Volume of the pycnometer	cm^3
R	Resistance of the solution	Ω
V	Voltage	V
I	Current	A
G	Conductivity of the solution	$\mu\text{S}/\text{cm}$
d_H	Hydrodynamic diameter	nm
k	Boltzmann's constant	J/K
T	Temperature	Celsius
D	Translational diffusion coefficient	m^2s^{-1}
U_E	Electrophoretic mobility	$\mu\text{m.cm}/\text{V.s}$
ϵ	Dielectric constant	F/m
ζ	Zeta potential	mV
$f(\kappa a)$	Henry's function	k
H_{foam}	Height of foam	cm
$H_{foam+liquid}$	Total height of foam and liquid	cm
H_{liquid}	Height of liquid	cm
σ	Surface tension	$\mu\text{m}/\text{m}$
$\Delta\rho$	Phases density difference	g/cm^3
H	Shape-dependent parameter	-

Chapter 1: Introduction and Fundamentals

1.1 Introduction

With the depletion of conventional reservoirs, energy shortage has become a global issue. Several countries drafted a national policy to overcome this problem, mainly focusing on recovering oil from nearly depleted reservoirs ([Jalal & Bodger, 2009](#)). Approximately 200 billion barrels of conventional oil and 500 billion barrels of crude oil are still trapped in the pore network because of the poor wettability condition and low sweep efficiency after primary and secondary oil recovery ([Muggeridge et al., 2014](#)). In order to improve production, Enhanced Oil Recovery (EOR) techniques have been successfully implemented in many fields ([Figure 1.1](#)) ([Vishnumolakala et al., 2020](#)). These EOR methods often include three major categories 1) chemical, 2) thermal, and 3) gas injection ([Green et al., 2018](#)). Several additives have been proposed as part of these methods to improve or retain the production, such as gas (CO_2 and N_2), polymer, alkaline, and surfactant ([Austad, 2013](#); [Paul et al., 2015](#); [Gbadamosi et al., 2019](#)). However, many parameters such as reservoir condition, formation mineralogy, and wettability condition may limit the application of any methods or additives used. Furthermore, environmental contamination, large particle size, operation expenses, instability under high-temperature conditions and salinity often adversely affect the EOR operation ([Muggeridge et al., 2014](#); [Tackie-Otoo et al., 2020](#)). Thus, it would be essential to develop a new economically feasible and environmentally friendly method to improve the oil recovery from conventional depleted reservoirs. This study attempts to develop a novel low salinity green surfactant nanofluid to enhance oil reservoirs production. A series of tests were conducted to extract, characterize and test a green surfactant from local plants, combined with salts and nanoparticles for interfacial tension reduction and wettability alterations. This EOR fluid might be a great asset towards production improvements from mature reservoirs if successful.

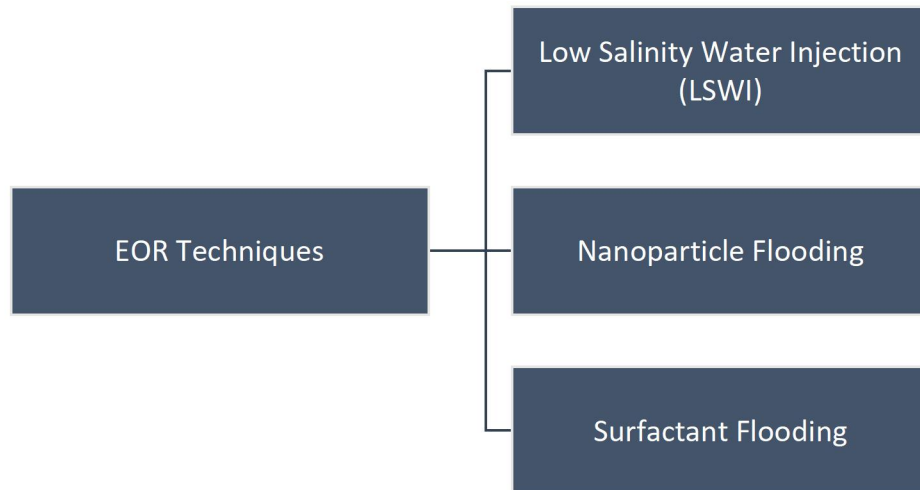


Figure 1.1: An overview of enhanced oil recovery techniques
(modified from [Vishnumolakala et al., 2020](#))

1.2 Background

1.2.1 Low Salinity Water Injection (LSWI)

The composition of traditional fresh water injected into the reservoirs for pressure maintenance did not raise significant concerns. The physical/chemical interaction between brine/oil/rock could not cause any production issues. However, this may not be the case once the composition of the injected water differs from the connate water ([Nadia Ariani, 2018](#)). Low salinity water injection (LSWI), which is also known as smart water flooding, was primarily adopted as a new water-based improved oil recovery (IOR) method in 1970 by British Petroleum ([Derkani et al., 2018](#)). During this period, substantial field tests were conducted to prove the effectiveness and capacity of LSW as an EOR method, which could target the trapped immobile oil reservoirs. As a multi-pattern technique, LSW is used during the secondary recovery but may act as a tertiary recovery method given the chemical reactions during and after its injection ([Lager et al., 2008](#)). Wettability alteration is the major mechanism during LSWI, followed by the electric double layer expansion, salting-in effect, multi-component ion exchange, and changes in pH ([Akbar et al., 2018](#)). Clay plays a critical role as a major mineral of sandstone reservoirs, given their permanent negative surface charges and large surface area. It has been documented that divalent ions (Ca^{2+} , Mg^{2+}) and organic matter can be substituted by monovalent cations, such as Na^+ , K^+ , and H^+ on the clay surface, increasing the local pH ([Al-Shalabi & Sepehrnoori,](#)

2016). As the pH rises, the chemical reaction between hydroxyl ion and the polar component of oil accelerates, weakening the hydrocarbon bonding/adhesion forces between oil and clay surface (Austad et al., 2010). As a result, oil recovery can be improved. However, LSW injection cannot always provide a good result, given the fact that the interactions of salt ions with the rock surface have not been understood yet. It should be noted that LSWI is insufficient at lowering the interfacial tension (IFT) at the oil-water interface, which is a critical factor in the oil recovery process. Moreover, it may trigger fine migration around the wellbore area, which leads to irreparable formation damage (Al-Sarihi et al., 2018).

1.2.2 Nanoparticle Flooding

Nanotechnology has been confirmed as a promising alternative that can overcome the drawbacks of LSWI and further surpass the current applications (Alsaba et al., 2020). With the nanosized scale (1-100nm), nanoparticles can easily penetrate the formations' pore throats and provide the required functionalities that the traditional recovery techniques lack (Ramezanzpour & Siavashi, 2019; Al-Samhan et al., 2020). Furthermore, a large surface area to volume ratio of nanoparticles can improve the system stability by weakening the non-equilibrium behavior between injected solution and rocks while substantially eliminating the issue of precipitation (Nikolov et al., 2019). Characteristic of high surface energy allows nanoparticles to be easily absorbed by the rock surface or bonded with the polar acid/base of oil droplets (structure transitioning) (Sun et al., 2017; Donath et al., 2019). A laboratory study by Hendraningrat et al. (2013) showed that the recovery rose to 40% of the original oil in place (OOIP) by injecting SiO₂ nano-flooding, where the wettability condition improved oil-wet into a water-wet status. Furthermore, Shah et al. (2009) demonstrated that nanoparticles could effectively raise the viscosity and density of the EOR solution. It turns out the viscosity of the solution increases by 140 times once only 1% of CuO nanoparticles are added. Besides, according to Nwidee et al. (2017), adding nano-NiO could reduce the contact angle from 88° to 42° and create a strongly water-wet system. Besides, it appears that nanoparticles, once adequately modified, can improve the IFT, permeability of the formation, and

viscosity of the EOR fluids (K. Li et al., 2018; Gbadamosi et al., 2019; Rostami et al., 2019; Alsaba et al., 2020). In order to deliver the performance mentioned above, multiple mechanisms have been addressed, such as nano-layer coating, structure transitioning (self-bonding and structuring), physical solid or chemical stability, entrapment mechanisms (log-jamming, gravity setting, deep-bed filtration, and particle adsorption), wettability alteration and structure disjoining force (Strambeanu et al., 2015; Zargartalebi et al., 2015; Negin et al., 2016; Sun et al., 2017). However, none of these mechanisms has been deeply understood. It also seems that nanoparticles are ineffective in changing the IFT, which is crucial to improving oil recovery. According to Agi et al. (2018), the effect of nanoparticles on the IFT reduction is not as much strength as the LSW flooding.

1.2.3 Green Surfactant

The use of surfactants to increase oil output can be dated back 80 years to the early twentieth century (Green et al., 2018). Many studies have shown that surfactants can significantly reduce the IFT between the injected fluids and the residual oil and contribute to a more efficient hydrocarbon transport toward the production wells (Ayirala et al., 2019; Sarmah et al., 2020; Tackie-Otoo et al., 2020). Surfactants are composed of two essential components: 1) a hydrophilic polar head and 2) a hydrophobic non-polar tail. The hydrophilic head exhibits a strong attraction to water molecules, whereas the hydrophobic tail exhibits a strong attraction to oil droplets (J. J. Sheng, 2015). The equilibrium of the surfactant's water-soluble head and oil-soluble tail confers to the surface-active agent its distinctive property. According to the ionic nature of the polar head, Surfactants are generally categorized as non-ionic (zwitterionic), cationic and anionic agents (Kronberg et al., 2014). However, being toxic and causing environmental pollution have restricted the application of these surface agent materials. Furthermore, a significant proportion of surfactants is absorbed by the reservoir porous media during the injection process, increasing the cost of operation and decreasing the effectiveness of the EOR solution (E. Hosseini et al., 2018; Peng & Nguyen, 2020). Thus,

generating a cost-effective, ecologically friendly, and non-toxic surfactant is necessary.

1.3 Problem Statement

The traditional chemical EOR techniques on mature reservoirs faced a limitation in oil recovery improvement, which could be caused by the complexity of fluid-lithology interactions, low sweep efficiency, pore-throat blockage, poor wettability condition, and surfactant adsorption. Although the combination of salts, nanoparticles, and surfactants has been proposed in recent years as a solution for oil recovery enhancement, the multi-interactions of those additives to affect foamability, IFT, and wettability have not been deeply understood. Traditional synthetic surfactants applied in the Petroleum industry are more expensive, toxic, non-biodegradable, and cause environmental pollution. The gap between the development of green surfactants and general engineering applications is large. Furthermore, when the surfactant is moving through porous media, a significant amount of surfactant is adsorbed by the reservoir formation for a variety of reasons, including rock formation/surfactant interaction and surfactant adsorption behavior, which adversely impact the oil recovery efficiency. As a result, prolonging the timing of EOR and incurring huge costs.

1.4 Research Questions

In order to accomplish this research, it is necessary to answer the following questions:

1. What would be the optimum technique/solvent to extract saponin from Soapnut and *Camellia oleifera* seed? What is the critical micelle concentration (CMC) of those saponins? What is the stability of the various condition?
2. What are the mechanisms involved in the IFT reduction and wettability alteration once the synergy fluid is used?
3. How to prevent the conglomeration of the nanoparticle? What is the best dispersion method?
4. What is the optimum combination of salts, nanoparticles, and green surfactants to deliver the optimum results?

1.5 Research Objectives

This study aims to deliver a high-performance green surfactant solution with nanoparticles and low salinity water. Brine is used as the base solution. Nano-glass flakes (NGF) are treated as sacrificial agents. Two new cost-effective green surfactants extracted from local plants have been developed as part of this study. The objectives of this research are:

1. To develop surfactant alternatives that are more environmental-friendly at the same time, without compromising the end product's performance.
2. To study the multi-mechanisms between new green surfactants, nanoparticles, salt, rock formation, and oil droplet to understand the IFT reduction and wettability alteration.
3. To design a mixing method for green synergy solution by combining low salinity water, nanoparticles, and green surfactants to improve the EOR process.
4. To examine the foamability and foam stability, IFT reduction, and wettability alteration of the green EOR solution on Mancos shale, Berea sandstone, and Malaysia sandstone and determine the optimum preparation sets.

1.6 Research Significance

EOR is capital and resource-intensive and expensive, primarily due to high injectant costs. Due to the complexity of formations associated with different sweep efficiency, IFT, and wettability, oil production is often restricted, even with traditional EOR techniques. In addition, the environmental pollution caused by EOR fluid has received increasing attention, so developing a greener solution without adversely affecting the overall performance is critical and essential. This study proposes developing environmentally-friendly, biodegradable, non-toxic surfactants extracted from local plants. It can serve as a reference for future studies of green surfactants.

1.7 Thesis Organization

This thesis provides a comprehensive guideline as to how saponin can be extracted from the plants and used to develop green surfactant solutions in order to serve as an alternative for improving oil recovery. Chapter 1 delivers the background study on the EOR methods, emphasizing the current problem of using commercial surfactant and the importance of developing green surfactant. Chapter 2 provides a thorough summary of previous studies performed on the EOR methods, such as nanoparticle and surfactant flooding. The relevant reservoir properties are also explained. This is followed by Chapter 3 and 4 where the synthesis and characterization of saponin surfactants are performed. Chapter 5 focuses on the foamability and foam stability of the synthesised surfactant, where the influence of temperature, salt and nanoparticles were examined. In Chapter 6 and 7, analytical studies related to EOR properties, such as IFT and wettability are presented to understand the mechanisms behind changes. Last but not least, chapter 8 gives a summary of findings and offers some discussion and conclusions, including recommendations for future studies.

Chapter 2: Literature Review

2.1 Introduction

EOR process is a well-known technique for improving oil production from the matured reservoir, but the unstable performance, high operation capital, and environmental contamination still restrict its widespread application ([Green et al., 2018](#); [Afolabi, 2019](#)). It is vital to understand the fundamentals of physical/chemical interactions and the mechanisms involved in other EOR techniques, including smart water flooding with green surfactants, even though a series of experimental studies on the laboratory scale shows positive results. Thus, a comprehensive theoretical study on different EOR methods and the physical/chemical interactions are involved in this chapter. A thorough observation of the interactions between salts,

nanoparticles, and surfactants is also presented to understand the synergy mechanisms.

2.2 Reservoir Properties Related to EOR Techniques

The interaction between fluids and rock in the reservoir significantly impacts oil production volume. Experiments on multi-phase flow have demonstrated that fluid behavior relies highly on interaction with other fluid rocks in reservoirs, where surface wettability, interfacial tension, capillary pressure, saturation, permeability, and porosity are discussed in detail in the following section.

2.2.1 Wettability

Wettability is defined as the ability of a fluid to wet a solid surface in the presence of another immiscible fluid, which can be schematically shown in [Figure 2.1 \(Kundu et al., 2011\)](#). It is commonly classified into three main categories: strong-oil wet, mixed wet, and strong-water wet systems. The inclination of fluid diffuses along the solid surface stands for the wetting condition of the liquid to that solid surface. This inclination can be quantified by measuring the contact angle of the fluid-rock surface based on the denser fluid compared to the rock surface ([T. Ahmed & Ahmed Phd Pe, 2010](#)). On this occasion, the degree of contact angle reflects the condition of wettability. More specifically, 0° to 30° indicates a completely water-wet system, 30° to 75° represents a moderately water-wet condition, 75° to 105° is a neutrally wet system, 105° to 150° gives a moderately oil-wet system, and 150° to 180° is a completely oil-wet system.

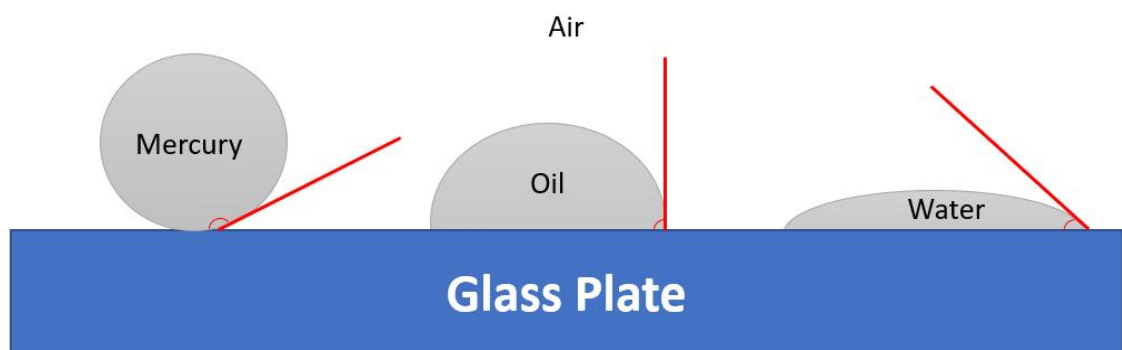


Figure 2.1: Interpretation of wettability by various fluids (modified from [Kundu et al., 2011](#))

2.2.2 Interfacial Tension

The free energy generated from the electrostatic force is located on the boundary of two immiscible phases. It is induced that the fluids fulfill the minimum area of the surface and form a membrane-like structure (Hiemenz et al., 2016). Under the circumstance of a multi-phase flow environment, it is essential to evaluate the impact of these forces on the contact region of two immiscible fluids. Interfacial tension is used to estimate the forces acting on the related interface; liquids, like water and oil, are specifically suitable for both phases. Moreover, surface tension targets the forces between two phases, such as gas and liquid, as illustrated in Figure 2.2 (Kundu et al., 2011).

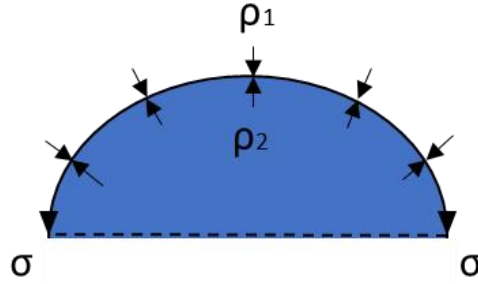


Figure 2.2: Interfacial tension that is acting on the surface of two immiscible phases (modified from Kundu et al., 2011)

A thin layer of membrane usually covers the surface of liquids. This membrane possesses a little resistant strength, induced by the attraction force between each molecule of liquids (Neumann et al., 2010). The mathematic equations of interfacial tension under gas-water conditions and oil-water conditions are present as:

$$\sigma_{gw} = \frac{rh\rho_w g}{2\cos\theta} \quad (\text{Eq. 2.1})$$

where σ_{gw} refer to the interfacial tension of the gas-water phase, mN/m; r refers to the radius, m; h refers to the height of the liquid, m; ρ_w refer to the density of water, kg/m³; g refers to the gravity acceleration, m/s²; θ refers to the contact angle, degree.

$$\sigma_{ow} = \frac{rhg(\rho_w - \rho_o)}{2\cos\theta} \quad (\text{Eq. 2.2})$$

where σ_{ow} refer to the interfacial tension of the oil-water phase, mN/m; r refers to the radius, m; h refers to the height of the liquid, m; g refers to the gravity acceleration, m/s²; ρ_w refer to the water density, kg/m³; ρ_o refer to the oil density, kg/m³; θ refer to the contact angle, degree.

2.2.3 Capillary Pressure

The capillary force in the formation reservoir is caused by wetting characteristics, pore size, and the IFT. When the two immiscible fluids get in touch with each other, a discontinuity pressure is formed between these two fluids in a small capillary tube which indicates the movement of fluids in a two or three fluid flow system (Tiab & Donaldson, 2011; Shi et al., 2018). The capillary pressure is described by Eq. 2.3:

$$P_c = P_{nw} - P_w \quad (\text{Eq. 2.3})$$

where P_c is the capillary pressure, psi; P_{nw} is the pressure of the non-wetting phase, psi, and P_w is the pressure of the wetting phase, psi, which for the reservoir condition is illustrated by Equation 2.4.

$$P_{cow} = P_o - P_w \quad (\text{Eq. 2.4})$$

where P_{cow} is the capillary pressure between oil and water phases, psi; P_o is the pressure in the oil phase, psi; P_w is the pressure in the wetting phase, psi.

$$P_{cgo} = P_g - P_o \quad (\text{Eq. 2.5})$$

where P_{cgo} refers to capillary pressure on the gas-oil system, psi; P_g refers to the gas phase's pressure, psi; P_o refers to the pressure of the oil phase, psi.

$$P_{cgw} = P_g - P_w \quad (\text{Eq. 2.6})$$

where P_{cgw} refers to capillary pressure on the gas-water system, psi; P_g refers to the gas phase's pressure, psi; P_w refers to the pressure of the water phase, psi.

2.2.4 Saturation

It has been confirmed that most formation pore spaces were filled with water prior to the oil migration and stuck in the pores. A portion of hydrocarbon has been displaced to the location hydrostatically by the equivalent amount of water, but the water traps in pores cannot migrate entirely by oil (Hendraningrat et al., 2013). Therefore, the reservoir formation generally comprises both hydrocarbon and

water. In the petroleum field, saturation is defined as the proportion of pore volume filled by a specific fluid (gas, oil, or water). The corresponding equation is shown (Tiab & Donaldson, 2011):

$$S_g = \frac{V_g}{V_p}, S_o = \frac{V_o}{V_p}, S_w = \frac{V_w}{V_p} \quad (\text{Eq. 2.7})$$

where V_p is pore volume, g/cm^3 ; S_g , S_o , and S_w are the saturation of gas, oil, and water, %; V_g , V_o and V_w are the volumes of gas, oil, and water, cm^3 .

It is worth noting that all saturations are based on pore volume instead of the gross reservoir volume. The saturation of each phase ranges between 0% and 100%. By definition, the sum of the saturation is 100%, which follows as (T. Ahmed & Ahmed Phd Pe, 2010):

$$S_g + S_o + S_w = 100\% \quad (\text{Eq. 2.8})$$

where S_g , S_o , and S_w are the saturation of gas, oil, and water, %.

2.2.5 Permeability

Permeability k is the formation capacity to transmit fluid through the porous medium. More generally, it reflects the degree of difficulty transmitting direction and flow rate of fluid flows through the formation. Darcy's law equation can express it as:

$$v = \frac{q}{A} = -\frac{k}{\mu} \frac{dp}{dx} \quad (\text{Eq. 2.9})$$

where v refer to the velocity of the fluid, m/s ; q refers to the volumetric flow rate, m^3/s ; A refers to the overall area of rock formation, m^2 ; k refers to the rock formation permeability, d ; μ refer to the dynamic fluid viscosity, $\text{N} \cdot \text{m}^2 \cdot \text{s}^{-1}$; dp/dx refer to the pressure variation over a distance, psi .

However, certain conditions need to be considered before adopting Darcy's Law. It is only suitable for incompressible Newtonian fluid with laminar flow and should not have slippage between fluid and boundary surface. Therefore, Darcy's Law cannot be used in the gas flowing under low-pressure conditions (Kundu et al., 2011).

2.2.6 Porosity

In terms of rock formation, porosity (\emptyset) estimates the storage ability to hold fluids.

The following equation defines it as:

$$\emptyset = \frac{\text{pore volume}}{\text{bulk volume}} \quad (\text{Eq. 2.10})$$

During sedimentation, a number of void spaces are generated and turn to isolated, which causes the inconformity of pore connection (T. Ahmed & Ahmed Phd Pe, 2010). As shown in Figure 2.3, most of the void spaces are interconnected, whereas the rest are entirely segregated, which results in two different porosities: absolute porosity and effective porosity (T. Ahmed, 2010). Absolute porosity is used when the rock may possess considerable porosity while rarely having interconnection pores, and the fluids cannot flow through it. Effective porosity is adopted for most calculation cases of reservoir engineering because it represents the interconnected pores (T. Ahmed, 2009). Both values can be obtained from Equations 2.11 and 2.12:

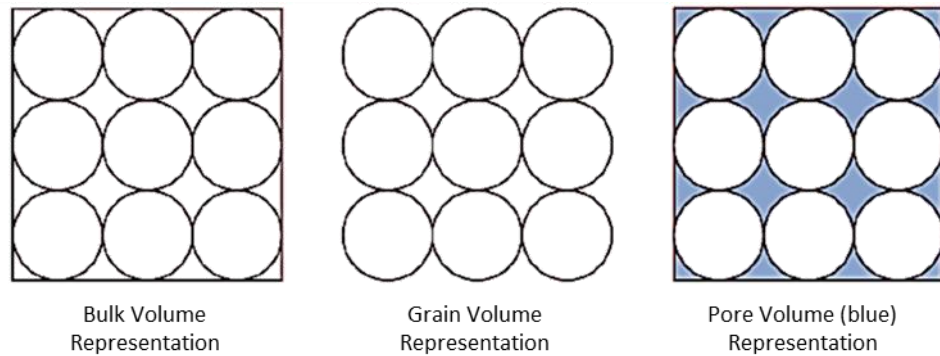


Figure 2.3: The illustration of bulk, grain, and pore volume (modified from T. Ahmed, 2010)

$$\emptyset_a = \frac{\text{total pore volume}}{\text{bulk volume}} = \frac{\text{bulk volume} - \text{grain volume}}{\text{bulk volume}} \quad (\text{Eq. 2.11})$$

where \emptyset_a refer to absolute porosity, %.

$$\emptyset = \frac{\text{interconnected pore volume}}{\text{bulk volume}} \quad (\text{Eq. 2.12})$$

where \emptyset refer to effective porosity, %.

2.3 Low Salinity Water Injection

Low Salinity Water Injection (LSWI) can improve oil recovery because of the interaction of salt ions with the reservoir rock. [Reiter \(1961\)](#) reported the first experimental result. It was indicated that the oil recovery could be improved by 12% by flooding the water with 75% less salinity than the connate reservoir water ([Martin, 1959](#); [McGuire et al., 2005](#)). LSWI can be applied in the secondary and tertiary oil recovery stages. In secondary flooding, the LSW is collected from the river and injected into the reservoir to increase the pressure and sweep the oil out macroscopically, as illustrated in [Figure 2.4 \(Fredriksen et al., 2018\)](#). In the tertiary stage, seawater or freshwater with low salt concentration (1000ppm to 3000ppm) is used ([He et al., 2015](#); [Al-Shalabi & Sepehrnoori, 2016](#)). This stage can decrease the residual oil concentration and improve the macroscopic sweep efficiency in the porous medium. Compared to other EOR techniques, the key advantages of LSWI are its maneuverable system, low cost, and low risk of environmental contamination ([Austad et al., 2010](#); [Ayirala & Yousef, 2014](#)). Several mechanisms have been proposed for LSWI during these decades, such as fines migration, multicomponent ionic exchange (MIE), electrical double layer (EDL), and pH effect, which are all discussed in the following sections ([Morrow & Buckley, 2011](#); [Katende & Sagala, 2019](#)).

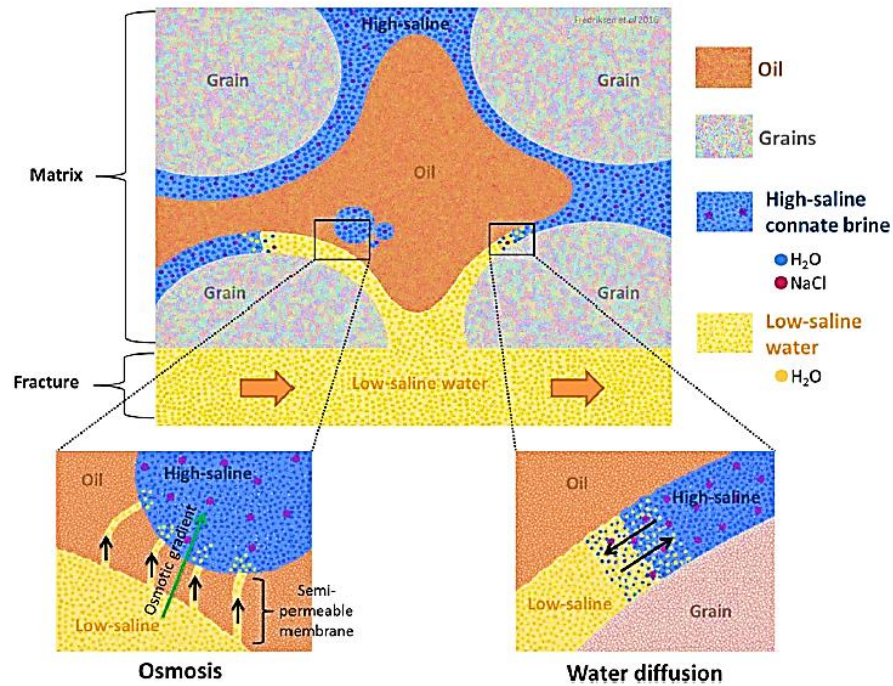


Figure 2.4: Illustration of low salinity water injection (Fredriksen et al., 2018)

According to the mechanisms stated above, LSWI would be successful if:

- 1) Clays such as kaolinite, smectite, and illite are included in the porous medium. It should be noted that the effectiveness of LSWI is directly proportional to the content of clay minerals (Cissokho et al., 2010; Alhuraishawy et al., 2018; Al-Maskari et al., 2019).
- 2) Polar organic components, such as acid and base, should be present in the oil droplet. No result has been found when the refined oil replaced the crude oil (Austad et al., 2010; Lashkarbolooki et al., 2014; Al-Saedi et al., 2020).
- 3) Connate water, also known as initial formation water, is always part of the pores medium. Salt concentration should be set between 1000 to 3000ppm for the best performance. Furthermore, divalent cations (i.e., Ca^{2+} , Mg^{2+}) must be present in the connate water or flooding water for higher efficiency (Cissokho et al., 2010; Ramly N. F. et al., 2020; Shabani & Zivar, 2020).

- 4) Temperature is not a critical parameter compared to other factors. However, according to the experimental results, LSWI would be effective once conducted under 100°C (Aksulu et al., 2012).
- 5) Recent reports show that the best results are obtained in poorly water-wet or intermediate-wet conditions (Zaeri et al., 2019; Chávez-Miyauch et al., 2020).
- 6) LSWI provides a good oil recovery when pH goes below five since polar organic compounds exhibit high adsorption rates in acidic environments (Pooryousefy et al., 2018; Rock et al., 2018; Dehaghani & Daneshfar, 2019).

2.3.1 Fines Migration

Tang and Morrow initially proposed the theory of fines migration in 1999 (Figure 2.5). It was found that the oil recovery increases when flooding low salinity water on the Berea sandstone reservoir (Y. Yang et al., 2020). During the aging process, most of the fine particles, including clays, have an oil or mix-wet system and prevent the movement of the crude oil (G.-Q. Tang & Morrow, 1999). During high salinity water flooding, these particles are untouched and would have their oil or mix-wet condition, which results in an ineffective displacement efficiency (Bernard, 1967; Al-Saedi et al., 2019). However, the electrical double layer of the particle starts to expand when the salinity of injection water drops to the range of 1000ppm to 3000ppm (Xie et al., 2019). The interaction with salt ions modifies the surface of clays, and wettability alteration takes place; therefore, the oil mobility improves (Nasralla & Nasr-El-Din, 2014). Some of the detached fine particles released from the surface of clays block the pore throats with higher permeability and divert the flow towards the un-swept zones, which further increases the sweep efficiency and oil production (Chakravarty et al., 2015a; Mehana & Fahes, 2018).

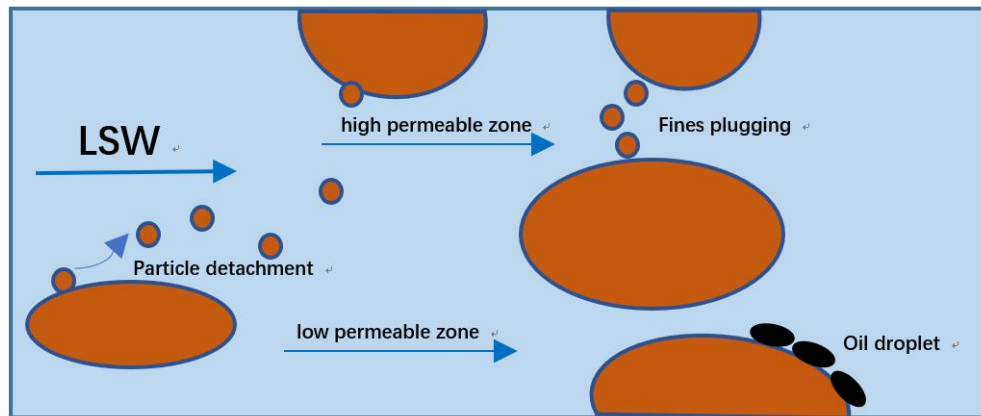


Figure 2.5: Fines migration mechanism during LSWI (modified from [G.-Q. Tang & Morrow, 1999](#))

2.3.2 Multicomponent Ionic Exchange

Multicomponent ionic exchange (MIE) in the water-oil-rock system might be one of the significant mechanisms during LSW flooding. They mentioned that the ion competition between the connected water and the exchange section of the clay surface improves production ([Lager et al., 2008](#); [Pouryousefy et al., 2016](#)). Multivalent cations, such as Ca^{2+} and Mg^{2+} , act as a "bridge" interconnecting the polar components between the oil droplet and the negatively charged clay surface, which have polar-organic compounds ([Austad et al., 2010](#); [Wissocq et al., 2018](#)). During the LSWI process, injection of water with low salt concentration can raise the repulsion force and reduce the electrostatic attraction force between the polar-organic compounds and the clay surfaces ([Kia, 1987](#); [Brady et al., 2015](#)). As a result, these organic compounds are desorbed from the rock surface and substituted by monovalent cations, shown in [Figure 2.6](#) ([Lager et al., 2008](#)). The wettability of the reservoir rock moves from oil/mix wet towards a water-wet condition, enhancing the oil recovery. The success of the MIE relies on various adsorption mechanisms, including cation exchange, cation bridging, ligand bridging, and water bridging, which is illustrated in [Figure 2.7](#) ([Sposito, 2016](#)).

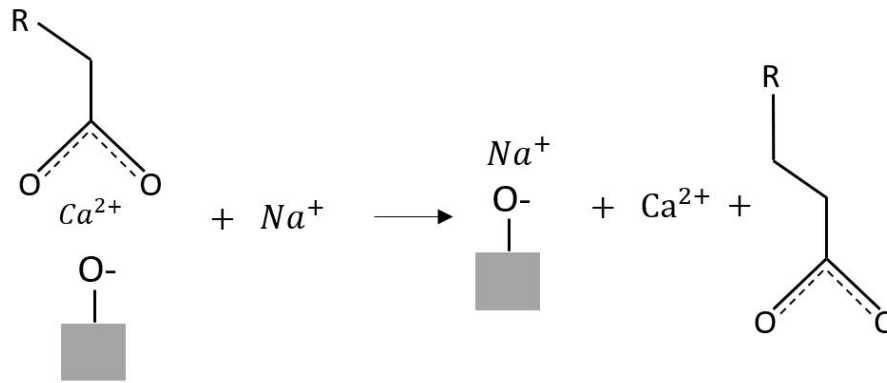


Figure 2.6: MIE mechanisms during LSWI (Lager et al., 2008)

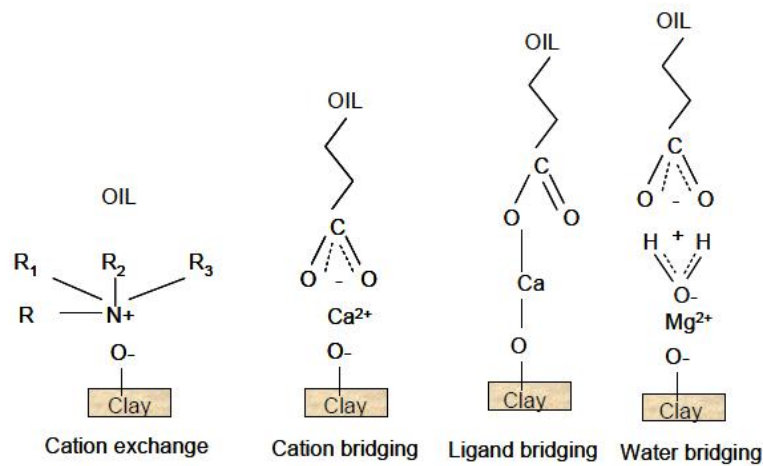


Figure 2.7: Adsorption mechanisms taking place on the clay surface (Sposito, 2016)

2.3.3 Electrical Double Layer Expansion

Electrical double layer expansion (EDL) was presented by [Ligthelm et al. \(2009\)](#) in view of the attraction/repulsion force located at the boundary surface of the rock/oil/water system. It is generated by the variation of the zeta potential of the surfaces, which results in an electrostatic repulsion force and van der Waals attraction force among ions with similar/opposite charges ([G. Tang & Morrow, 1999](#); [Xie et al., 2019](#)). The decreasing salinity of injection fluids would enhance the negative electrostatic surface potential among the oil/water interface and clay surface, leading to an increase in the repulsive force between them ([Y. Zhang & Morrow, 2006](#); [RezaeiDoust et al., 2011](#)). Consequently, the monovalent cations adsorbed on the clay surfaces are replaced by the divalent cations, followed by the polar organic compounds' desorption from the clay surface, pushing the surface to

become water-wet (Ayirala & Yousef, 2014). As schematically shown in Figure 2.8, the EDL is structured by three layers (S.-J. Park & Seo, 2011). The first layer is called the Stern layer, which comprises the immovable contrary charged ions with a thickness of 1nm (S. Y. Lee et al., 2010). The second layer is a buffer region between the stern and diffuse layers. This layer cannot move freely and is formed by ions with positive and negative charges (Nasralla & Nasr-El-Din, 2014). The third layer, the diffuse layer, comprises the exchangeable ions that are slightly bonded to the surface and migrate among the relevant interfaces. The thickness of this layer is around 1 to 500nm (Hiemenz et al., 2016).

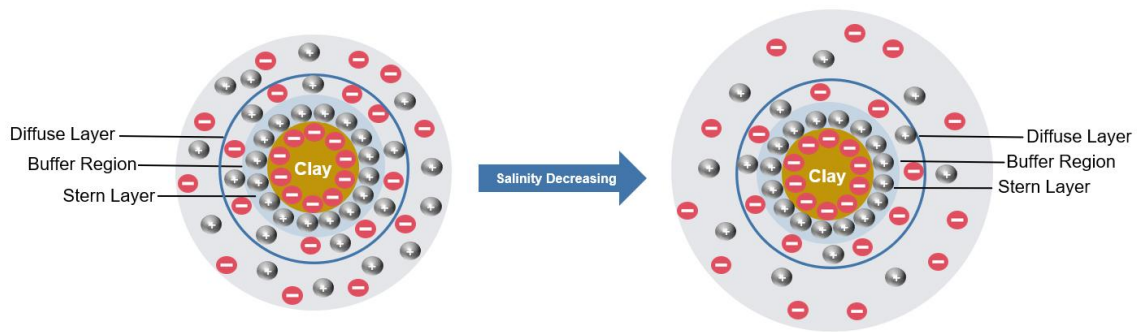


Figure 2.8: Illustration of electric double layer (modified from S.J. Park & Seo, 2011)

The degree of ions movement is controlled by the competition between the Coulomb attraction force and the electrostatic repulsion force. In the reservoir environment, the EDL is induced at the boundary surface of clays and the interface of water/oil (Esmaeili & Maaref, 2019). During the high salinity water flooding, the thickness of EDL reduces, which allows the organic compounds to be adsorbed from the oppositely charged clay surfaces (Kia, 1987; Nassabeh et al., 2019). When the total salinity of the solution decreases, the zeta potential (also named electrokinetic potential) between clay surface and oil droplet becomes more negative. Therefore, the electrostatic repulsion force increased. After that, the correlative double layers start to expand and overlap, the amount of electrostatic repulsion force of similar charged clay surface and oil droplet can overcome the binding force. Thus, the oil droplet desorbs from the clay surface also the clay surface becomes more water-wet, as shown in Figure 2.9 (Ding & Rahman, 2017).

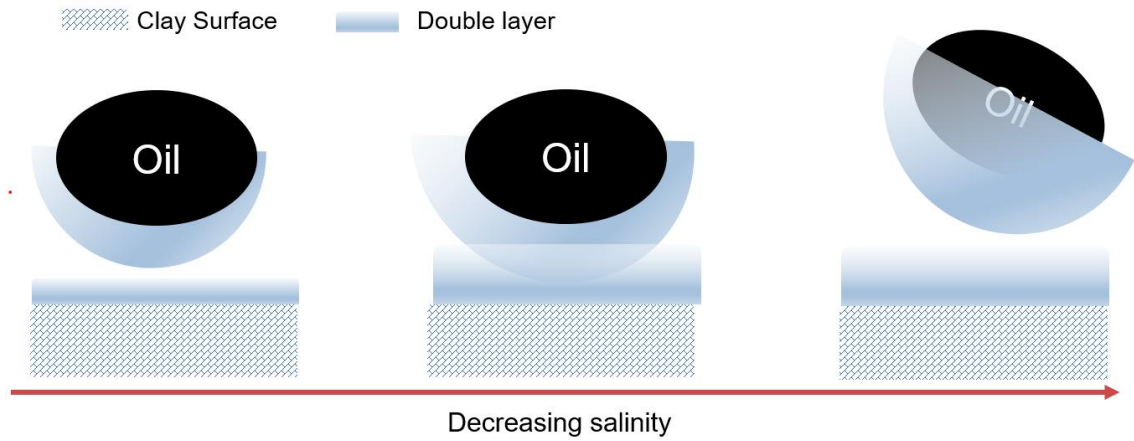


Figure 2.9: Electrical double layer expansion and overlapping (modified from [Ding & Rahman, 2017](#))

2.3.4 pH Effect

Tang and Morrow (1999) proposed a pH effect when they observed that the local pH rises during the LSWI on Berea sandstone ([Kia et al., 1987](#); [G.-Q. Tang & Morrow, 1999](#); [Katende & Sagala, 2019](#)). In an initial reservoir condition, the pH of the connate water is around five because of the dissolved acidic gases, such as carbon dioxide and hydrogen sulfide. In this environment, the polar-organic compounds tend to be adsorbed on the surface of clays by the "bridge" cations (divalent cations) ([Chen et al., 2019](#)). Injection of low saline water can "break" this bridge, release the oil droplet and increase the pH. This pH rise can be due to the dissolution of minerals and cation exchange ([Chavan et al., 2019](#)). Carbonates are the primary minerals that can increase the pH since many hydroxyl ions are released once carbonates are dissolved in low salinity water ([Elakneswaran et al., 2020](#)). The chemical reactions involved are expressed in the following equations:



The cation exchange is triggered by the interaction of the low saline water with the clay particles. In this reaction, hydrogen ions from the brine solution possess more ionic strength and will be replaced by the cations located at the surface of rocks ([Y. Zhang et al., 2007](#)). As shown in [Figure 2.10](#), as the

concentration of hydrogen ions decreases and the amount of hydroxyl ions increases, the pH increases (Austad et al., 2010; RezaeiDoust et al., 2011).

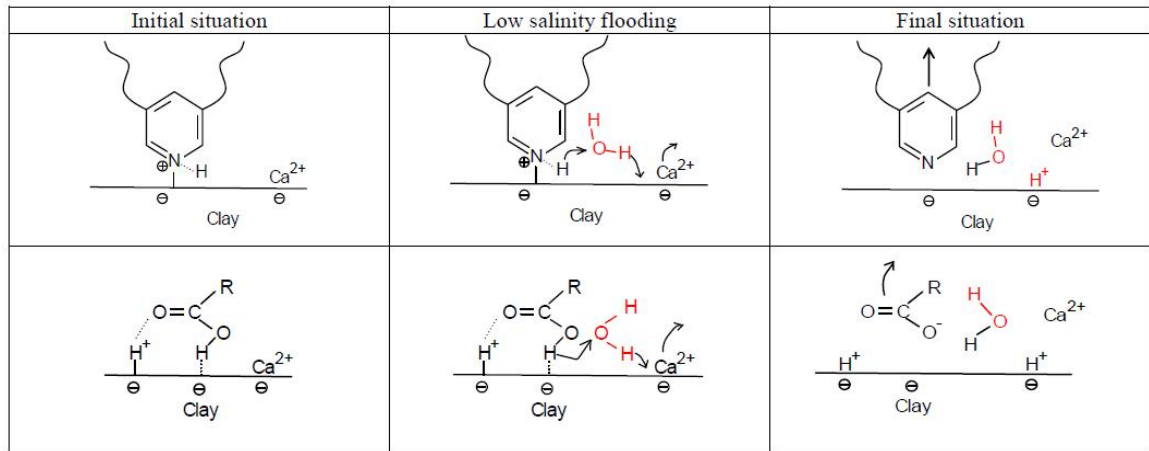


Figure 2.10: pH effect of LSWI (Austad et al., 2010)

2.4 Nanoparticle Flooding

Most of the reservoirs worldwide are reaching their limitation for oil/gas production (Nwidee, 2017). Therefore, the priority objective is extending the abandonment while inventing a better technique to overcome the drawbacks. Nanotechnology has been gaining attention recently, especially in the petroleum industry. This technology is defined as the study of understanding/fine-tuning particles within the size of approximately 1-100 nanometer scale, where unique properties generate novel applications (Denney, 2011; Ayatollahi & Zerafat, 2012; Esfandyari et al., 2014). As a new EOR method, nanoparticles are combined with surfactant or brine injected into oil formation to alter the wettability and improve the sweeping efficiency. The advantages of employing nanoparticles in the EOR process can be summarised as follows:

- High profitability: they can deliver excellent performance in small dosages (Alnarabiji & Husein, 2020; Alsaba et al., 2020).
- Environmentally friendly: most of the raw materials used to produce nanoparticles come from natural substances, such as SiO_2 , which is the main component of sandstone (Sofla et al., 2019).
- Great stability: nanoparticles can withstand high temperatures and pressure environments (Sadatshojaei et al., 2019).

- iv. Extremely small size: nanoparticles can flow through the un-swept areas and drive the oil out of pores ([Rostami et al., 2019](#)).
- v. High surface energy and large surface area: they are readily adsorbed on the surface of rocks and change the surface characteristics such as wettability ([Ramezanpour & Siavashi, 2019](#)).

2.4.1 Classification of nanoparticles

Nanoparticles are particles that possess a zero-dimension structure and are smaller than 100nm in size diameter ([Serrano et al., 2009](#)) and can be classified into three subtypes: metallic, magnetic, and oxidized metal ([Alsaba et al., 2020](#)).

Metallic nanoparticles have been getting much attention recently. It possesses the characteristics like a large surface area to volume ratio, high surface energy, and excellent suppression effect of particle self-aggregation behavior during flooding ([Sciau et al., 2009](#); [Rezvani et al., 2020](#)). The standard categories of metallic nanoparticles include aluminum, titanium, zinc, silver, and copper. According to the laboratory study, the size and shape of metallic nanoparticles are highly dependent on the resonance oscillation since the degree of oscillation is directly related to the density of electron clouds ([White et al., 2009](#); [Almao, 2012](#)). Moreover, it has been confirmed that the presence of metals can accelerate the splitting decomposition process of heavy crude oil, which can further reduce the viscosity and bring oil recovery improvement ([Hashemi et al., 2012](#)).

As a result of its magnetic feature, high surface-to-volume ratio, and strong magnetic field, magnetic nanoparticles have been widely used in petroleum, biological and environmental industries ([Jun et al., 2007](#); [Murugesan et al., 2016](#)). Several metals can be used as base materials, such as iron, cobalt, and ferric oxide. The property of surface functionalization enables these particles to deliver outstanding performance on separate oil/gas from water or hybrid flooding; they also behave as catalytic agents, increase the speed of the chemical degradation process and improve the stability of nanoparticles under high-temperature, high-pressure environments ([Jauhari et al., 2011](#); [Pastrana-Martínez et al., 2015](#); [Alnarabiji & Husein, 2020](#)). The team of Qing Wang successfully separated residual

oil droplets from connected water by synthetic magnetic nanoparticles. They intentionally turn the nanoparticles' surface charge to positive by coating them with polymer molecules (Q. Wang et al., 2018). The positively charged nanoparticles can bond with negative charged polar oil components by electrostatic attraction force, and then the magnets will be introduced to drag the oil out from the fluid (Avendano et al., 2012; L. Morrow et al., 2015). Furthermore, magnetic nanoparticles are widely applied in oil/gas exploration and geological surveys. It is treated as a contrast agent by blending with fracture fluids and injecting them into the reservoirs (Jauhari et al., 2011; Rahmani et al., 2015).

Oxidized metal nanoparticles are the most widely used kind, especially for the petroleum and chemical industries. The common types contain silicon dioxide, iron oxide, titanium trioxide, zinc oxide, nickel oxide, and aluminum oxide (Alsaba et al., 2020; Al-Samhan et al., 2020). These particles present unique chemical and physical properties. Specifically, the thermal conductivity capacity was boosted up to 40% by introducing metal oxide nanoparticles into the solution (Yu et al., 2008). The relevant application targets fines migration control, oil recovery enhancement, fluid injection improvement stability, and crude oil reduction viscosity (Hendraningrat & Torsæter, 2015; Roustaei & Bagherzadeh, 2015). More importantly, metal oxide nanoparticles can effectively improve the tolerance of hybrid solutions injected into high-pressure, high-temperature reservoir conditions (Esfandiyari et al., 2014). The scheme of the structure of different nanoparticles is present in Figure 2.11.

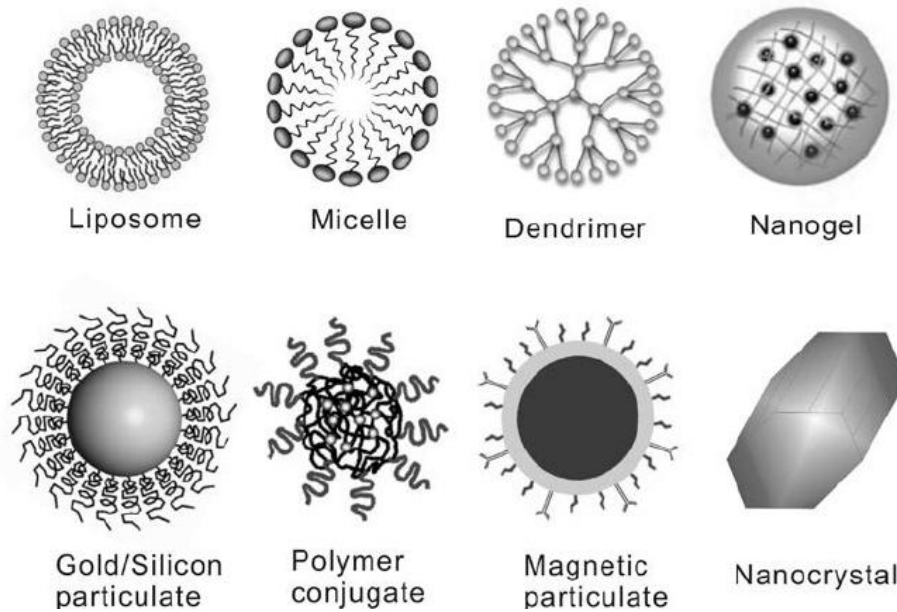


Figure 2.11: Illustration of the structure of various nanoparticles (Q. Wang, 2014)

2.4.2 Wettability Alteration

Wettability is the most critical feature governing the volumetric sweep efficiency of an EOR method (Sadatshojaei et al., 2019). It controls the degree of difficulties of driving oil out of the pore spaces from wetting or non-wetting formations. Reservoir wettability condition is determined by the inter-relationship between rock, oil, and water system, the distribution of oil droplets in the pore structure, and the bonding intensity between oil compounds and the rock surface (Ju et al., 2012; Mousavi Moghadam & Baghban Salehi, 2019; Nikolov et al., 2019). Numerous experimental studies have shown that the formation wettability changes from an oil-wet or mix-wet condition to a strongly water-wet system by applying nanoparticles (Liang et al., 2019; Mohajeri et al., 2019). However, the efficiency of wettability alteration depends on the nanoparticle distribution at the interface of injecting solution and the rock formation.

On the other hand, surface cleaning and surface coating concepts. In the surface cleaning mechanism, hydrophilic nanoparticles with high surface energy can be easily bonded to the lipophilic molecules on the rock surface, therefore breaking their structure and improving the wettability condition (Aminian & ZareNezhad, 2019b). In the nanoparticle coating mechanism, nanoparticles adhere and cover the

rock surface with their self-forming nanostructure and change the wetting condition, as shown in [Figure 2.12 \(Ali et al., 2018\)](#). For example, nano-silica particles with hydrophilic features tend to be adsorbed on the lipophilic rock surface and coat the surface with a hydrophilic nanostructure shield, thereby changing the rock surface from an oil-wet to a water-wet system ([S. Li et al., 2018](#)).

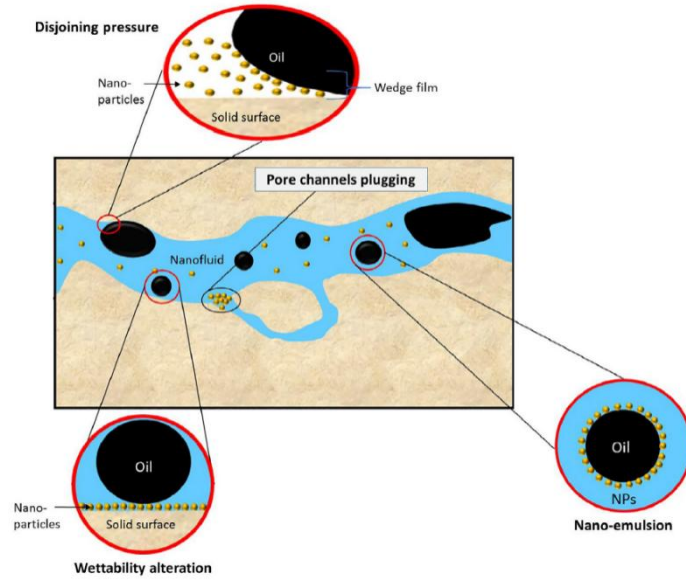


Figure 2.12: Mechanisms of wettability alteration of nano-flooding ([Ali et al., 2018](#))

According to [Zhang et al. \(2010\)](#), the effectiveness of nanoparticles also depends on the type of emulsion formed. As illustrated in [Figure 2.13](#), the hydrophilic nanoparticles coalesce into oil-in-water emulsion and self-assemble on the interfacial surface. In contrast, the lipophilic nanoparticles prefer to coalesce into the water-in-oil emulsion ([T. Zhang et al., 2010](#)). Additionally, hydrophilic nanoparticles possess a water-wet attribute, which is crucial for an effective water-wet alteration ([Negin et al., 2016](#); [Jin et al., 2018](#)). On the contrary, lipophilic nanoparticles are more likely to contact oil instead of water and move towards an oil-wet system. However, the extent of this alteration greatly depends on the size and concentration of nanoparticles ([Aminian & ZareNezhad, 2019b](#)).

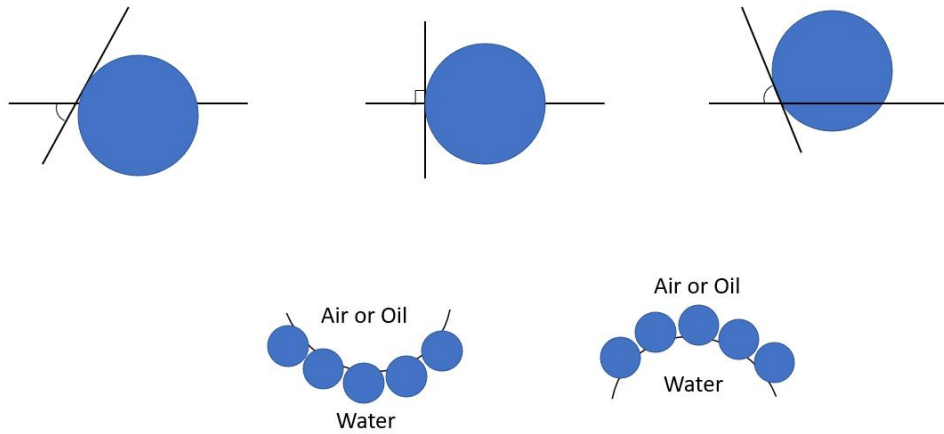


Figure 2.13: Contact angle of different nanoparticles and their related emulsion state (modified from [T. Zhang et al., 2010](#))

2.4.3 Structure Disjoining Pressure

Nanoparticles in the EOR injection fluid tend to self-aggregate or layering into the wedge-film structure at the interface between the solid substrate (rock) and the injection aqueous ([Chengara et al., 2004](#); [Nikolov et al., 2019](#)). These nanoparticles would trigger a pressure known as the structure disjoining pressure, which pushes the particles and injection fluid spread along the contact surface ([H. Zhang et al., 2014](#)). This disjoining pressure is directly related to the fluids' ability to propagate through the surface of the substance and is caused by an uneven distributed interfacial force on the surface of fluid/oil/rock ([Agista et al., 2018](#); [Gbadamosi et al., 2019](#)). Due to this force, the contact angle between the EOR fluids (with nanoparticles) changes, driving the fluids to spread along while forcing the oil droplet to detach from the rock surface, as shown in [Figure 2.14](#) ([Wasan et al., 2011](#)).

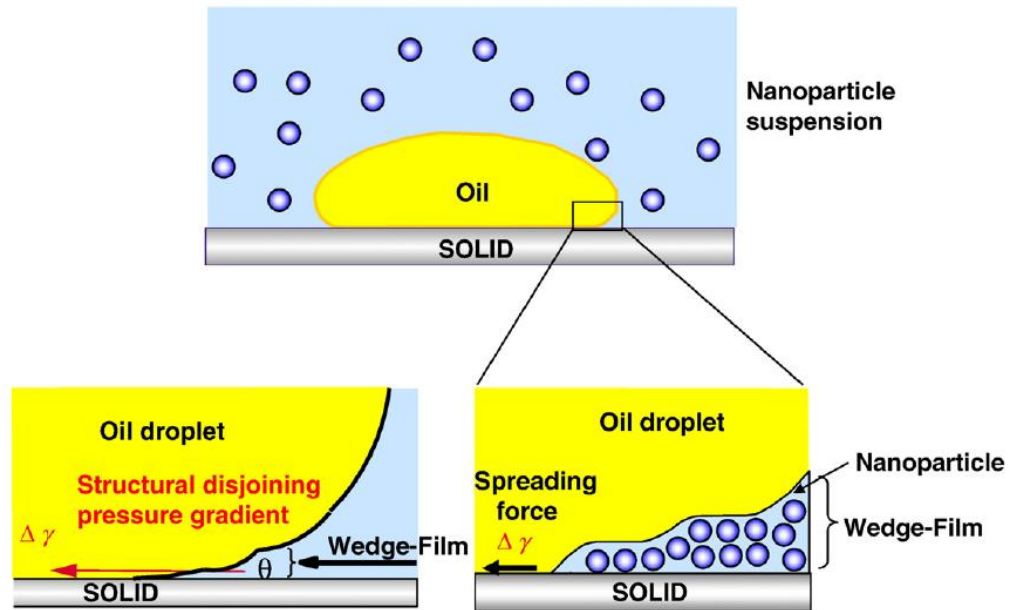


Figure 2.14: Mechanism of the structure disjoining pressure (Wasan et al., 2011)

The correlative energy that motivates this disjoining pressure is the electrostatic repulsion force and the Brownian motion (Negin et al., 2016). Although the repulsion force generated by an individual nanoparticle is small, the pressure can reach 50 kPa on the vertex (Mcelfresh et al., 2012). In addition, the particle size, charge density, and concentration also affect the magnitude of the repulsion force among these particles (Kazemzadeh et al., 2019). As a rule of thumb, the lesser the size of particles, the bigger the particle charge density, and the higher the repulsion force. In addition, this force rises as the concentration of nanoparticles increases (Salem Ragab & Hannora, 2015; K. Li et al., 2018).

2.5 Surfactants Flooding

2.5.1 Surfactant Classification

Surface-active agents, also known as surfactants, are chemical compounds comprising mainly of polymeric molecules that can be adsorbed on the surface of substrate or interface of fluids in a low concentration (Negin et al., 2017; Sarmah et al., 2020). The main characteristic is its ability to reduce the interfacial tension between oil and water in a reservoir (Belhaj et al., 2020). Surfactants possess a unique molecular structure that includes a hydrophilic head group (polar part) that

exhibits a strong affinity for water, together with a group of the hydrophobic tail (nonpolar part) that have a strong affinity for oil compounds (Green et al., 2010). The structure of a surfactant is shown in Figure 2.15 (Massarweh & Abushaikh, 2020). The feature of surface-active is induced by the equilibrium between hydrophilic and lipophilic parts of the surfactant molecule (Green et al., 2018). More specifically, the hydrophobic tail is generally composed of a long linear hydrocarbon chain, and the amount of carbon atoms on this chain dedicates the water solubility. A surfactant is considered hydrophilic when the chain has less than 12 carbons, and the hydrophilic head can bond with water molecules (Kamal et al., 2017; Schramm, 2000). On the contrary, when the number of carbon is larger than 14, the surfactant is treated as hydrophobic since the long hydrocarbon chain hinders the water solubility (Green et al., 2018).

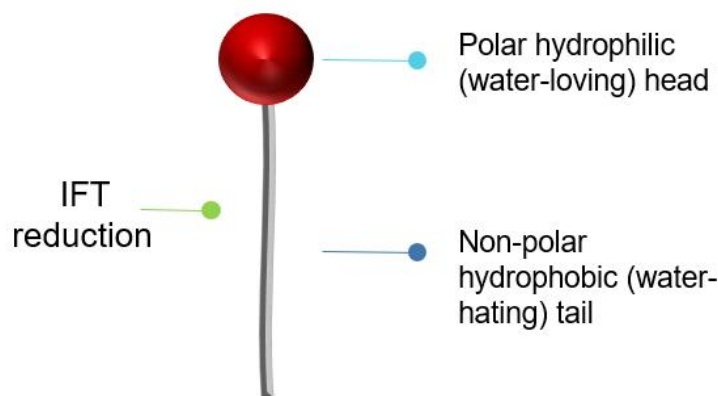
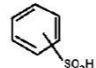
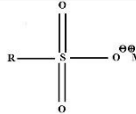

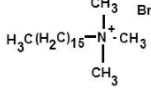
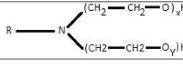
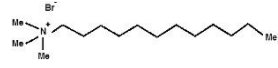
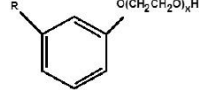


Figure 2.15: Structure of a surfactant molecule (modified from Massarweh & Abushaikh, 2020)

Surfactants are classified based on the ionic nature of the hydrophilic head into three categories of ionic (cationic and anionic), nonionic and zwitterionic (J. J. Sheng, 2015; Negin et al., 2017). Each of these groups possesses specific properties. For instance, surfactants with a cationic head possess a positive charge in the solution, while an anionic head has a negative charge (Kronberg et al., 2014; Green et al., 2018). The head group of nonionic surfactants is non-dissociating. It will not pose a charge in the solution, while the zwitterionic surfactant presents both negative and positive charges when ionizes in the aqueous solution. Some of the most common surfactants are summarized in Table 2.1 (Kronberg et al., 2014;

Sheng, 2015; Paul et al., 2015; Negin et al., 2017; Green et al., 2018; Aziz et al., 2019).

Table 2.1: Some of the example surfactants used in the industry (Kronberg et al., 2014; Sheng, 2015; Paul et al., 2015; Negin et al., 2017; Green et al., 2018; Aziz et al., 2019)

Ionic type	Name of surfactant	Molecular structure
Anionic	Alkyl aryl sulfonate	$\text{CH}_3(\text{CH}_2)_m\text{CH}(\text{CH}_2)_n\text{CH}_3$ 
Anionic	Alkyl sulfate	
Anionic	Sodium dodecyl sulfate	
Cationic	Cetyl trimethyl ammonium bromide	
Cationic	Ethoxylated alkyl amine	
Cationic	Dodecyl trimethyl ammonium bromide	
Nonionic	Alkyl ethoxy carboxylate	$\text{RO}(\text{CH}_2\text{CH}_2\text{O})_x\text{CH}_2\text{COO}^- \text{M}^+$
Nonionic	NEODOL ethoxylate 91-8	$\text{RO} - (\text{CH}_2\text{CH}_2\text{O})_n - \text{H}$
Nonionic	Polyethoxylated alkylphenols	

2.5.2 Surfactant lost behavior

Surfactant is considered a primary cause of the cost of chemical EOR flooding, and losing it will result in many economic losses. In general, the expenditure on surfactants accounts for 50% or more than 50% of the entire process outlay (R. Zhang & Somasundaran, 2006; Peng & Nguyen, 2020). Unfortunately, surfactant losses are an inevitable phenomenon and can only be minimized. The physical retention induces the formation of pores (adsorption and surfactant precipitation) or injected solution trapped in the porous media (Abbas et al., 2020). In addition, the factors like surfactant type (anionic, cationic, and nonionic), salinity, ionic strength, temperature, pressure, pH, and concentration also affect the intensity of surfactant adsorption rock formation (Ayoub et al., 2019; Yekeen et al., 2019). Thus,

minimizing the degree of surfactant adsorption is important for delivering successful surfactant flooding.

Under the state of low concentration, surfactants tend to adsorb on the rock surface as monomeric structures (J. Zhang et al., 2016). When the concentration rises, these monomers start to agglomerate together and assemble as micelles. Meanwhile, electrostatic interactions among each surfactant molecule will force these monomers/micelles situated on the rock surface (Barati-Harooni et al., 2016). The adsorption mechanisms can be summarized as electrostatic attraction, hydrophobic interactions, ion-binding, hydrogen bonding, and chemical interactions (S. Park et al., 2015; Saha et al., 2017).

2.5.3 Application of Surfactant in the Petroleum Industry

Nowadays, various surfactants have been widely used in the petroleum industry for decades, especially for foam/emulsion drilling, enhanced oil recovery, fracturing, waterflooding, acidizing, and corrosion inhibition (Paul et al., 2015; Negin et al., 2017; Schramm, 2000). Due to the complexity of the reservoir environment, waterflooding, as a traditional secondary recovery technique, has already reached its limit exhibiting a decrease in oil recovery, leaving 50% to 75% of original oil in place (Flaaten et al., 2008). As part of the chemical EOR, surfactant flooding is one of the most adopted techniques to improve oil production under these circumstances. In this method, one or multiple types of surfactant are added to the injected fluid to effectively improve the reservoir wettability and the interfacial tension between the oil and water, as shown in Figure 2.16 (Schmiedel & Rybinski, 2007; Hou et al., 2015; Sarmah et al., 2020).

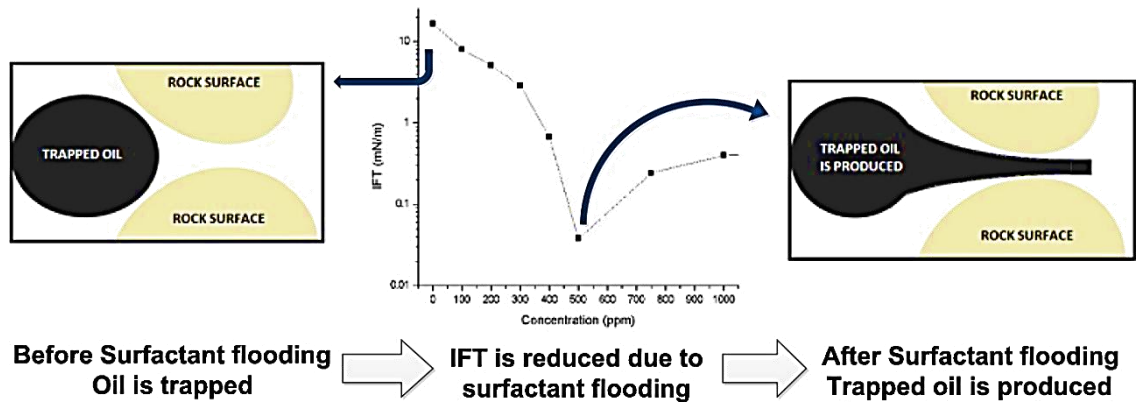


Figure 2.16: Mechanism of surfactant-assisted water-flooding (Kumar & Mandal, 2017)

During surfactant flooding, co-surfactant and polymers are also injected along with the surfactant to improve the resistance of the solution to the extreme environment (Mahdavi et al., 2017). However, the efficiency of a hybrid surfactant solution is not consistent over time since surfactants are easily adsorbed on the surface of rocks or trapped in the complicated structure of porous media (Ayoub et al., 2019; Belhaj et al., 2020). Thus, a successful surfactant flooding should maximize the oil recovery while minimizing the loss of surfactants.

2.5.4 Limitations of Synthetic Surfactants

Surfactant is considered a primary cause of the enormous cost behind the chemical EOR flooding. In general, the expenditure on surfactants accounts for more than 50% of the entire process outlay (R. Zhang & Somasundaran, 2006; Peng & Nguyen, 2020;). However, a large portion of surfactant tends to be adsorbed by reservoir formation when flowing through porous media for several reasons, such as rock formation/surfactant interaction and surfactant adsorption behavior. They are raising the cost of operation and reducing the performance of the EOR solution (Belhaj et al., 2020). Unfortunately, surfactant loss is inevitable and can only be minimized. The physical retention induces the formation of pores (adsorption and surfactant precipitation) or trapping the injected solution in the porous media (Abbas et al., 2020). In addition, surfactant type (anionic, cationic, and nonionic), salinity, ionic strength, temperature, pressure, and pH also affect the intensity of

surfactant adsorption in the rock formation (Ayoub et al., 2019; Yekeen et al., 2019). Thus, minimizing the surfactant adsorption during EOR is significantly essential for the success of surfactant flooding. In a low concentration, surfactants also tend to adsorb on the rock surface as monomeric structures (J. Zhang et al., 2016). When the concentration rises, these monomers' molecules formate together and assemble as micelles. As a result, surfactants lose their functionality and may change the properties of the EOR fluid, reducing the oil recovery significantly (Barati-Harooni et al., 2016).

Mainly, the surfactant is classified into two classes: natural and artificially synthesized. Both surfactant classes lead to IFT reduction and wettability alteration. However, synthetic surfactant is more expensive, toxic, non-biodegradable, and causes environmental pollution. Therefore, researchers have started to develop a new series of green surfactants as a substitute to replace the traditional synthetic surfactant

2.5.5 Green Surfactants

Recently, the study of natural surfactants has become popular among researchers. Chhetri et al. (2009) studied the application of Soapnut saponin on oil recovery by conducting IFT reduction experiments at various surfactant concentrations. The results showed that IFT between oil and water was decreased from 19 dyne/cm to 2.5 dyne/cm. (M. A. Ahmadi et al., 2012) investigated the natural surfactant extracted from Glycyrrhiza Glabra. An IFT reduction was observed, decreasing from 33 dyne/cm to 9 dyne/cm. (Deymeh et al., 2012) developed a natural surfactant from the *Seidlitzia Rosemarinus* plant, and by using pendant drop methods, IFT results significantly dropped from 32 dyne/cm to 9 dyne/cm. (Pordel et al., 2012a) successfully extracted a natural surfactant from the local plant Ziziphus Spina Christi, and the relative IFT performance was examined. IFT was decreased from 48 dyne/cm to 9 dyne/cm. In addition, (Zendehboudi et al., 2013) reported that this surfactant could reduce the IFT of crude oil from 32 dyne/cm to 11 dyne/cm. (M. A. Ahmadi et al., 2014) discovered that the IFT decreased from 43.9 dyne/cm to 17.9 dyne/cm by injecting the surfactant solution extracted from the leaves of the

Mulberry tree. Natural surfactants extracted from Glycyrrhiza Glabra leaves by (Arabloo et al., 2015), Henna leaves by (Rahmati et al., 2015), Matricaria Chamomilla by (S. S. Shadizadeh & Kharrat, 2015), Soap Nut by Saxena et al. (2019), and Anabasis Setifera by Nowrouzi et al. (2020) possess extraordinary performance on IFT reduction between oil and water. Therefore, all these plant extracts can be utilized to decrease IFT. The details of the comparison between various surfactants are summarized in Table 2.2.

Table 2.2: Natural surfactants summary and comparison

Natural Surfactant	Ionicity	IFT (mN/m)	Reference
Soapnut	Non-ionic	19-2.5	(Chhetri et al., 2009)
Seidlitzia Rosmarinus	Cationic	32-8.9	(Deymeh et al., 2012)
Glycyrrhiza Glabra	Non-ionic	33-9	(M. A. Ahmadi & Shadizadeh, 2012)
Zizyphus Spina-Christi	Non-ionic	48-9	(Zendeboudi et al., 2013)
Mulberry leaf	Cationic	43.9-4.01	(Rahmati et al., 2015)
Henna	Cationic	43.9-3.05	(Rahmati et al., 2015)
Prosopis leaf	Cationic	36.5-15	(Khorram et al., 2015)
Spistan leaf	Cationic	36.5-20	(Khorram et al., 2015)
Olive leaf	Cationic	36.5-14	(Khorram et al., 2015)
Matricaria chamomilla	Nonionic	30.63-12.57	(Khorram et al., 2015)
Trigoonella Foenum-Graceum	Non-ionic	75-23.5	(Barati-Harooni et al., 2016)

2.5.6 Synthetic Surfactants versus Green Surfactants in Cost Aspect

Surfactant flooding can decrease the interfacial tension between water and oil and alter the wettability through surfactant adsorption behavior, enhancing oil recovery

(Massarweh & Abushaikh, 2020). However, a large portion of surfactant tends to be adsorbed by reservoir formation when flowing through porous media for several reasons, such as rock formation/surfactant interaction and surfactant adsorption behavior. They are raising the cost of operation and reducing the performance of the EOR solution (Belhaj et al., 2020). Mainly, the surfactant is classified into two classes: natural and artificially synthesized. Both surfactant classes can lead to IFT reduction and wettability alteration. Nevertheless, synthetic surfactants are more expensive, toxic, non-biodegradable, and cause environmental pollution than green surfactants. Therefore, researchers have started to develop a new series of green surfactants to replace the traditional synthetic surfactant. Table 2.3 presents the research summary on the use of synthetic surfactants and green surfactants in chemical EOR.

Table 2.3: Research on the use of synthetic surfactants and green surfactants in EOR

Reference	Surfactants Applied	Surfactants Type	IFT Reduction (mN/m)
(Liu et al., 2022)	Sodium dodecyl sulfate (SDS)	Synthetic Anionic	3.46
(Luan et al., 2019)	Alkyl aryl monosulfonate (AMS)	Synthetic Anionic	29.2
(Qi et al., 2022)	Cetyltrimethylammonium bromide (CTAB)-R4	Synthetic Cationic	1.18
(Qi et al., 2022)	Dodecyltrimethylammonium bromide (DTAB)-R2	Synthetic Cationic	1.8
(Sarmah et al., 2020)	Alkylpolyglycoside (APG)-F1	Synthetic Nonionic	0.47
(Massarweh & Abushaikh, 2020)	Tergitol 15-s-7(Tg7)	Synthetic Nonionic	27.8
(Khorram et al., 2015)	Olive leaf	Natural Cationic	14
(Khayati, 2020)	Soapnut	Natural Nonionic	9.89

According to Table 2.3, synthetic and natural surfactants can deliver a proper IFT reduction. However, the overall performance of natural surfactants was wake

than the synthetic one. Therefore, the natural surfactants may be co-surfactants in the EOR process to reduce cost and environmental pressure.

In order to deliver a successful EOR surfactant flooding, not only does the technical process and viability need to be comprehensively mastered, but the economic feasibility is also a crucial parameter. It is highly affected by the oil price and surfactant purchase cost (especially at the field scale). The general expense of EOR surfactant flooding is related to the surfactant ([Sajjad et al., 2019](#)). Overall, the capital expenditure on surfactants can divide into two parts: 1) Minority: the cost of surfactant purchase; 2) Majority: the cost of re-purchase losing surfactant caused by adsorption behavior ([Nowrouzi et al., 2020](#)). This project's Soapnut and Camellia oleifera seed study are natural and inexpensive surfactant materials. It can be widely obtained in Asian and Middle East areas. Compared to other typical commercial surfactants, the Soapnut saponin and Camellia oleifera saponin possesses two significant advantages:

- It is present as a natural and cheap surfactant. Compared to other commercial surfactants used in industry, such as NEODOL, Sodium dodecyl sulfate (SDS), and Alkyl sulfate (AS), it is 100% biodegradable, non-toxic, environmentally friendly, and a fantastic sustainable natural resource ([Samanta et al., 2013](#); [Saxena et al., 2019](#)).
- It possesses a similar performance and contains the same structure as synthetic surfactants. The stock price of Soapnut and Camellia oleifera seed in the source area is as low as 0.65 US\$/kg and 1.15 US\$/kg, respectively ([Anhui Changfu Chinese Medicine Co., Ltd.](#)). Based on the extraction efficiency provided by [Köse & Bayraktar. \(2016\)](#), the saponin extraction yield was approximately 75% by water. Then the prices of extracted saponin from Soapnut and Camellia oleifera were roughly located at 0.87 US\$/kg and 1.53 US\$/kg. For the typical synthetic surfactants used in the Petroleum Industry, the price has been reported around 4 US\$/kg ([Nowrouzi et al., 2020](#)). Therefore, it approximately can reduce the cost by 78.3% with Soapnut saponin and 61.8% with Camellia oleifera saponin as surfactant alternatives.

2.5.7 Surfactants Application in LSWI

Low salinity water injection (LSWI) has been introduced in the petroleum industry as a brand-new technique for oil recovery recently. Several mechanisms such as electrical double layer expansion, multicomponent ionic exchange, pH increase, and fines migrations are major mechanisms that mobilize oil and enhance oil recovery (Qiao et al., 2016). Surfactant flooding has been proven to be a mature technology to enhance oil recovery by numerous studies and field tests (Shabani & Zivar, 2020; Tale et al., 2020; Y. Yang et al., 2020). The oil has been mobilized and re-produced by wettability alteration and decreased capillary force because of the reduction of IFT between oil and water phases. However, a large amount of surfactant loss during the surfactant injection process that causes by adsorption, mechanical trapping, and precipitation (Moradi et al., 2019).

Alagic et al. (2010) presented a hybrid EOR flooding technique that combines surfactant flooding with LSWI named low salinity surfactant (LSS) flooding. This new technique brings several advantages to LSWI and surfactant flooding. One of the key advantages is that LSS can reduce surfactant adsorption to the rock compared with traditional surfactant flooding (M. A. Ahmadi & Shadizadeh, 2018). Furthermore, it can further decrease the IFT that avoids re-trapping the mobilized oil compared with traditional LSWI. In specific, several multi-mechanisms have been discovered: 1) LSWI can increase the local pH level, thereby weakening the surfactant adsorption behavior (Hosseinzade et al., 2016); 2) the low ionic strength ion contributed by LSWI can weaken the ionic bonding between polar oil modules and clay surface, thus further improve the surface wettability from less water-wet condition to more water-wet condition together with surfactant (Chávez et al., 2020); 3) the low ionic strength solution environment can effectively maintain surfactant stay in water phase where the oil-in-water microemulsion form Rissoen (2012); 4) the IFT reduction ability brought by the surfactant can prevent re-trapping of the mobilized oil at lower capillary pressure during low salinity water environment (Alagic et al., 2011). Several experiments have been conducted on sandstone cores. As shown in Figure 2.17 presented by Rissoen (2012), the oil

recovery rises from 64% OOIP (LS) to 94% OOIP (LSS), and the corresponding residual oil saturation decrease from 0.3 (LS) to 0.05 (LSS). Furthermore, the traditional LS flooding can only bring 2% oil recovery of OOIP, but the LSS flooding can boost the recovery up to 26% OOIP. Similar results also observed by [Moradi et al. \(2019\)](#) that the IFT successfully reduced from 15 mN/m to 7.2, 9.1 and 12.5mN/m by additional natural surfactant (Tribulus Terrestris Extract) to saline water that contains SO_4^{2-} , Mg^{2+} and Ca^{2+} , respectively ([Figure 2.18](#)).

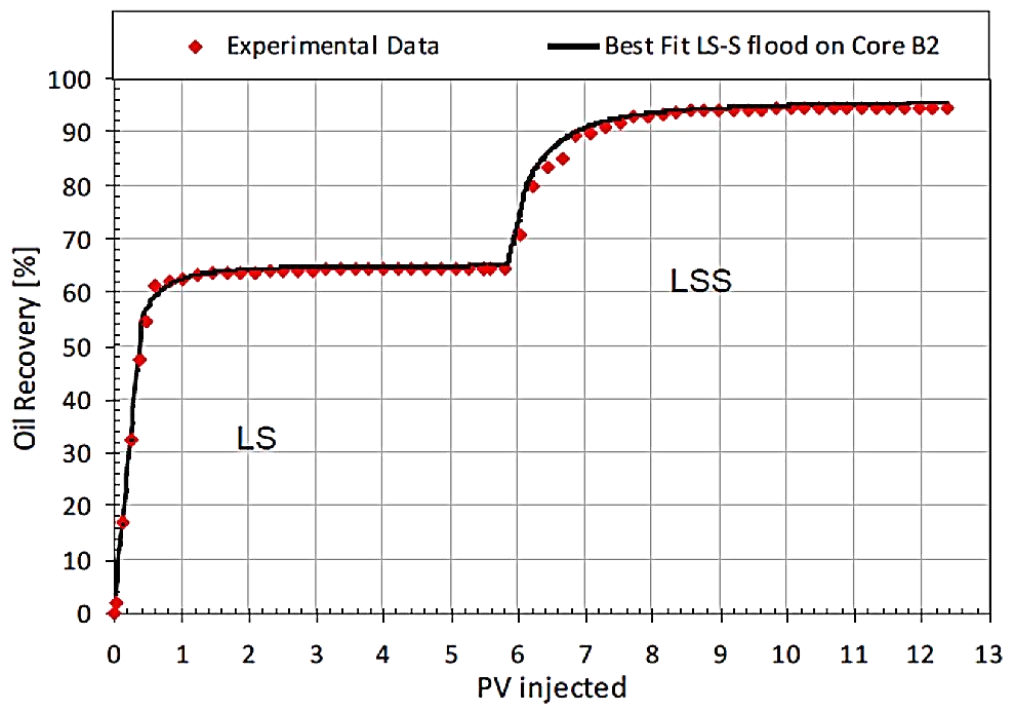


Figure 2.17: Oil recovery by LS flooding and LSS flooding ([Rissoen, 2012](#))

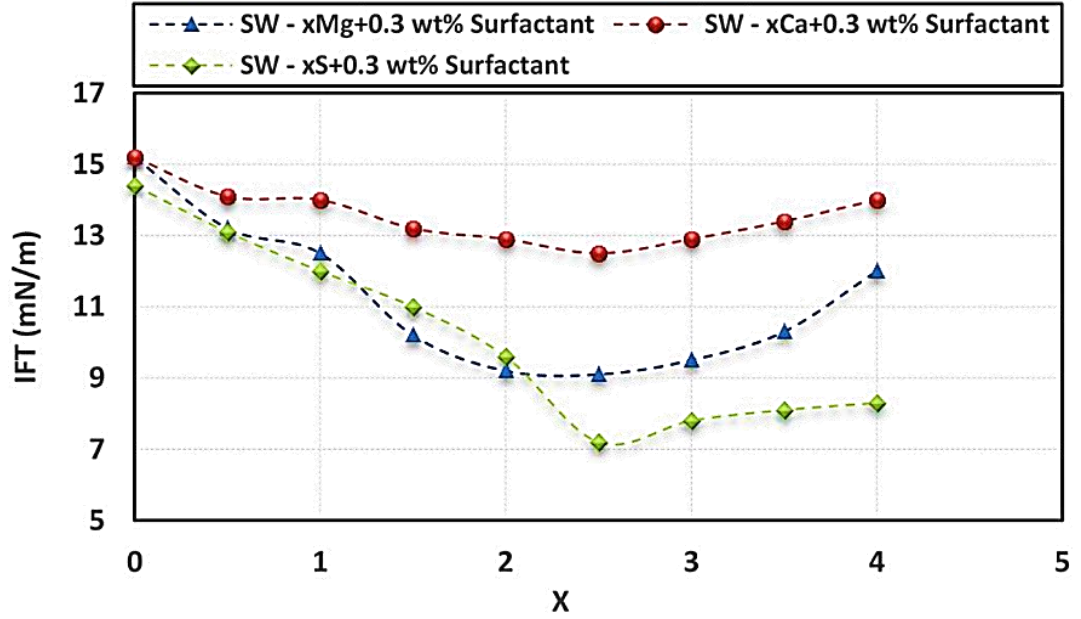


Figure 2.18: IFT reduction induced by addition of surfactant in saline water (Moradi et al., 2019)

2.6 Foamability and Foam Stability

2.6.1 Introduction

Foam in porous media is defined as a gaseous dispersion in a liquid phase that is continuously flowing. According to the two-dimensional foam slice shown in Figure 2.19, the general foam structure is defined at the bottom by a large amount of bulk liquid and at the top by a second large amount of bulk phase, in this instance, gas (Marinova et al., 2009). The many components of the foam structure are more clearly visible inside the magnified section of the image. In this case, a two-dimensional interface is used to separate the gaseous phase from the thin liquid film. When it comes to the physical qualities of gases and liquids, there is no strong dividing line between them. The physical behavior of this interfacial region is approximated by a two-dimensional surface phase, which is dictated by mathematical convenience (the Gibbs surface) (Yisong et al., 2022). A lamella is defined as the region that includes the thin film itself, the two interfaces on either side of the thin film, and a portion of the junction with other lamellae. The plateau boundary is defined as the intersection of three lamellae that meet at an angle of 120° . The aqueous solution containing surfactant that is in contact with a gas can be disturbed, resulting in foam formation (Tran et al., 2022). Stabilization of thin liquid

films is accomplished through the adsorption of surfactant molecules. The characteristics of liquid films are critical in foam stability because they influence the way foam expands and contracts.

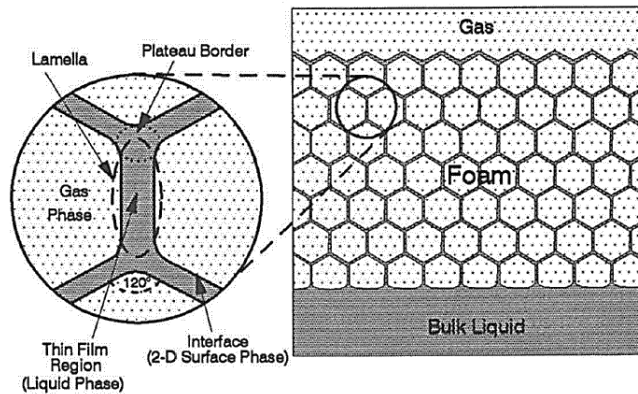


Figure 2.19: Two-dimensional foam structure (Marinova et al., 2009)

2.6.2 Foam formation

Unlike bubbles in pure water, they do not coalesce (merge). Instead, they form a 3D structure that possesses a specific mechanical strength. Due to their high interfacial free energy, they are usually not thermodynamically stable. However, the presence of surfactants stabilizes the foam films, making them metastable. When an interface absorbs surfactant, its surface area can be modified, which causes a change in its surface tension (AlYousef & Schechter, 2019). For example, the surface tension increases if an interface is expanded and vice-versa. It is also known as the Gibbs effect.

Over time, a perturbed interface will return to its equilibrium surfactant surface coverage. The surfactant will be transported to or from the perturbed surface during relaxation. Figure 2.20 illustrates that the disturbed foam film results in film thinning, which increases the local surface area. The surface tension in the locally thinned region is higher than in the surrounding regions due to the Gibbs effect (Kawale, 2012).

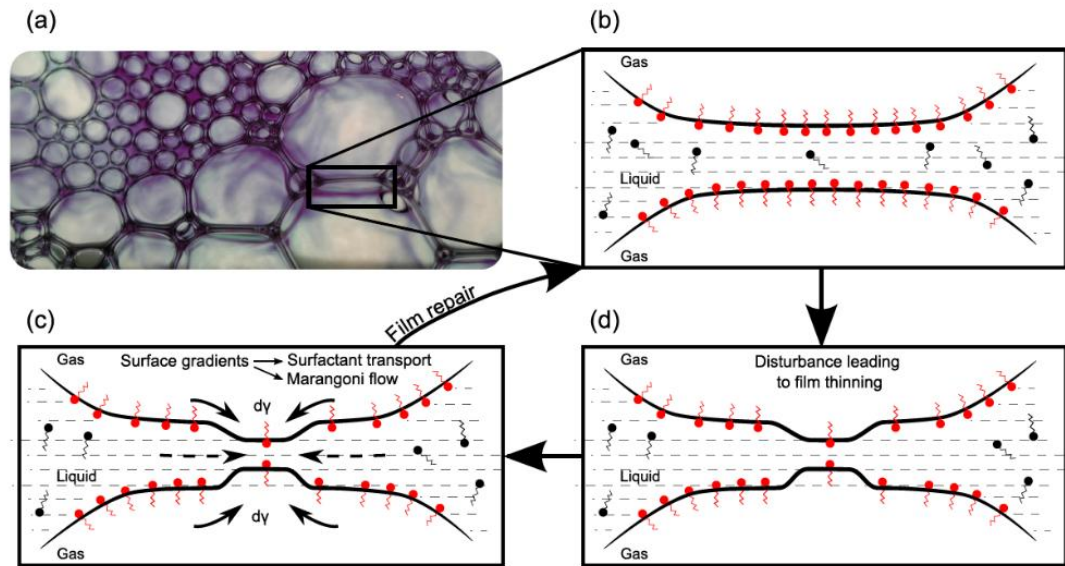


Figure 2.20: Marangoni Flows' foam structure and internal molecular film repair mechanism (Kawale, 2012)

These surface tension gradients across the thinned region deliver the liquid mass, from the low surface tension (healthy film region) to the high surface tension region (thinned film region). These flows are also known as Marangoni flows which can lead to stabilization. When Gibbs and Marangoni's effects are combined, the repair of the thinned film could be improved (Mustan et al., 2022a). For a successful film repair instance to occur, sufficient liquid mass must be transported to the thinned region before the surface tension gradients disappear (Skauge et al., 2020).

2.6.3 Foam application in EOR

Foam is used in various oil and gas industry applications, including enhanced oil recovery, drilling, and well stimulation. The primary goal of EOR is to increase the efficiency of both microscopic displacements and volumetrics (Yisong et al., 2022). Mobility control can be used to increase the displacement efficiency of a system. Ideal mobility ratios can be reached by increasing or decreasing the viscosity of one of the fluids, depending on the situation (Y. Sheng et al., 2022). It is possible to produce capillary trapped oil by lowering the interfacial tension between the displaced and displacing phases during the flooding process. As investigated in this

project, foam is considered part of the novel chemical EOR solution of nanoparticles, low salinity water, and green surfactant.

Most of the time, the foam has been utilized in EOR procedures to adjust the mobility ratio or block off undesirable inflow during good treatments ([Rattanaudom et al., 2022](#)). Using a combination of surfactant, gas, and water/low saline water to form foam in a reservoir can help alleviate the issues during gas injections while also increasing the efficiency of sweeps, allowing for more remarkable oil recovery. When combined with other additives (salt and nanoparticles), these distinctive properties can boost the ultimate recovery of mature oil reservoirs ([Aziz et al., 2019](#)). One of the most significant obstacles to the successful application of foam in EOR is the negative impact of crude oil on foam stability and describe the complicated reaction between them. The studies of bulk foam indicate an apparent contradiction between the effect of crude oil on foam stability. Some researchers indicate that crude oil causes the foam to break and prevents the foam from accumulating with each other ([L. Zhang et al., 2019](#)). On the other hand, other researchers have demonstrated that stable foams can be formed in the presence of crude oil if a suitable foaming agent is used ([Osama Al, 2015](#)).

2.6.4 Properties of Foamability and Foam Stability

As an unstable thermodynamical system, the foam will break at last. Over time, the foam column undergoes irreversible evolution as the shrinks of lamella's interfacial area (decreasing interfacial free energy). The capacity of surfactants to create foam, regardless of the foam qualities, is known as foamability. Moreover, foam stability is considered one essential feature of foam description because it determines how well the foam withstands bubble collapse or coalescence ([Amani et al., 2021](#)). However, it is challenging to regulate because it is influenced by several factors, including the concentration and amount of foaming agent used and the method applied to prepare the foam. In order to quantify foam stability, it is necessary to determine its half-life, which can be determined by observing changes in the liquid content of foam as a function of time ([Osama Al, 2015](#)). Three mechanisms govern foam half-life: 1) Coarsening, which is caused by the diffusion of gas from adjacent

smaller bubbles to large bubbles); 2) Bubble coalescence, which is caused by rupture of the liquid film between adjacent bubbles; 3) Foam drainage, which is described by the liquid mainly flowing out of the foam through the plateau boundary and node under the action of gravity (L. Zhang et al., 2019). In the case of foam in the porous medium, the major mechanisms are summarized as 1) Capillary pressure; 2) Capillary suction; 3) Disjoining pressure, and 4) Interfacial elasticity (Petkova et al., 2021). The foam stability is also directly influenced by the chemical characteristics of the surfactants. A number of mechanisms are discussed in the following sub-sections.

2.6.4.1 Gravity drainage

Gravitational force is the most evident force operating on foam, causing the liquid to drain between the air bubbles. Increasing bulk liquid viscosity can facilitate drainage, defined as the irreversible flow of liquid through a foam film membrane via plateau borders (Jones et al., 2016). As the water drains by gravity, the top of the foam quickly turns dry, with only 1% liquid, while the bottom remains wet. Under the impact of drainage, the shape of the bubbles changes from slightly spherical to polyhedral (Figure 2.21) (Ataei et al., 2020). As a result of this draining mechanism, these foam bubbles become less stable and more prone to breaking.

The bubble size plays an important role too. Usually, the foam bubbles have diameters $> 10 \mu m$ and may be larger than $1000 \mu m$. For instance, when the foam is associated with smaller bubbles, the viscous dissipation is greater, and the drainage will be slower (Almobarky et al., 2018). Some foams will be the most stable if the bubble size distribution is substantially weighted toward the smaller sizes (Schramm, 1994). Gravity drainage is a recovery technique in which gas fills the void volume, and gravity is the primary driving force.

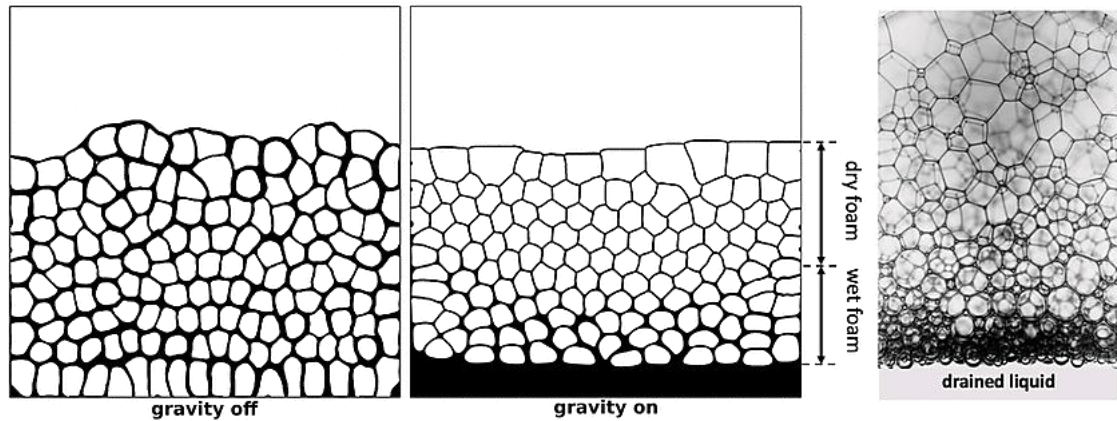


Figure 2.21: The influence of gravity on foam drainage ([Ataei et al., 2020](#))

2.6.4.2 Surface elasticity

It is a direct consequence of the surfactant adsorption at the contact, often referred to as the "self-healing" effect. The foam formation section states that the Gibbs-Marangoni effect is the mechanism underlying this occurrence. Generally, it can tolerate minor deformations without rupturing ([Schramm, 1994](#)). As illustrated in [Figure 2.22](#), when the lamellae are stretched and restored, the surface elasticity should exist so that the foaming, which requires the diffusion of the surface-active component from the bulk solution to the newly formed surface, can be sufficiently slow ([Ueno et al., 2016, p. 201](#)). Else, the surface adsorption will reduce surface tension, causing the temporary stretch of the foam lamella to become permanent, leading to weak lamellae. Stability is dependent on elasticity. As the surfactant concentration increases, the film's elasticity decreases, causing the foam to collapse quickly, resulting in poor stability ([Skauge et al., 2020](#)).

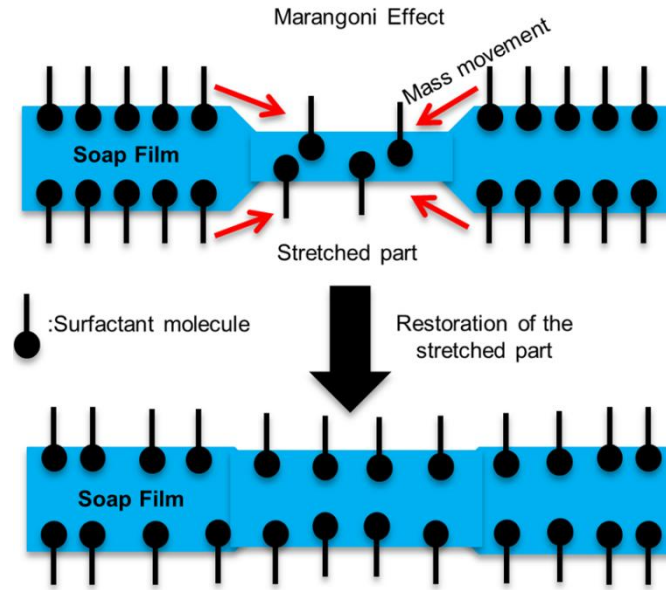


Figure 2.22: A diagram illustrating the Gibbs-Marangoni effect (Ueno et al., 2016, p. 201)

2.6.4.3 Laplace Capillary pressure

Laplace capillary pressure is the differential pressure between the inside and outside of a curved surface. The liquid will flow from the films to the plateau borders, causing the films to thin and lead to rupture and foam collapse (Beneventi et al., 2001).

The mechanism can be explained with the Yong-Laplace equation (Eq. 2.15). As the radius (R) of the curved surface increases, the pressure difference between the gas and liquid phases changes.

$$\Delta P = P_G - P_L = \frac{2Y}{R} \quad (\text{Eq. 2.15})$$

where P_G denotes gas pressure, psi; P_L denotes liquid pressure, psi; Y denotes surface tension, N/m. The quantity P_G and P_L is also referred to as the capillary pressure P_C , psi. The radius of curvature at the Plateau border, R (unit m), is less than the radius of curvature of the thin liquid film, but the gas pressure P_G in the bubble is the same.

2.6.4.4 Disjoining pressure

Under the influence of capillary pressure, the thin liquid film formed between bubbles is thinning. When the film thickness is reduced to 300-200nm, the capillary

pressure slows down the film drainage. Disjoining pressure, defined as the interaction between the film surfaces, affects film drainage ([Yaminsky et al., 2010](#)). Three components govern the disjoining pressure: van der Waals force, electrostatic force, and steric repulsion force. In particular, the attractive van der Waals forces contribute negatively to the disjoining pressure. And the electrostatic forces stabilize the foam film. When two equally charged interfaces approach each other, and their electric double layers overlap, repulsive forces are created, contributing to disjoining pressure ([Y. Sheng et al., 2022](#)). The steric forces are caused by each atom in a molecule occupying a specific amount of space; they are repulsive and only observed on a concise length scale. Molecule size can play a role in steric interaction. The disjoining pressure is only considered for thin films (i.e., 100 nm). The disjoining pressure is not expected to be significant for thicker films.

2.6.4.5 Foams stabilized by ions

Other chemicals (additives) added to the surfactant solution have improved foam surface properties, eventually strengthening the lamellae. Specific additives may synergize with the surfactant to increase the foam stability in numerous ways, such as improving lamellae elasticity, decreasing liquid phase drainage, and increasing surface viscosity. Polymers, particles, and electrolytes are just a few additives that can stabilize foam ([Mustan et al., 2022b](#)).

Salts are either naturally present or added to a variety of foam applications. The adsorption of surfactant molecules at the air-water interface can be influenced by salt, which changes the charge at the interface ([Amani et al., 2021](#)). As a result, the presence of salt has a significant impact on foam adsorption and stability. In addition, salts containing the same ions can exhibit significant differences in surfactant adsorption. With increasing salt concentration, the film thickness decreases smoothly. By investigating two surfactant concentrations (0.01wt% and 0.3wt%), [Farajzadeh et al. \(2008\)](#) discovered that the film was prepared with 0.01wt% surfactant was thicker than the film prepared with 0.3wt% surfactants. It is because surfactant is an electrolyte, and its concentration determines the ionic strength of the solution at low salt concentrations.

2.6.4.6 Surfactant concentration

Several researchers have revealed the effect of surfactant concentration on foam generation, stability, and bubble coalescence in the presence and absence of salts. Some reported that increasing surfactant concentration could increase foam stability, while others reported that increasing surfactant concentration could only increase foam stability until a specific concentration was reached ([Osama-Al, 2015](#)). Changes in surfactant concentration have a significant impact on foam generation ability. Surfactant concentrations in EOR foam are typically in the range of 0.1-1wt% (for economic reasons).

2.6.4.7 Crude oil presence

In EOR, the oil presence plays an essential role in foam applications. Numerous studies have been conducted on the effect of oil on foam stability. The parameters that most influence foam-oil interactions are the Entering (E), Spreading (S), and Bridging (B) coefficients, as well as the Lamella number (L) ([Lin et al., 2021](#)).

An oil droplet or a hydrophobic particle must first enter the gas-water interface after emerging from the aqueous phase to rupture a foam film. The entry coefficient determines whether it is thermodynamically advantageous for the oil droplet to enter the solution gas surface ([Hadian et al., 2020](#)). If the coefficient is negative, the oil droplet is prevented from entering the foam interface, and the surfactant solution thoroughly wets the oil drop.

In a second step after this entry, some oil from the droplet can spread on the solution-gas interface. A new gas-oil surface and water-oil interface are created when an oil drop spreads over the gas-water surface, and a spreading coefficient measures the change ([Simjoo et al., 2013](#)). Spreading oils has a negative impact on the stability of the foam. When the value is positive, the oil will spread along with the gas solution or remain at its position.

2.7 Conclusion

In order to sustain the high-consumption energy market, it is necessary to recover and mobilize more oil from the matured reservoir formation. Three technologies are applied for oil recovery: primary, secondary, and EOR. Unfortunately, the conventional recovery processes (primary and secondary) did not work all the time perfectly, especially on reservoir formations with complex geological properties and structures ([Muggeridge et al., 2014](#)). According to [Green et al. \(2018\)](#), only 33% of the original oil in place was produced through conventional methods, while the residual 77% can partially achieve by EOR. EOR has been a widely used method for more than sixty years in the oil industry. Substantial oil was trapped in the pore structure after primary and secondary recovery because of viscous and capillary forces. Compared with the conventional oil recovery technique, EOR can displace the oil left in the swept zone by improving wettability and lowering the interfacial tension between the injected liquid and residual oil. However, several limitations restrict the wide application of EOR, such as 1) Unstable performance due to the intricacy of reservoir condition, wettability variation, and formation mineralogy; 2) Serious environmental contamination caused by chemical additives; 3) Potential risk of pore throat blockage because of the large particle size; 4) Instability of high temperature, pressure, and salinity condition; 5) Expensive financial expense since lots of additives were adsorbed by the rock formation. Therefore, developing a new cheap hybrid solution is crucial to improve oil recovery with less environmental contamination amongst these limitations.

LSWI was first introduced in 1961 ([Reiter, 1961](#)). It has been confirmed by many researchers/fields that it can improve oil production by injecting low salinity water (1000ppm to 3000ppm) into the reservoir rock ([Saikia et al., 2018](#); [Ebrahim et al., 2019](#); [Katende & Sagala, 2019](#); [J. H. Lee & Lee, 2019](#); [Chávez-Miyauch et al., 2020](#); [Mofrad & Saeedi Dehaghani, 2020](#); [Shabani & Zivar, 2020](#)). With the mechanisms of fines migration, multicomponent ionic exchange, electrical double layer, and pH effect, LSW can decrease the residual oil concentration and improve the macroscopic sweep efficiency in the porous medium. However, it shows no

apparent improvement in wettability alteration and may trigger fines migration around the new wellbore region ([Al-Sarihi et al., 2018](#)).

Nanoparticle flooding is an advanced method that blends the nano-size particles (1-100nm) into the injection flood. These particles can easily penetrate the pore throat without blockage with the nanosized scale. Furthermore, the large surface area to volume ratio can increase the system stability by weakening the non-equilibrium behavior. The high surface energy enables nanoparticles to efficiently adsorb on the rock surface or bond with the polar acid/base oil droplet. With the multiple mechanisms, such as structure disjoining, entrapment, and nano-layer coating, significant oil recovery has been observed after nano-flooding. However, it also appears that nanoparticles are not very effective in changing the IFT; merely a 2% improvement has been found by [Bayat et al. \(2015\)](#). Therefore, it is necessary to introduce surfactants into this project. Numerous studies show that surfactants can enormously reduce the IFT between the oil-water interface, leading to a better wettability condition. Surfactant molecules comprise a hydrophilic head (polar) and a hydrophobic tail (nonpolar). The hydrophilic head has a strong attraction to water molecules. Instead, the hydrophobic tail has a strong affinity to the oil droplet. A small amount of surfactant can effectively improve the reservoir wettability and the overall sweep efficiency by decreasing the IFT. However, the drawbacks such as expensive, toxic, environmental pollution restrict synthetic surfactants' development.

In consequence, natural green surfactants have been proposed in this study. It has several advantages: cheap, environmentally friendly, non-toxic, and 100% biodegradable. Furthermore, it also can contribute similar performance in IFT reduction and wettability alteration to synthetic surfactants. Therefore, the newly introduced natural surfactants, Soapnut saponin, and *Camellia oleifera* saponin are appropriate for chemical EOR.

Chapter 3: Green Surfactant Extraction

3.1 Introduction

Most of the surfactants used in the industry are marked as chemical compounds. They generally have toxic ingredients and can increase the toxic load on the environment ([Ahmadi and Chen, 2020](#)). According to the United States Centers for Disease Control and Prevention (CDC), when the concentration of surfactant exceeds certain limits, the growth of algae and the rest of the microorganisms is disrupted ([CDC, 2018](#)). Significant underground contamination and negative environmental effects have also been reported, such as rising the toxic load of underground water and impacting microbial diversity ([Kaczerewska et al., 2020](#)).

In contrast to chemical surfactants, surfactants extracted from plants have attracted great attention ([Bachari et al., 2019](#); [Sar et al., 2019](#); [Saxena et al., 2019](#); [Guzmán et al., 2020](#)). Natural surfactants possess several remarkable properties, including 1) cost-effective; 2) environment-friendly; 3) biodegradable; 4) completely renewable; 5) non-toxic to humans and other living creatures; 6) providing similar performance as the chemical surfactants ([Ahmadi & Shadizadeh, 2018](#); [Moradi et al., 2019](#)). This project mainly focuses on extracting non-toxic green surfactants from the pericarp fruit (Soapnut) and *Camellia oleifera* seed ([Figure 3.1](#)). Soapnut is a fruit of the *Sapindus mukorossi*, widely distributed in tropical and sub-tropical continents, including Asia, Europe, the Middle East, and America ([Köse & Bayraktar, 2016](#)). *Sapindus mukorossi* is also called ritha tree. It is growing lushly in India, Pakistan, Malaysia, China, Iran, and many other countries. The fruit, Soapnut, is also commonly known as a soapberry. It is a brownish glaze-skinned dried nut with a diameter of 1 to 2 centimeters and can be divided into two parts (pericarp and seed) ([Samal et al., 2017](#); [Saxena et al., 2018](#)). It contains a fatty ester of tetracyclic triterpenoids and glycosides. Saponin is one of the secondary metabolites which can be primarily extracted from the pericarp of Soapnut ([Jassal et al., 2016](#)). Pericarps are typically used as traditional cleaning detergents for laundry, shower, and body treatment for centuries because of their foam-forming ability in water ([Muntaha & Khan, 2015](#)). *Camellia oleifera* is a tiny evergreen shrub or tree native to the

subtropics with excellent nutritional and therapeutic properties, widely distributed and cultivated extensively in Southeast Asia (including Malaysia, Thailand, and Vietnam) and China. It has been widely used as the primary source of *Camellia oleifera*-oil production since the seed of *camellia oleifera* contains high-quality cooking oil and its rare monounsaturated fatty acids.



Figure 3.1: Green surfactants. Top: *Camellia oleifera*; a) Fruit diameters around 4cm; b) Seed opening; c) Fruit structure; d) *Camellia oleifera*-oil extracted from seeds, Bottom: e) Soapnut fruit; f) Soapnut kernel; g) Soapnut pericarp ([Chen et al., 2015](#))

These species have large evergreen leaves with dark green color, measuring three to five inches long by two to three inches wide. This huge shrub or small tree blooms in late October with single, fragrant white flowers and grows to a height of 20 feet with slender, upright, numerous trunks and branches. The crown forms a rounded or oval vase when the lower limbs are removed. Its seeds resemble the

shape of a spherical moon and are produced between September to October. Several researchers have been identified 249 compounds from *Camellia oleifera*, including saponin (Chen et al., 2015). The chemical structure of saponin extracted from Soapnut and *Camellia Oleifera* are shown in Figure 3.2 and Figure 3.3.

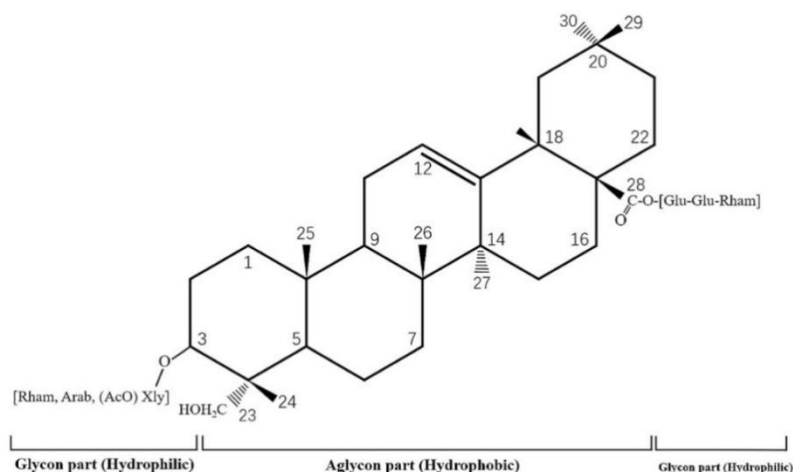


Figure 3.2: The chemical structure of saponin extracted from Soapnut (Gundewadi et al., 2018)

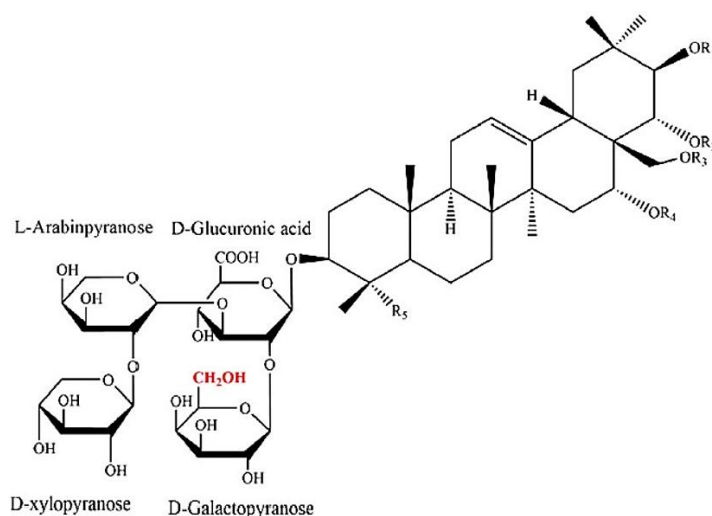


Figure 3.3: The chemical structure of saponin extracted from *Camellia Oleifera* (Fan et al., 2018; Zhang et al., 2021)

Meanwhile, three additional green surfactant plants have been tested: *Glycyrrhiza*, *Tribulus Terrestris*, and Mulberry leaf. The process for extracting saponin from natural plants can be summarised in four sections: 1) raw materials purchase and treatment; 2) extractions with four various techniques; 3) filtrate out

1000ml vacuum filter manufactured by Merck was used to filter the impurities from the green surfactant solution. Petronas Carigali Sdn Bhd - Miri Crude Oil Terminal (MCOT) provided the crude oil used in this section, the properties of crude oil are shown in [Table 3.1](#).

3.2.2 Chemical Additives

All solvents and chemicals used in the extraction process were analytical grades; methanol and ethanol were purchased from Merck, procured from commercial sources, and used without further treatment.

3.2.3 Plant Materials Pretreatment

As shown in [Figure 3.5](#) below, the fruit of *Sapindus mukorossi* (Soapnut), *Camellia oleifera* seed, *Glycyrrhiza*, *Tribulus Terrestris*, and Mulberry leaf was selected from the local variety and purchased from the native market.

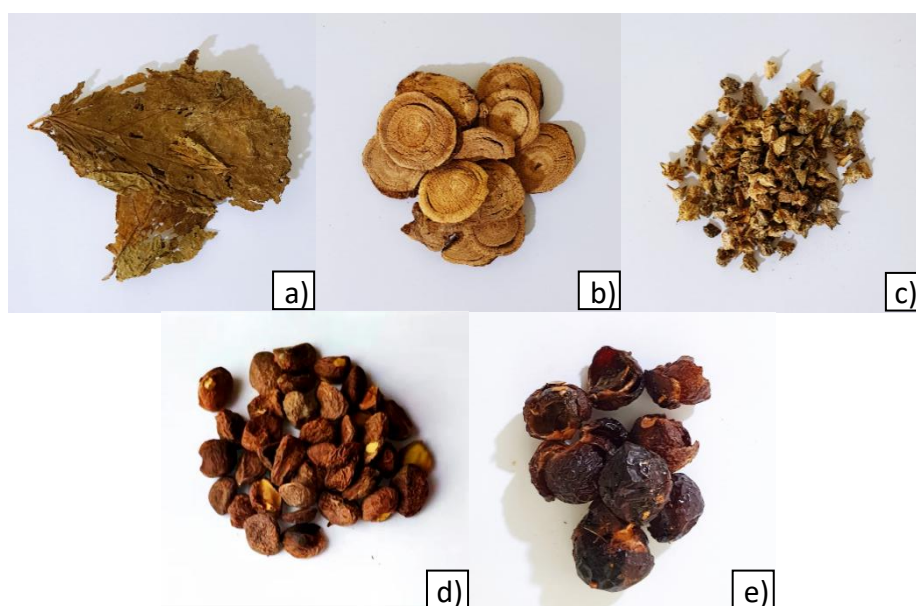


Figure 3.5: Potential green surfactant plants. a) Mulberry leaf, b) *Glycyrrhiza*, c) *Tribulus Terrestris*, d) *Camellia oleifera* seed, e) *Sapindus mukorossi* (Soapnut)
The pericarps of Soapnut were separated from the kernels with the assistance of a local vendor, and only the ripe pericarps were collected because they had the highest concentration of saponin components. The damaged parts were discarded,

while only the fruits have leathery shrunken skinned with dark brownish color were selected to ensure the high quality of raw materials. These selected pericarps of Soapnut, seeds of *Camellia oleifera*, *Glycyrrhiza*, *Tribulus Terrestris*, and Mulberry leaf were stored in a refrigerator at 2°C in vacuum containers for preservation before further treatments. A voucher specimen has been deposited in the Petroleum Laboratory, Curtin University Malaysia.

In order to eliminate the moisture from the plants, they were first washed and then placed in an oven with maximum hot air ventilation at 61°C for 96 hours. To maximize the mass transfer efficiency of extraction and enhance solvent penetration. With the grinder (Panasonic PSN-MXAC400), the natural plants (pericarps, seeds, or leaves) were ground into coarse powders separately from the plants. The oversized particles were removed using a succession of Merck mesh sieving of #20 (0.841mm), #40 (0.42mm), and #60 (0.25mm). Furthermore, oversized particles were collected and ground again with final sieving. After that, all crushed coarse powder was followed by uniform hand ground the coarse powders by mortar-pestle. Finally, the finalized saponin powders were stored in several 250ml airtight borosilicate glass reagent bottles with a screw closure. Meanwhile, the reagent bottle's body was covered with aluminum foil for light exposure prevention.

3.2.4 Green Surfactant Selection

It is critical to select suitable plants that contain practical green surfactants. Therefore, drop shape analyzing, also known as the pendant drop method, has been applied in this section. This method is precise enough to analyze the IFT between oil and liquid phases. Three grams of raw plant powder from the five plants (Soapnut pericarps, *Camellia oleifera* seeds, *Glycyrrhiza*, *Tribulus Terrestris*, and Mulberry leaf) were mixed with 100ml ultra-pure water, respectively. Then each solution was filtered by the vacuum filter with grade 4 filter paper (pore size of 20 to 25 μm). After that, each green surfactant solution was filled in the glass cuvette for the IFT test. A drop shape analyzer (DSA) 100B made by Kross GmbH was used to calculate the IFT, and the shape of the oil droplet was analyzed by its embedded software.

Fisher Scientific provided a 3ml syringe and a 0.5mm J-shaped stainless steel needle for oil injection. The test solutions were filled into the 5cm x 5cm x 5cm Glass-cuvette, and the syringe and J-Shaped needle were filled with oil, as indicated in Figure 3.6, during the IFT measurement.

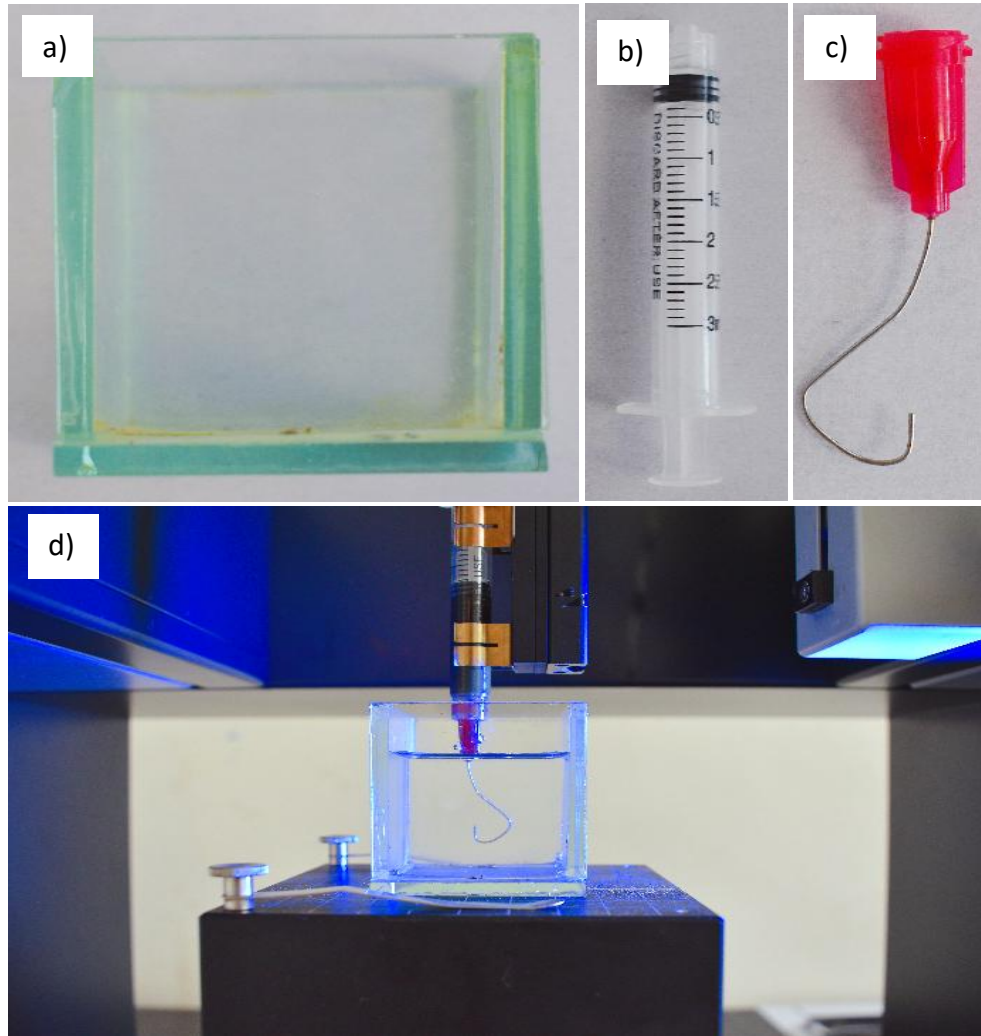


Figure 3.6: The equipment for the DSA test. A) glass box, b) oil injection syringe, c) J-shape needle, d) IFT measurement

Before each test, a dynamic IFT measurement was performed on pure water/oil interfaces to validate the absence of contaminants. Design solutions were introduced into the glass chamber during each IFT measurement. The pendant drop method was then used to generate an oil droplet from the tip of a needle at the solution-needle contact. The IFT for a specific time interval was then determined

using DSA 100B. The syringe (with a J-shape needle) was filled with crude oil, the composition, characteristics ratio, and properties of reservoir crude oil are shown in [Table 3.1](#).

Table 3.1: The composition, physical and chemical properties of crude oil ([Petronas Carigali Sdn Bhd MCOT, 2021](#))

	Unit	Miri Crude Oil
Density at 15°C	kg/L	0.842
American petroleum institute (API)	API degree	36.5
Carbon preference index (CPI)	-	1.10
Total acid number (TAN)	mg KOH/g	2.52
Barrel factor	BBL/T	7.483
Pour point	°C	-6
Viscosity at 20°C	Pa.s	4.08
Viscosity at 40 °C	Pa.s	2.51
Reid vapor pressure	Kpa	20
Saturation hydrocarbons	% w/w	65.5
Aromatic hydrocarbons	% w/w	18.4
Nitrogen, sulphur and oxygen (NSO)	% w/w	16.1
Asphaltenes	% w/w	0.11
Resins	% w/w	29.81
Pristane/phytane	-	3.9
Pristane/nC ₁₇	-	1.2
Pristane/nC ₁₈	-	0.3

The IFT results are summarized in [Table 3.2](#). It can be observed that the Glycyrrhiza, Tribulus Terrestris, and Mulberry leaf only slightly affect IFT (reduce around 2.6-2.9 mN/m). In contrast, Soapnut and Camellia oleifera significantly decrease the IFT between the water and oil interface (11.65 and 12.77, respectively). Therefore, it is decided to use those two natural plants as the source of natural surfactants.

Table 3.2: Fundamental IFT results of green surfactant plants selection

Natural Surfactant Plants	Amount of Plants Powder (gram)	Solvent Volume (ml)	Reference IFT, pure-water (mN/m)	IFT (mN/m)
Soapnut	3	100	17.8	6.15
Camellia oleifera	3	100	17.8	5.03
Glycyrrhiza	3	100	17.8	14.9
Tribulus Terrestris	3	100	17.8	15.8
Mulberry leaf	3	100	17.8	15.2

3.2.5 Saponin Extraction

Extraction is the most crucial step to obtain the targeted substance from specific raw materials. In order to deliver a successful extraction process with high efficiency, it is necessary to take into account the raw materials particle size, the extraction cost, the solids-to-liquids ratio, the duration extraction effect, and the extraction temperature (Jassal et al., 2016; Köse & Bayraktar, 2016). According to earlier research, saponin would precipitate in saline water, and as a result, ultrapure water was applied as the extraction solvent. Furthermore, saponin extracted from Soapnut and Camellia oleifera is a thermolabile component, meaning that it changes, decomposes, or is destroyed when exposed to high temperatures (Muntaha & Khan, 2015). Therefore, the extraction process was done through several stages to achieve extraction efficiency and preserve the green surfactants.

It all starts with the maceration, shown in Figure 3.7a. This procedure for extracting the thermolabile chemical is straightforward, but it has a low extraction efficiency and requires a lengthy extraction period. Three kinds of solvents were prepared. The first was pure water in order to get the lowest extraction cost, and the second was a 1:1 blend of ethanol and ultrapure water to produce the highest extraction yield. The third one was made entirely of ethanol. A total of ten grams of the Soapnut and Camellia oleifera powders were poured into six glass beakers respectively. The beakers labelled with No.1, No.2 and No.3 were filled with Soapnut powder, while No.4 to No.6 were filled with Camellia oleifera powder. For No.1 and No.4, the solvents used were 100ml of ultra-pure water (solid/liquid ratio follow 1:10) while for No.2 and No.5, the solvents were changed to 100ml of

ethanol-water mixture. For No.3 and No.6, 100ml of pure ethanol was mixed with both Soapnut and *Camellia oleifera* powders. All the beakers were covered by the aluminum foil and sealed tightly by parafilm to avoid light. The solutions were cured at 30°C for 36 hours (Figure 3.5a). During the curing period, a magnetic stirrer was used to stir the mixture at 600rpm constantly.

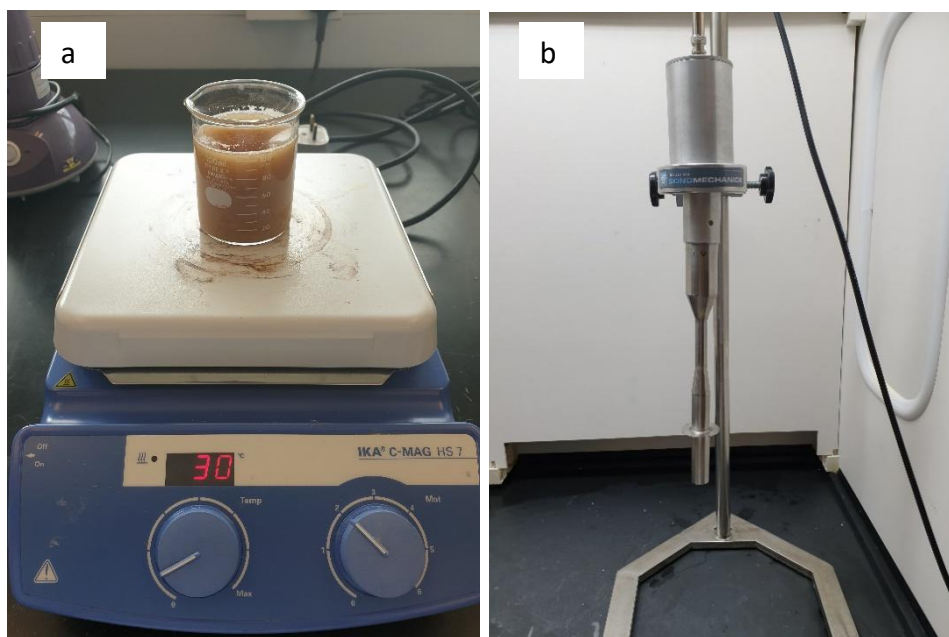


Figure 3.7: Extraction process. a) Maceration process of Soapnut powder and b) Ultrasonic homogenizer

After that, the solutions were transferred to the sealed stainless-steel beakers, where they were subjected to an ultrasonic-assisted extraction (UAE) procedure for 2hr. UAE is a cutting-edge green technology with a high extraction efficiency while requiring a small amount of solvent. Saponin can be dissolved and diffused into a solvent as a result of the mechanical effects of acoustic cavitation caused by the ultrasonic wave ([Azwanida, 2015](#)). [Figure 3.7b](#) was accomplished using an ultrasonic homogenizer with a digital control system, which operated at a frequency of 20kHz and with a constant power of 250 watts. In order to minimize overheating and irreparable damage to the saponin solution, the ultrasonic homogenizer was set to 50% amplitude and run for 7s with a 2s interval. The sealed stainless steel beakers were positioned centrally in the ultrasonic bath, containing a

3L water depth of 8cm. After 2hr of sonication, the solutions cooled down to room temperature for further process.

Following that, all saponin solutions were subjected to 6 minutes of microwave irradiation at a power grade of 20% to prevent overheating. Microwave-assisted extraction (MAE) is another environmentally friendly extraction technology developed for this project to increase extraction yield while reducing solvent consumption ([Guru et al., 2020](#)). The rapid heating caused by the microwave's radiation interacts with the polar substance through mechanisms such as molecule rotation and ionic conduction (water or organic solute). It contributes to the disruption of membrane-bound organelles, hence speeding up the extraction process ([Schmitt et al., 2014](#)). The microwave used in this project has a frequency of 2.45 GHz and a maximum installed power of 500W, which were both appropriate for the application.

These solutions were transferred to the percolators one at a time after being brought back to room temperature. During the percolation, the soluble constituents are completely replaced by a new solvent, drop by drop, as a batch process, rather than a continuous process. Firstly, a grade 4 filter paper with a pore size of 20 to 25 microns was placed on the bottom of the percolator before gently placing the moistened Soapnut/Camellia oleifera powder on top of it. Then, another filter paper was placed on top of the powder. The sample was kept in the percolator up to 36hr before collecting the leachate (consists of high concentration of active chemicals) at a slow pace. An additional 50ml of solvent was added to the percolator for 24hr. Once the percolation has ended, a pressing was undertaken to recuperate the residual liquid, which was then added to the leachate. -

3.2.6 Isolation, Purification, and Dehydration of Saponin

After several extraction processes (maceration, ultrasonic-assisted extraction, microwave-assisted extraction, and percolation), all solutions were gone through isolation and purification. Each solution was placed into four 50ml centrifuge tubes and spun at 4000rpm for 20 minutes at 2°C using a Hettich Universal 320R Benchtop centrifuge. The surfactant solution was collected from the supernatant fluids, and

the contaminants that had accumulated at the bottom of the tube were discarded. Following that, the collected supernatant fluids were put back into a centrifuge tube and centrifuged again at the same settings. It was necessary to repeat this procedure five times until all contaminants were removed, as depicted in [Figure 3.8](#) (Chemat et al., 2019).

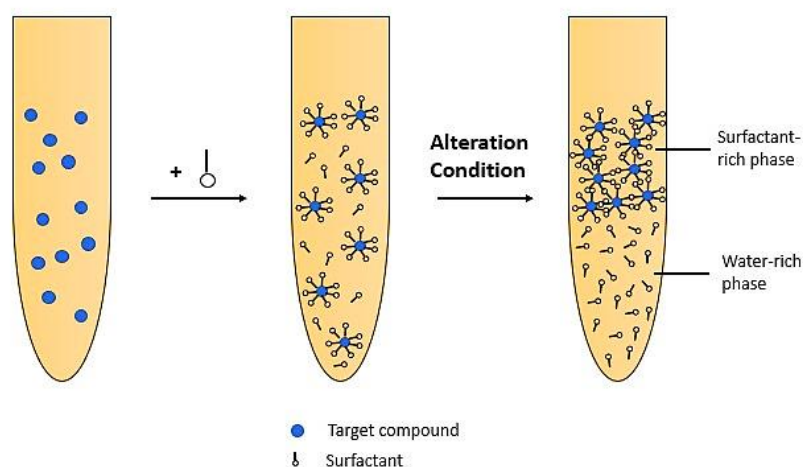


Figure 3.8: Diagram of the surfactant separation technique (modified from [Chemat et al., 2019](#))

Following that, vacuum filtration was used to filter the solutions. The Buchner funnel was lined with two layers of Grade 1 filter papers, and the mixture of solid and fluid was poured through the filter paper into the vacuum flask. The vacuum pressure was set to low in the case of a filter paper burst. It was necessary to repeat this procedure three times for each sample until no solid particles were left on the filter papers. Finally, clear light brownish solutions containing a high concentration of saponin components were obtained. The isolation, purification, and dehydration of the saponin process are summarized in [Figure 3.9](#).

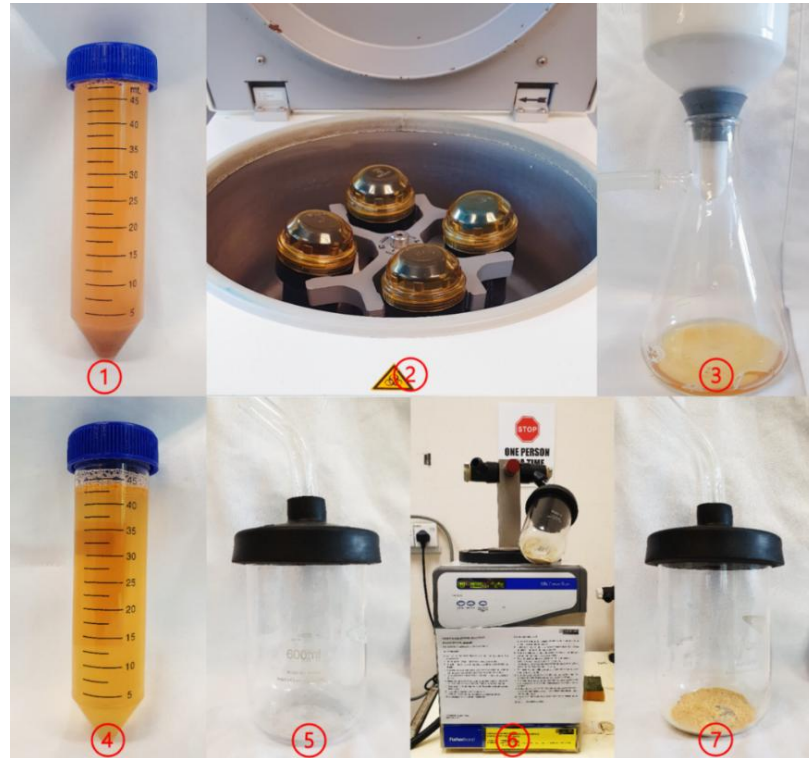


Figure 3.9: Purification and dehydration of Saponin. 1) Saponin solution; 2) Centrifuge tube assembling; 3) Centrifuge under 4000rpm for 20 minutes; 4) The filtered Saponin solution; 5) 600ml Freeze-dryer beaker; 6) Freeze-drying process; 7) Extracted Saponin powder

Meanwhile, these final solutions were stored in three glass beakers individually at 20°C, which were covered by aluminum foil for light-avoiding and sealed tightly by parafilm. The freeze-drying process was adopted for dehydrating saponins (Köse and Bayraktar, 2016; Smutek et al., 2016). It is a process for removing water at low temperatures that utilize material freezing, pressure decrease, and heating to desorb the water molecule. Before putting these solutions into the freeze dryer, the samples were transferred from the glass beakers to three 200ml wide mouths round ultimate plastic bottles. For the next 48 hours, they were placed in the laboratory's ultra-low temperature freezer at -80°C. Following that, each sample was immediately transported to a freeze drier for 96-hour drying phase, during which all of the water molecules in the saponin solution were sublimated. In order to facilitate subsequent testing, the final extract saponin

powders were placed into three 250ml airtight borosilicate glass reagent bottles with a screw lid and stored at 2°C for further analysis.

3.3 Results and Discussion

The final extracted saponins were summarized as 1) brownish powder for the pure water, 2) light yellowish powder for the ethanol-water mixture, 3) brightly yellowish powder for pure ethanol. The weight of each powder was recorded by MS-TS precision balance for further analysis. The equation used to calculate the extraction yield is expressed by Eq. 3.1 (Saxena et al., 2019).

$$\text{Extraction yield, (wt\%)} = \frac{\text{amount of total extracted, g}}{\text{amount of feedstock, g}} \times 100\% \quad (\text{Eq. 3.1})$$

Differences in the yield percentage of saponin extraction could be due to various solvents used. However, the yield percentage, the cost of extraction, the complexity of the extraction process, production safety, and environmental sustainability all played a role in determining the optimal solvent system for the extraction. Saponins generated from Soapnut pericarps and *Camellia oleifera* seeds were easily dissolved in water. After soaking, more water molecules can penetrate the Soapnut/*Camellia oleifera* tissue matrix, releasing (leaching) more saponins from it. Thus, a longer soaking period enables more self-contained sugar to dissolve, which enhances the permeability of the Soapnut/*Camellia oleifera* cell membranes and further accelerates the process of saponin diffusion from the tissue matrix into water. As a result, insufficient soaking time can induce the yield percentage with the same solid-liquid ratio and solvent system.

According to Table 3.3 shown below, the extraction yield percentage with different solvent systems was between 76wt% to 84wt%. All the extraction solvents went through the same extraction conditions, including 1) the maceration at room temperature for 36 hours with 600 rpm stirring; 2) ultrasonic-assisted extraction at 50% amplitude for 2 hours; 3) microwave-assisted extraction at 20% powder grade for 6 minutes; 4) the percolation at room temperature for 60 hours; 5) and the same solid to liquid ratio of 1:10. Thus, the combination of ethanol and water would be the best choice for the extraction process. However, using an ethanol-water mixture would not be practical since ethanol is expensive, not environmentally

friendly (as compared to water), extremely inflammable, and requires extra effort for preparation. In contrast, the water provided an extract yield about 3wt% lesser than the ethanol-water mixture. Consequently, water is recommended as the solvent for the experiments that will take place in the following stages of this research.

Table 3.3: Summary of yield percentages of the different solvent system

Solvent System	Solid/Liquid Ratio (g/ml)	Yield Percentage Soapnut (wt%)	Yield Percentage <i>Camellia oleifera</i> (wt%)
Ultra-pure water	1:10	81	79
Ethanol-water mixture 50% v/v	1:10	84	81
Pure ethanol	1:10	78	76

3.4 Conclusions

This chapter selected Soapnut pericarps, *Camellia oleifera* seeds, Glycyrrhiza, *Tribulus Terrestris*, and Mulberry leaf as potential natural surfactant plants and went through the IFT test. Soapnut and *Camellia oleifera* has been chosen as the source of natural surfactants provider since both can reduce the IFT between water and oil interface as high as 72%. A serious natural surfactant extraction technique follows to extract the saponin from its tissue matrix with maximum extraction efficiency, which includes: maceration, ultrasonication, microwave-assisted, percolation, isolation and purification, and dehydration (freeze-drying).

In order to determine the optimum extraction solvent, three different solvent systems were applied to the extraction process, including ultra-pure water, ethanol-water mixture, and pure ethanol. It was found that the mixture of ethanol and water delivers the best result (84wt% for Soapnut and 81wt% for *Camellia oleifera*), followed by pure water (81wt% for Soapnut and 79wt% for *Camellia oleifera*) and pure ethanol (78wt% for Soapnut and 76wt% for *Camellia oleifera*). However, the high purchasing price, toxicity, inflammability, and redundant mixture requirements make ethanol-water mixture less favorable, even though it presents the highest yield percentage. Instead, water is extremely cheap, safe,

environmentally friendly, and accessible, and it only delivers around 3wt% less than the ethanol-water mixture. Therefore, pure water has been chosen and recommended as the solvent system for the subsequent experiments in this project.

Chapter 4: Saponin Characterization

4.1 Introduction

Due to the lack of study on the new green surfactants that can be applied to enhance oil recovery, it is important to identify the morphology and particle size distributions of saponin particles by scanning electron microscope (SEM) and physicochemical properties through a series of experiments, such as density, pH, conductivity, solubility, critical micelle concentration (CMC), particle size and zeta potential. Ultraviolet-visible spectroscopy (UV-Vis) and Fourier-transform infrared spectroscopy (FTIR) tests are crucial since natural surfactants are extracted from plants. Furthermore, the effectiveness/survivability of extract surfactant (Saponin) must also be tested under a high-temperature environment. At last, to assess the thermal stability of the material as well as the amount of weight loss during combustion, the extracted surfactants were gone through the thermogravimetric analysis (TGA).

4.2 Methodology

4.2.1 Experimental Apparatus

The pH meter manifested by Mettler Toledo was used to measure the pH of the Soapnut saponin and Camellia oleifera Saponin with various mixture ratios. Sartorius Quintix 412-1S digital scale was adopted to weigh the saponin extracts. Vacuum filtration set (Buchner flask and funnel) with grade 4 filter papers (25 μ m particle retention) were applied to separate the impurity from the solution and improve the accuracy of the results. The Zetasizer Nano ZS, manufactured by Malvern Panalytical, determined the extracted Saponin's particle size and zeta potential. An electrical conductivity meter was applied to measure the electrical conductivity and total dissolved solids (TDS) of the saponin surfactant solutions. Ultrapure water with the resistivity of 5.4 M Ω .cm supplied by the Elga water purification system was used for the solvent of saponin solution. IKA® C-MAG HS7 digital stirring hot plates were used to heat the solution and stir the mixture. A Laboratory thermometer was applied to measure the temperature of the saponin

surfactant solutions. The dynamic light scattering method employed Malvern Zetasizer Nano ZS to measure the surfactant's zeta potential and particle size. The Quattro-S ESEM by ThermoFisher Scientific with dual 180-degree energy-dispersive X-ray spectroscopy (EDS) and wavelength dispersive X-ray spectroscopy (WDS) to study the morphology and particle size distribution of saponin particles of Soapnut and *Camellia oleifera*. Lambda 25 UV-Vis Spectrometer manufactured by Perkin Elmer was used to confirm the presence of dissolved Saponin inside the solution. Agilent Cary 630 FTIR was introduced to identify and characterize the extracted saponins and the different functional groups. Syringe filters (4mm diameter and 0.2µm pore size) made by Merck were used to remove the impurities in the test solution. 3,500 µL Quartz cuvette manufactured by Mettler Toledo was used to retain the test solution during the UV-Vis experiment.

4.2.2 Experimental Materials

Ultra-pure water was used as the solvent and base fluid to dissolve saponin surfactants in all experiments, which had a density of 0.9970 g/ml, pH of 6.70, resistivity of 18.18 MΩ.cm and viscosity of $8.90 \times 10^{-4} \text{ kg} \cdot \text{m} \cdot \text{s}^{-1}$ at 25°C. Ultra-pure water was also used as the reference in the measurements of pH and conductivity of the surfactant solution with various concentrations. A sodium hydroxide (NaOH) pellet was used to increase the saponin surfactant solution's pH to test the Saponin's effectivity (survival condition) under the alkaline environment. It possessed a reagent-grade requirement (98% purity) and was produced by Merck Millipore. Moreover, hydrochloric acid (HCl) was applied to reduce the saponin surfactant solution's pH to verify the Saponin's effectivity (survival condition) under the acidic environment. It has 37% purity and is made by Merck Millipore. Methanol and ethanol fulfilled the analytical grade and were applied to the operation of Zetasizer Nano ZS. Extracted Soapnut saponin powder and *Camellia oleifera* saponin (also named *Camellia oleifera* saponin) powder was used to test several physical/chemical characteristics.

4.2.3 Preparation of Surfactant Solutions

All the surfactant solutions were prepared by dissolving the saponin extract into the ultra-pure water and mixed based on the ratio given in [Table 4.1](#). For example, preparing 1wt% of saponin surfactant solution requires 1g of saponin extract mixed with 100ml of ultra-pure water. Sartorius Quintix 412-1S digital scale was adopted to weigh the right amount of ultra-pure water into the glass beaker. At the same time, a more precise balance, Mettler Toledo's analytical balance, was applied to measure the weight of saponin extracts. Because of the tendency of saponin molecules to agglomerate or cluster, all of the produced solutions were well mixed before being tested. Surfactant solutions were homogenized by an ultrasonic homogenizer for 60 seconds at 20% amplitude with a specified circulation rate (running 7 seconds and pulse 2 seconds) in order to achieve a steady and uniform dispersion of surfactant solution, followed by transferring to a water bath device (4 hours) and mixed by a magnetic stirrer at 40°C (4 hours). The mixture process was carried out at ambient temperature.

Because of the natural tendency for self-agglomeration, low saponin concentration was adopted in this research to achieve optimum recovery efficiency with uniform particle dispersal. With an increased concentration in saponin surfactant, the downsides such as agglomeration and clustering also increase, eventually weakening the green saponin surfactant solution's performance during EOR operation. Such downsides can induce the reduction of formation permeability and pore throat blockage, then further trigger the formation damage. Furthermore, the cost of surfactants is another critical factor brought to the forefront, both in terms of environmentally and economically feasibility. It is essential to deliver the optimum performance with minimum surfactant consumption during the EOR process, especially on a large oil field. Therefore, a small concentration of green surfactants was used in this study.

Table 4.1: Mixture ratio of different green surfactant solutions

Weight Percentage (wt%)	Amount of saponin extract (g)	Amount of ultra-pure water (ml)
1	1	100
2	2	100
3	3	100
4	4	100
5	5	100
6	6	100
7	7	100
8	8	100
9	9	100

4.2.4 Density, pH, and Conductivity Determination

A pycnometer measured the density and weight of the saponin solutions. All the measurements were obtained using the equation below:

$$\rho = \frac{w_{filled} - w_{empty}}{V} \quad (\text{Eq. 4.1})$$

where ρ is the density of the solution, g/cm³; w_{filled} is the weight after pycnometer filled by solution, g; w_{empty} is the weight of the empty pycnometer, g; V is the volume of the pycnometer, cm³.

The accurate pH values of the saponin mixtures with various concentrations were determined by the Mettler Toledo pH meter at room temperature. The measurements were repeated three times for consistency purposes.

Conductivity is related to the ion concentration of the solution, and it is proportional to the electric current that is transmitted through these free moved ion electrodes (Bai et al., 2013). A conductivity meter is the most used device in the laboratory that measures the quantity of electrical current or conductance of the solution. High conductivity solution is generated by the material containing high molar conductivity ions that are fully dissociated (Kronberg et al., 2014). On the contrary, a low conductivity solution is linked to the material containing low molar conductivity ions that were partially dissociated (Tadros, 2015). The molar conductivity of ions is presented in Table 4.2. The results of the conductivity were calculated using the following equations:

$$R = \frac{V}{I} \quad (\text{Eq. 4.2})$$

$$G = \frac{1}{R} \quad (\text{Eq. 4.3})$$

where R is the resistance of the solution, Ω ; V is the voltage, V; and I refers to the current, A; while G is the conductivity of the solution, $\mu\text{S}/\text{cm}$.

Table 4.2: Molar conductivity of common anions and cations

Types	Ion	Molar Conductivity ($\text{S L mol}^{-1}\text{cm}^{-1}$)
Anions	OH^-	0.1986
	Cl^-	0.0764
	CH_3COO^-	0.0409
Cations	H^+	0.3498
	Na^+	0.0501
	K^+	0.0735

4.2.5 Critical Micelle Concentration (CMC)

CMC is considered an important characteristic of a surfactant. It is defined as the concentration boundary of surfactant that the solution surface is saturated with surfactant molecules, and the additional surfactant will induce micelles to form (Nesměrák & Němcová, 2006; Y. Yang et al., 2013). Based on environmental perspectives and economic feasibility, injecting extra surfactants into the solution above the CMC point is regarded as waste since these additional surfactants will no longer effectively benefit from reducing the surface tension (Tadros, 2015; Saxena et al., 2019). The CMC determination was obtained using conductometry, the most common electrochemical method in this study. Due to the characteristics of surfactant monomers, when the concentration of surfactant reaches the CMC point, the aggregated micelles will reveal an apparent change on the conductivity meter (Nowrouzi et al., 2020). This agglomeration can be identified by analyzing different conductivity values against the saponin concentration, where changes from the straight lines can be identified as the CMC (Saxena et al., 2018). The CMC point of

Soapnut saponin and *Camellia oleifera* saponin were identified using the multi-range Mettler Toledo Seven Multi™ conductivity/pH combo meter.

4.2.6 Temperature

In order to verify the effectiveness/survivability of the saponin surfactant under the harsh environment of the reservoir saponin mixtures with various concentrations were tested by the conductivity meter on different temperature scales ([Saad et al., 2015](#)). As mentioned in section 4.2.4, the saponin solution could transmit electrical current and reveal apparent changes on the conductivity meter by different concentrations. Therefore, the conductivity value was chosen as a reference for the survivability/effectiveness test of the saponin extract. Eighteen portions (9 Soapnut saponin and 9 *Camellia oleifera* saponin) of the saponin surfactant were mixed with ultra-pure water based on their relevant weight percentage (1wt% to 9wt%). Then they were transferred in eighteen 250ml glass beakers. The mixing procedure described in section 4.2.3 was used, and each saponin mixture was then placed in the IKA® C-MAG HS7 digital hot plates for the heat process. At the same time, the laboratory thermometer was placed in the solution for temperature monitoring. Meanwhile, the magnetic stirrer continuously stirred the mixture at 200 rpm to avoid agglomerate/cluster. The conductivity test was conducted at the temperature of 25°C, 40°C, 50°C, 60°C, 70°C, 80°C and 100°C. Each measurement was repeated three times.

4.2.7 Particle Size Distribution

It was necessary to measure the saponin extracts' particle size distribution (PSD) to understand their physical properties better and forecast the synergistic influence of other additives (nanoparticles and salts) on their properties. This method can also be used to determine the stability of a suspension by examining the size and distribution of the particles in the solution ([Saxena et al., 2018](#)). The saponin particle size was determined using the Zetasizer Nano ZS, which Malvern Panalytical manufactured. Dynamic light scattering (DLS) is the approach that Zetasizer employed to determine particle size and evaluate the specific distribution of the

particles (Gundewadi et al., 2018). This technique was developed on the basis of the interaction between the electrical field and the light emitted by a particle/molecule. It determines the diffusion velocity of Brownian particles. The diameter and size distribution of the average hydrodynamic particle are determined using the Stokes-Einstein equation, denoted by Eq (4.4) (Tadros, 2015).

$$d_H = \frac{kT}{3\pi\mu D} \quad (\text{Eq. 4.4})$$

where d_H is the hydrodynamic diameter, nm; k is the Boltzmann's constant, J/K; T is the temperature, Celsius; μ refers to the viscosity of the solution, $\text{N.m}^2\text{s}^{-1}$; D is the translational diffusion coefficient, m^2s^{-1} .

0.5 grams of saponin extract was mixed with 100ml ultra-pure water and homogenized for 60 seconds at 20% amplitude with a predetermined circulation (7 seconds running and 2 seconds pulse) using an ultrasonic homogenizer. Ultrasonication was utilized because it provides the following benefits: 1) a homogenized and stable saponin solution, 2) the removal of air bubbles, and 3) the breaking up of any potential agglomerates. Following ultrasonication, the solution was diluted with 30ml ultra-pure water and filtered using a $0.2\mu\text{m}$ syringe filter. All the solutions were evaluated immediately after the preparation to avoid contamination and self-agglomeration.

4.2.8 Zeta Potential

The zeta potential is a fundamental feature of particles' electrokinetic potential that is defined by the amount of their electrostatic or electric charge of attraction/repulsion (Saxena et al., 2019). It can provide precise information on the factors that contribute to clustering, agglomeration, and dispersion and can be used to enhance the stability of EOR systems. The zeta potential of saponin extract was determined in this experiment using the Malvern Panalytical Zetasizer Nano ZS, which operates on the basis of Henry's equation, as discussed below.

$$U_E = \frac{2\varepsilon\zeta}{3\eta} f(\kappa a) \quad (\text{Eq. 4.5})$$

where U_E is the electrophoretic mobility, $\mu\text{m.cm/V.s}$; ε is the dielectric constant, F/m; ζ is the zeta potential, mV; η is the viscosity, $\text{N.m}^2\text{s}^{-1}$; $f(\kappa a)$ is the Henry's function, k.

For the zeta potential measurement, 0.2 gram of saponin extract was combined with 100ml of ultra-pure water and ultrasonicated for 60 seconds at 20% amplitude with a predetermined circulation (7 seconds running and 2 seconds pulse). Then, the solution was filtered through a $0.2\mu\text{m}$ syringe filter and injected into a zeta cell. The injected solution moves towards the electrode with the external electric field opposite the saponin extract particles. The pH of the mixture was in the range of 4.45 to 4.62 (natural pH of Saponin). All the solutions were evaluated immediately after the preparation to avoid contamination and self-agglomeration. Each measurement was performed three times to ensure uniformity.

4.2.9 Thermogravimetric Analysis

Thermogravimetric analysis (TGA) is the approach that can quantify the peak of decomposition and degradation temperature of the surfactant as well as provide the moisture content (water loss), thermal stability, and the amount of weight loss under combustion ([Mathiarasi et al., 2017](#); [Nowrouzi et al., 2020](#)). TGA can be used to determine the peak of decomposition and degradation temperature of a surfactant and the moisture content (water loss), thermal stability, and amount of weight loss under combustion conditions ([Nowrouzi et al., 2020](#)). This work quantified the green surfactants (saponins) extracted from Soapnut and Camellia oleifera using a PerkinElmer thermogravimetric analysis STA 6000 instrument. There were weights assigned to each sample, and the temperature program was configured for a temperature range of 100°C to 900°C with a temperature scanning rate of 50°C/minute . The measurements were carried out with nitrogen as the balancing gas, which was injected at a rate of 30ml/min .

4.2.10 SEM Analysis

SEM is an electron microscope that generates images of the test sample by scanning the surface with a focussed stream of electrons. When electrons contact atoms in a

sample, they produce a variety of signals that reveal information such as surface morphology and particle size interaction about the sample's surface. The high-intensity electron beam of electrons was fired and scanned at a specific small area of the sample's surface with a zig-zag type pattern (raster scan pattern), and the image was created by combining the beam's position with the strength of the detected signal. At very high magnifications, levels of detail lower than 0.5 nm resolution can be achieved because electrons scan the sample. This chapter scanned Soapnut saponin extracted powder and Camellia oleifera saponin extracted powder by a low-vacuum SE detector (LVD) of SEM. The magnification level starts from 300 to 5000x. Both saponin extracts did not go through the coating process since they are electrical conductivity and may destroy the surface information about a failure mechanism. The electron beam accelerating voltage was set between 7.50 kV to 10.00 kV (HV condition). The spot size setting was in the range between 2.0 and 3.0.

4.2.11 UV-Vis Analysis

UV is a method of measuring how much light is absorbed and dispersed by a sample, which means it uses visible and neighboring light. The color of the substances involved is directly affected by their absorption or reflectance in the visual spectrum. Molecules with bonding and non-bonding electrons can absorb ultraviolet or visible light to excite these electrons to higher anti-bonding molecular orbitals. The longer the wavelength of light it can absorb depends on how quickly the electrons can be excited. This chapter targeted UV-Vis to identify Saponin's presence in Soapnut saponin extract and Camellia oleifera saponin extract ([J. Zhang & Qu, 2013](#)). The UV-Vis spectra were tested at 25°C in absorption mode within the wavelength range between 190 to 700 nm. The reference solution was ultra-pure water.

The operational process can be summarized as 1) the test solution is placed between the photodetector and the light source; 2) then the intensity of a light beam is determined both before and after it passes through a sample. The wavelength-dependent extinction spectrum of the sample is quantified by comparing these observations at each wavelength. Typically, the data is shown as

extinction versus wavelength. During the test solution preparation period, 10mg of Soapnut saponin and Camellia oleifera saponin were mixed with 100ml ultra pure water in a 250ml plastic beaker. The solutions were sent to an orbital shaker manufactured by Lab Companion SKF-2075 for 48 hours at room temperature to maximize the solubilization of Saponin in ultra-pure water. After that, the solutions were centrifuged at 4000 rpm for 30 minutes to separate the undissolved Saponin or impurities from the solution. Then, each solution was filtered by a 0.2 μ m syringe filter then injected into a 3,500 μ L quartz cuvette for the UV-Vis test. (Adiukwu et al., 2017). Then, each solution was filtered by a 0.2 μ m syringe filter then injected into a 3,500 μ L quartz cuvette for the UV-Vis test. All experiment apparatus was thoroughly cleaned, and all the test solutions were freshly made to deliver high accuracy results.

4.2.12 FTIR Analysis

FTIR analyses organic and inorganic substances quantitatively and qualitatively. FTIR reveals chemical bonds inside a molecule by generating an infrared absorption spectrum. The spectra generate a profile of the sample, a unique molecular fingerprint that can be used to screen and scan for a wide variety of components (Almutairi & Ali, 2015). The FTIR is an efficient analytical technique for detecting functional groups and analyzing covalent bonding information. The FTIR spectrum of the Soapnut saponin extract and Camellia oleifera saponin extract was tested, and the preparation process was similar to section 4.2.11. The analysis conditions were set at eight scans, with a resolution of 4cm⁻¹ measured between 650-4000cm⁻¹.

4.3 Result and Discussion

4.3.1 Density

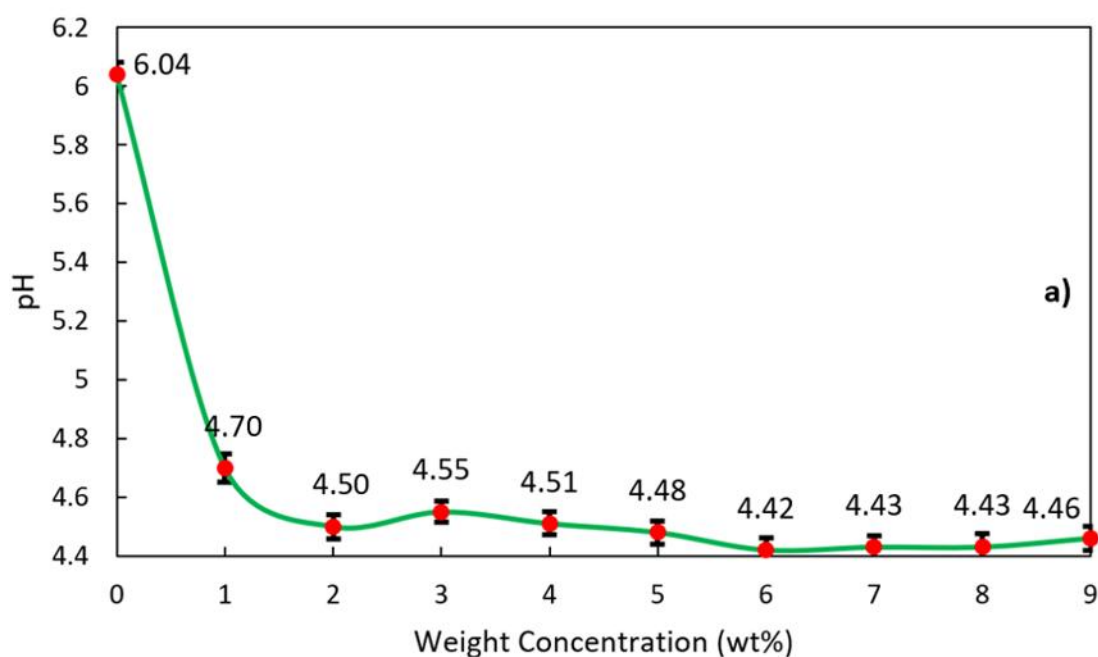
Table 4.3 shows the densities for both saponin solutions. The impact of density is considered insignificant.

Table 4.3: Densities of the Soapnut saponin and Camellia oleifera saponin solutions

Fluid	Liquid W(g)	Pycnometer volume V(cm ³)	Density ρ (g/cm ³)
Ultra-pure water Reference	24.99	25.00	0.99976
Soapnut Saponin solution 1	22.46	25.00	0.89840
Soapnut Saponin solution 2	22.51	25.00	0.90040
Soapnut Saponin solution 3	22.49	25.00	0.89960
Density Average			0.89957
Ultra-pure water Reference	24.99	25.00	0.99976
Camellia oleifera saponin solution 1	23.11	25.00	0.92430
Camellia oleifera saponin solution 2	23.03	25.00	0.92121
Camellia oleifera saponin solution 3	23.29	25.00	0.93150
Density Average			0.92567

4.3.2 pH

pH measurements were performed for nine saponin solutions for each Saponin (Soapnut and Camellia oleifera) with different concentrations (weight percentage) from 1wt% to 9wt%. The results obtained are shown in [Figure 4.1](#).



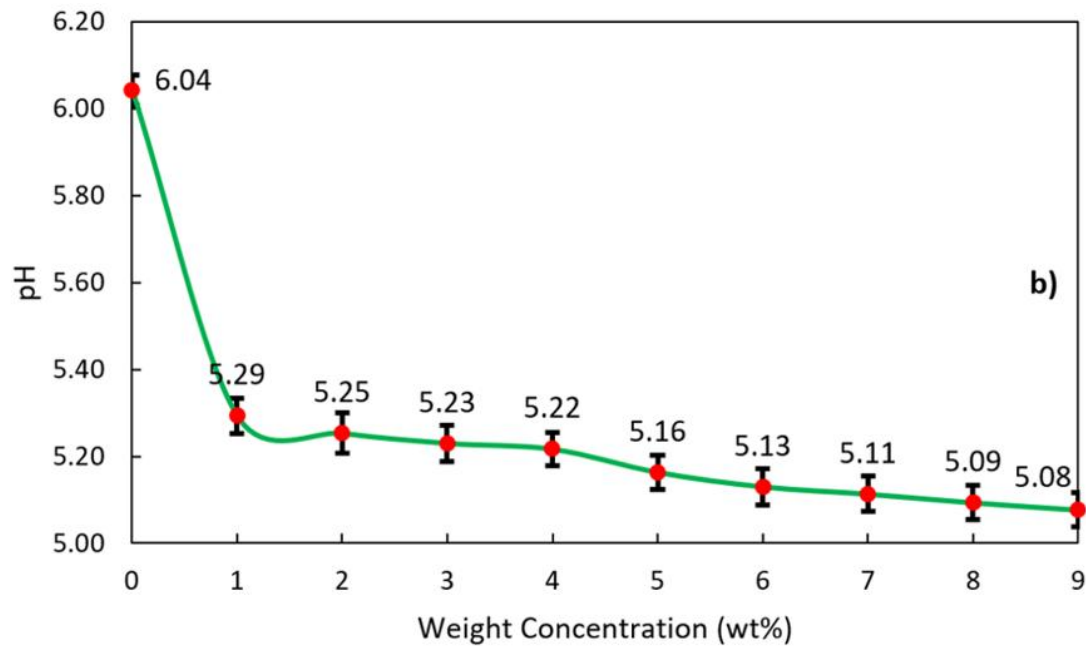


Figure 4.1: pH variation of the saponin extract vs. concentration. a) Soapnut saponin; b) *Camellia oleifera* saponin. The error bars were the standard deviation of the three independent measurements

Figure 4.1a shows that when the concentration of Soapnut saponin increased, the pH of the solution dropped from 4.70 at 1wt% to 4.46 at 9wt%. The existence of contaminants in the extracted surfactant that have not been eliminated could be associated with a little increase in pH fluctuation at a concentration of 3%. As a result, the Soapnut surfactant produces a slightly acidic solution, and the Soapnut saponin extract is a weak-acid natural surfactant (Azam et al., 2013; Muntaha & Khan, 2015; Mehana & Fahes, 2018). For *Camellia oleifera* saponin, Figure 4.1b shows a steady decreasing trend as the concentration increases. The pH of the solution sharply dropped from 6.04 to 5.29 when 1wt% *Camellia oleifera* saponin was added to the solution. After that, the pH of the solution gently decreased in the range of 0.01 to 0.06. Finally, the pH reached 5.08 at 9wt%. Therefore, like Soapnut saponin, *Camellia oleifera* saponin also created a slightly acidic solution, and it can be considered a weak-acid natural surfactant. According to Belhaj et al. (2020), the acidic surfactant solution can impact reservoir rock and other EOR fluid addition. Various studies confirmed that the adsorption of

surfactants increased with decreasing pH (Azam et al., 2013; Mehana & Fahes, 2018).

4.3.3 Conductivity and Solubility

Eighteen different saponin extract solutions (9 for Soapnut saponin and 9 for *Camellia oleifera* saponin) were prepared with different concentrations (1 wt% to 9 wt%). Based on Figure 4.2, the surfactants showed good solubility since the increased gradient of conductivity was stable and continuous. The conductivity number is proportional to the electrical current flows among the electron ions, which is directly related to the dissolved ions from the substance. Thus, the increasing concentration can increase the number of ions, improving the conductivity.

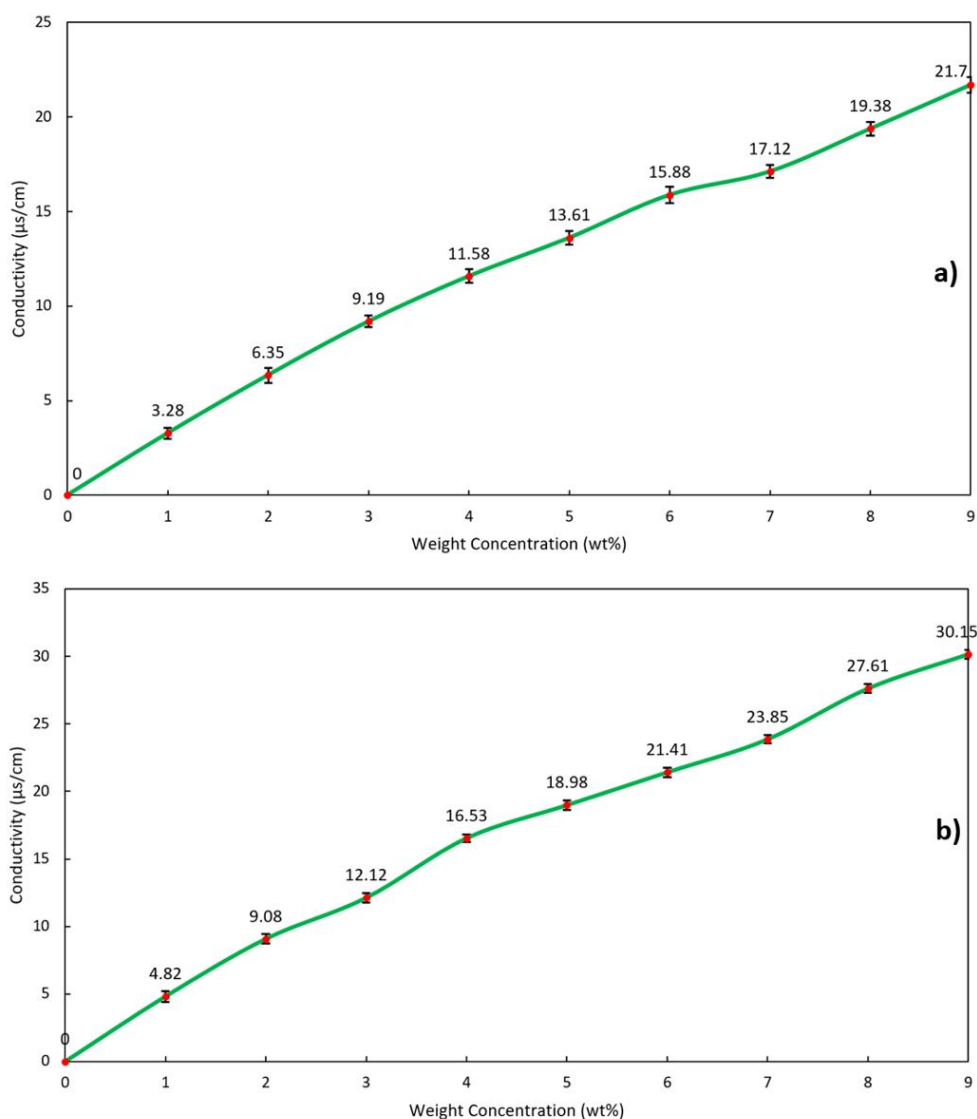


Figure 4.2: The conductivity of saponin extract with increasing concentration. a) Soapnut saponin; b) *Camellia oleifera* saponin. The error bars were the standard deviation of the three independent measurements

4.3.4 CMC Point Identification

In this study, the conductivity measurement was used to calculate the CMC point, which was done in accordance with William's approach. According to William's method, the CMC point is marked by the deviation in the straight-line slope obtained by plotting the conductivity against the surfactant concentration. Based on Figure 4.3, it appears that the CMC point of Soapnut saponin is near 4.6wt%, at which time the slope of the conductivity begins to diverge from its initial value. For the *Camellia oleifera* saponin, the CMC point was present in 4wt%.

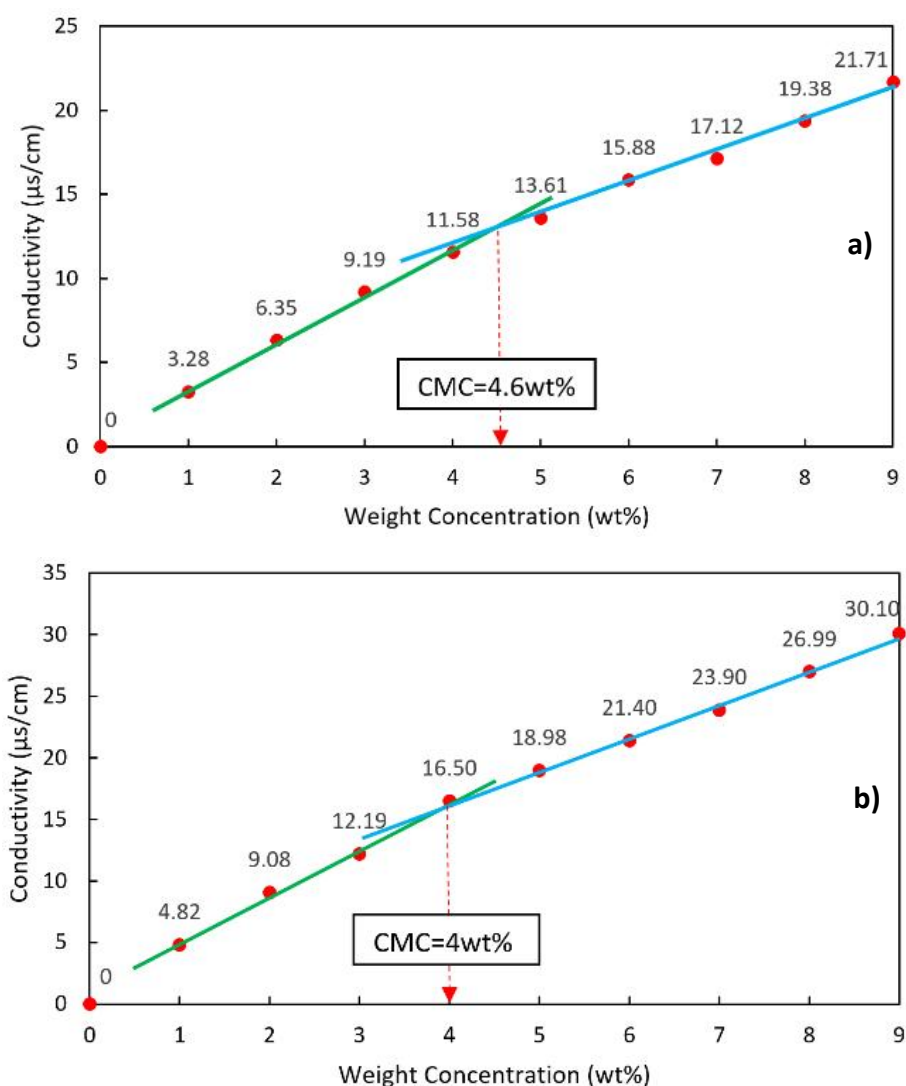


Figure 4.3: CMC point of a) Soapnut saponin extract solution; b) *Camellia oleifera* saponin extract solution

CMC is a key characteristic of surfactants since it represents the highest concentration of surfactants that may be dissolved in water without agglomerating. Molecular self-agglomeration and micelle formation occur after the CMC point, leading to lower electric conductivity since dispersed saponin molecules (monomers) were considered suitable electrolytes with a higher ionization degree (Saxena et al., 2018; Sar et al., 2019). Micelles cause similarly charged hydrophilic surfactant heads to oppose each other (electrostatic repulsion force) and interact with the hydrophobic surfactant tails of other molecules in the solution, reducing the binding site for electro-activation and partially neutralizing the charges. This behavior has the effect of lowering the net electrostatic charge and the level of ionization (Cosgrove and Cosgrove, 2010).

4.3.5 Temperature Effect and CMC Variation

To determine the surfactant's effectiveness at elevated temperatures (reservoir condition). The saponin mixtures with various concentrations were tested at different temperatures, ranging from 40°C, 50°C, 60°C, 70°C, 80°C, and 100°C. The results obtained are presented in Figure 4.4. It is observed that the conductivity increased as the temperature increased from 25°C to 100°C, but the slope of the trend started to decrease when the temperature reached 100°C. As discussed earlier, the number of electron ions generated from the Saponin possessed excellent solubility. As the temperature increases, the ion mobility/activity associated with molecular vibration and rotation increases (Cosgrove and Cosgrove, 2010; Sauerheber and Heinz, 2016).

Moreover, the Brownian motion in the solution increases with the temperature, which reduces the solution viscosity (Tadros, 2015). Therefore, the mobility of ions is further stimulated, leading to a decline in resistivity and an increase in conductivity. However, the conductivity slightly decreases or maintains a constant above 80°C. This could be due to the self-agglomeration. The larger molecular with less charged ions could not produce enough ions mobility in the solutions. The CMC point was also examined at various temperatures up to 100°C with concentrations ranging from 1 to 9 wt% to evaluate the performance of the

Soapnut surfactant and *Camellia oleifera* surfactant's high temperatures, and the outcomes are demonstrated in Figure 4.5 and Figure 4.6.

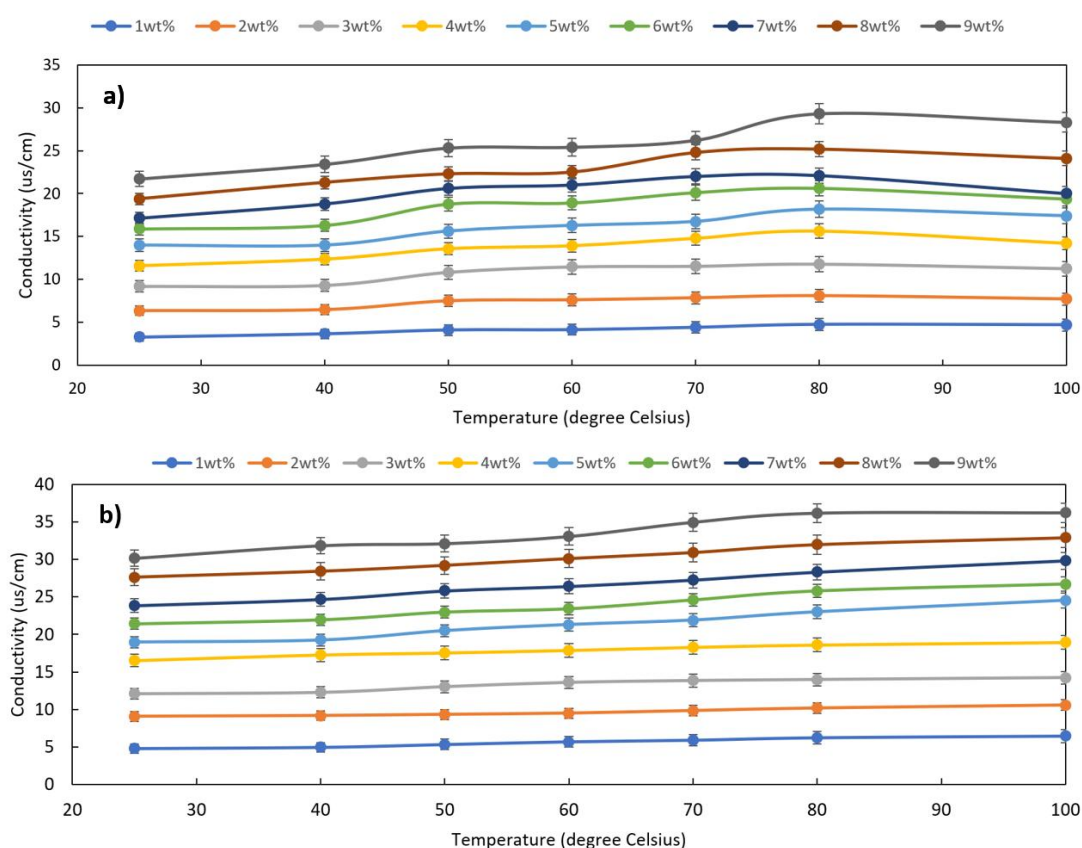


Figure 4.4: Conductivity of the saponin solutions at various concentrations under different temperatures. a) Soapnut saponin and b) *Camellia oleifera* saponin. The error bars were the standard deviation of the three independent measurements

It is noticed that the CMC point shifted towards a higher concentration with increasing temperature. [Chen et al. \(1998\)](#) and [Saxena et al. \(2019\)](#) explained that this rise in the CMC point could be due to a delay in saponin molecules aggregation. With increasing temperature, electron mobility increases due to molecule vibration and rotation. Therefore, the structural water connected to the hydrophobic group has a tendency to change the balance between monomers and micelles toward the monomers ([Kumar and Mandal, 2017](#); [Saxena et al., 2018](#)).

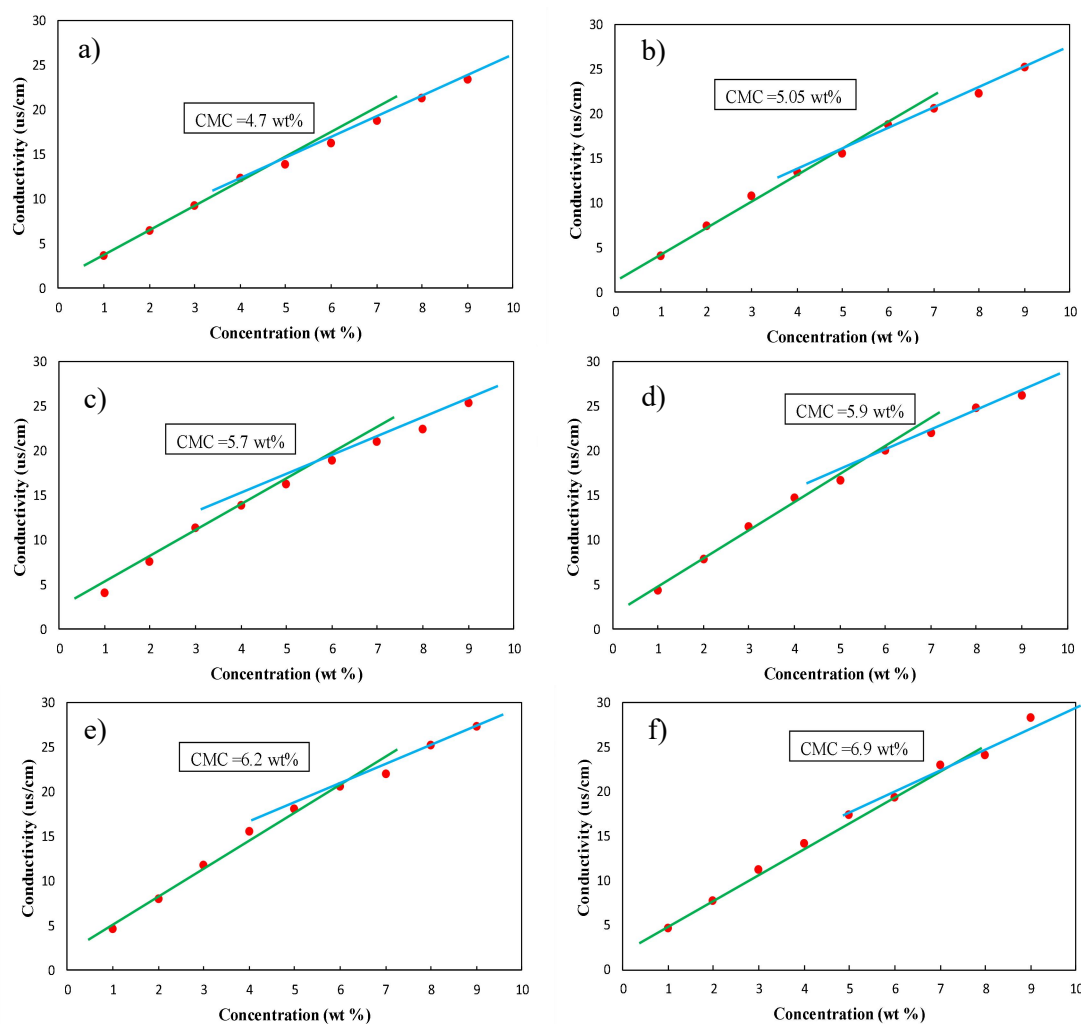


Figure 4.5: Temperature effect on the CMC of Soapnut saponin with varying concentrations. a) 40°C; b) 50°C; c) 60°C; d) 70°C; e) 80°C; f) 100°C

In other words, elevated temperatures cause the alkyl group's water structure to break down ([Chen et al., 1998](#); [Saxena et al., 2019](#)), resulting in the aggregation of saponin molecules at a higher concentration. The increase in adsorption sites can also explain this as a result of the rise in surface curvature, which increases with rising temperature ([Moeini et al., 2014](#); [Bizhan et al., 2020](#)). As a result, the saponin enters the solution more slowly, increasing the CMC. In summary, the derived saponins from both plants perform well at elevated temperatures.

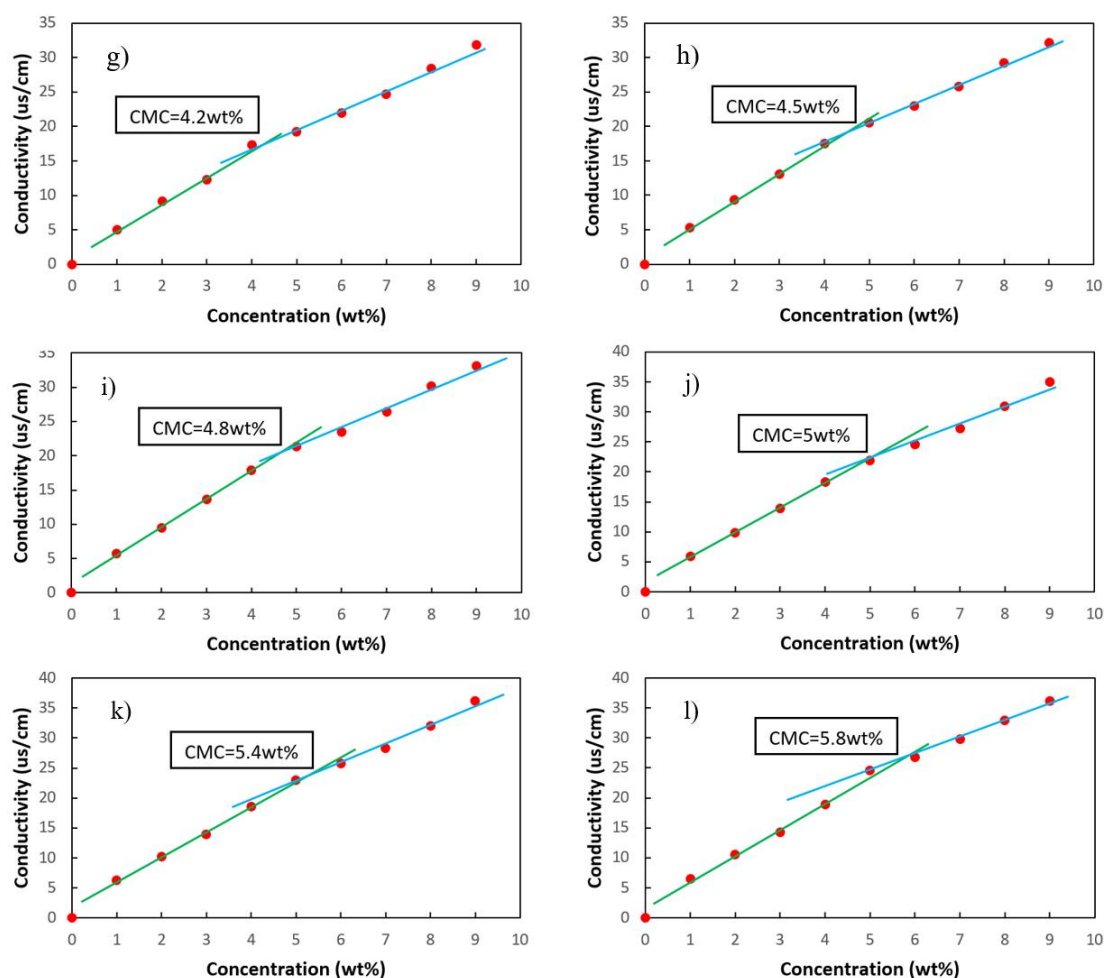


Figure 4.6: Temperature effect on the CMC of Camellia oleifera saponin with varying concentrations. g) 40°C; h) 50°C; i) 60°C; j) 70°C; k) 80°C; l) 100°C

4.3.6 Particle Size Distribution and Zeta Potential

The particle size distribution and zeta potential of saponins were determined using the Malvern Panalytical Zetasizer Nano ZS. As shown in Tables 4.4 and 4.5, the average particle size of Soapnut saponin extract and Camellia oleifera saponin extract in liquid suspension were around 103.4nm and 123.6nm, respectively.

Table 4.4: Average particle size of saponin surfactant extracted from the Soapnut

Test	Z-Average (d.nm)	Pdi	Zeta Potential(mV)
Test 1	103	0.569	-6.93
Test 2	103.9	0.586	-6.10
Test 3	103.3	0.572	-6.03
Average	103.4	0.576	-6.35

Table 4.5: Average particle size of surfactant extracted from the Camellia oleifera

Test	Z-Average (d.nm)	Pdi	Zeta Potential(mV)
------	------------------	-----	--------------------

Test 1	123.3	0.580	-21.5
Test 2	122.5	0.584	-23.4
Test 3	125.0	0.593	-22.2
Average	123.6	0.586	-22.4

For Soapnut saponin, the average polydispersity index (Pdl) was 0.576, while for *Camellia oleifera* saponin, it was 0.586. This shows that the saponins are soluble in water and will not obstruct the creation of pore throats during the EOR injection procedure. The average zeta potential of the Soapnut saponin extract was determined to be -6.35mV. Soapnut extract surfactant was classified as a nonionic surfactant because the average value was near 0 mV, which was consistent with previous investigations ([Balakrishnan et al., 2006](#); [Chhetri et al., 2009](#); [Du et al., 2014](#); [Schmitt et al., 2014](#); [Tmáková et al., 2016](#)). *Camellia oleifera* saponin's average zeta potential was identified as -22.4mV, so it is considered an anionic surfactant.

The zeta potential reading presents the electrokinetic behavior on the cell surface. The majority of plant fruits include various naturally occurring coagulants, such as tannins. Tannins (tannic acid) are a class of polyphenolic macromolecules that interact with and precipitate proteins and other organic compounds such as amino acids and alkaloids ([Nowrouzi et al., 2020](#)). Tannis, in combination with other naturally occurring coagulants, can adsorb and deposit on the saponin molecular surface, resulting in the shift of the share plane position in the electrical double layer then giving a negative charge of Soap-nut saponin on Zeta-Sizer ([Nowrouzi et al., 2020](#); [Saxena et al., 2019](#)). When saponins are extracted from raw plants, they may contain ionic contaminants that influence their zeta potential. Specifically, the interfaces between the molecules of surfactant and water are energy-intensive; thus, they tend to recombine to decrease the total interfacial area ([Mohanty & Mukherji, 2013](#)). Moreover, the metastability of surfactant solution (water + surfactant) is accomplished by the adsorption of amphiphilic molecules (nonionic in this case). According to [Hunter \(1981\)](#), neutral ion adsorption affects the chemical-specific adsorption of nonionic ions on the interface, affecting the reading of zeta potential. Many commercial nonionic surfactants have discovered ionic contamination, and those contaminants sometimes are surface-active ([Mohanty &](#)

Mukherji, 2013; Pal et al., 2018; Kumar & Mandal, 2019). Thus, a slight negative charge was observed on the surface of the surfactant solution. Furthermore, the equipment, glassware, surfactant container, and the floating particles in the air may become the potential source of ionic contamination. This phenomenon was not only happened during this study; other researchers also observed it. The zeta potential has been found to show -11.4 mV on pure TX 100 (famous commercial nonionic surfactant) solution (Yekeen et al., 2019). Hou et al. (2015) also found out that the zeta potential value on the TX-100 solution was shown as -8mV. -2.1 mV zeta potential was found when Ayirala et al. (2019) applied Ethoxylated alcohol (nonionic surfactant) in the study. Therefore, according to the above discussion, it can consider Soapnut Saponin a nonionic surfactant even the zeta-potential shows -6.35 mV. Furthermore, Camellia oleifera saponin is considered an anionic surfactant since the zeta-potential shows -22.4mV.

4.3.7 TGA

The thermal stability and degradation analysis of saponin extract were conducted by PerkinElmer thermogravimetric analysis STA 6000. Two kinds of extracted Saponin were analyzed (Soapnut and Camellia oleifera). Specifically, Soapnut saponin is extracted by ultra-pure water, and Camellia oleifera saponin is extracted by ultra-pure water. The original weight of each sample was 5mg. The temperature program was set from 100°C to 900°C at the rate of 10°C/min under a nitrogen supply of 10mL/min, and the weight loss percentages as a function of temperature were obtained, as shown in Figure 4.7. TGA plots indicated that the Saponin extracts were experienced in three successive phases. It can be seen in the samples that abnormally increased at the beginning (first phase) for both saponins. For Soapnut saponin, the weight increased from 5mg to 5.11mg (2.27%) between 100°C and 150°C, and Camellia oleifera saponin raised from 5mg to 5.09mg (1.93%) between 100°C to 153°C. Two possible reasons can explain it. Firstly, it may trigger by the error of the sample weighting component. It requires weighing the sample at the analytical balance before sending it to the TGA (error 1), and the weighting components of the TGA itself also will weigh automatically (error 2). Secondly, the

nitrogen gas used in TGA may not be pure and mix a few portions of carbon dioxide or oxygen, leading to an oxidation reaction. The mass increase may trigger adsorption from the substance in the atmosphere. Such as, if the atmosphere contains carbon dioxide or oxygen, the mass of Saponin may increase due to CO₂/O₂ adsorption, turning the oxide into a carbonate (Chiang et al., 2009). The results of TGA can provide analysis in three phases.

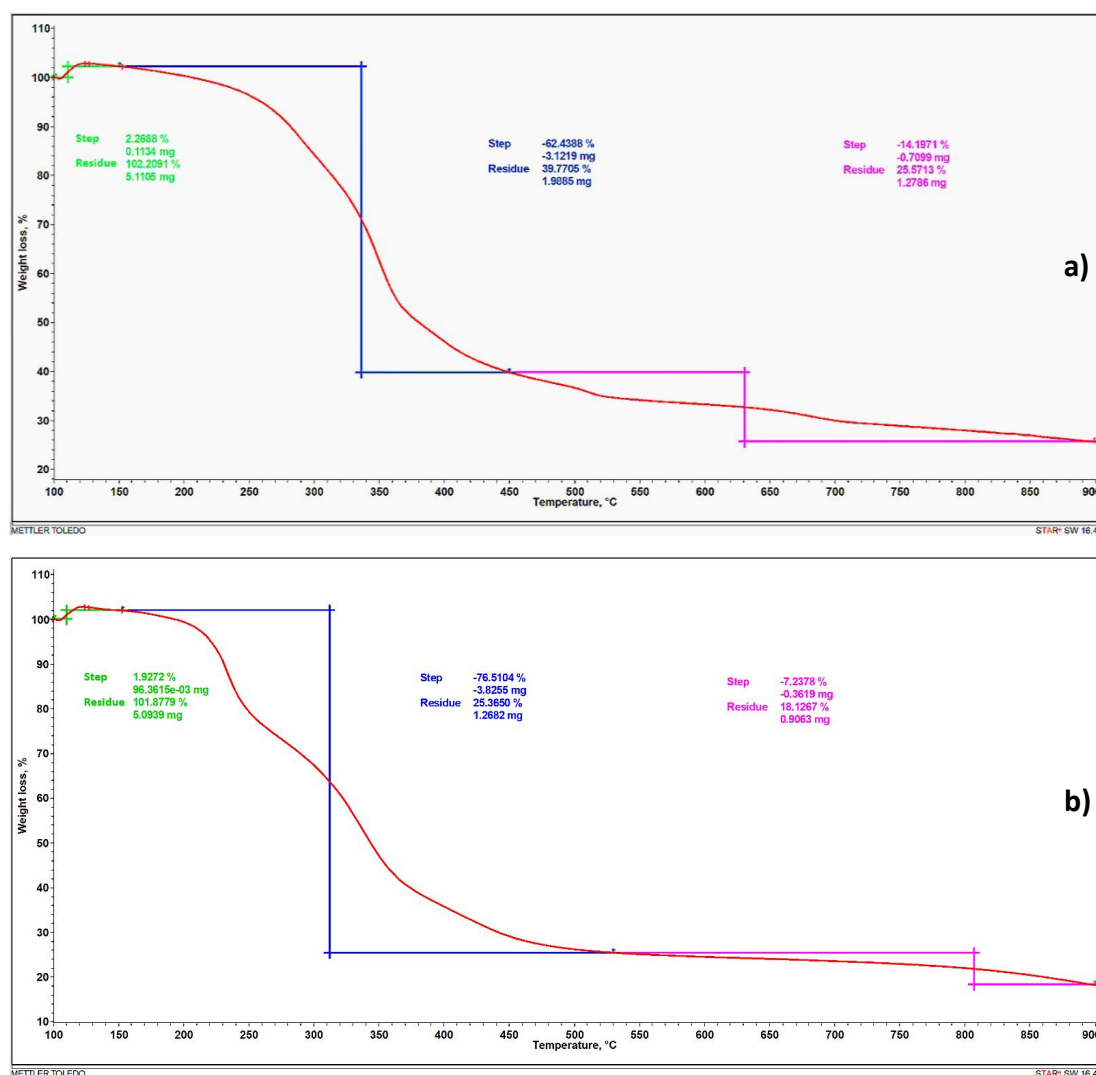


Figure 4.7: TGA results of a) Soapnut saponin and b) Camellia oleifera saponin

For Soapnut saponin, the second disintegration phase occurred between 150°C to 450°C, with a weight loss of roughly 62.44% (3.12mg). The final peak occurred at about 450°C, where the surfactant degraded. The third phase occurred between 450°C to 900°C, with 14.20% weight loss (0.71mg). Camellia oleifera saponin's second decomposition phase was observed from 150°C to 530°C, with

approximately 76.51% loss in weight (3.83mg). The third phase happened between 530°C to 900°C, with a 7.24% weight loss (0.36mg). The second phase involved the extraction of moisture (bound water) from the surfactants ([J. Yang et al., 2021](#)) and the breakdown of any oxides found in the extracted surfactants as contaminants ([Shen et al., 2021, p. 20](#)). It demonstrated that the Saponin surfactant exhibits exceptional thermal stability, even at high reservoir temperatures. The last phase is probably associated with the formation of gases from the reactions of oxygen and carbonaceous leftovers (such as CO and CO₂) ([El Barky, 2020](#)).

4.3.8 SEM

Scanning Electron Microscopy (SEM) is a technique for determining particles' shape, size, and arrangement. This approach has been particularly successful in the research field because it is minimally intrusive and can attain the needed resolution of a micrometer down to the nanometer range ([Hlawacek et al., 2013](#)). This section introduced SEM to analyze the morphological of the individual and agglomerated structure of extract saponins from Soapnut and Camellia oleifera in dry status. Both specimens are tested under dry powder conditions. Low vacuum mode - low vacuum detector (LVD) observed magnification from 0.6x to 5000x. In order to provide a high standard image quality, double-sided carbon conductive tape was adhered to the SEM's sample holder, then the powder of saponin was evenly spread on the top of the tape. According to [Figure 4.8](#), most saponin particles demonstrated a uniform spherical structure, primarily in the agglomerated form. It also showed that both saponin types have an apparent preference for adhering to each other.

Furthermore, it can be observed that there are lots of small irregular fragments, which were probably caused by the ultrasonic extraction that broke up some saponin particles. For Soapnut saponin, the majority are spherical shape particles (65%), amorphous shape particles (25%), and a minority as less rounded particles (10%); whereas for Camellia oleifera saponin: the majority are spherical shape particles (45%), amorphous shape particles (35%), and a minority as less rounded particles (20%). Meanwhile, numerous small amorphous shape particles

were attached/bonded to form a large cluster. It may be caused by the large adhesion/cohesion forces or intermolecular attraction force of Van der Waals forces (Yisong et al., 2022). Therefore, aggregates cluster of saponin particles dominates the most parts in both SEM images.

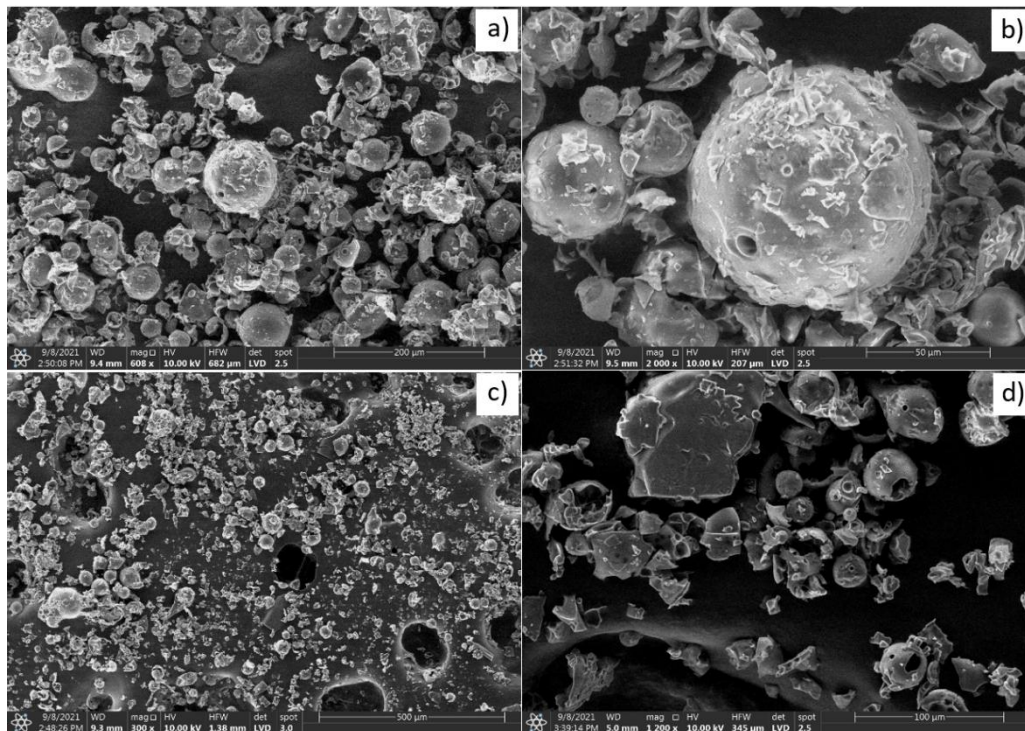


Figure 4.8: SEM images of extracted Soapnut saponin and *Camellia oleifera* saponin under drying powder status. a) an overall image of Soapnut saponin; b) Soapnut saponin particle; c) an overall image of *Camellia oleifera* saponin; d) *Camellia oleifera* saponin particle

4.3.9 UV-Vis

Ultraviolet-visible spectroscopy (UV-Vis) has been used to identify the extract saponins from Soapnut and *Camellia oleifera*. The experiment was conducted in batch mode, with a series of saponin solutions at various concentrations. Each batch contained seven tubes with an increasing amount of Soapnut saponin powder or *Camellia oleifera* saponin powder mixed with ultra-pure water. Maximum wavelength is the component exhibiting the farthest absorbance recorded in this section. Figure 4.9a shows that most Soapnut saponin compounds exhibit a significant absorption peak in the region of 200 and 350nm, of which the maximum

absorption peak (λ_{\max}) was measured at 200nm. For *Camellia oleifera* saponin (Figure 4.9b), the absorption peak was observed between 200-380nm. Specifically, the maximum absorption peaks at 215, 270, and 350nm.

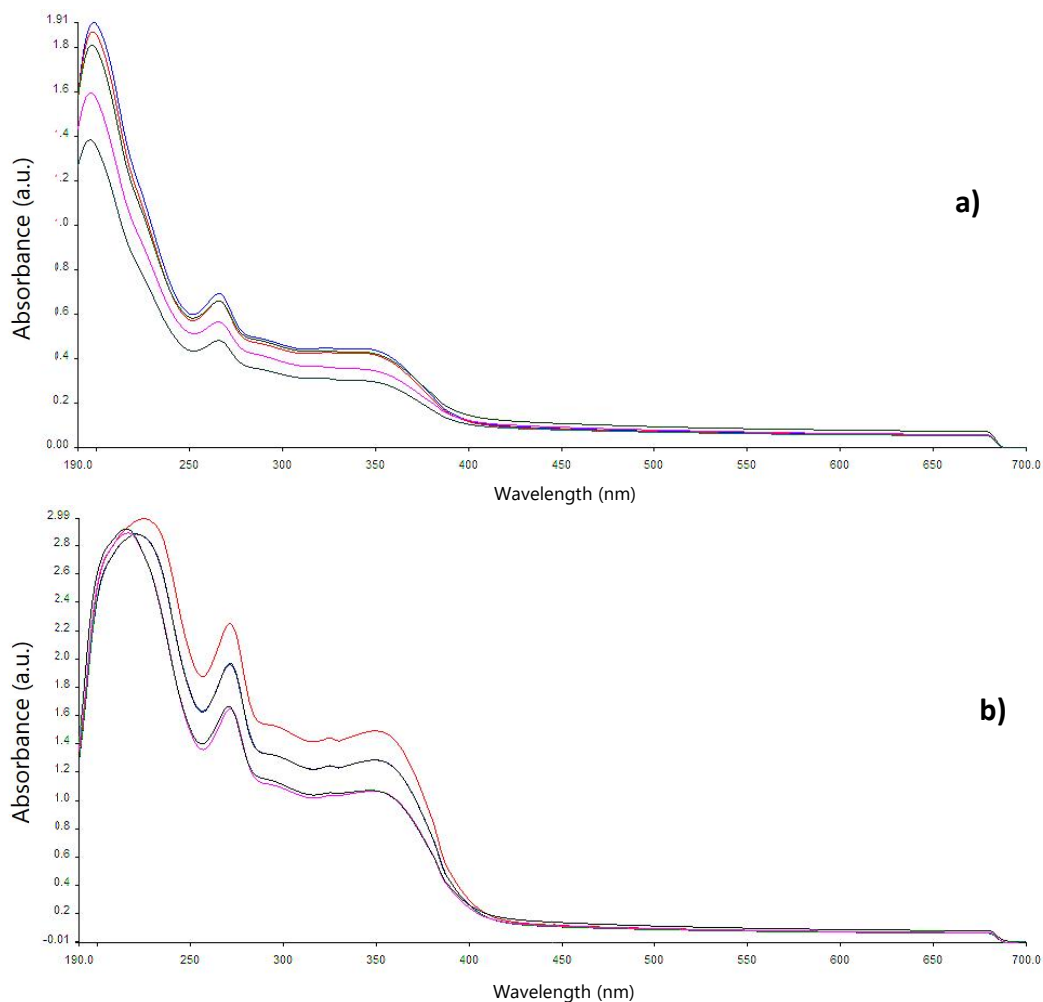


Figure 4.9: UV-Vis of saponins. a) Soapnut saponin and b) *Camellia oleifera* saponin with increasing concentrations

4.3.10 FTIR

The infrared absorption spectrum testified saponin (dry powder). The spectrum of pure saponin has several indicative frequencies that can be used to identify numerous functional groups, confirming the saponin body's complexity. The results achieved were similar to that of saponins investigated by other researchers. Figure 4.10 presents the FTIR results of Soapnut saponin, where the peak validated the

alcoholic hydroxyl group (-OH) caused by O-H stretching at 3317cm⁻¹. In addition, the C-H bending of alkanes was discovered at the peak of 1385cm⁻¹ (Basu et al., 2015).

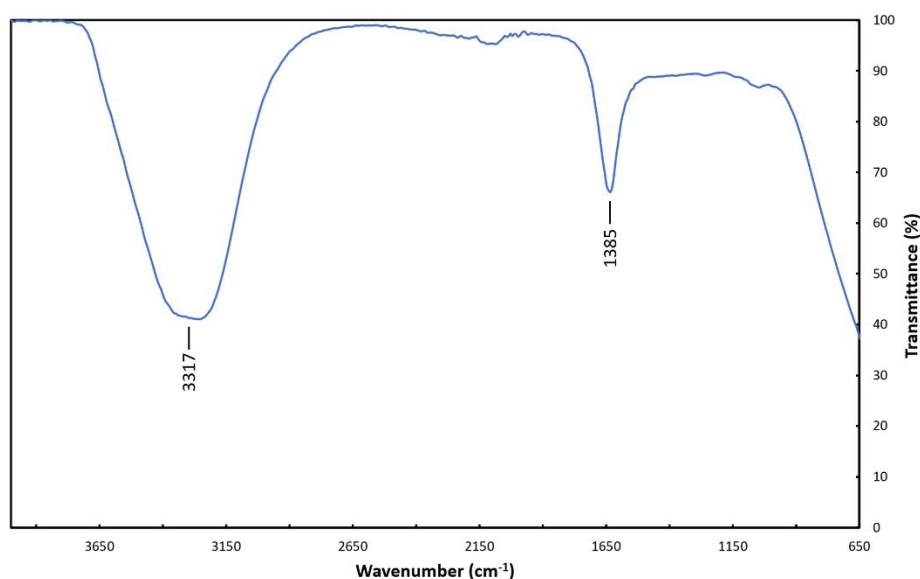


Figure 4.10: FTIR absorption spectral data of Soapnut saponin

Figure 4.11 presents the FTIR results of *Camellia oleifera* saponin, where the distinctive bands of infrared adsorption were exhibited at 3312cm⁻¹ for the hydroxyl group (-OH) that stretched arising from the surface hydroxyl groups (Yuan et al., 2018). The absorbance of aliphatic carbon-hydrogen (C-H) was observed at 2923cm⁻¹. The absence of absorption between 2500 and 1900 cm⁻¹ shows no double or triple bond buildup. At 1378 and 1239 cm⁻¹, the symmetric deformation vibration peak and the antisymmetric deformation peak -CH- were identified (Yuan et al., 2018). In addition, the absorbance of functional groups of carboxylic acid or ester (C=O) was determined at 1728 cm⁻¹. The peak at 1619 cm⁻¹ may probably be due to C=C bonds in the saponin moiety. In the 1029 cm⁻¹ area, oligosaccharide linkage absorptions to sapogenins, specifically C-O-C, were observed (Almutairi & Ali, 2015). Those mentioned above infrared functional group absorptions, which are characteristic of saponins, have been attributed to the presence of the oleanolic acid-ester. As indicated by the C=O infrared absorbance, these triterpenoid saponins are bidesmosides due to two glycones connecting them to the sapogenin via glycosidic and ester groups (Yuan et al., 2018).

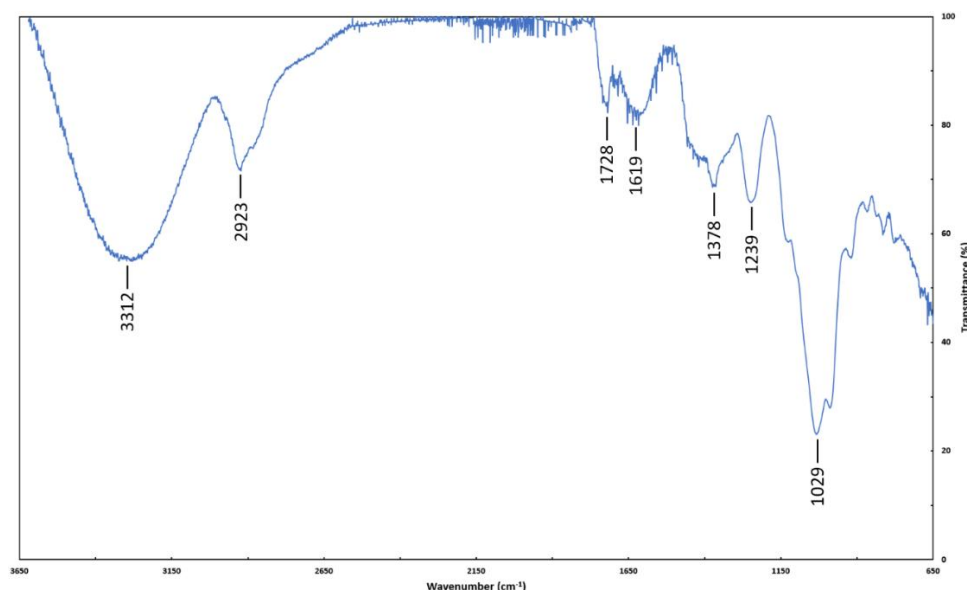


Figure 4.11: FTIR absorption spectral data of *Camellia oleifera* saponin

4.4 Conclusions

This chapter examined several properties of Soapnut and *Camellia oleifera* saponins, including density, pH, conductivity, critical micelle concentration (CMC), particle size distribution, zeta potential, thermal degradation, SEM, UV-Vis, and FTIR. Furthermore, the performance of green surfactants under high temperatures was also identified. The following conclusions are eventually drawn:

- 1) The average density of the extract green surfactants is 0.89957 g/cm³ for Soapnut saponin and 0.92567 g/cm³ for *Camellia oleifera* saponin.
- 2) The pH of Soapnut and *Camellia oleifera* saponins decreases as surfactants' concentration increases. Both extracted saponins are considered weak-acid natural surfactants.
- 3) Both Saponin extracts possess excellent solubility and conductivity. Furthermore, the CMC point of Soapnut saponin was estimated at 4.6wt%. For *Camellia oleifera* saponin, the CMC point was located at 4wt%.
- 4) The conductivity of saponin solutions increases as a temperature function but stops at 80°C due to self-agglomeration. Therefore, 80°C can be considered the temperature threshold for the saponin solution, especially at a high concentration. For the CMC points, it was discovered that the CMC

- point increases as the temperature increases due to the imbalance between monomers and micelles, with the highest CMC point being attained at 100°C.
- 5) The average particle sizes of Soapnut saponin extract and *Camellia oleifera* saponin extract are around 103.4nm and 123.6nm, respectively. The average polydispersity index that indicates the width of overall distribution was 0.576 for Soapnut saponin and 0.586 for *Camellia oleifera* saponin.
 - 6) The zeta-potential of Soapnut saponin shows -6.35mV and is considered a nonionic surfactant. For *Camellia oleifera* saponin, the zeta-potential is determined as -22.4mV, and it is considered an anionic surfactant.
 - 7) For TGA analysis, the results fall into three stages: 1) 100–150°C, the Soapnut saponin experienced about 6.2% weight loss, and the *Camellia oleifera* saponin showed approximately 6.2% weight loss; 2) 150–450°C, the Soapnut saponin experienced about 20.24% weight loss, and the *Camellia oleifera* saponin shows around 19.83% weight loss; 3) 450–900°C, the Soapnut saponin experienced about 8.43% weight loss, and the *Camellia oleifera* saponin shows about 7.99% weight loss. Both surfactants will be degraded at 450°C, which shows good thermal stability under reservoir conditions.
 - 8) According to the images captured by SEM, most saponin particles (Soapnut saponin and *Camellia oleifera* saponin) revealed a uniform spherical structure without any sharp edges. It was also found that most of the spherical shape particles were aggregates together, forming complex structures.
 - 9) The UV-Vis results show that most Soapnut saponin compounds exhibit a significant absorption peak in the region of 200–350 nm, of which the maximum absorption peak (λ_{max}) was measured at 200 nm. For *Camellia oleifera* saponin, the absorption peak was observed between 200-380 nm. Specifically, the maximum absorption peaks are at 215, 270, and 350 nm.
 - 10) The FTIR results revealed that the hydroxyl group (-OH) was located at 3312cm^{-1} ; the absorbance of aliphatic carbon-hydrogen (C-H) was observed at 2923cm^{-1} ; the symmetric deformation vibration peak and the

antisymmetric deformation vibration peak -CH- were identified at 1378 and 1239 cm^{-1} ; the carboxylic acid or ester (C=O) was determined at 1728 cm^{-1} ; the peak at 1619 cm^{-1} may probably due to C=C bonds in the saponin moiety. In the 1029 cm^{-1} area, oligosaccharide linkage absorptions to sapogenins, specifically C-O-C, were observed.

Chapter 5: Foamability and Foam Stability

5.1 Introduction

Foam is a mixture of liquid, gas, and foaming agent, whereby the liquid is transformed into the continuous dispersion phase, while the gas is transformed into the discontinuous dispersed phase. The lamellae, or thin liquid films, divide gas bubbles into bulk foam. Foamability and foam stability are two concepts that are commonly used to characterize the foaming capabilities of solutions that contain surfactants. Foamability is defined as the ability of the surfactant solution to create foam under specific conditions, whereas foam stability refers to the differentiation or continuous period of the foam bubbles (usual variations in height or volume) as a function of time instantly following foam generation ([Kedir et al., 2022](#)).

In order to determine the properties of foam, several parameters must be considered, such as the surfactant type (anionic, cationic, or nonionic), surfactant concentration, gas structure (including the amount of oxygen present), brine concentration and composition (including salinity), crude oil interaction, temperature, and pressure. Therefore, it is essential to understand foam-stabilizing agents' properties, tolerances, limitations, and performance.

A number of experiments have been carried out to investigate the foamability and foam stability for both extracted green surfactants (Soapnut saponin and *Camellia oleifera* saponin) under 5 conditions, which were 1) different concentrations of surfactant; 2) variation of salinity; 3) under the influence of temperature; 4) the fluid system contained nanoparticles, salt, or both; and 5) the crude oil-foam interaction.

5.2 Methodology

5.2.1 Experimental Apparatus

Ultrasonic homogenizer used to mix the solution and manufactured by SONOMECHANICS Industrial evenly thoroughly. Mettler Toledo manufactured the analytical balance used to measure substances. Sartorius Quintix 412-1S digital scale was adopted to weigh the right amount of ultra-pure water. An orbital shaker

manufactured by the Lab Companion SKF-2075 was used to completely dissolve the solute (salt and surfactant) into the solvent system. 50ml centrifuge tubes manufactured by Fisher Scientific are used as a solution container. An electrical conductivity meter manufactured by Mettler Toledo Seven Multi™ was applied to measure the solution's electrical conductivity and total dissolved solids (TDS). The microscope used to investigate the foam structure was manufactured by LEICA Microsystem CME Compound Binocular.

5.2.2 Experimental Materials

The oil supplied by Miri Crude Oil Terminal was the reservoir oil without any gas (dead oil), with a density of 0.84 kg/L. The composition and the properties of crude oil are the same as the one used in the Chapter 3, which is shown in [Table 3.1](#). The salt sodium chloride (NaCl) was used to evaluate the salinity effect and purchased from Merck Millipore. Nano-glass flake (NGF) was also part of this study for the green solution development, purchased from Glassflake Ltd, with a purity of >98%. This inorganic nanoparticle was applied because of its excellent stability (physical and chemical), low toxicity, and ability to be functionalized with other materials. Ultra-pure water with a resistivity of 5.4 MΩ.cm was used as a solvent. Extracted green surfactants from the previous chapters (Soapnut saponin and *Camellia oleifera* saponin) were applied as foaming agents.

5.2.3 Preparation of Green Surfactants Solutions

In order to measure the foamability, foam stability, salinity effect, and oil-foam interaction of the extracted green surfactants, several batches of the solutions were prepared. NaCl was used as the salt and NGF as the nanoparticle. Only a small amount of nanoparticles should be used to avoid agglomeration ([Rezvani et al., 2020](#)). In this study, all the solutions were prepared by a high-frequency ultrasonic homogenizer to ensure a uniform dispersion. This sonication could: 1) produce a homogeneous and stable hybrid solution; 2) eliminate any air bubbles from the solution; and 3) disperse any potential agglomerates/clustering. The ultrasonic amplitude was fixed at 35% with a set circulation (running 7 seconds and pulse 2

seconds) for 15 minutes to prevent over-heating and structural damage (Singh & Mohanty, 2020). Various concentrations of NaCl, NGF, and green surfactants (Soapnut and Camellia oleifera saponin extract) were considered. The conductivity measurement was conducted right after the end of the mixing process.

5.2.3.1 Salinity Effect Measurement

The conductivity test probe was calibrated by a standard solution to obtain accurate readings for salinity effect measurement. The experiments were repeated three times. Three different solutions were prepared as described in the followings:

- 1) The solute for the first batch was pure NaCl. Different concentrations of NaCl (1000 ppm to 55000 ppm) solutions were prepared and poured into the centrifuge tubes with 10ml of ultrapure water. A total number of 25 centrifuge tubes containing varied salt concentrations were moved to an orbital shaker for 24 hours, where they were stirred at a speed of 300 rpm throughout the entire time. The conductivity measurements were carried out immediately following that.
- 2) The solute for the second batch was NGF nanoparticles. 25 portions of 5mg NGF (0.05 wt%) were added to each centrifuge tube. For the next 24 hours, the orbital shaker rotated at 300 rpm, mixing the solutions. After that, sonication at a 50% amplitude for 20 minutes was applied to the solutions (7 seconds running and 2 seconds pause) (Singh & Mohanty, 2020).
- 3) The solute for the third batch was extracted from green surfactants (Soapnut and Camellia oleifera saponin). On the basis of the second batch, 25 portions of 50mg green surfactants (0.5wt%) were weighed by the analytical balance and added to centrifuge tubes. All of these solutions were transported immediately to the ultrasonic homogenizer, where they were mixed at a 35% amplitude for 20 minutes (7 seconds running and 2 seconds pause) until all solutes were completely dissolved (Singh & Mohanty, 2020).

5.2.3.2 Foamability, Foam Stability, and Bubble Structure

Foaming and foam stability can reduce the mobility ratio between the displaced and displacing phases while providing a better movement for the solution by decreasing the capillary pressure, especially in low permeability formations ([Osama Al, 2015](#); [Skauge et al., 2020](#)). The amount of foam produced increases as the surfactant concentration is increased until it reaches the CMC point. The impact is insignificant when exceeding the CMC ([Aziz et al., 2019](#)). Four different types of solutions were created for the foamability and foam stability tests in this investigation, having the following characteristics:

- 1) The first batch of solutions' solute was pure Soapnut saponin and Camellia oleifera saponin. Eighteen portions of green surfactants (10mg to 800mg) were weighed independently by the analytical balance and added into centrifuge tubes. Each tube contains 10ml ultrapure water. These tubes were then moved to an orbital shaker for 12 hours at a speed of 200rpm for mixing, followed by 10 minutes of ultrasonication at 35% amplitude (7 seconds running and 2 seconds pause) until all surfactants were present dissolved. Following that, foamability and foam stability tests were performed.
- 2) The second batch of solutions contained the identical solute to the previous batch. Following the same technique as the previous batch, these tubes were moved to a hot water bath and exposed to a temperature of 85°C. Following that, foamability and stability tests were undertaken.
- 3) The third batch of solutions contained a solution of NaCl, NGF, and saponins. Thirty-four portions of NaCl (10mg to 1000mg), NGF (5mg), and saponins (50mg) were individually weighed on the analytical balance and then transferred into 34 centrifuge tubes. Each tube contains 10ml ultrapure water. These 34 tubes were then moved to an orbital shaker for 24 hours at a speed of 400rpm for mixing, followed by 30 minutes of ultrasonication at a 35% amplitude (7 seconds running and 2 seconds pause). Following that, foamability and stability tests were performed.

- 4) The final batch of solutions contained a solution of NaCl, NGF, saponins, and crude oil. Thirty-four portions of NaCl (10mg to 1000mg), NGF (5mg), saponins (50mg), and 2ml crude oil were individually weighed on an analytical balance and then transferred to centrifuge tubes. Following the same technique as with the third batch. The foamability and stability tests were performed.

In order to determine the link between foam stability and bubble size, the LEICA LEICA microsystem CME compound binocular microscope (BC43) was used to observe the foam structure in detail right after the foam was created at the four solutions shown above. In this study, the Bartsch method was used to create foams, whereby each sealed 50ml centrifuge tube containing the mixture was shaken ten times by hand with the same amplitude (Saxena et al., 2018). A camera and a computer were used to monitor and analyze the height of the foam column during its growth and decay, as illustrated in Figure 5.1. In this test, the time the foam completely disappeared was recorded. In the stability test, the time consumed to lose 50% of the foam volume (half-decay time) was measured (AlYousef & Schechter, 2019). Additionally, the LEICA Microsystem CME Compound Binocular microscope was utilized to observe the foam structure in detail and determine the link between foam stability and average bubble size. The foam height was determined by subtracting the overall height (foam and liquid) from the liquid height, as defined in Eq. 5.1:

$$H_{foam} = H_{foam+liquid} - H_{liquid} \quad (\text{Eq. 5.1})$$

where H_{foam} refer to the height of foam, cm; $H_{foam+liquid}$ refer to the total height of foam and liquid, cm; H_{liquid} refer to the height of liquid, cm.

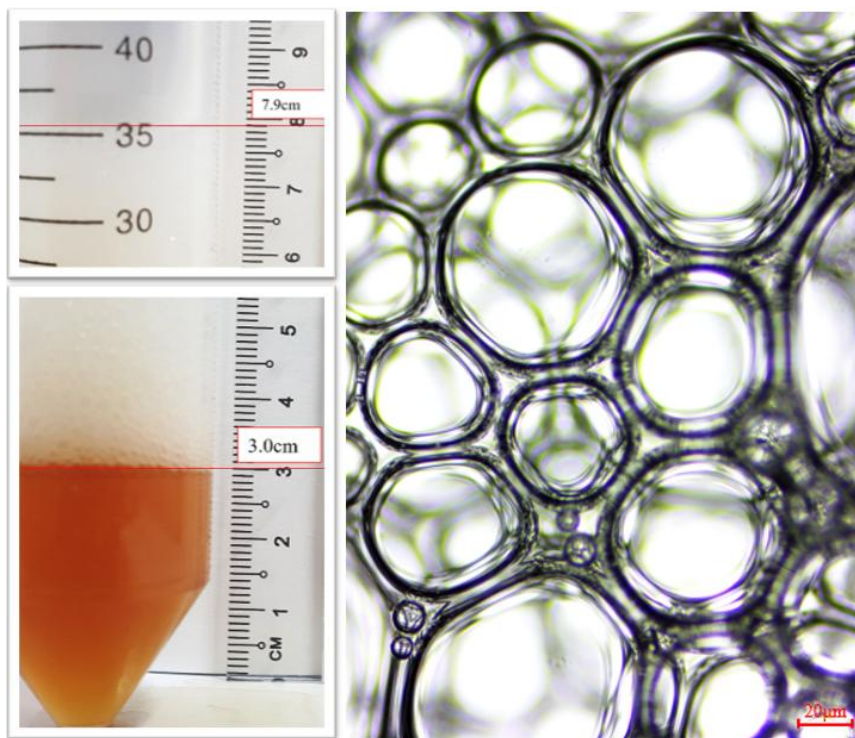


Figure 5.1: The foamability and bubble structure of 2wt% Soapnut saponin at 25°C

5.3 Results and Discussions

5.3.1 Salinity Effect

Overall, 100 solutions were mixed with a specific ratio for the conductivity test conducted in this section. The results are summarized in [Table 5.1](#).

For the 1st batch (pure NaCl), as the concentration of NaCl increases from 1000ppm to 55000ppm, the conductivity increase. It is because of the total dissolved ions and the overall ionic strength, which increased by increasing the concentration of salt conductivity. For instance, conductivity raised from 2.53ms/cm at 1000ppm to 118.2ms/cm at 55000 ppm. In the 2nd solution containing NaCl and NGF, the rise in conductivity was not as consistent as that of the 1st batch. It was found that the conductivity of the 2nd batch was slightly higher than the 1st batch (31.13ms/cm for 1st batch and 31.2ms/cm for 2nd batch at 14000ppm) before reaching 16000ppm salinity since the nanoparticles were extremely small particles with low ionic strength.

Table 5.1: Results of the conductivity tests on the green fluids

Salt Concentration (ppm)	NaCl Conductivity (mS/cm)	NGF Weight Percent (wt%)	NaCl+NGF Conductivity (mS/cm)	Soapnut saponin Weight Percent (wt%)	NaCl+NGF+ Soapnut saponin Conductivity (mS/cm)	Camellia oleifera saponin Weight Percent (wt%)	NaCl+NGF+Camellia oleifera saponin Conductivity (mS/cm)
1000	2.53	0.05	2.57	0.5	2.83	0.5	2.95
2000	4.16	0.05	5.49	0.5	6.66	0.5	6.7
3000	7.1	0.05	7.79	0.5	7.72	0.5	7.81
4000	9.05	0.05	10.6	0.5	10.45	0.5	11.02
5000	11.49	0.05	12.58	0.5	12.4	0.5	12.8
6000	13.1	0.05	14.51	0.5	13.99	0.5	14.59
7000	15.98	0.05	16.65	0.5	16.25	0.5	17.1
8000	17.2	0.05	17.9	0.5	17.75	0.5	18.42
9000	18.99	0.05	21	0.5	20.85	0.5	21.9
10000	20.53	0.05	22.8	0.5	23.15	0.5	24.21
12000	26.94	0.05	27.15	0.5	28.1	0.5	29.98
14000	31.13	0.05	31.2	0.5	31.6	0.5	32.79
16000	36	0.05	35.6	0.5	36.8	0.5	37.5
18000	41.2	0.05	39.8	0.5	43.5	0.5	45.21
20000	46.5	0.05	43.2	0.5	47.2	0.5	48.1
22000	50.82	0.05	47	0.5	52.1	0.5	53.4
24000	53.1	0.05	50.9	0.5	54	0.5	56.23
26000	57.7	0.05	53.5	0.5	57.5	0.5	58.95
28000	63.41	0.05	58.2	0.5	62.46	0.5	63.91
30000	69.8	0.05	63	0.5	70.3	0.5	71
35000	80.9	0.05	72.2	0.5	80.15	0.5	81.8
40000	89.8	0.05	82	0.5	90.3	0.5	92.03
45000	99.54	0.05	91.1	0.5	98.94	0.5	100.05
50000	108	0.05	101.5	0.5	107.5	0.5	110.2
55000	118.2	0.05	109	0.5	119.1	0.5	122.54

After passing 16000ppm, the conductivity of the solution starts to decrease. In fact, it was reduced from 46.5ms/cm (in 1st batch) to 43.2ms/cm (in 2nd batch) at 20000ppm salinity, 63.41ms/cm (in 1st batch) to 58.2ms/cm (in 2nd batch) at 28000ppm salinity, and 118.2ms/cm (in 1st batch) to 109ms/cm (in 2nd batch) at 55000ppm salinity. It could be due to the surface charge of nanoparticles and the electrostatic attraction force between salt molecules and nanoparticles ([Petkova et al., 2021](#)). Increasing the concentration of salts would bring more dissociated ions (Na^+ and Cl^-) into the solution, which would be adsorbed on the surface of nanoparticles (nanoparticles have high surface energy).

In the 3rd batch (NaCl+NGF+Soapnut saponin) and 4th batch (NaCl+NGF+Camellia oleifera saponin), 50mg of extracted saponin was added to each sample. In those solution systems, the specific conductance is dependent on the nature of the ions generated upon ionization, the nanoparticles added, and the presence of salt (NaCl). Both dispersed saponin molecules (monomers) are considered good electrolytes with a higher ionization degree. The conductivity increased from 2.83ms/cm to 119.1ms/cm (Soapnut saponin) and 2.95ms/cm to 122.54ms/cm (Camellia oleifera saponin) at 1000ppm and 55000ppm salinity, respectively. For 3rd batch and 4th batch, the conductivity was increased due to the addition of green surfactants. For example, at 18000ppm salinity, the 3rd batch and 4th batch conductivity showed 43.5ms/cm, and 45.21ms/cm, respectively, but it only achieved 39.8ms/cm at the 2nd batch. This is because the existence of saponin increases electrostatic repulsion and reduces the electrical charge density at the micellar surface ([Tran et al., 2022](#)). On the other hand, higher polar molecules' alignment is associated with a higher dielectric constant. The addition of saponin molecules would lower the polar molecules' average alignment, therefore decreasing the dielectric constant ([Y. Sheng et al., 2022](#)). Thus, the reduction of conductivity induced by the nanoparticles for 2nd batch could be compensated by surfactant, and the presence of salts did not have any detrimental impact on the performance of the green surfactants.

5.3.2 Foamability and Stability Test

Overall, 190 solutions have been tested at room temperature with designed additives and a specific mixing ratio. A camera monitored the height of growth and decay of the foam column after 0 hours, 1 hour, 3 hours, 5 hours, 8 hours, 10 hours, 15 hours, 23 hours, 29 hours, 39 hours, 51 hours, 57 hours, 61 hours and 80 hours. After capturing the photos, they were transferred to a computer for analysis.

5.3.2.1 Pure Saponins

This section conducted the foamability and foam stability tests on the pure Soapnut saponin and *Camellia oleifera* saponin with an increasing concentration from 10mg to 800mg (0.1wt% to 8wt%), respectively. The results obtained are shown in [Figure 5.2](#) and [Figure 5.3](#). As can be seen, both saponins can generate a large amount of foam (great foamability). It increased from 16mm at 0.1wt% to 83mm at 8wt% (Soapnut saponin) and 18.2mm at 0.1wt% to 90mm at 8wt% (*Camellia oleifera* saponin). The maximum length of the foam column increases linearly with the saponin concentration until it reaches its CMC point at 4.6wt% (Soapnut saponin) or 4wt% (*Camellia oleifera* saponin), which is 83mm or 90mm, respectively. In the foamability aspect, the *Camellia oleifera* saponin shows slightly better than Soapnut saponin, which contributes an extra 7mm foam length. In the foam stability aspect, both saponins deliver a great stable foam. The foam generated by *Camellia oleifera* saponin could last 61 hours, while the foam created by Soapnut saponin could stand 57 hours (both mixed with small saponin concentrations from 0.1wt% to 0.5wt%). The foam generation is mainly contributed by micelles formation, which indicates the foam with higher concentration tends to break and results in a rapid draining process.

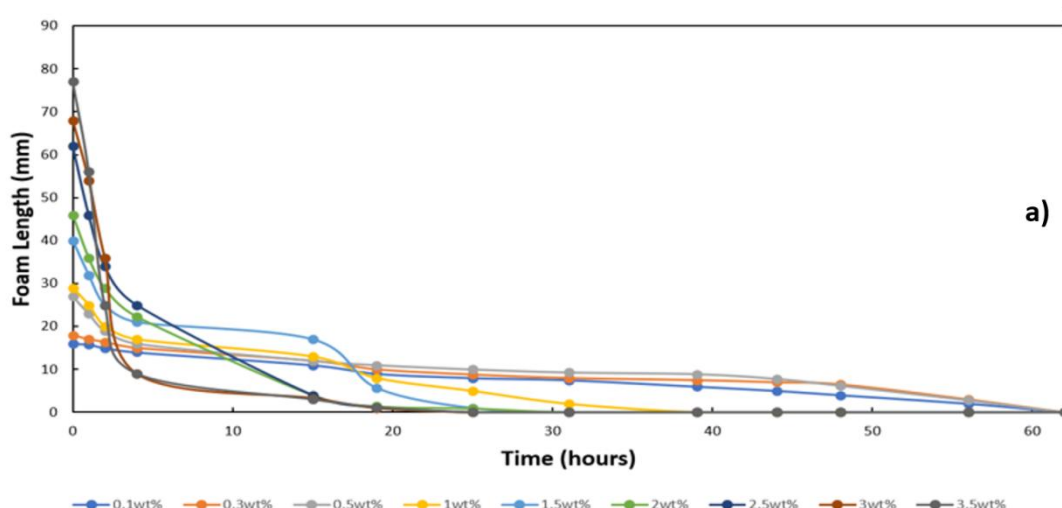
With all saponin concentrations, the height of foam declined as time went by. Moreover, the speed of the foam's structural collapse was proportional to the concentration of the saponins. A foam with a higher saponin concentration breaks down more quickly than foam with a lower concentration of saponin. Specifically, the foam generated by Soapnut saponin was able to last 57 hours (2.8mm) at 0.5wt%, whereas it was reduced to 10 hours (0.9mm) when the concentration was

raised to 7wt%. It was also observed that the surfactant concentration would highly influence foamability and foam stability. Take Soapnut saponin, for instance. The highest concentration ranged was 0.1wt% to 0.3wt%, could have its foam standing for 56 hours, while the shortest period of foam structure collapse was observed from the surfactant with 8wt% that stood only for 19 hours. And *Camellia oleifera* saponin reveals a similar behavior (the longest period was 61 hours at the concentration from 0.1wt% to 0.3wt%, and the shortest period only lasted 10 hours at 8wt%). The foam structure's collapse rate was essentially identical for saponin concentrations greater than the CMC. Most of the foam was only able to stand for less than 10 hours, and the foam length decreased along with the concentration (from 1mm to 0.8mm). It is mainly caused by the foam film's Gibbs elasticity declines with rising saponin concentration ([Petkova et al., 2021](#)). Furthermore, the rising saponin concentration also enhanced the impact of graviton force on foam drainage resulting in continuous liquid drainage from the space between bubbles, breaking the liquid films, and causing foam coalescence ([Mustan et al., 2022b](#)).

Specifically, two major mechanisms are related to the bubble's self-break (foam coalescence): liquid foam drainage and dynamic interfacial dilatational elasticity properties ([Peng et al., 2021](#)). Liquid drainage is an inevitable behavior. It occurs naturally due to gravitational force and differential surface pressure within the film lamellae and at the plateau's border. It leads to both lamellae and border thinning and raises their surface tension gradient, which reduces the relative amount of bulk liquid among the interfaces and pushes the liquid flow from the lowest surface tension to the thinner region ([Almobarky et al., 2018](#)). Therefore, foam bubbles approach one another and may collide, resulting in their collapse. Usually, the high liquid foam drainage behavior causes the reduction of net foam volume, and it occurs at the initial phase after the foam is generated. At first, the foam includes an excessive amount of liquid, making it moist. As the liquid drains, the volume proportion of liquid in the foam decreases, so the foam volume decreases ([Jones et al., 2016](#)). The foam becomes dry when drainage is nearly complete, particularly in the upper section (higher gas volume fraction vs. liquid). Dry foams have extremely thin lamellae, which enhances the potential of foam

collapse. The second mechanism, dynamic interfacial dilatational elasticity properties, occurred after the liquid foam drainage process. The saponin molecules or micelles start to diffuse, reorientate and adsorb on the interface and decrease the surface tension (Jones et al., 2016). Increasing the saponin concentration increases the amount to which saponin molecules adsorb at the contact. Surface tension does not change significantly compared to the interface's surface area, so elasticity decreases. It had stated that low elasticity results in a less stiff foam structure that is prone to collapse.

In terms of surfactants ionicity, the anionic surfactant (*Camellia oleifera* saponin) was expected to generate more stable foam films at much lower surface coverage (i.e., increased surface mobility) due to increased surface mobility and due to the significant electrostatic repulsion between the charged surfactant molecules on the film surfaces (Petkova et al., 2020). In contrast to the foam films of nonionic surfactant (Soapnut saponin), with the extremely high surface coverage and a high dynamic Gibbs elasticity, they stabilized primarily through steric interactions with very short ranges, and complete adsorption layers were required to stabilize foam and emulsion films (Peng et al., 2021). Therefore, the *Camellia oleifera* saponin performed better than Soapnut saponin in terms of foamability and foam stability.



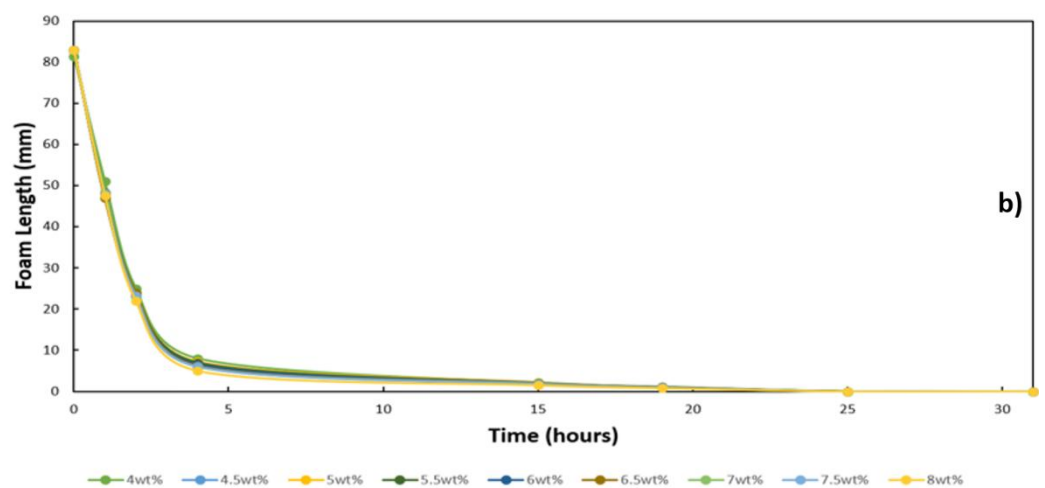


Figure 5.2: Foam height vs concentration of Soapnut saponin. a) 0.1wt%-3.5wt%, and b) 4wt%-8wt%

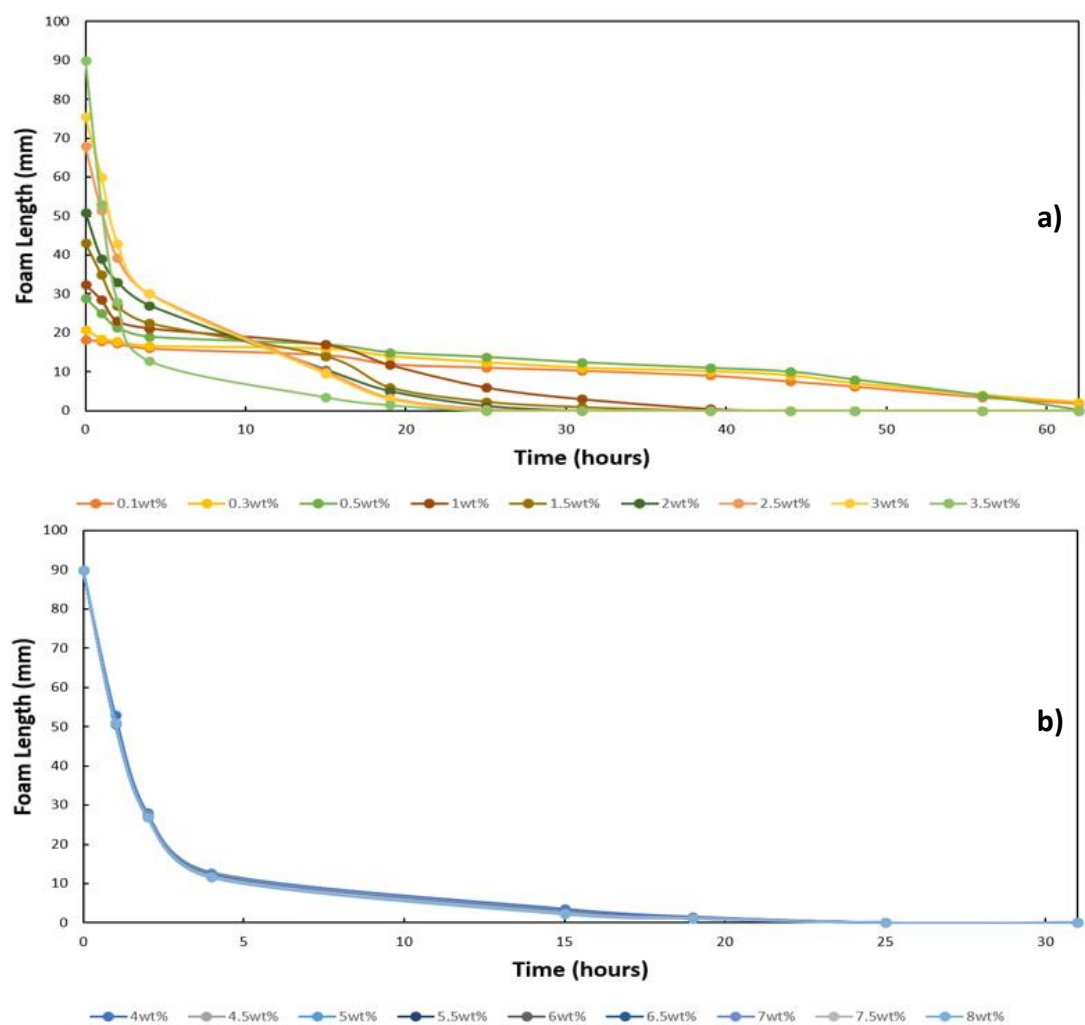


Figure 5.3: Foam height vs. concentration of Camellia oleifera saponin. a) 0.1wt%-3.5wt%, and b) 4wt%-8wt%

5.3.2.2 Foam Bubble Structure (Soapnut saponin and Camellia oleifera saponin)

The link between foam stability and the average foam bubble size was determined and depicted in Figure 5.4. An ascending trend was observed for the average bubble diameter when the saponin concentration was increased until approaching the CMC point. For Soapnut saponin, the average bubble diameter increased from 18.9 μm to 48.3 μm when the concentration raised from 0.1wt% to 8wt%. Camellia oleifera saponin's average bubble size is slightly larger than the bubble generated by Soapnut saponin. The bubble diameter remained almost constant, passing the CMC (4.6wt% for Soapnut saponin and 4wt% for Camellia oleifera saponin).

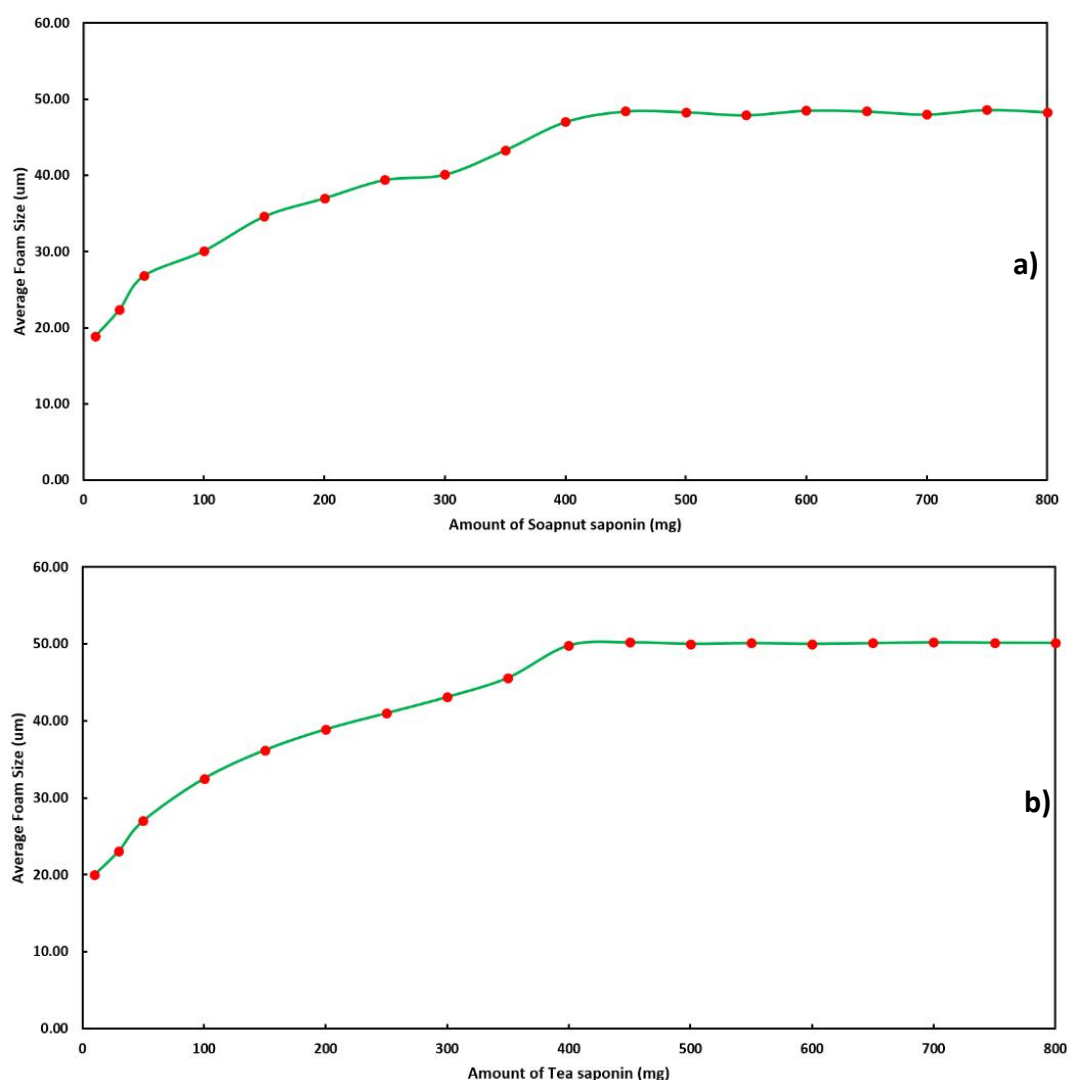


Figure 5.4: Average foam size of saponins. a) Soapnut saponin, and b) Camellia oleifera saponin with various concentrations

The bubble diameter variation seems to be directly related to the concentration of saponin surfactant. The increasing saponin concentration brings more saponin molecules to the bubble surface ([Marčelja, 2006](#)). It promotes the frequency of collisions between bubbles and further stimulates bubble coalescence, in which the adjacent bubbles in a liquid medium coalesce a larger bubble. Surfactants influence the kinetics of bubble diameter by affecting the interface's wettability condition, the dynamic adsorption (DA) of saponin molecules at the liquid/gas interface in microchannels, and the liquid phase's physical properties ([Giribabu et al., 2007](#)). Hence, the diameter of bubbles was influenced by both capillary quantity and the wetting qualities of the bubble surface.

Furthermore, capillary pressure and gas concentration gradient also has been reported that influence the bubble size. At ambient temperature and pressure, the bulk fluid around bubbles was saturated with gas, and it is not anticipated that any mass transfer will occur within the bulk fluid due to the air concentration gradient between the bulk fluid and the bubbles' interfaces ([Jones et al., 2016](#)). Nevertheless, pressure variation (capillary pressure variation) has been recorded between the neighboring bubbles because of their size difference. The pressure inside the smaller bubble is greater than the larger bubbles. As a result of the Young–Laplace effect, the air is transported (adsorbed) from the small bubble to the adjacent larger bubble, resulting in coarsening of big bubbles while small bubbles vanish and therefore increase the bubble size ([Pasdar et al., 2018](#)). This behavior is also called inter-bubble gas diffusion or disproportionation.

It is worth noting that bulk fluid cannot dissolve and retain additional air inside itself at atmospheric pressure, and any dispersed air added to the bulk fluid by small bubbles will be devoured by large bubbles via inter-bubble gas diffusion ([Parhizkar et al., 2015](#)). As a result, small bubbles become smaller as large bubbles become larger, causing the bubble's size to continue to expand to the larger diameter at a rate largely dependent on the air diffusivity, shown in [Figure 5.5](#).

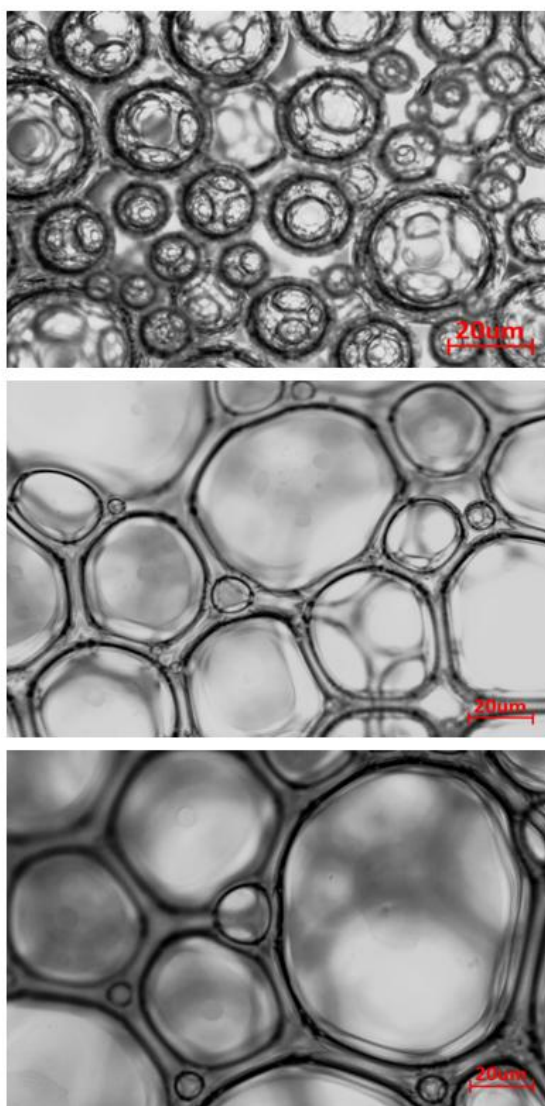


Figure 5.5: Average bubble size at the Soapnut saponin of 0.3wt% (top), 3wt% (middle), and 5.5wt% (bottom)

5.3.2.3 Pure Saponins at 85°C

In order to evaluate the foamability and foam stability of the extracted green surfactants at an actual reservoir temperature, 36 portions of the saponins solutions were tested and presented in [Tables 5.2 and 5.3](#). It was observed that the foamability (height of foam) of both saponins increases substantially (approximately twofold) when the temperature increases to 85°C. For Soapnut saponin, with the same concentration of 0.1wt%, foam height increased from 16mm at room temperature (25°C) to 30mm when the temperature increased to 85°C. For *Camellia oleifera* saponin, under the same concentration of 4wt%, the foam height increased

almost double from 81mm at 25°C to 157mm at 85°C. Physicochemical parameters of the saponin solution, such as viscosity and density, are affected by temperature.

Both tend to decrease when the solution of temperature increases, further promoting the bubble coalescence and boosting. The reason for this phenomenon was simple: the increasing temperature resulted in increased bubble velocity and a corresponding enhancement in the rate of saponin molecules being transported to the rising bubble surface through the convective diffusion; then this impact occurred as a result of the growing bubble deformation rate (the rise in the bubble diameter by enhanced drag force on column walls, which attributed to the wall effect) ([Borkowski & Zawala, 2021](#)). Specifically, the saponin adsorption density, buoyancy force, dilational and interfacial shear modulus also increased with increasing temperature. Therefore, the small bubbles generated by saponins became easier to merge and shift to the larger size. Furthermore, the increasing temperature also increases the bubble terminal velocity ([Oetjen et al., 2014](#)).

Table 5.2: Foamability and foam stability test of Soapnut saponin at 85°C

Weight Percent (%)	Amount (mg)	Ultrapure water (ml)	0 hrs Length(mm)	0.5 hrs Length(mm)	1 hr Length(mm)	1.5 hrs Length(mm)	2 hrs Length(mm)	4 hrs Length(mm)	8 hrs Length(mm)	16 hrs Length(mm)	24 hrs Length(mm)
0.1	10	10	30	25	19.5	15	12	10	7.6	5	0
0.3	30	10	34	28.6	21	18	15	12.8	9	7	0
0.5	50	10	49	41	28	17	15.3	13	9.8	8.2	0
1	100	10	58	50	34.1	22	17	15.8	13	11	0
1.5	150	10	76.5	62	45	30	20	18	14.6	8	0
2	200	10	89	70	55.2	41	29	25	14	6.7	0
2.5	250	10	120	92	71	49	25	20.3	13	6.5	0
3	300	10	138	106	80	40	22.3	18	12.2	6	0
3.5	350	10	148	113	69.5	38	23	16.2	13	5.8	0
4	400	10	155	108	68	37.6	24	17	12.8	6	0
4.5	450	10	166	96.5	68	36	23.4	17	13	6	0
5	500	10	166	97	66.6	37	22.8	16.3	13	6.3	0
5.5	550	10	166	98	67.2	36.2	23	17	12.9	6.1	0
6	600	10	166	97.2	67	37	23.2	17.4	13	6.1	0
6.5	650	10	166	97	67.5	37.1	22.9	16.8	12.5	6	0
7	700	10	166	97	66	36	23.5	15	13.2	6.2	0
7.5	750	10	166	97.4	67.5	36.7	23.8	17	13	6	0
8	800	10	166	97.8	67.6	36	23	16.5	12.7	6	0

Table 5.3: Foamability and foam stability test of Camellia oleifera saponin at 85°C

Weight Percent (%)	Amount (mg)	Ultrapure water (ml)	0 hrs Length(mm)	0.5 hrs Length(mm)	1 hr Length(mm)	1.5 hrs Length(mm)	2 hrs Length(mm)	4 hrs Length(mm)	8 hrs Length(mm)	16 hrs Length(mm)	24 hrs Length(mm)
0.1	10	10	38.7	36	24	20	16.2	12	10	8	0
0.3	30	10	49	42	29.6	26	21	17.5	14	10.3	0
0.5	50	10	58	50.1	35	31.4	27	21	17.5	14	0.3
1	100	10	76	65	41	35	30	25	20	13.5	0.2
1.5	150	10	89.3	78.5	50	42.8	37	30.4	23	13	0.2
2	200	10	100	90	62	50	41.2	29	21.4	12.1	0.1
2.5	250	10	138.5	101	69.8	56	40	25.1	19	11.6	0
3	300	10	150	116.2	73	55.4	37	21	17.5	11.1	0
3.5	350	10	157	120	80	49	34.8	19.6	15	10.4	0
4	400	10	166	129.3	89.8	40.1	31	18	13.6	9	0
4.5	450	10	166	129	94	39.5	30.5	16	14	11	0
5	500	10	166	129.5	90	43	34	18	13.8	9.3	0
5.5	550	10	166	129	91	40	29.5	18	15	10	0
6	600	10	166	129	90.8	41	30.8	17.5	14	9.8	0
6.5	650	10	166	129.2	88	39	28	22	17.2	8.5	0
7	700	10	166	128.9	90.6	39.6	30.6	17.6	13.9	9	0
7.5	750	10	166	129.4	90.2	38.5	29	21.3	14	10	0
8	800	10	166	129	91	42	33	17	14.5	9.5	0

When the foam height achieved the highest level, the new foam creation with bubble coalescence and foam drainage reached equilibrium. Coarsening behavior is when bubbles move between adjacent ones, altering their structure and topology as liquid travels through the film (lamella) (Thakore et al., 2020). It is related to the Ostwald ripening phenomena and pressure variation, in which gas spreads from smaller bubbles to larger bubbles. In this case, bubble coarsening to enhance the foam height was caused by the lamellae break between neighboring bubbles triggered by temperature fluctuations (Rodríguez et al., 2020). Drainage includes gravity-driven via the plateau borders or the liquid network inside foams and capillary suction-driven from the lamellae into the plateau borders. In general, three factors may contribute to boosting the foam coalescence to form a higher foam height at high temperatures (H. Wang et al., 2017):

- 1) The increasing temperature increases the diffusion kinetics in saponin's molecules allocation at the air-water interface, and a variation influences the film drainage in hydrodynamic boundary conditions.
- 2) The increasing temperature changed the surface rheology, weakening the liquid film between neighboring bubbles and promoting bubble coarsening.
- 3) Furthermore, when the temperature is above the lower critical solution temperature, the saponin aggregate and causes the bubble's thin films to bridge since the surface shear modulus (changes from viscous to elastic) and dilatational modulus increase along with the temperature.

However, it negatively affects the bubble coalescence process by attenuating the liquid film thickness that splits each bubble, which slightly boosts the foam height while substantially reducing the foam stability (Issaoui & Ben Mansour, 2019). Furthermore, it is worth noting that foamability was greater along with the temperature, but the foam was less stable at the higher temperature. When the temperature increased from 25°C to 85°C, the stability of the foam decreased from 57 hours to 16 hours (Soapnut saponin), and *Camellia oleifera* saponin reduced from 61 hours to 24 hours. The foam stability was dominated by three factors: coalescence, liquid drainage, and coarsening. Coalescence is the process by which gas diffuses over the liquid film between adjacent bubbles due to

a variation in Laplace pressure (Thakore et al., 2020). Liquid drainage behavior is defined as a downward liquid movement caused by gravity. Usually, foams can become more stable by minimizing the liquid drainage behavior. Coalescence happens when the volume fraction of the liquid interface reaches equilibrium status, and it leads to the bubble's lamella breaking, isolating each bubble until it completely evaporates over time (Rodríguez et al., 2020). Therefore, two reasons are responsible for the decreased foam stability (shorter foam life) at higher temperature: 1) Higher temperature decrease the surface viscosity and boost the gas diffusion rate, therefore, inducing faster liquid drainage among bubble's lamella; 2) Higher temperature enhanced the kinematic velocity of the ions then triggered a higher frequency of ion collisions (Brownian motion) (Thakore et al., 2020).

5.3.2.4 The Combination Between Saponins, Nanoparticles, and Salt

The structure of the foam changes irrevocably over time due to four different activities: 1) film drainage, 2) capillary suction, 3) gas diffusion and 4) particles interaction. The term "foam stability" indicates preserving the foam's structure over an extended period while being thermodynamically unstable (Petkova et al., 2021). As discussed previously, nanoparticles' extremely small size, high surface energy, huge surface area to volume ratio, and physical/chemical stability enable them to efficiently improve the solution's stability. Additionally, salts can increase the efficacy of macroscopic sweeps in porous media and affect the wettability condition. Therefore, in this section, three substances, including NaCl, NGF, and Soapnut/Camellia oleifera saponin, were mixed with a specific ratio and blended with 10ml ultrapure water. Overall, this section contains 52 solutions within two parts. All solutions have the same saponin concentration (0.5wt%) since they could produce the longest foam stability. The first part includes 14 solutions (7 for Soapnut saponin and 7 for Camellia oleifera saponin), and the only additive was nanoparticle (NGF), with the concentration increased from 0.001wt% to 0.005wt%. The second part contained 38 hybrid solutions, including salt (NaCl) and nanoparticle (NGF) as additives. The NGF concentration remained at 0.003wt%

because it can deliver the best foam stability. And the saponin concentration was the same as above.

5.3.2.4.1 The Presence of Nanoparticles

All the tests were conducted at room temperature. According to [Figure 5.6](#), the foam length of both saponins increased along with the NGF concentration until it reached the threshold (0.003wt%). For Soapnut saponin, it increased from 27.1mm (0.001wt%) to 28mm (0.003wt%), then decreased to 26.8mm (0.005wt%). Similar results also happened in *Camellia oleifera* saponin. The foam length started to increase from 29.5mm at 0.001wt% to 30.6mm at 0.003wt%, then decreased to 29.3mm at 0.005wt%. Compared to the tests conducted by only pure saponins, the additional NGF was able to add approximately 2mm foam length. And it successfully improves the foam stability from 57 hours to 80 hours. The optimum concentration of NGF was located at 0.003wt% for both saponins. The foam could stand from 28mm until 80 hours at 1.3mm. The results show slightly better for *Camellia oleifera* saponin, mainly contributed by the electrostatic repulsion forces between similar charged NGF particles and *Camellia oleifera* saponin (negative charged) ([Almubarak et al., 2020](#)). It starts at 30.6mm and lasts 80 hours at 2.3mm.

The added NGF generally contributes to the enhancement of nanoparticle (NGF) on foam's stability could effectively adsorb and aggregate at bubble films and Plateau borders, thereby raising the maximum capillary pressure and particle detachment energy prior to foam coalescence, decreasing the direct interface contact between adjacent bubble's lamella, slows film drainage, gas diffusion and mitigate the tendency of bubble break ([Shojaei et al., 2021](#)). In foam systems, detachment energy is the energy required to detach particles from the liquid-gas interface. Due to the high surface energy (or detachment energy in this case) of NGF, the adsorption at the liquid-gas interface of bubbles is considered non-reversible, whereas other common additives experience an easily adsorb and desorb process ([Z. Xu et al., 2020](#)). Furthermore, the particle's dispersibility is enhanced through saponin molecules adsorbed onto the NGF surfaces. Consequently, the surface activity increased, and the interface layer structure improved. Thus, both the

maximum capillary pressure and the strength of the bubble's film were enhanced in the company of NGF.

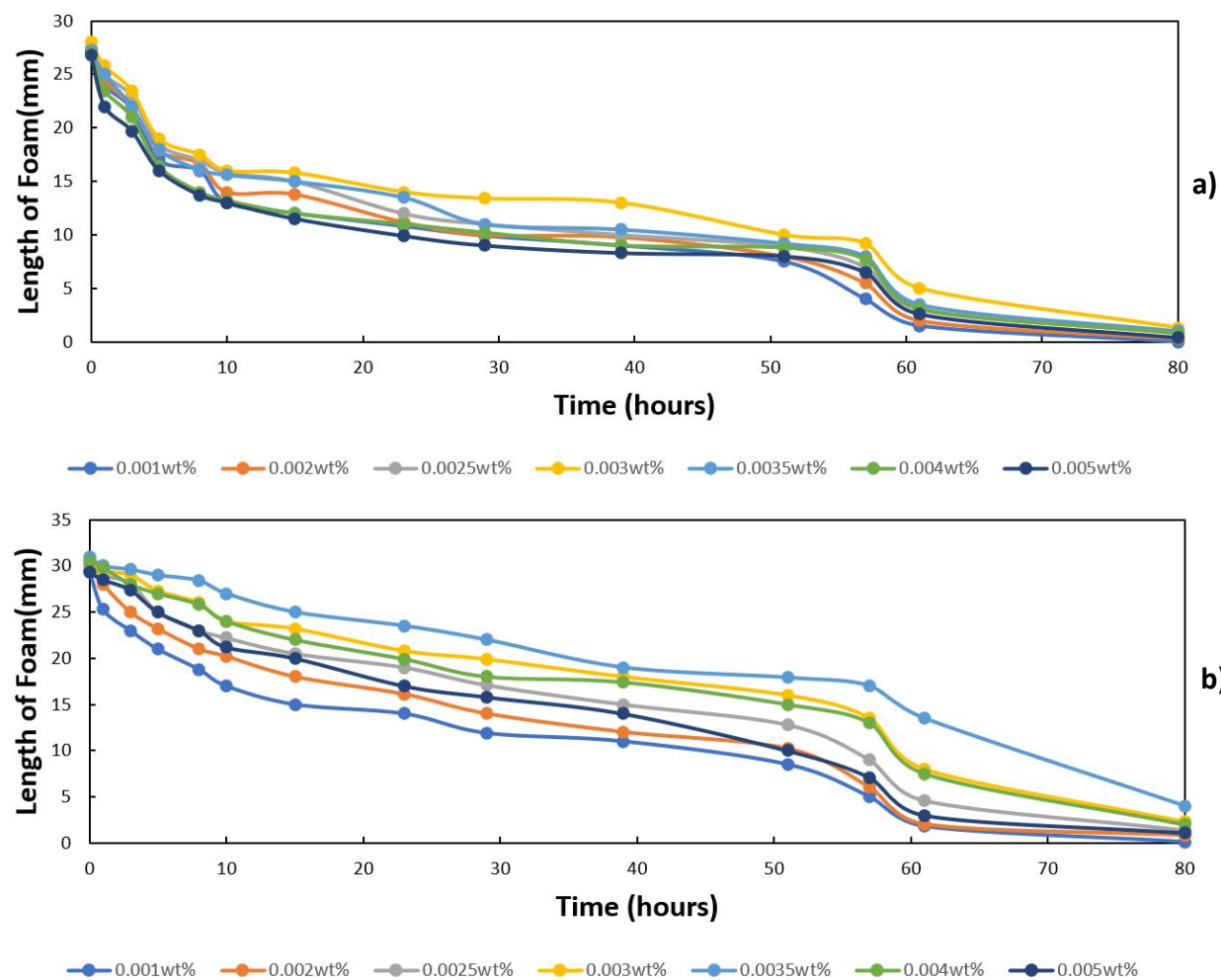


Figure 5.6: The saponin foam height vs. time under increasing NGF concentration. a) Soapnut saponin, and b) Camellia oleifera saponin

In addition, with the extremely small size, NGF can easily penetrate the liquid film and arrange themselves as a monolayer of bridging particles, and a densely packed bilayer of particles, aggregating into a network at the liquid-gas interface (Almubarak et al., 2020). It also is verified that the extremely small size can generate stronger foam due to their increased diffusivity and interface. NGF can also further lower the interfacial rheological properties (bubble's surface tension) and capillary pressure by reducing the gas diffusion rate and pressure variation between neighboring bubbles, lowering the bubble's film permeability to gas and promoting foam generation, propagation, and stability (Prodanovic & Johnston, 2017). Furthermore, the presence of NGF produces dense solid bubble film (higher viscosity) that efficiently inhibits the gas diffusion in the foam column and mitigates the foam liquid membrane from thinning/drainage process. As a result, the bubble's coalescence and disproportionation are slowed. The thickness of the bubble's film reduces as capillary pressure rises, eventually leading the bubbles to rupture when the pressure overcomes the threshold (maximum capillary pressure) (AlYousef & Schechter, 2019). The nanoparticles can cause a pressure drop (pressure variation) and generate firmer foam, increasing along with the nanoparticle's concentration. It is worth noting that the bubbles containing NGF break from the boundary, while the bubbles without NGF develop by diffusion-controlled coarsening.

5.3.2.4.2 The Presence of Salt

Salt has an uncertain influence on the foamability and foam stability of froth. While some researchers have discovered that additional salt accelerates the foam's collapse and destabilizes the foam, others have discovered that salt can increase the stability or have a neutral effect. In order to get a better understanding of the relationship between the effect of salt/salinity, a series of experiments (19 sets for each saponin) were carried out to evaluate the influence of salinity on foamability and foam stability. Like the previous tests, the longest time scale (80 hours) was applied in order to make sure to record all effects on foamability and foam stability. Both saponin concentration (0.5wt%) and NGF concentration (0.003wt%) were kept constant throughout the tests, while the salinity was varied (increased from

1000ppm to 100000ppm). According to the results presented in [Figure 5.7](#) and [Figure 5.8](#) below, it is readily apparent that the foamability/foam height increases along with the concentration of NaCl until it exceeds the limitation (for Soapnut saponin is 60000ppm, and Camellia oleifera saponin is 80000ppm). The addition of NaCl has a substantial impact on the volume of foam (foamability). For Soapnut saponin, the length of foam increased almost twofold when the salinity reached 20000ppm, from 28mm to 47mm. Camellia oleifera saponin also presented similar results: foam length boost from 30.6mm to 50mm when salinity increased from 0 to 20000ppm. The highest foam length was achieved by Soapnut saponin was at 20000ppm salinity with 47mm. For Camellia oleifera saponin, it shows 50mm foam length at 20000ppm salinity. However, the addition of NaCl significantly reduces the foam's stability. For Soapnut saponin, the foam stability decreased from 80 hours at 1.3mm to 57 hours at 0.1mm. For Camellia oleifera saponin, the foam stability declined from 80 hours at 2.3mm to 57 hours at 1mm.

The salt concentration directly controls the number of saponin molecules absorb at the air/water interface, consequently, the foam length. The salt contained several ions (Na^+ and Cl^- for NaCl), and ions with different valences influence the saponin adsorption because of the screening of electrostatic charge ([Obisesan et al., 2021](#)). It mainly leads to variations in the counterions' hydration radius and significantly diminishes the interface potential through their binding. The length of foam is determined by the diffusional movement of saponin from the bulk solution to the air/water interface, and the thin foam film governs the foam stability and film drainage, which is directly related to the van der Waals forces, London dispersion forces, electrical double layer, hydration, gravitational force, viscous force, and surface tension ([Majeed et al., 2020](#)). The foam length of Soapnut saponin starts to increase from 1000ppm (28mm) until it reaches the threshold of 20000ppm (47mm), and Camellia oleifera saponin rises from 1000ppm (29.8mm) until it reaches the threshold of 20000ppm (50mm). It significantly improved Soapnut and Camellia oleifera saponin's foamability compared to the original foam length of 28mm and 30.66mm, respectively. The relatively low salt concentration slightly increases the zeta potential shrinks the electrostatic double-layer, causing a lesser electrostatic

repulsion force between the colloid particles ([Hadian et al., 2020](#)). It favors the diffusivity and absorption of the saponin molecules throughout the bulk solution also slows down the instance bubble burst after foam formation.

Furthermore, the appropriate salt concentration may improve the foam structure from thermodynamically unstable to stable by electrostatic repulsion force modification. Due to the reduced electrostatic double-layer repulsion force, the bulk solution produced smaller and stronger bubbles, enabling the liquid lamella to be packed tightly between bubbles ([Behera et al., 2014](#)). The additional NaCl also reduces the solubility in the solution, thus decreasing the hydrophobic interaction between water and saponin molecules and increasing the foam stability by slowing the bubble coalescence rate. The film thickness also plays an essential role since it may become less than the critical thickness due to the formation of the Newton black film ([Majeed et al., 2020](#)). Therefore, more saponin molecules adsorb at the air/water interface and enhance foamability.

However, the foam length of Soapnut saponin drastically decreased from 40mm (30000ppm) to 16mm (100000ppm) and 46.3mm (30000ppm) to 18mm (100000ppm) for *Camellia oleifera* saponin. On the other hand, the zeta potential dropped as the salinity increased, owing to the increased concentration of Na^+ and Cl^- along with the interface. As mentioned before, in the presence of salt (NaCl), the foamability and foam stability are mainly controlled by foam film related to the van der Waals forces, film drainage, electrical double layer, and electrostatic repulsion force ([Obisesan et al., 2021](#)). In the presence of salt, Newton black films are located at the bobble wall (lamellar) with a thickness between 4nm to 50nm. Short-range forces easily influence this kind of thin metastable film, and the thick films with a thickness larger than 100nm it generally affected by electrostatic repulsion force and van der Waals forces ([Tran et al., 2022](#)). When the NaCl concentration is sufficiently high, the formation of micellar structures inside the foam film becomes incapable, and the film's stability is reduced. The high NaCl concentration thins the foam film through drainage, forcing the counterions to congregate in a small area. And the double layers on each surface start to approach and overlap (electrical double layer expansion) ([Hadian et al., 2020](#)).

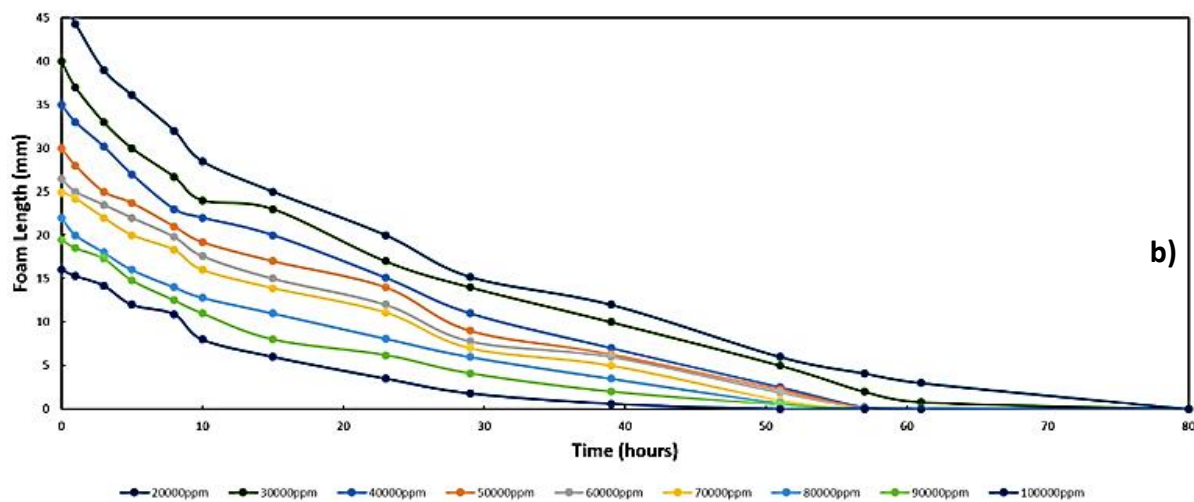
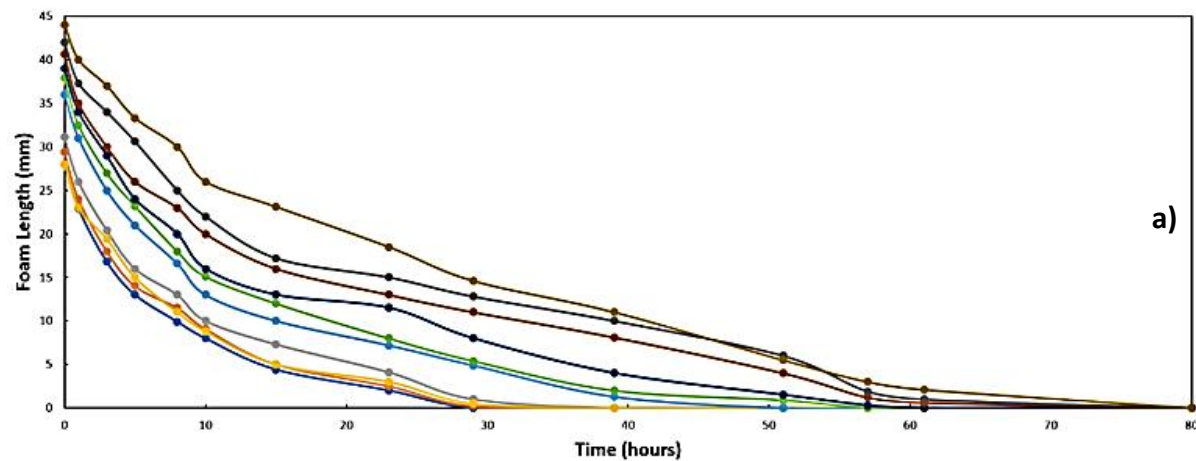
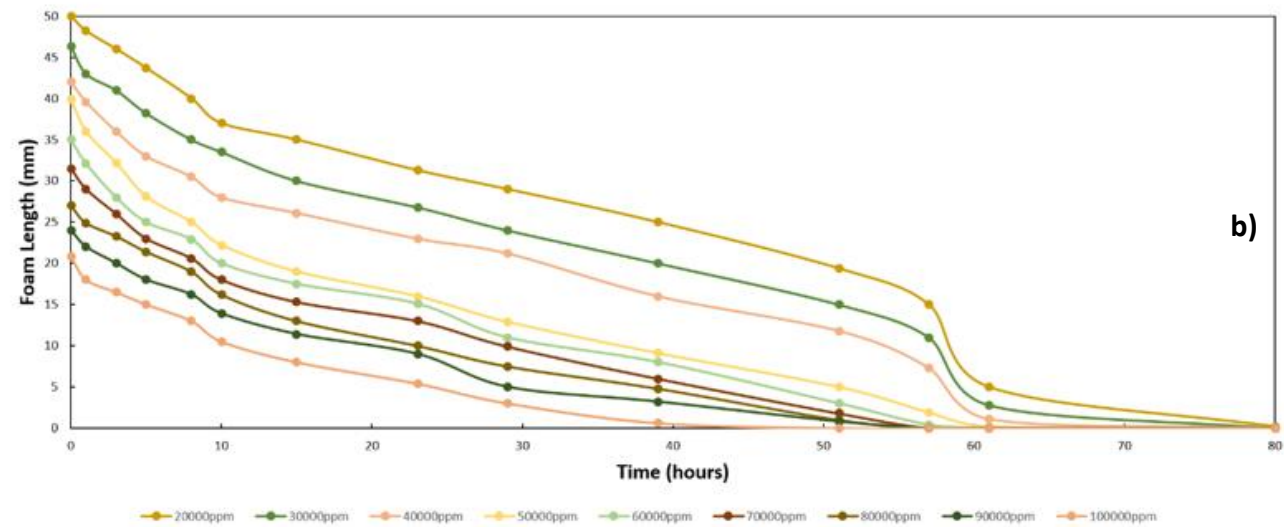
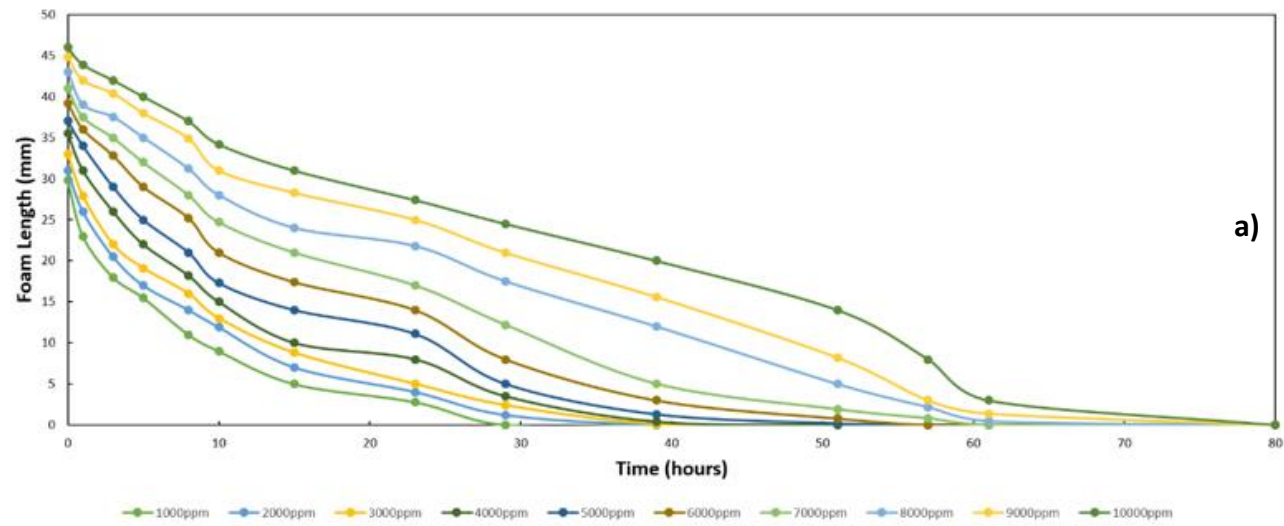


Figure 5.7: Soapnut saponin foam height vs. Time with NGF under increasing salinity. a) 1000ppm-10000ppm, b) 20000ppm-100000ppm



Then the counterions bonding with excessive NaCl ions decreases Debye length and surface potential, which diminishes the electrical double layer repulsion force in the foam film. As a result, the foam stability decreased from 80 hours at 28mm to 39 hours at 0.6mm (Soapnut saponin). And for Camellia, oleifera saponin was reduced from 80 hours at 30.6mm to 39 hours at 1mm.

5.3.2.4.3 The Presence of Crude Oil

When the generated foam contacts with oil, it must maintain its stability to provide reasonable mobility control successfully. Although there is a wide range of experiment data related to the foam–oil interaction, it still lacks consistent/well-accepted results. This section added 2ml of crude oil separately in 4 solutions. In order to compare the difference in foamability and foam stability, the composition and weight percentage are the same as in the last section (5000ppm or 20000ppm NaCl with 0.003wt% NGF and 50mg saponin). According to previous research, the presence of oil has a destabilizing effect on the foam since the foam stability is determined by the low molecular weight components of crude oil and causes a shorter lifespan of foam films. The foamability and foam stability mechanisms in the presence of crude oil are mainly summarized as 1) liquid film thinning, 2) oil droplets diffusing at the air/water interface, 3) unstable oil bridges in foam films, 4) and the stability of the pseudoemulsion film. The capacity of crude oil to access the air/water interface is an essential requirement for the rupture of foam lamellae.

Furthermore, the stability of the pseudomeulsion film also plays a critical factor in foam stability since it will directly lead to the burst of foam lamellae. The entering crude oil further aggravates the unstable condition of foam thermodynamics by thinning the pseudoemulsion film and invasion the lamella layer ([Lin et al., 2021](#)). After that, the air/water interface grows due to the crude oil spreading heavier and oil-form bridging. Then the foam film becomes thinner until it is finally ruptured ([Mustan et al., 2022a](#)).

The results are presented in [Figure 5.9](#). Both saponins solutions could generate the most stable foam when no crude oil was present. The foam decay period is first generalized by a rush fall in foam length, followed by a relatively

extended moderate degradation rate. For Soapnut saponin that contains 5000ppm salinity, the foam length of "solution without oil" was able to stand 39 hours at 1.3mm, while the stability of "solution with oil" dropped to 29 hours at 1.1mm. Similar results were shown in *Camellia oleifera* saponin; the longest foam stability was achieved by the "solution without oil" at 51 hours (0.2mm), whereas the foam column decreased to 39 hours (0.9mm) when oil was introduced. As shown in Figure, the foam height immediately went into a sharp degradation period once the foam was generated until the time reached 10 hours. It is worth noticing that the degradation rate of the "solution with oil" was higher than the "solution without oil." It was mainly caused by the bubbles coalescing at the top of the foam column, resulting in the broader bubble size distribution, altering the foam texture ([Hadian et al., 2020](#)). After that, the changed texture repartitioned the crude oil position in the foam column by localized accumulation. With the gravity drainage mechanism, the accumulated crude oil droplets were drained through the lamellae to the Plateau borders and formulated an extra oil phase at the air/water interface, resulting in a faster bubble coalescence rate ([L. Zhang et al., 2019](#)). Thus, the foam column of Soapnut saponin went through a harsh decaying period from 36.5mm to 7mm at 5000ppm and 48mm to 27.3mm at 20000ppm. Likewise, in the first 10 hours, the foam length of *Camellia oleifera* saponin decreased from 36.8mm to 14mm at 5000ppm and 51.5mm to 35.1mm at 20000ppm.

After passing 10 hours, the foam column presented a similar trend to "solution without oil." It decreased almost linearly with time over a long period, demonstrating a stable diminish of the volume of bubbles. However, the foam height and the stability were notably less in the case of "solution with oil." For Soapnut saponin, the foam length slowly decreased from 7mm to 1.1mm after 19 hours at 5000ppm and dropped from 27.3mm to 0.2mm after 51 hours at 20000ppm. *Camellia oleifera* saponin also presents similar results, in which the foam column reduced from 14mm to 0.9mm after 29 hours at 5000ppm and declined from 35.1mm to 3mm after 51 hours at 20000ppm. At the same time scale (23 hours) and salinity (20000ppm), the foam length of Soapnut saponin decreased from 20mm to 17mm, and *Camellia oleifera* saponin dropped from 31.3mm to

26mm in the presence of oil. Therefore, it can conclude that the presence of oil diminishes the stability of the foam

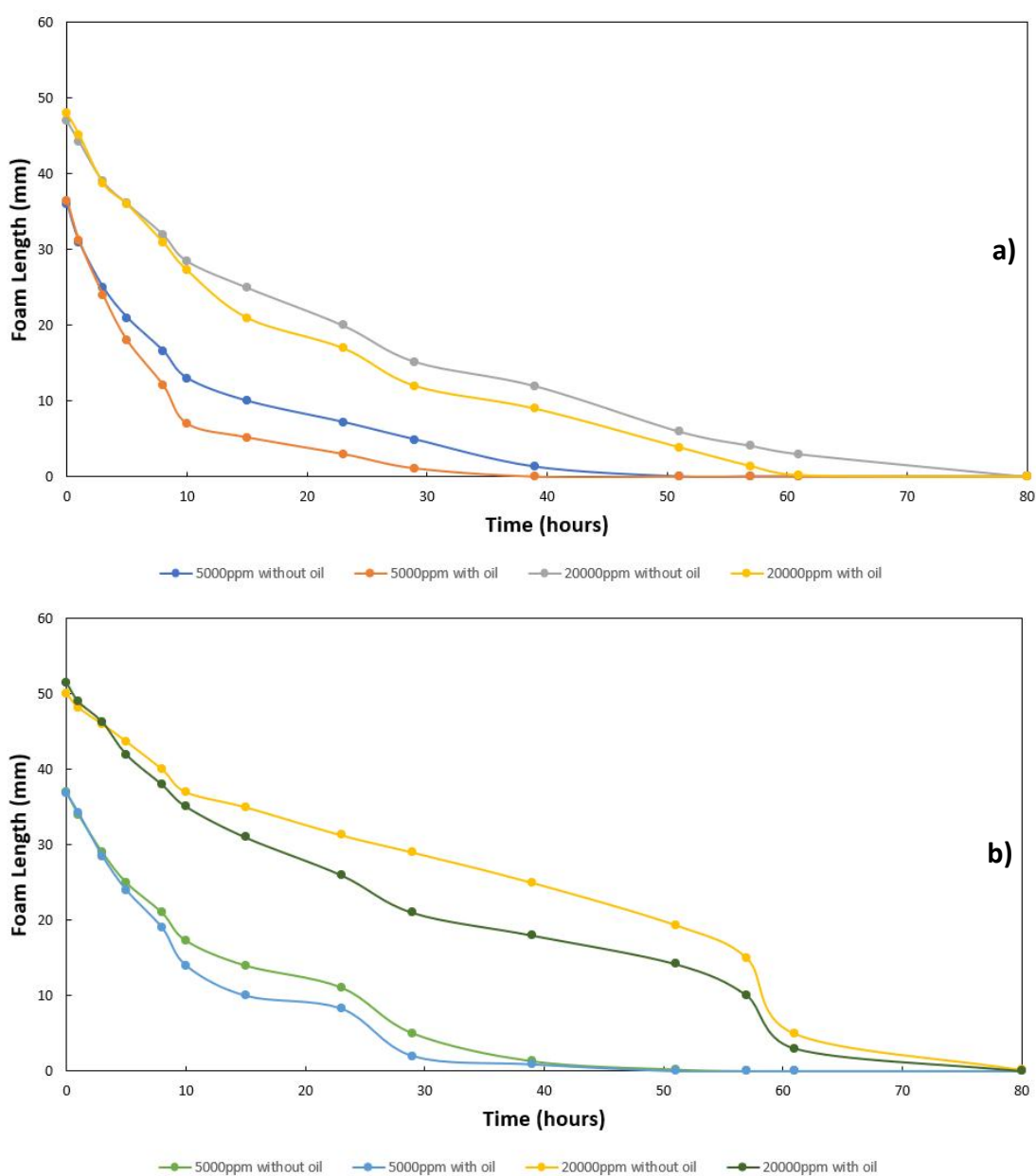


Figure 5.9: Soapnut saponin foam length vs. time in the absence and presence of crude oil. a) Soapnut saponin and b) Camellia oleifera saponin

Also, the Camellia oleifera saponin possesses better foamability and stability in the presence of crude oil. As mentioned above, the rapid foam decomposition during the "first 10 hours" period was mainly caused by gravitational drainage. However, this mechanism became weak when the bubble distribution became

much wider, and the size of the bubbles showed disunity during the "after 10 hours" period. The dominant mechanisms governing the foam stability at the "after 10 hours" period can be summarized as Ostwald ripening and bubble coalescence. The crude oil droplets tend to dissolve in micelles formed by saponins and reduce the number of micelles by decreasing electrostatic repulsion force. It hinders the stratification behavior occurrence in foam films, resulting in a continuous disintegration of the foam column (Behera et al., 2014). Furthermore, crude oil's presence also enhances the disjoining pressure at the air/water interface by emulsification and imbibition of oil. As a result, the thinning rate of the pseudoemulsion films was able to reduce and bring a relatively mild foam rupture period (Obisesan et al., 2021).

5.4 Conclusion

In this chapter, a series of tests were conducted to evaluate the performance of the green surfactants under different conditions in the presence of temperature, salt (NaCl), nanoparticles (NGF), and Crude oil. The following conclusions were then drawn:

- 1) In the solutions with only salt (NaCl), the conductivity increases with increasing salt concentration. On the other hand, in the solution with both salt and nanoparticles (NaCl and NGF), the conductivity only increases up to 18000ppm salinity. In the solution with NaCl, NGF, and extracted saponins, the conductivity substantially increases along with the saponin concentration. These results could be linked to the presence of active ions in the solutions that could change the conductivity. Furthermore, this is also contributed by the nanoparticle's surface charge and the electrostatic force of attraction between the salt molecules and nanoparticles. That salt concentration will lead to more dissociated ions (Na^+ and Cl^-) being adsorbed on the surface of large nanoparticles in the solution. The increase in salt concentration also enhances the propensity of nanoparticles to bond with salt molecules through electrostatic force attraction. Consequently, the

solution's overall quantity of ions/molecules will decrease from any salt concentration.

- 2) In the solution only contained green surfactants (Soapnut saponin and *Camellia oleifera* saponin), the maximum foam height enhances in direct proportion to saponins concentration until it reaches its CMC point at 4.6wt% (Soapnut) and 4wt% (*Camellia oleifera*), which are 83mm and 90mm, respectively. The foam column increased from 16mm at 0.1wt% to 83mm at 8wt% (Soapnut saponin) and 18.2mm at 0.1wt% to 90mm at 8wt% (*Camellia oleifera* saponin). However, the foam stability highly depends on the saponin concentration. The solution with a higher concentration experienced a faster foam structural collapse. The foam generated by Soapnut saponin was able to last 57 hours (2.8mm) at 0.5wt%, whereas it was reduced to 10 hours (0.9mm) when the concentration was raised to 7wt%. The longest concentration range was 0.1wt% to 0.3wt%, which could have its foam standing for 56 hours, while the shortest period of foam structure collapse was observed for the surfactant with 8wt% that stood only for 19 hours. The *Camellia oleifera* saponin also shows similar results. It is primarily because the Gibbs elasticity of the foam sheet decreases as the saponin concentration increases. Additionally, the increasing saponin concentration amplified the gravitational force's effect on foam drainage, resulting in continuing liquid drainage from the area between bubbles, rupturing the liquid coatings, and culminating in foam coalescence. In terms of surfactants ionicity, the anionic surfactant (*Camellia oleifera* saponin) performed better than the nonionic surfactant (Soapnut saponin) in foamability and foam stability, which was caused by the variation in surface coverage and surface mobility.
- 3) The foam bubbles' average diameter raised with the increasing saponins concentration until it reached the CMC point. For Soapnut saponin, the average bubble diameter increased from 18.9 μ m to 48.3 μ m when the concentration raised from 0.1wt% to 8wt%. For *Camellia oleifera* saponin, the average bubble size is slightly larger than the bubble generated by

Soapnut saponin. It shows an increase from 20.0 μ m at 0.1wt% to 50.13 μ m at 8wt%. The possible causes for this phenomenon are mainly affected by physical differences in the decay behavior between the porous media foam and the bulk foam. A bulk foam declines were mainly due to coarsening (gas diffusion), gravity drainage, and coalescence, with the mechanisms leading to a rise of the bubble average size and finally became a dry bulk foam with polyhedral construction. On the other hand, the foam in a porous medium has a smaller degree of freedom and cannot form a polyhedral structure; instead, it is a gas dispersion in the liquid phase in the form of ganglia separated by foam lamellae. Capillarity and saturation also play a pivotal role in situ foam performance. The nonionic surfactant is charged at approximately zero. Increasing the surfactant concentration will increase the load on the molecular structure and thus weaken the lamellae of the foam and lower its stability of the foam.

- 4) The foamability (height of foam) of both saponins increases substantially (approximately twofold) when the temperature increases to 85°C. For Soapnut saponin, with the same concentration of 0.1wt%, foam height increased from 16mm at room temperature (25°C) to 30mm when the temperature increased to 85°C. For *Camellia oleifera* saponin, under the same concentration of 4wt%, the foam height increased almost double from 81mm at 25°C to 157mm at 85°C. It is mainly caused by the increased temperature leading to an increase in bubble velocity and a corresponding increase in the rate of saponin molecules delivered to the rising bubble surface via convective diffusion; this effect happened due to the increasing bubble deformation. However, the foam stability experienced an adverse effect. When the temperature increased from 25°C to 85°C, the stability of the foam decreased from 57 hours to 16 hours (Soapnut saponin), and *Camellia oleifera* saponin reduced from 61 hours to 24 hours. The stability of foam is affected by the coarsening of the foam and drainage of the foam. At higher temperatures, foam drainage occurs faster, in which the foam dries faster and coalesces. Foam coarsening happens at a higher rate at elevated

temperatures as the permeability of the foam films to the gas increases as the temperature rises, resulting in a decrease in the consistency of the foam. Furthermore, the increased temperature reduces the surface viscosity and increases the rate of gas diffusion, resulting in faster liquid drainage between bubble lamella. And increased temperature increased the kinematic velocity of the ions, resulting in a higher frequency of ion collisions (Brownian motion).

- 5) For the solutions containing only nanoparticles (NGF), the foam length of both saponins increased along with the NGF concentration until it reached the threshold (0.003wt%). For Soapnut saponin, it raised from 27.1mm (0.001wt%) to 28mm (0.003wt%), then decreased to 26.8mm (0.005wt%). Similar results also happened in *Camellia oleifera* saponin. The foam length increased from 29.5mm at 0.001wt% to 30.6mm at 0.003wt%, then decreased to 29.3mm at 0.005wt%. Compared to tests using only pure saponins, the addition of NGF increased roughly 2mm foam length. Additionally, it successfully increased the foam's stability from 57 to 80 hours. For both saponins, the optimal concentration of NGF was 0.003wt%. The resultant enhancement of foam stability is generally due to the addition of NGF that effectively adsorb and aggregate at bubble films and Plateau borders, thereby increasing the maximum capillary pressure and particle detachment energy prior to foam coalescence, decreasing direct interface contact between adjacent bubble's lamella, slowing film drainage, and gas diffusion, and mitigating bubble break tendency. Additionally, due to their incredibly small size, NGF can easily penetrate the liquid film and form a monolayer of bridging particles or a densely packed bilayer of particles at the liquid-gas interface, aggregating into a network. Additionally, it can be verified that the incredibly small size results in stronger foam due to its higher diffusivity and interface.
- 6) With saponins and nanoparticles (NGF), the foamability/foam height increases along with the concentration of NaCl until it exceeds the limitation (for Soapnut saponin is 60000ppm, and *Camellia oleifera* saponin is

80000ppm). For Soapnut saponin, foam's length nearly doubled when the salinity reached 20000ppm (28mm to 47mm). *Camellia oleifera* saponin also had comparable results, increasing the foam length from 30.6mm to 50mm as salinity increased from 0 to 20000ppm. Soapnut saponin produced the longest foam length of 47mm at a salinity of 20000ppm. It demonstrates a 50mm foam length for *Camellia oleifera* saponin at a salinity of 20000ppm. Based on the results, 20000ppm salinity was the optimum salt concentration for both saponins. When the concentration of NaCl increases, more ions like Na^+ and Cl^- are hydrolysis into the solution to spread non-uniformly between each bubble at the contact surface, which can slow down the rate of drainage of liquid foam by producing an interface that is still in motion. The immobile interface thus induces slower coalescence of the foam bubbles; thus, the foam becomes more potent at higher salt concentrations. Due to the relatively low salt concentration, the zeta potential is slightly increased, the electrostatic double-layer shrinks, and the electrostatic repulsion force between the colloid particles is reduced. It increases the diffusivity and absorption of saponin molecules in the bulk solution and the time required for a bubble burst after foam formation. Additionally, by modifying the electrostatic repulsion force, the appropriate salt content can transform the foam structure from thermodynamically unstable to stable. However, adding NaCl decreases the foam's stability greatly. Foam stability dropped from 80 hours at 1.3mm to 57 hours at 0.1mm in the case of Soapnut saponin. Foam stability decreased from 80 hours at 2.3mm to 57 hours at 1mm in the presence of *Camellia oleifera* saponin. Continuously increasing the salinity will increase the concentration of Cl^- which carries the negative charge and thus raises the repulsion forces and ionic strength within the structure of bubbles, thus weakening the foam lamellae and lowering the foam stability.

- 7) The presence of crude oil accelerates the foam collapse/reduces the foam stability, and merely affects foamability. For Soapnut saponin containing 5000ppm salinity, the foam length of "solution without oil" remained stable

for 39 hours at 1.3mm, whereas "solution with oil" only remained stable for 29 hours at 1.1mm. Similar to the results obtained with *Camellia oleifera* saponin, the "solution without oil" exhibited the longest foam stability at 51 hours (0.2mm). However, the foam column fell to 39 hours (0.9mm) when added oil. It was primarily due to the bubbles aggregating near the top of the foam column, which resulted in a more significant dispersion of bubble sizes and hence altered the foam texture. The altered roughness then redistributes crude oil inside the foam column via localized accumulation. Gravity drainage caused the collected crude oil droplets to drain through the lamellae and generate an additional oil phase at the air/water interface, resulting in a quicker bubble coalescence rate. Thus, the foam column of Soapnut saponin degraded rapidly from 36.5mm to 7mm at 5000ppm and from 48mm to 27.3mm at 20000ppm. Ostwald ripening and bubble coalescence are also considered the major mechanisms. The crude oil droplets prefer to disintegrate in saponin-derived micelles, which reduces the number of micelles by decreasing their electrostatic repulsion force. It inhibits the formation of stratification in foam sheets, resulting in the column's ongoing disintegration.

Chapter 6: Interfacial Tension Study in Low Salinity Green Surfactant Nanofluid EOR Solutions

6.1 Introduction

When liquid-liquid or gas-liquid come into touch, they form an interface with only a few molecular layers. There are no identical molecules out of the interface of two immiscible fluids, and hence an inward-directed force strives to decrease the surface area by drawing it into the shape of a spherical ([Nowrouzi et al., 2020](#)). This surface activity forms a tensioned film of molecules, which is determined by the interface's specific free energy. It is critical to study the interaction behavior of immiscible fluids ([Alonso, 2020](#)). There is a significant hydrocarbon left/trapped in the rock formation, and the presence of gas and liquids phases provides a multi-phase interaction system. Knowledge of the characteristics related to the interaction between the immiscible phases is critical throughout the development phases and implementing a practical oil recovery approach for different reservoirs. The characteristics mainly focus on the properties of phases, chemical/physical reactions, and the saturation profile ([Divandari et al., 2020](#)). IFT is considered one of the most important secondary and enhanced oil recovery parameters since it can recover the residual oil by complicated rock-oil-brine interactions. It defies the forces at the interfaces of two fluids (water and oil) in a reservoir and impacts porous media's microscopic efficiency.

Many researchers have identified salt, nanoparticles, and surfactants as suitable modifiers in IFT reduction, although the performance consistency, particle interactions, and kinetics are not yet fully understood and challenges remain ([Nowrouzi et al., 2020](#)). Therefore, it is necessary to investigate further the physical/chemical interaction and multi-mechanisms of salt/nanoparticles/green surfactants in two-phases or three-phases systems. Therefore, this chapter tested the IFT of the new low salinity-nanoparticle-green surfactant formulations. Two extracted saponins (Soapnut saponin and Camellia oleifera saponin), nanoparticle (NGF), and salt (NaCl) were examined systematically as a function of concentration

and rock formation type. The drop shape analysis technique for pendant drop has been applied to determine the IFT in the oil-liquid system. Aspects containing different green surfactants, salt concentration, nanoparticles' concentration, and the mixture of those components are addressed in this chapter. Furthermore, the optimum concentration or ratio that leads to the lowest IFT is also investigated in this chapter. At last, the comparison and sensitivity analysis of each solution are addressed.

6.2 Methodology

6.2.1 Experimental Apparatus

Aluminum Panel Magnetic Hot Plate Stirrer was used to mix the solution. Mettler Toledo manufactured the analytical balance used to measure substances. Sartorius Quintix 412-1S digital scale was adopted to weigh the right amount of ultra-pure water. An orbital shaker was used to completely dissolve the solute (salt and surfactant) into the solvent system, and Lab Companion SKF-2075 made it. Drop shape analyzing, also known as the Pendant Drop method, is one of the IFT determination methods between oil and liquid phases. DSA100B manufactured by Krüss GmbH measured the IFT at ambient conditions. The shape of the oil droplet was analyzed by DSA100B embedded software. 0.5mm J-Shaped stainless needle and 3ml syringe manufactured by Fisher Scientific were used for oil injection. The glass box was filled with a mixture solution during the experiment, and the syringe (with a J-shape needle) was filled with oil. As shown in [Figure 6.1](#), the glass box (5cm x 5cm x 5cm) was used to measure the IFT in an oil-liquid two-phase system. The Quattro-S ESEM by ThermoFisher Scientific was used to study the particle interaction and bonding behavior between salt, saponin, and nanoparticle. All used equipment was thoroughly cleaned to maintain the high accuracy and repeatable results, especially the tip of the needle was well-treated cause the oil tended to attach to its outer surface.

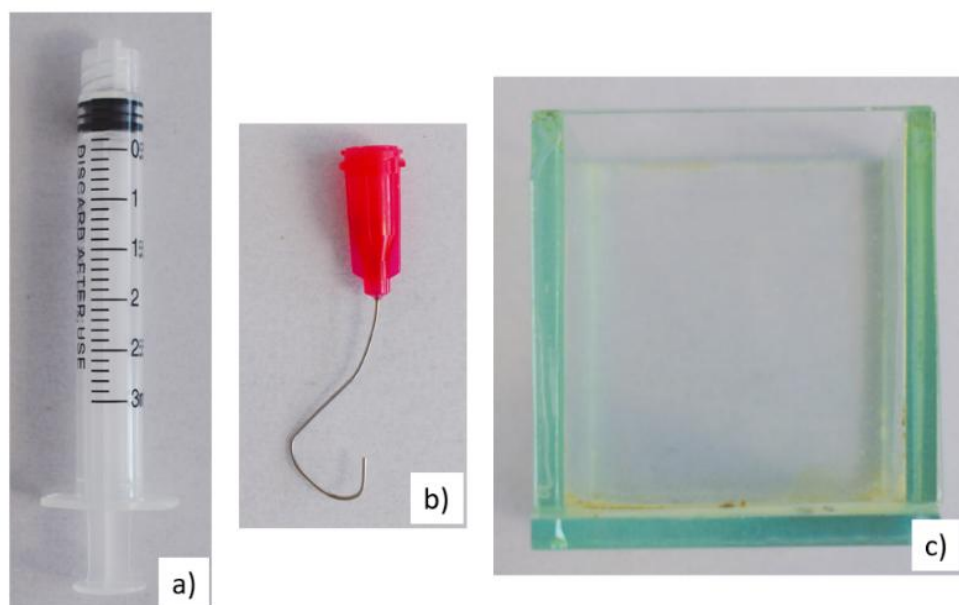


Figure 6.1: IFT measurement equipment. a) 3ml syringe, b) 0.5mm J-shape stainless needle, and c) glass box for IFT measurement

6.2.2 Experimental Materials

Ultra-pure water was used as the solvent and base fluid to dissolve additives in all experiments. It had a density of 0.9970 g/ml, pH of 6.70, resistivity of 18.18 MΩ.cm, and viscosity of $8.90 \times 10^{-4} \text{ kg}\cdot\text{m}\cdot\text{s}^{-1}$ at 25°C. The surfactants used in this chapter were extracted from natural plants: Soapnut saponin (extracted from Soapnut fruit) has a density of 0.89957 g/cm³, and pH 4.50, Camellia oleifera saponin (extracted from Camellia oleifera seed) has a density of 0.92567 g/cm³ and pH 5.17 (shown in [Figure 6.2](#)). Sodium Chloride (NaCl), 99.5% purity, and Calcium Chloride (CaCl₂), 99.5% purity, made by Merck Millipore, were used for brine preparation (shown in [Figure 6.3](#)). Ultra-thin ECR Glassflake (NGF), 98% purity, unmilled grade GF100nm provided by Glassflake Ltd was used as the nanoparticle. The size of NGF was around 100nm, and the surface area was 50-700 m²/g. The transmission electron microscope (TEM) image of the NGF is shown in [Figure 6.4](#). The oil used in this chapter supplied by Miri Crude Oil Terminal was the actual reservoir oil without any gas (dead oil), which has a density of 0.84 kg/L. The composition and the properties are similar to [Table 5.1](#).

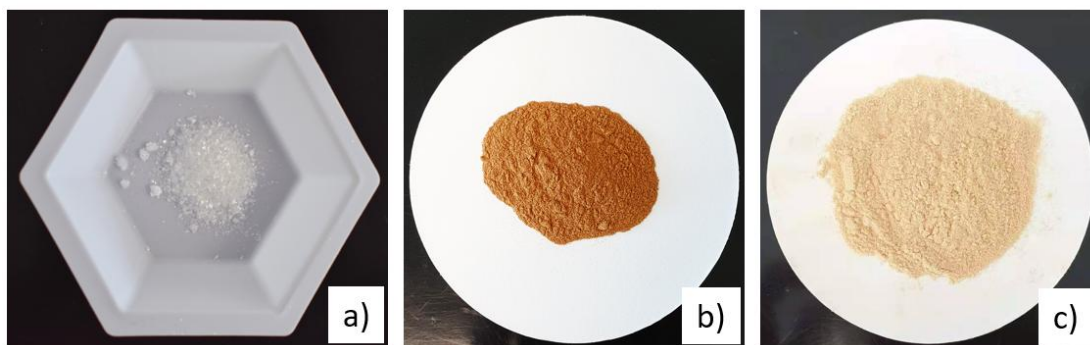


Figure 6.2: Additives applied in this study. a) Nano-glass flakes (NGF), b) Soapnut saponin, and c) *Camellia oleifera* saponin

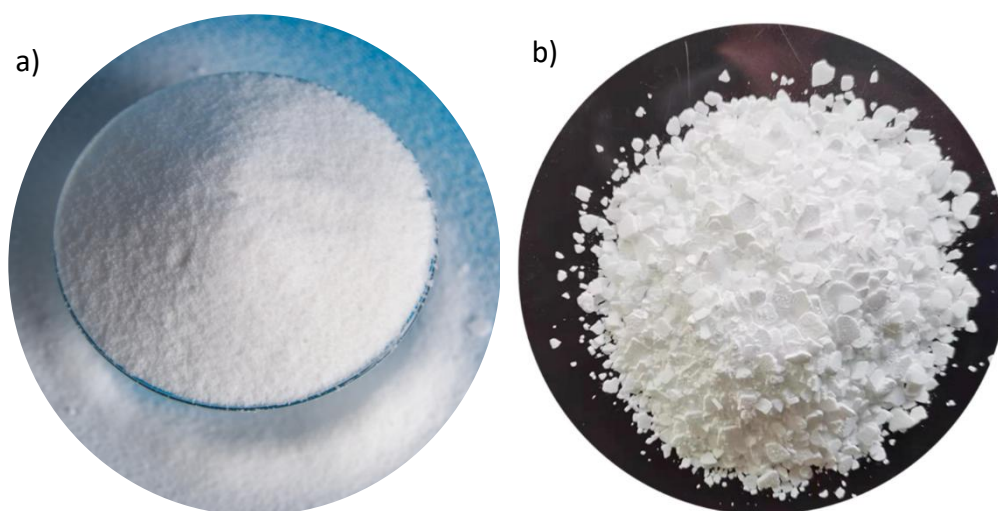


Figure 6.3: Salt used in this study. a) NaCl, and b) CaCl_2

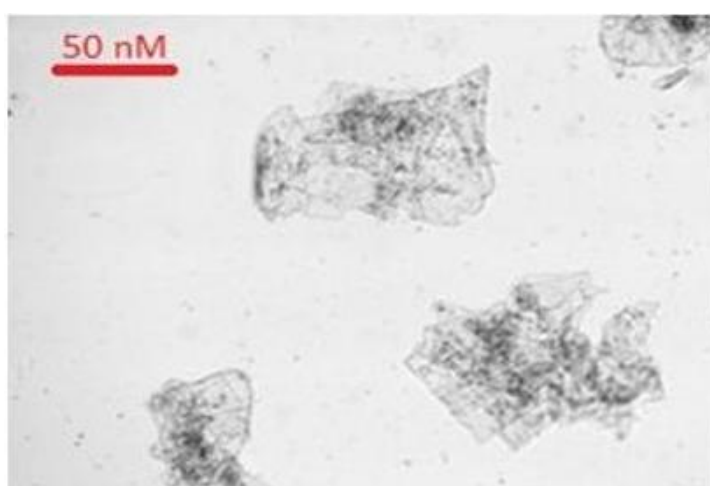


Figure 6.4: TEM image of NGF

6.2.3 Test Fluids Preparation

Sodium chloride (NaCl) was used as the salt and NGF as the nanoparticle. A small portion of nanoparticles can yield a stable and evenly diffused solution, but the solution may face an agglomeration issue ([Rezvani et al., 2020](#)). Thus, a high-frequency ultrasonic homogenizer evenly disperses nanoparticles in the solutions. Sonication could: 1) deliver a homogenized and stable hybrid solution, 2) remove air bubbles, and 3) break any potential agglomerates/clustering. The ultrasonic amplitude was fixed at 35% with a set circulation (running 7 seconds and pulse 2 seconds) for 15 minutes to prevent over-heating and structure damage ([Singh & Mohanty, 2020](#)). Ultrapure water with a resistivity of 5.4 MΩ.cm was used as the solvent during preparation. An orbital shaker manufactured by Lab Companion SKF-2075 was used to completely dissolve the solute (salt and surfactant) into the solvent system.

6.2.3.1 Crude Oil Preparation

The oil supplied by Miri Crude Oil Terminal was used for the IFT and Wettability test. In order to minimize the potential impurities dissolved in the oil, the oil was filtered by the filter paper and stored in the 250ml blue cap bottle ([Figure 6.5](#)).

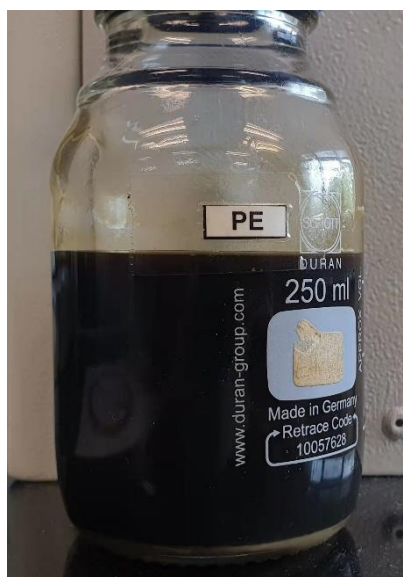


Figure 6.5: Crude oil sample after filtration

6.2.3.2 Pure Saponin Solution Preparation

For pure saponin solution preparation, a designed amount of Soapnut saponin or *Camellia oleifera* saponin is mixed with 50ml of ultra-pure water. The concentration was set at 0.1wt%, 0.3wt%, 0.5wt%, 1wt%, 2wt%, 3wt%, 4wt%, 4.5wt%, 5wt%, 6wt%, 7wt%. The proper amount of ultra-pure water was weighed using a Sartorius Quintix 412-1S digital scale. At the same time, the weight of saponin was measured using a more precise Mettler Toledo analytical balance. In order to create a homogenized solution, all samples were sent to the orbital shaker for 12 hours, then mixed with by magnetic stirrer at 40°C for 6 hours.

6.2.3.3 Mixed Solution Preparation

Most preparation steps are similar to pure saponin solution preparation for the solution containing salt (NaCl or CaCl₂), nanoparticle (NGF), or both. After the magnetic stirrer mixed process, solutions were transferred to the orbital shaker for 24 hours to completely dissolve the additives (salt, nanoparticles, or both). Because of the potential for agglomeration or clustering of saponin molecules and NGF particles, all prepared solutions need to be ultrasonic for 2 minutes at 15% amplitude with a specified circulation (running 5 seconds and pulse 1 second) before the test begins. Overall, solutions prepared for IFT and contact angle measurement were divided into four parts in this chapter:

- 1) The additives for the first part were pure saponins (Soapnut saponin or *Camellia oleifera* saponin): 24 portions for IFT measurement (12 for Soapnut saponin and 12 for *Camellia oleifera* saponin), 72 portions for contact angle measurement (24 for Berea sandstone core slice, 24 for Shale core slice, and 24 for Malay sandstone core slices). Various concentrations were prepared and mixed with 50ml ultra-pure water. The concentration of saponins was set at 0.1wt%, 0.3wt%, 0.5wt%, 1wt%, 2wt%, 3wt%, 4wt%, 4.5wt%, 5wt%, 6wt%, 7wt%. The mixing methods were explained above. This part mainly focused on investigating the effect of the saponin concentration on IFT in the oil-liquid system and the contact angle in the three-phase system (oil-liquid-rock). Most of all, it is required to determine the optimum saponin

concentration that can deliver the lowest IFT and contact angle.

- 2) The additives for the second part were saponins (Soapnut or *Camellia oleifera*) and NGF: 14 portions for IFT measurement (7 for Soapnut saponin and 7 for *Camellia oleifera* saponin), 48 portions for contact angle measurement (16 for Berea sandstone core slice, 16 for Shale core slice, and 16 for Malay sandstone core slices). The concentration of the saponin was fixed at optimum point and the concentration of NGF was set at 0.001wt%, 0.002wt%, 0.0025wt%, 0.003wt%, 0.0035wt%, 0.004wt%, and 0.005wt%. The mixing methods were explained above. This part aimed to investigate the effect of NGF concentration on the IFT and wettability in the presence of saponin. Furthermore, it also required estimating the optimum NGF concentration that can deliver the lowest IFT and contact angle in saponin solution.
- 3) The additives for the third part were saponins (Soapnut or *Camellia oleifera*) and salt (NaCl or CaCl_2): 32 portions for IFT measurement (16 for Soapnut saponin and 16 for *Camellia oleifera* saponin), 96 portions for contact angle measurement (32 for Berea sandstone core slice, 32 for Shale core slice, and 32 for Malay sandstone core slices). The saponin concentration was fixed at the optimum point, and the concentration of NaCl or CaCl_2 was set at 1000ppm, 2000ppm, 3500ppm, 5000ppm, 10000ppm, 20000ppm, and 40000ppm. The mixing methods were explained above. This chapter aimed to investigate the IFT and wettability condition affected by salt concentration and the type of salt (monovalent salt NaCl and divalent salt CaCl_2). In addition, the optimum salinity that can bring the lowest IFT and contact angle were also investigated in this part.
- 4) The additives for the last part were the combination of saponins (Soapnut or *Camellia oleifera*), salt (NaCl or CaCl_2), and NGF: 32 portions for IFT measurement (16 for Soapnut saponin and 16 for *Camellia oleifera* saponin), 96 portions for contact angle measurement (32 for Berea sandstone core slice, 32 for Shale core slice, and 32 for Malay sandstone core slices). The concentrations of saponins and NGF were fixed in all samples, determined

by the point reaching the lowest IFT or contact angle in the last part. For example, 4.5wt% for pure Soapnut saponin, 4wt% for *Camellia oleifera* saponin, and 0.003wt% for NGF. The concentration of NaCl or CaCl₂ was set at 1000ppm, 2000ppm, 3500ppm, 5000ppm, 10000ppm, 20000ppm, and 40000ppm. The mixing methods were the same as above. Also included in this section is an investigation into the optimum salinity capable of achieving the smallest IFT and contact angle.

This experiment used low concentrations of saponins and nanoparticles to ensure optimal recovery efficiency and homogeneous particle dispersion. With higher nanoparticle concentrations, drawbacks such as agglomeration and clustering occur, lowering the effectiveness during EOR operations ([Sadatshojaei et al., 2019](#)). For Soapnut saponin and *Camellia oleifera* saponin, the CMC was estimated at 4.6wt% and 4wt%, respectively. IFT reduction and wettability alteration performance tend to be similar when the concentration is above CMC. Therefore, increasing the concentration of green surfactants and nanoparticles is meaningless and may eventually lead to formation permeability declination, pore throat occlusion, and formation destruction. Furthermore, the expense of surfactants has been brought to the forefront, not only in terms of environmental considerations but also in economic feasibility. It is critical to achieving maximum performance while using the least surfactant possible throughout the EOR process, especially on a major oil field. As a result, a low dosage of green surfactants was used in this experiment.

6.2.4 IFT Measurements

Pendant/Rising drop is one of the most widely applied methods in IFT measurement. A drop of crude oil is discharged into the solution, and the droplet's shape is mainly affected by the equilibrium between surface force and gravitational force. DSA-100B (manufactured by Krüss GmbH) measured the IFT between the designed solution and crude oil. The crude oil was placed in a 3ml syringe with a 0.5mm J-shape stainless needle (manufactured by Fisher Scientific). The glass box (5cm x 5cm x 5cm) was filled with a test solution. The J-shape needle was positioned in the glass

box and fully immersed in the test solution during measurement. The crude oil droplet was carefully dispensed at the tip of the needle, and DSA-100B's camera captured the picture of the droplet. A schematic image of the IFT measurement apparatus is shown in Figure 6.6.

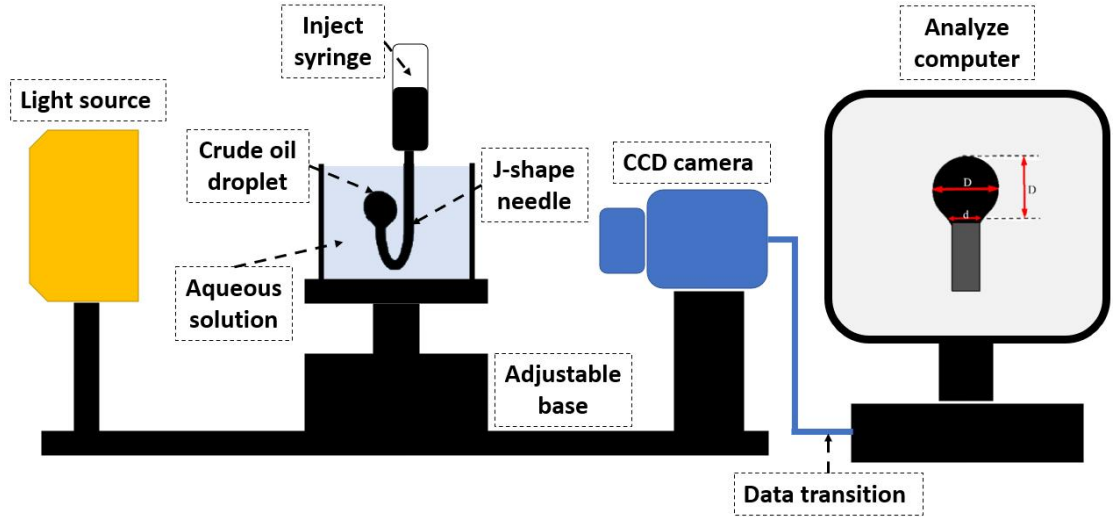





Figure 6.6: Schematic diagram of DSA-100B apparatus used for IFT measurement

It is critical to make sure that the oil droplet maintains its equilibrium position only due to buoyancy rather than injection force before leaving the tip of the needle. The software automatically recorded the results every second (with image taking), and the time was set for 30 minutes to make sure the oil droplet achieved an equilibrium status in the oil/test solution environment (as shown in Table 6.1). At last, the equilibrated static surface tension was automatically calculated by embed software followed by the Young-Laplace equation (Eq 6.1). Figure 6.7 illustrates the schematic diagram of the experimental steps that were used.

$$\sigma = \frac{\Delta \rho g D^2}{H} \quad (\text{Eq 6.1})$$

where σ is the surface tension, $\mu\text{m}/\text{m}$; $\Delta \rho$ is the phases density difference, g/cm^3 ; g is the gravity acceleration, m/s^2 ; D is the maximum horizontal oil diameter, mm ; H is the shape-dependent parameter, no unit.

Table 6.1: Effect of Soapnut saponin concentration on the IFT at oil/water interface

Concentration	0wt%	4.5wt%	7wt%
Image			
IFT (mN/m)	17.8	3.8	6.3

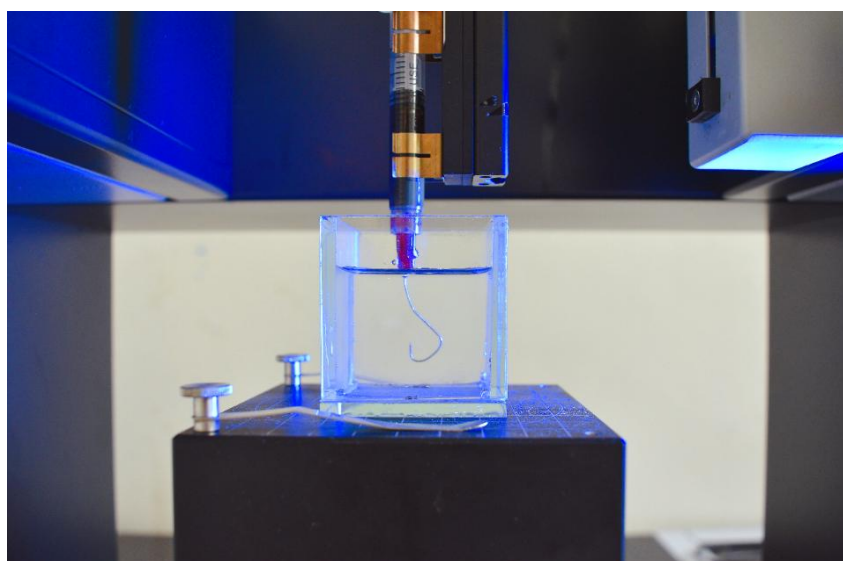


Figure 6.7: IFT measurement in DSA-100B

It is worth noticing that the base solution was not consistent for all IFT tests. The base solution is ultra-pure water for the first batch containing saponin. For the second batch that contains saponin and NGF, the base is the solution with 4.5wt% Soapnut saponin or 4wt% *Camellia oleifera* saponin (optimum concentration). For the third batch that contains saponin and salt, the base is the solution with 4.5wt%

Soapnut saponin or 4wt% *Camellia oleifera* saponin (optimum concentration). For the last batch that contains saponin, NGF, and salt, the base is the solution with 4.5wt% Soapnut saponin or 4wt% *Camellia oleifera* saponin and 0.003wt% NGF. Each measurement was repeated three times, and the average result was used. All tests were conducted at room temperature (20°C) and 14.7psia.

6.2.5 Transmission Electron Microscopy (TEM) Characterization

TEM is considered one of the electron microscopy techniques commonly utilized to characterize particles. At spatial resolutions down to atomic dimensions (1nm), TEM can provide immediate high-resolution pictures and detailed qualitative/quantitative information about particles ([Zhang et al., 2019](#)). Quattro-S ESEM (ThermoFisher Scientific) was applied in this part, which comprised the electron gun, electromagnetic lenses, condenser, and other precision components. The sample specimen and its position and how the data are obtained from the sample are fundamentally different in a TEM mode compared to a typical SEM mode. TEM uses a high-energy electron beam to penetrate an ultra-thin sample and produce a detailed image ([Smith, 2015](#)). Therefore, in this part, TEM was used to observe the particles' bonding behavior before and after core slices were immersed in the designed solution. As the electron beam passes through the core slices, electron-electron interactions between the beam and the test sample convert the incident electrons to unscattered or scattered electrons ([Muneesawang & Sirisathitkul, 2015](#)). Shadow image with various darkness was generated based on the density of unscattered electrons. To allow electrons to pass through, the solution that contained saponins, nanoparticles, and salt was freeze-dried into a fine powder. Then, the powder was evenly dispersed onto the support grids. In order to deliver a clearer and sharper image ([Figure 6.8](#)), a high voltage model was used (10.00 kV to 30.00 kV), and the magnification was varied from 500x to 120000x. The spot size was fixed between 3.0 and 3.5.

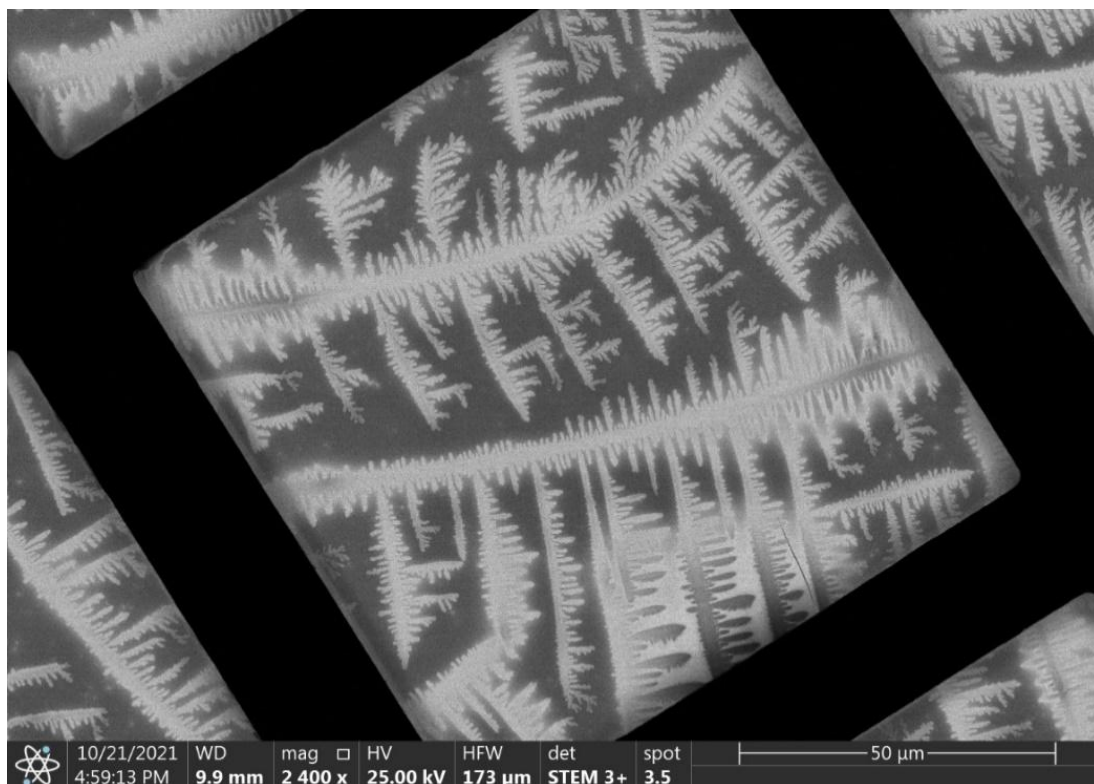


Figure 6.8: TEM image of Soapnut saponin in the designed solution that contains NaCl and NGF

6.3 Results and Discussions

6.3.1 IFT Measurements

A comparative examination of Soapnut saponin's effect or *Camellia oleifera* saponin's effect on the IFT modification as a surfactant and nanoparticle concentration, salt type, and salinity was estimated through a series of IFT measurements. Furthermore, this section also included a comprehensive explanation of the contributing mechanisms of the combination of surfactant, salt, and nanoparticles applied in IFT variation. The optimum concentration of salt, nanoparticles, and surfactants has been determined since it is important for effective oil recovery. The reference IFT values (as a benchmark) were estimated when the variable additives were not added to the test solution. And the values are summarized in [Table 6.2](#).

Table 6.2: Summary of benchmark IFT for each batch test

Base additives	Variable additives	Solution Environment	Benchmark (mN/m)
-	Soapnut saponin	Ultra-pure water	17.8
-	Camellia oleifera saponin	Ultra-pure water	17.8
Soapnut saponin	NGF	4.5wt% Soapnut saponin	3.8
Camellia oleifera saponin	NGF	4wt% Camellia oleifera saponin	3.72
Soapnut saponin	NaCl or CaCl ₂	4.5wt% Soapnut saponin	3.8
Camellia oleifera saponin	NaCl or CaCl ₂	4wt% Camellia oleifera saponin	3.72
Soapnut saponin	NaCl or CaCl ₂	4.5wt% Soapnut saponin 0.003wt% NGF	3.24
Camellia oleifera saponin	NaCl or CaCl ₂	4wt% Camellia oleifera saponin 0.003wt% NGF	2.97

6.3.1.1 IFT Modification by Extracted Green Surfactants

The influence of saponins (both Soapnut saponin and Camellia oleifera saponin) concentration on the IFT of the oil-aqueous phase has been shown in [Figure 6.9](#). Both IFT values experienced a rapid decrease with a small amount of saponin (less than 1wt%) at the beginning, then remained gentle declined until they reached CMC. For Soapnut saponin, the IFT was initially changed from 17.8mN/m at 0wt% to 6.82mN/m at 1wt% with a sharp decrease, followed by a gentle fluctuation to 6.3mN/m at 7wt%. For Camellia oleifera saponin, the IFT variation path was similar to Soapnut saponin. It reduced from 17.8mN/m to 5.72mN/m at 1wt%, then fluctuated to 4.1mN/m at 7wt%, which shows a better ability at IFT reduction. Based on the results of IFT measurements, the lowest IFT value was determined to be 3.8mN/m with 4.5wt% for Soapnut saponin. For Camellia oleifera saponin, the IFT was further reduced to 3.72mN/m with 4wt%. It was mainly caused by the electrostatic interactions acting more in anionic surfactants (Camellia oleifera saponin) than nonionic surfactants (Soapnut saponin) ([Qi et al., 2022](#)). The higher lateral electrostatic interactions drive the Camellia oleifera saponin further

adsorbed at the oil/aqueous interface thereby leading to the smaller IFT value (Moslemizadeh et al., 2021). Both surfactant concentrations are in close agreement with the CMC measured by the electrical conductivity meter in the previous chapter.

The reduction percentage of IFT was approximately 78.7% and 79.1% for Soapnut saponin and Camellia oleifera saponin, respectively. These results show that the extracted natural surfactants can lower the IFT of the oil-aqueous phase to an acceptable level without other additives. The IFT variation with saponin concentration can be divided into three stages. A sharp decrease in IFT was observed at 0wt% to 1wt%, mainly caused by the rapid diffusion of saponin molecules in solution and the saponin monomers adsorbed on the oil-aqueous interface hydrogen bonding (Arabloo et al., 2016). The adsorption level was controlled by the charge on the electrical double layer at the oil/aqueous interface. In other words, when saponin was added to a solution containing water and oil, the saponin molecules began exchanging water with the oil molecules present at the oil-water interface (Daghlian et al., 2016). The oil-water-surfactant system's molecular exchange mechanism was characterized by two unique types of interactions: 1) On one side, the surfactant's hydrophilic (polar) groups align themselves and engage with the water molecule; 2) On the other side, the surfactant's hydrophobic (non-polar) groups position themselves and interact with the oil molecule (Kamal et al., 2017; Peng and Nguyen, 2020). Finally, a thin layer of aligned saponin molecules was applied to the oil-water interface. The presence of a saponin disrupts the contact force (cohesive forces) at the interface between water and oil molecules (which becomes significantly weaker in comparison to its initial state); hence, the IFT is lessened (Nowrouzi et al., 2020b). At intermediate concentration (Soapnut saponin is 1wt% to 4.5wt%, Camellia oleifera saponin is 1wt% to 4wt%), a further rise in the saponin concentration leads to a relatively stable IFT reduction. The decrease rate drops from 61.7% at the first stage to 44.3% (Soapnut saponin) and 67.6% to 35.4% for Camellia oleifera saponin. Saponin molecules tend to concentrate at the interface since they experience less free energy than bulk solutions. As a result, intermolecular forces become weaker, and the IFT diminishes. Furthermore, the monomers generated from the first stage start

to aggregate to form mixed micelles and generate a stable emulsion when the saponin concentration increases (Rezaei et al., 2021). The newly formed micelles significantly decrease the number of saponin monomers in solution, and the lateral electrostatic interactions drive the saponin further adsorbed at the oil/aqueous interface. This results in a gentle period of IFT reduction due to the fewer saponin micelles in the solution replacing the water and oil molecules at the original oil/aqueous interface (Moslemizadeh et al., 2021).

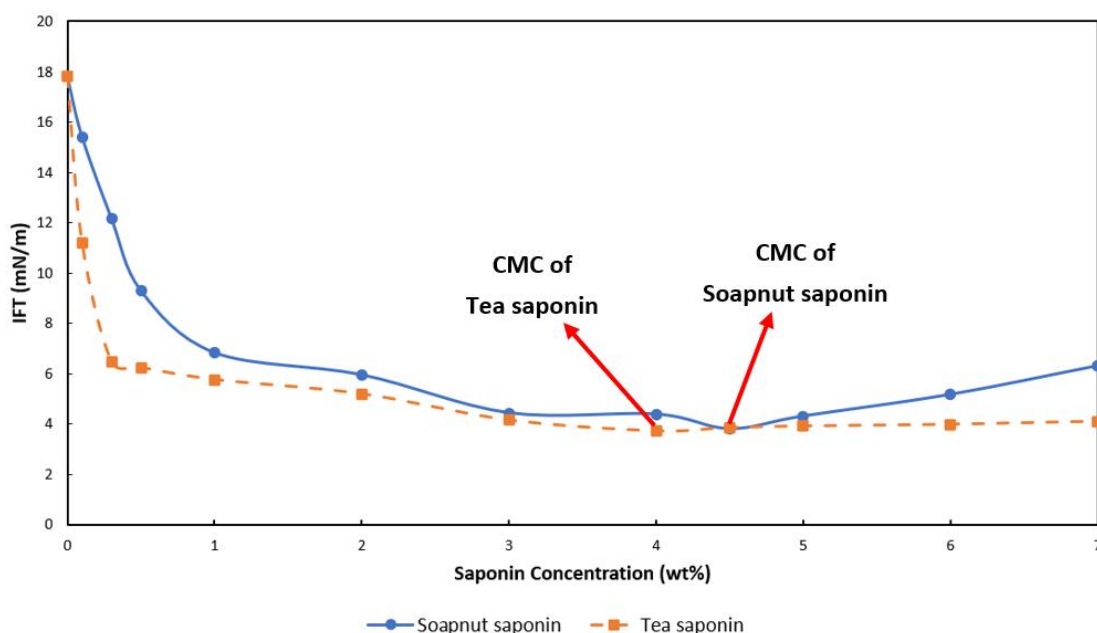


Figure 6.9: IFT results for both saponins against concentration

However, aberrant activities have been seen when the concentration of Soapnut saponin exceeds 4.5wt% and *Camellia oleifera* saponin exceeds 4wt%. The results indicate a small rise from 4.3mN/m (5wt%) to 6.3mN/m (7wt%) for Soapnut saponin and 3.85mN/m (4.5wt%) to 4.1mN/m (7wt%) for *Camellia oleifera* saponin. Generally, when surfactant concentration is above its CMC point, the surfactant molecules begin to self-organize into micelles (Sarmah et al., 2020). At the same time, when the concentration is above the CMC point, the surface tension does not decrease further (M. Ahmadi & Chen, 2020). However, at concentrations greater than CMC points of both saponins, there was a small increase in IFT. This abnormal behavior is explained by the existence of 1) Natural coagulants (which synthesize extremely small amounts of membrane flocculate material) and 2) Impurities.

Numerous naturally occurring coagulants, including tannins, are present in most plant fruits. Tannis (tannic acid) are polyphenolic macromolecules that covalently link to and precipitate proteins and other organic substances such as amino acids and alkaloids (Nowrouzi et al., 2020). Tannis, in combination with other natural coagulants, has the ability to adsorb and deposit on the saponin surfactant molecular, thereby preventing sections of the molecular from adsorbing into the oil-water interface (Saxena et al., 2019; Nowrouzi et al., 2020). The presence of a trace amount of membranous flocculate material in the solution may be sufficient to initiate it (shown in Figure 6.10).

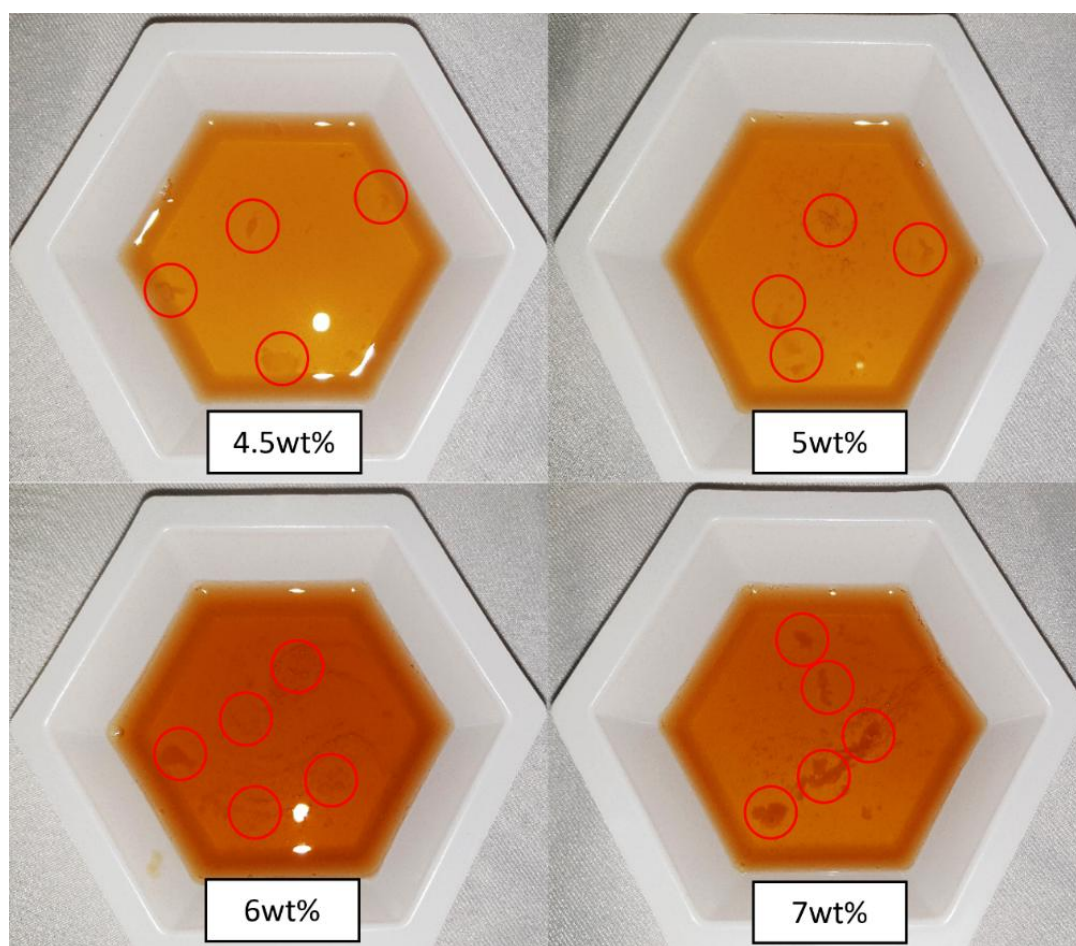


Figure 6.10: Formation of membranous flocculate substance against saponin concentration

When saponin concentration is greater than CMC, the membranous flocculate material forms. Saponin from raw Soapnut fruit or *Camellia oleifera* has contaminants that impair its surfactant efficacy. Impurities reduce the overall

number of effective components (saponin surfactant), which results in a drop in IFT (Jalali et al., 2019; Haghighi et al., 2020). As a result, as the saponin surfactant concentration grows, the total number of contaminants increases, limiting the IFT lowering ability.

6.3.1.2 Influence of Green Surfactants and Nanoparticle's Interaction on IFT Modification

According to the results achieved from the previous section, both saponins possess excellent surface/interface activity. Various researchers have widely reported that nanoparticles are frequently used in conjunction with surfactants (Almahfood & Bai, 2018; AlYousef & Schechter, 2019; Ayoub et al., 2019; Alsaba et al., 2020; Almubarak et al., 2020; Divandari et al., 2020; Jiang et al., 2021;), but there is a lack of consistency regarding IFT reduction. Therefore, this part focused on investigating the combination and interaction of the saponin and NGF on interface properties of fluids and the effect of nanoparticles concentration (NGF) on IFT in saponin solution. In this section, the constant was the optimum concentration achieved from the last section, and the variable was the concentration of NGF. Specifically, all test solutions contain the same saponin concentration: 4.5wt% for the Soapnut saponin batch and 4wt% for the Camellia oleifera saponin batch. Consequently, the reference IFT was 3.8mN/m for Soapnut saponin and 3.72mN/m for Camellia oleifera saponin. Then, the NGF was added with increasing concentration from 0.001wt% to 0.005wt%. According to Figure 6.11, compared to the case of only saponin, the presence of NGF leads to a further IFT decrease in saponin solution along with the NGF's concentration until it reaches its optimum point. It is worth noticing that the decreasing rate of IFT with NGF was much lower than the solution that only contains saponin. For Soapnut saponin, the IFT reduction rate drops from 61.7% (without NGF) to 14.7% (with NGF). For Camellia oleifera saponin, the decreasing rate reduced from 67.6% to 20.2%. However, the IFT starts to increase when the concentration of NGF passes its optimum point.

Overall, the IFT variation with NGF concentration can be divided into two stages. A gentle decrease of IFT observed from 0.001wt% at 3.71mN/m to

0.003wt% at 3.24mN/m (Soapnut saponin), and 3.67mN/m (0.001wt%) to 2.97mN/m (0.003wt%) for *Camellia oleifera* saponin. Saponin molecules tend to adsorb on the NGF surface to form monolayers due to the high surface-to-volume ratio and high surface energy of NGF (Jiang et al., 2021). At the solution's interface, the saponin and NGF are distributed so that the saponin monolayer concentrates at the liquid interface, while the NGF are distributed underneath the monolayer in the diffuse layer. It offers a more powerful driving force for the assembly to migrate toward the interface (Jalil & Hussein, 2019). The addition of NGF to the dispersed solutions of saponin introduces the non-DLVO forces (steric forces) and promotes the interfacial layers' interactions, such as electrostatic repulsion force/Coulomb force (Saïen & Bahrami, 2016). The surface charge of NGF was negative for all pH conditions. Thus, the saponins with an anionic head group (*Camellia oleifera* saponin) were experienced more drive to migrate toward the interface by the negative surface charge of NGF by electrostatic repulsion interactions (Belhaj et al., 2020). Additionally, saponin adsorption on NGF pushed the NGF toward the interfaces due to their enhanced hydrophobicity (Saïen & Fadaei, 2018). The electrostatic repulsion force between NGF particles and saponin boosts the saponin diffuse in solution, resulting in a drop in IFT. Furthermore, the intensive interaction between NGF and saponin ions brings negative free energy for saponin adsorption and micelle production (Mohajeri et al., 2019). Consequently, the interfaces ions do less work, resulting in decreasing IFT.

Then the IFT starts to increase after passing the 0.003wt%. For Soapnut saponin, the IFT rise from 3.24mN/m at 0.003wt% to 5.38mN/m at 0.005wt%. For *Camellia oleifera* saponin, the IFT increased from 2.97mN/m at 0.003wt% to 4.12mN/m at 0.005wt%. Therefore, it can conclude that excessive nanoparticle leads to a mildly negative effect on IFT in the presence of saponin solution. As mentioned before, saponin molecules tend to adsorb on the NGF surface due to the high surface energy of NGF. The excessive concentration substantially increases the number of NGF in saponin solution, removing the saponin molecules from the interface (Sadatshojaei et al., 2019). As a result, the surfactant efficiency was reduced, and IFT increased.

Moreover, redundant NGF adsorbed at the oil/water interface reduces the interfacial area covered by saponin and increases IFT. Superabundant NGF's presence also aggravates aggregation and enhances the electrostatic interaction between saponin and NGF particles (A. Ahmed et al., 2019). It also may affect the adsorption behavior of naturally occurring amphiphiles in crude oil by steric hindrance. A similar situation was found in Sun et al. (2014). As shown in Figure 6.11, 0.003wt% of NGF is the optimum concentration for both saponins, and the minimum IFT values were 3.24mN/m (Soapnut saponin) and 2.97mN/m (Camellia oleifera saponin). Furthermore, compared with the solution only containing saponin, 0.003wt% NGF can further reduce the IFT by approximately 0.56mN/m (Soapnut saponin) and 0.75mN/m for Camellia oleifera saponin. Therefore, it can conclude that the appropriate amount of NGF can further decrease the IFT in the saponin solution.

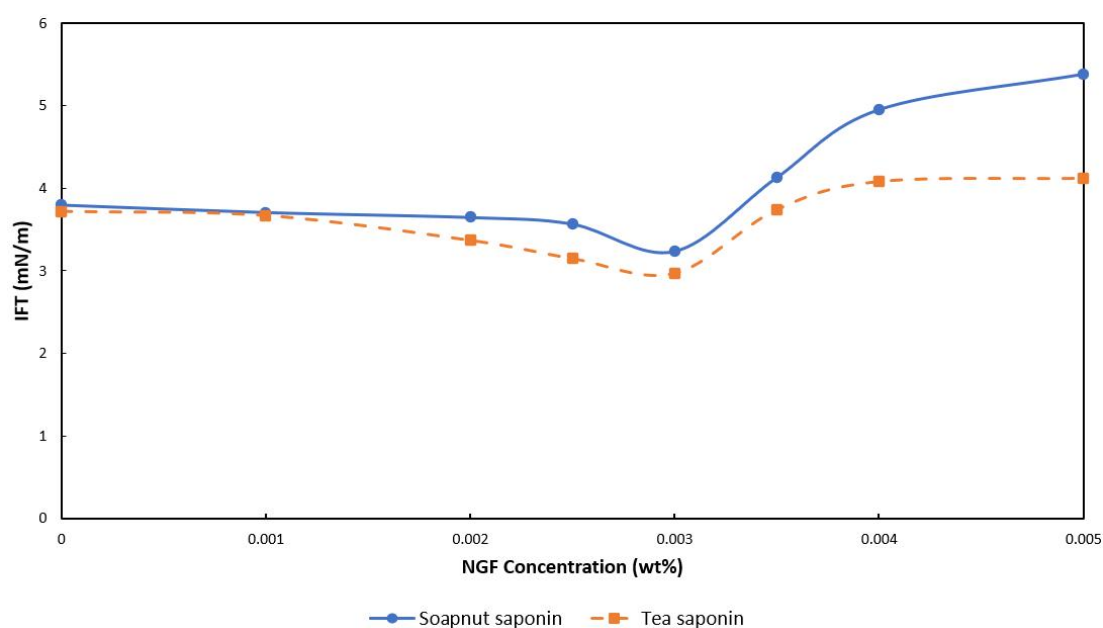


Figure 6.11: IFT results for both saponins against NGF concentration in saponin solution

6.3.1.3 Influence of Salt Type and Salinity on IFT Modification of Green Surfactant Solutions

Salt ions can interact with saponin's function group, modifying their microscopic assembly and physicochemical properties through high molar electrolytes (Wan & Poon, 1969). Furthermore, the concentration and valence of salt ions can affect the solubility of saponin in water and the IFT of the oil/water interface (Mokhtari et al., 2019). This phenomenon is named a salt-surfactant synergistic effect. This part has mainly investigated the influence of salt type (NaCl and CaCl₂) and salt concentration (1000ppm, 2000ppm, 3500ppm, 5000ppm, 10000ppm, 20000ppm, and 40000ppm) on the IFT performance of saponin. Like the last part, all test solutions include the same concentration of saponin: 4.5wt% for the Soapnut saponin batch and 4wt% for the Camellia oleifera saponin batch. As a result, the reference IFT for the Soapnut saponin batch was 3.8mN/m, and the reference IFT for Camellia oleifera saponin was 3.72mN/m. As shown in Figure 6.12 and Figure 6.13, the presence of NaCl or CaCl₂ decreases the IFT until the concentration reaches its optimum value. For Soapnut saponin, the IFT decreased from 3.73mN/m at 1000ppm to 2.91mN/m at 3500ppm (NaCl). In the presence of CaCl₂, the IFT dropped from 3.75mN/m at 1000ppm to 3.42mN/m at 3500ppm. In terms of Camellia oleifera saponin, the IFT was diminished from 3.67mN/m at 1000ppm to 2.7mN/m at 3500ppm (NaCl) and 3.59mN/m at 1000ppm to 3.27mN/m at 3500ppm (CaCl₂). This can be explained by salting in effect. The additional salt (NaCl or CaCl₂) with low concentration disassembles the structure of organic particles in crude oil that formed around the water, enhancing their solubility in water (Nowrouzi et al., 2020). It also improves the solubility of saponin in the solution, driving them to move to the oil/water interface. Eventually, the IFT was further reduced. Furthermore, electrolytes (Na⁺, Ca²⁺, Cl⁻) have improved adsorption and aggregation processes by lowering electrokinetic repulsion or the double-layer screening effect (Mofrad & Saeedi Dehaghani, 2020). NaCl or CaCl₂ can ease the dissociation reaction of saponin monomers, reduce the desorption rate of saponins, and thin the ionic atmosphere surrounding the saponin monomers (Budhathoki et al., 2016). According to Greshfeld, creating the monolayer of non-dissociated monomers can

drop the IFT. The lowest results achieved by *Camellia oleifera* saponin was 2.7mN/m at 3500ppm salinity (NaCl), and Soapnut saponin was 2.91mN/m at 3500ppm salinity (NaCl), where the saponin disperses evenly between the water and oil phases, yielding in the lowest IFT.

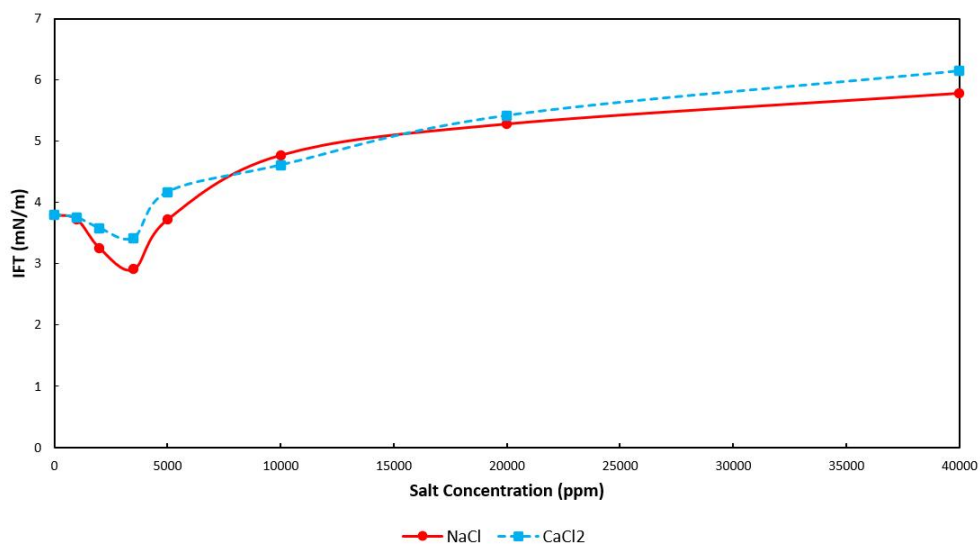


Figure 6.12: IFT results for Soapnut saponins against salt type and concentration in saponin solution

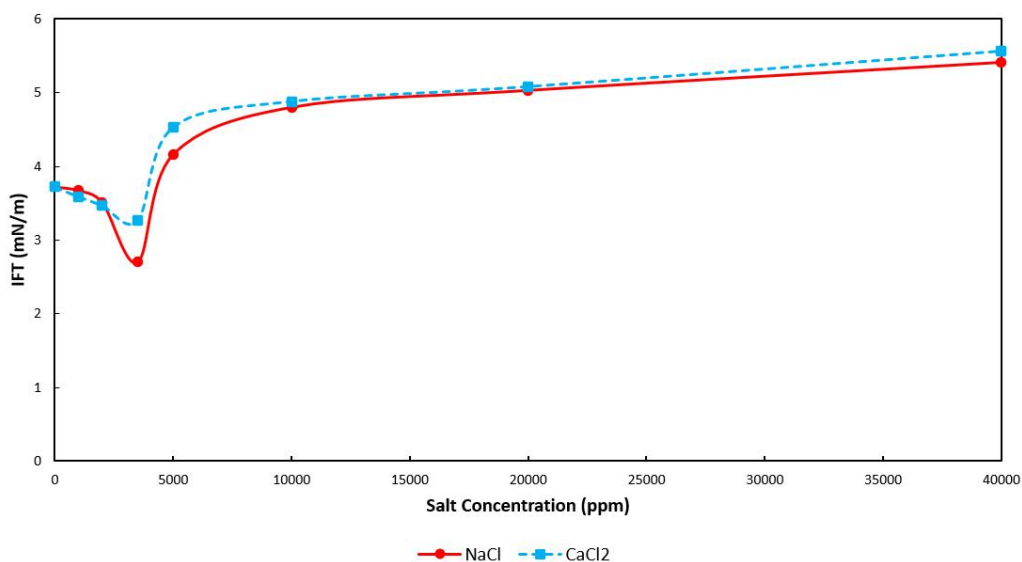


Figure 6.13: IFT results for *Camellia oleifera* saponins against salt type and concentration in saponin solution

Nevertheless, the IFT increases when the optimum salinity passes (3500ppm). For Soapnut saponin, the IFT increased to 5.78mN/m and 6.15mN/m at 40000ppm for NaCl and CaCl₂, respectively. For Camellia oleifera saponin, the final IFT reached 5.41mN/m for NaCl and 5.56mN/m for CaCl₂ at 40000ppm. Increasing salinity enhances the electrostatic repulsion force between particles, weakens the double layer expansion, and induces the hydration repulsion effect, restraining saponin from further dissolving into water (Belhaj et al., 2020). It also forces saponin to be drawn away from the oil/water interface. Most saponins dissolve in the water at low salt concentrations but remain in the oil phase at high salt concentrations. As a result, the IFT increased. In term of IFT reduction ability, the monovalent salt (NaCl) deliver better results than divalent salt (CaCl₂). For Soapnut saponin, NaCl could further decrease IFT than CaCl₂ by 0.51mN/m. For Camellia oleifera saponin, this value increased to 0.57mN/m. The difference in IFT between NaCl and CaCl₂ is mainly caused by the salt dissolution rate (degree of hydration), adsorption rate, ion valence, ionic charge, and ion activity (Abbas et al., 2020). In this case, NaCl release Na⁺ and Cl⁻, CaCl₂ release Ca²⁺ and Cl⁻. Divalent cations, Ca²⁺, have a higher charge and stronger interaction with the negatively charged head groups of saponin than monovalent cations Na⁺. Furthermore, the smaller size of Ca²⁺ also causes higher hydration energy, stronger connections with saponin molecules, and a faster stabilization process (Yekeen et al., 2019).

Na⁺ requires a higher concentration because its larger size results in a lower surface charge. Therefore, the saponin solution containing CaCl₂ was greater than those containing NaCl and caused the IFT difference under the same conditions (Olayiwola & Dejam, 2019). In addition, the presence of Na⁺ and Ca²⁺ can generate acid/base interactions at the interface, affecting the solubility of the polar organic matter in the solution (Chávez et al., 2020). The solution containing Ca²⁺ appears to dissolve harder than the one with Na⁺. In terms of ionic charge, divalent cation Ca²⁺ possesses higher electrostatic repulsion forces than monovalent cation Na⁺; therefore, the aggregation tendency of saponin is higher in CaCl₂ solution and hence induces the elevated IFT (Ebaga-Ololo & Chon, 2018). In addition, Na⁺ is far more active in the salt-saponin synergistic effect than Ca²⁺. Specifically, Na⁺ appears to

have the strongest interaction moiety since it is more easily dissociated from its hydration sphere. However, Ca^{2+} has weaker salt-saponin connections due to its Columbia interactions being filtered by strongly bonded solvation water molecules (Katende & Sagala, 2019). Based on the presented results, it can be seen that the variation of IFT in the presence of salt is small since saponin is insensitive to salinity. It also can be concluded that 3500ppm was the optimum salinity for both salts (NaCl and CaCl_2) in saponin solution (Soapnut saponin or *Camellia oleifera* saponin). In addition, *Camellia oleifera* saponin presents a better IFT reduction ability than Soapnut saponin. At last, it is worth noting that the monovalent salt (NaCl) shows a superior ability of IFT reduction than nanoparticles (NGF). Compared with 2.91mN/m for Soapnut saponin and 2.7mN/m for *Camellia oleifera* saponin in the presence of NaCl, the lowest IFT achieved by NGF was only 3.24mN/m for Soapnut saponin and 2.97mN/m for *Camellia oleifera* saponin.

6.3.1.4 Influence of Salt Type and Salinity on IFT Modification of the Solution Contain Green Surfactants and Nanoparticles

The combination of surfactant, salt, and nanoparticles has recently received lots of attention. It can improve several rheological characteristics of the fluid system and further decrease the IFT between the oil/water interface. The mechanisms involved in nanoparticles (NGF) and salt (NaCl or CaCl_2) in saponin solution became more complicated than in previous tests. Derjaguin-Landau-Verwey-Overbeek (DLVO) and non-DLVO theories significantly contribute to the aggregation, dispersion, and interactions behaviors of the multi-particle system and the IFT variation at the oil/water interface (Rostami et al., 2019; Sanaei et al., 2019). According to the DVLO theory, an equilibrium status occurred at the initial status of the saponin solution between electrostatic repulsion forces and attractive forces. The repulsion forces generate an energy barrier that prevents particles from contacting each other (Vatanparast et al., 2018). In contrast, the attractive forces (Van der Waals force) draw particles together to break through the barrier, resulting in particle coalescence. Regarding the non-DLVO theory, several forces responsible for the IFT

variation in salt-surfactant-nanoparticles systems are hydration, steric, and magnetic forces ([Rostami et al., 2019](#)).

However, there is still a lack of agreement on the optimum combination ratio and the study of how salinity affects the IFT of the solution containing saponin and nanoparticles. Hence, this part was focused on investigating the influence of the salt type (NaCl and CaCl₂) and salinity (from 1000ppm to 40000ppm) on the IFT variation of the solution containing saponin and nanoparticles (NGF) in order to discover the combined influence of salt and nanoparticles in green surfactant solution. Similar to the previous section, all tested solutions contain the same saponin concentration and NGF: 4.5wt% for the Soapnut saponin batch, 4wt% for the Camellia oleifera saponin batch 0.003wt% NGF for all solutions. The reference IFT value for the Soapnut saponin batch and Camellia oleifera saponin batch was 3.24mN/m and 2.97mN/m, respectively. According to [Figure 6.14](#), under the low salinity (ppm), the IFT decreases with an increase in the concentration of NaCl and CaCl₂, and it reaches the lowest value at the optimum salinity (3500ppm). For Soapnut saponin, the IFT dropped from 3.11mN/m at 1000ppm to 2.52mN/m at 3500ppm (NaCl). In the presence of CaCl₂, the IFT dropped from 3.15mN/m at 1000ppm to 2.67mN/m at 3500ppm. For Camellia oleifera saponin, the IFT decreased from 2.89mN/m at 1000ppm to 2.14mN/m at 3500ppm under NaCl condition and dropped from 2.91mN/m at 1000ppm to 2.55mN/m at 3500ppm under CaCl₂ condition. In contrast to the pure saponin solution, the addition of nanoparticles (NGF) and salt (NaCl or CaCl₂) significantly affect the IFT behavior of saponin in the oil/water system. In the absence of salt, saponin molecules tend to adsorb on the NGF surface, generating the double layer by its high surface energy and surface-to-volume ratio ([Harikrishnan et al., 2017](#)). The creation of microemulsions occurs as a result of the electrostatic forces and hydrophilic interactions between head groups of saponin and NGF, and hence the saponin molecules were distributed at the oil/water interface randomly ([Vatanparast et al., 2018](#)). As a result, the IFT results achieved were 3.24mN/m (4.5wt% Saponin saponin + 0.003wt% NGF) and 2.97mN/m (4wt% Camellia oleifera saponin + 0.003wt

% NGF).

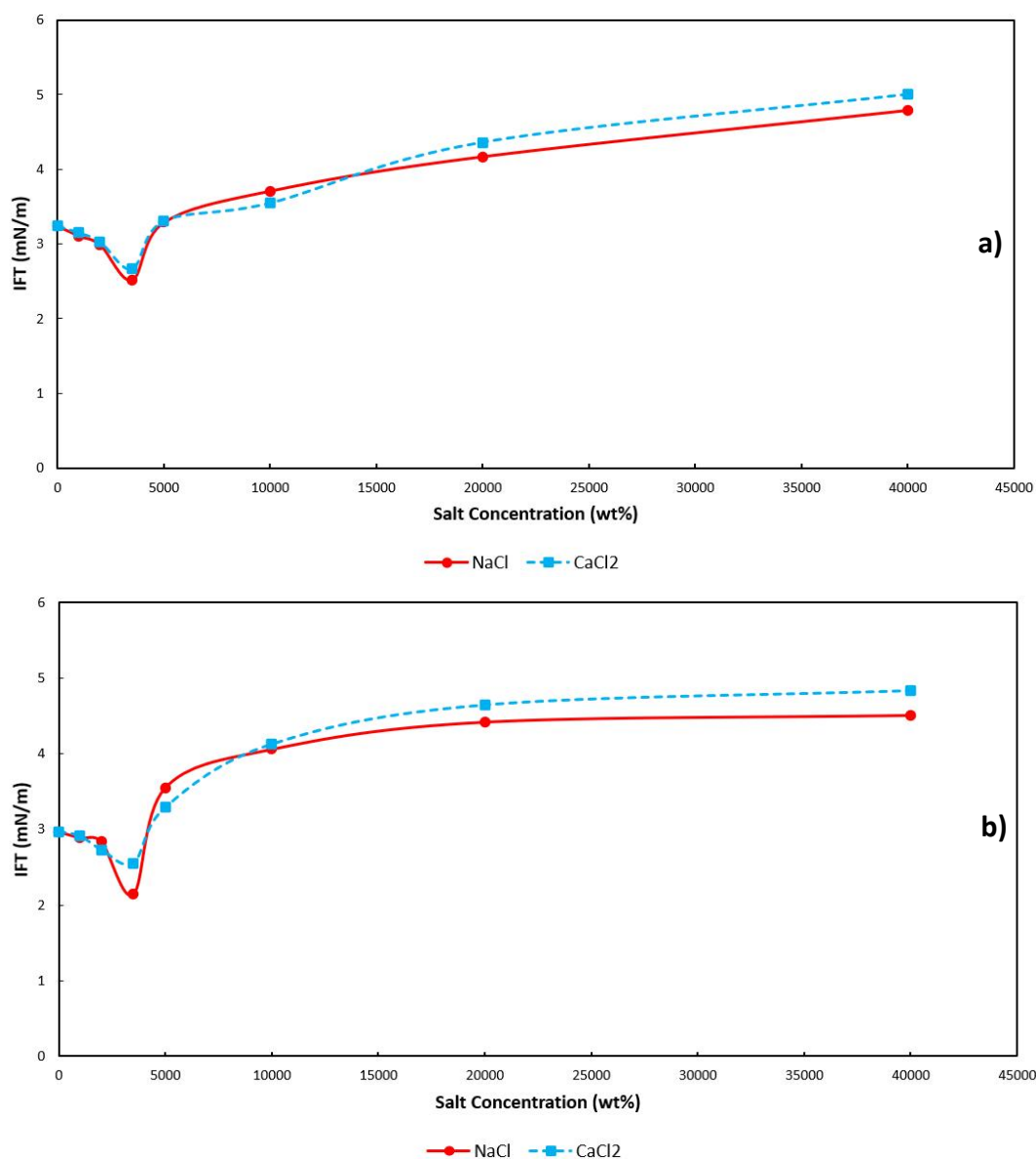


Figure 6.14: IFT results for the combination of saponin and NGF. a) 4.5wt% Soapnut saponin and 0.003wt% NGF, and b) 4% Camellia oleifera saponin and 0.003wt% NGF, in increasing salinity

When NaCl or CaCl₂ was added into the solution with a low concentration (ppm), the counterions of salt screen electrostatic repulsion of the polar head groups of saponin; Consequently, saponin molecules got even closer to each other and arranged a more compact layer at the oil/water interface (Yekeen et al., 2019). As a result, the IFT decreased. A certain amount of saponin molecules and NGF

were dispersed or pushed to the interface due to the Brownian motion and electrostatic repulsion forces between similarly charged saponin head groups and NGF, resulting in the IFT reduction (Olayiwola & Dejam, 2019). On the other hand, the increasing salt concentration enhances the repulsive Coulomb interactions among similarly charged particles (including saponin coated NGF) and induces more saponin molecules to move to the interface (Aminian & ZareNezhad, 2019b). Furthermore, to balance the repulsive force, NaCl or CaCl₂, NGF, and saponin ions deplete one another, resulting in negative free energy for saponin adsorption and micelle generation. The saponin molecules at the interface experience less free energy than in the bulk solutions. Consequently, the interfaces ions do less work, decreasing IFT (Ebag-Ololo & Chon, 2018). It is worth mentioning that the IFT reduction also is contributed by the nanoparticles' negative surface charge (caused by saponin adsorption). Consequently, nanoparticles function as transporters of saponin molecules into the interface by Brownian motion, thereby decreasing the IFT. Hence, the IFT values were able to further decrease from 3.24mN/m to 2.52mN/m (NaCl) or 2.67mN/m (CaCl₂) for Soapnut saponin. Similarly, the IFT results of Camellia oleifera saponin also experienced a drop from 2.97mN/m to 2.14mN/m (NaCl) or 2.55mN/m (CaCl₂). So far, the lowest IFT results were presented by the combination of saponin, NGF and salt compared with the previous tests. The optimum combination concentration was: 4.5wt% Soapnut saponin or 4wt% Camellia oleifera saponin + 0.003wt% NGF + 3500ppm NaCl or CaCl₂.

However, the IFT increased almost twofold when the salinity was above the threshold (3500ppm), just like in the previous tests. For Soapnut saponin, the IFT increased to 4.79mN/m and 5mN/m at 40000ppm for NaCl and CaCl₂, respectively. For Camellia oleifera saponin, the final IFT reached 4.51mN/m for NaCl and 4.84mN/m for CaCl₂ at 40000ppm. When salinity exceeds its limitation of 3500ppm, parts of saponin molecules interact with NGF, resulting in microemulsions, while others interact with salt ions and form cylindrical micelles. Consequently, two agglomerates form in the solution and significantly decrease the number of saponin molecules at the interface. Thus, the IFT increase along with the salt concentration. The presence of salt acts as the stabilizing agent. When the salinity is below

3500ppm, the system consisting of water, oil, surfactant, salt, and nanoparticles is governed by the proton exchange, which enhances the surface potential (Belhaj et al., 2020). Saponin molecules occupy most space of the oil/water interface; saponin-coated nanoparticles become more hydrophobic and move to the interface with saponin molecules (Kumar & Mandal, 2019). However, parts of saponin-coated nanoparticles started to accumulate and precipitate along with the rising dissociation group and surface potential (salinity exceeds 3500ppm), and the amount of precipitation rose in proportion to the salinity. After that, nanoparticles were formed a nano-saponin layer adjacent to the interface, preventing the saponin molecules from accessing it (Olayiwola & Dejam, 2019). The high salinity also decreased the CMC of saponin and caused more micelles to be generated. Therefore, the total concentration of the active saponin molecules in the solution contributes to the IFT reduction. On the other hand, the formed micelles prefer to adsorb on nanoparticles (by Coulomb attraction force) or form a network with nanoparticles than move toward the interface (Ma et al., 2008). Consequently, fewer saponin molecules could reach the interface, leading to an IFT increase. Although Na^+ or Ca^{2+} can enhance surface activity, it also screens the electrostatic repulsion interactions between similarly charged saponin and nanoparticles (Zargartalebi et al., 2014). Therefore, the repulsion force among particles almost fades away. As a result, the IFT increased almost double with the range between 2.29mN/m to 2.37mN/m.

Figure 6.15 and Figure 6.16 demonstrated that the monovalent salt (NaCl) has superior IFT reduction capabilities when compared to the divalent salt (CaCl_2) in the solution of saponin and nanoparticles (NGF). In the case of Soapnut saponin, NaCl was more effective at decreasing IFT than CaCl_2 by 0.15mN/m. This value increased to 0.41mN/m for the Camellia oleifera saponin. The mechanisms that caused this variation were similar to previous tests. The divalent cations Ca^{2+} possess a higher charge and smaller ionic radius than monovalent cations Na^+ . The bigger the ion diameter, the faster the interface fills, and the fewer ions can be deposited on the water-oil interface (Safari et al., 2022). Additionally, because smaller ions have a greater capability to block oil components inside the aqueous

phase, Na^+ is more effective at weakening the IFT. Furthermore, the electrostatic attraction between saponin molecules and nanoparticles was highly affected by the surface charge (zeta potential) (Shabani & Zivar, 2020). With the formation of the micelles and plural hemimicelles, the divalent Ca^{2+} can further enhance the zeta potential than the monovalent Na^+ . Therefore, the solution containing CaCl_2 prevented more saponin molecules from moving to the interface than the NaCl solution. The cations (Na^+ and Ca^{2+}) interact with crude oil's acidic components, lowering their surface concentration and allowing the migration of additional saponin molecules to the oil/water interface (W. Li et al., 2020). This behavior is performed better in monovalent cations (smaller positive charge) than in divalent cations, resulting in the IFT engendered by CaCl_2 being larger than the NaCl . It can be concluded that the optimum concentrations of several additives: 3500ppm for salts (both NaCl and CaCl_2), 4.5wt% for Soapnut saponin, 4wt% for *Camellia oleifera* saponin, and 0.003wt% for NGF.

Additionally, 3500ppm was the optimal salinity for sodium chloride and calcium chloride in both saponin solutions (Soapnut saponin and *Camellia oleifera* saponin). The combination of 4.5wt% Soapnut saponin or 4wt% *Camellia oleifera* saponin, 0.003wt% NGF, and 3500ppm NaCl or CaCl_2 generated the lowest IFT in its batch tests. The lowest IFT was presented by combining 4wt% *Camellia oleifera* saponin, 0.003wt% NGF, and 3500ppm NaCl , 2.14mN/m. Apart from that, *Camellia oleifera* saponin exhibits superior IFT lowering abilities compared to Soapnut saponin. Finally, it is worth mentioning that the solution's additional nanoparticles could reduce further IFT (between 2.27mN/m to 2.37mN/m) than the solution containing saponin and salt.

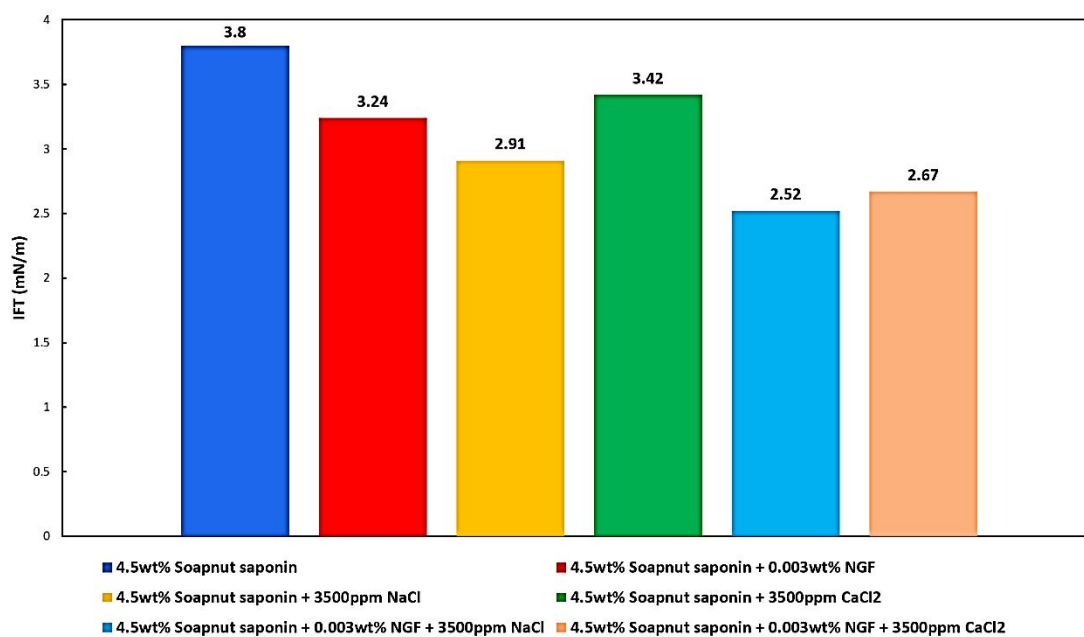


Figure 6.15: The summary of IFT reduction ability of Soapnut saponin in the presence of different additives and combinations

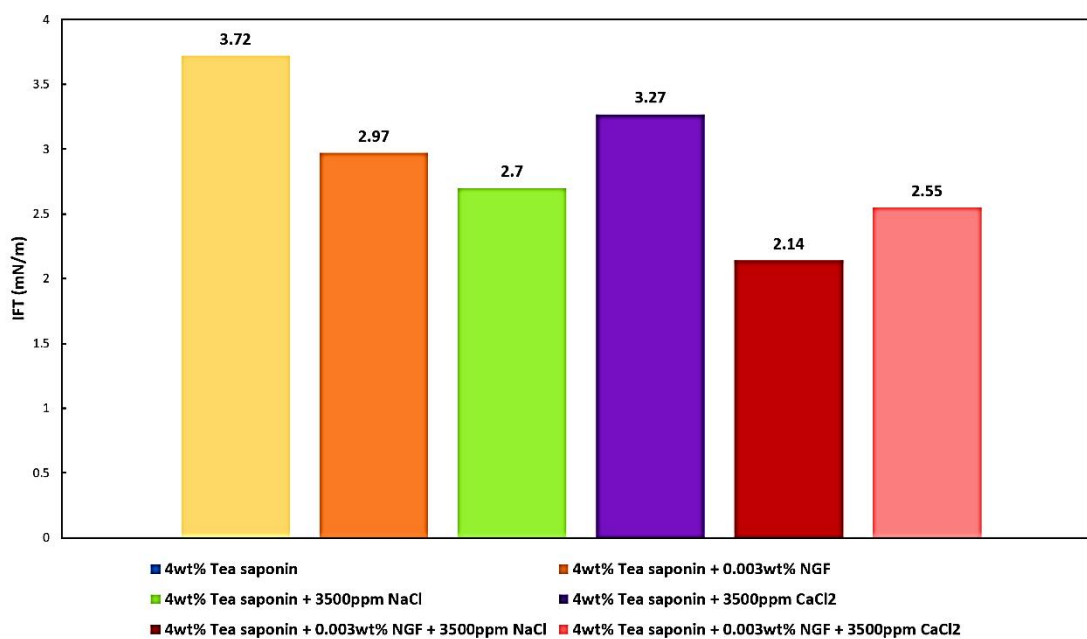


Figure 6.16: The summary of IFT reduction ability of Camellia oleifera saponin in the presence of different additives and combinations

6.3.2 TEM

The effectiveness of IFT reduction of the combination of saponin, nanoparticles, and salt has been proven in the above sections. However, it is still a lack of information about the bonding and interactions among the additives. Therefore, TEM was applied in this section to investigate the morphological characteristics and microstructure of the green smart nanofluid. The optimum concentration ratio (4.5wt% Soapnut saponin or 4wt% Camellia oleifera saponin, 0.003wt% NGF, and 3500ppm NaCl) generated the lowest IFT was used. The solutions were fresh and homogenously prepared (followed section 6.2.3.3), then thoroughly dried by the freeze dryer into fine powder. After that, 1mg powder was placed on the carbon-coated grid with an additional thin carbon film layer. As shown in [Figure 6.17](#), A series of crystallization processes happened.

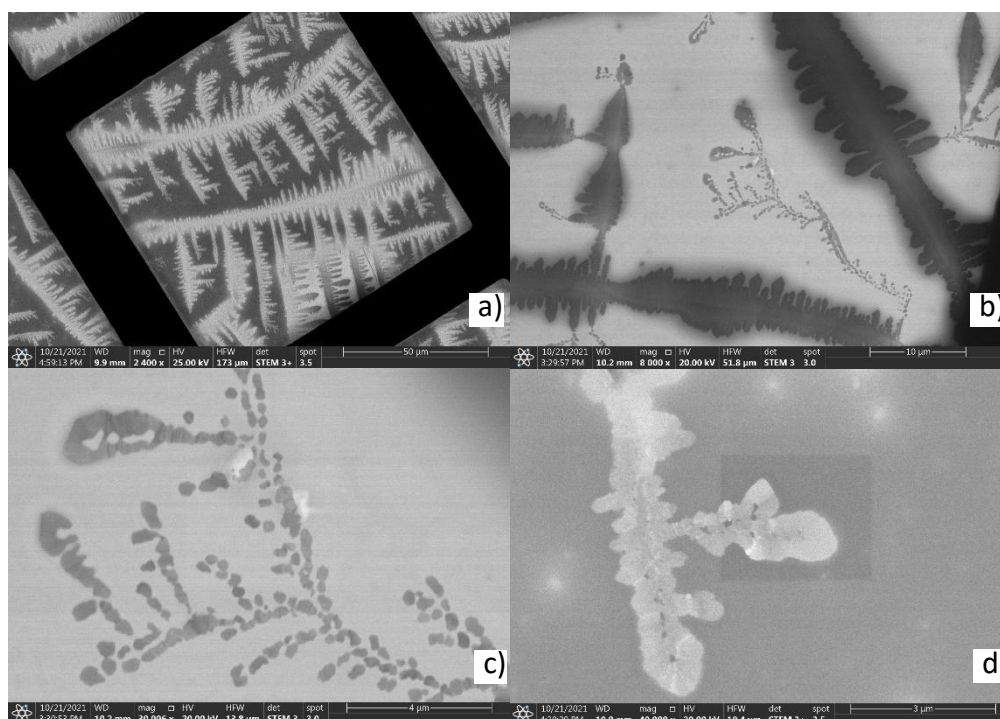


Figure 6.17: TEM images of the Fern-like crystal structure formed by the combination of saponin, NGF, and NaCl. a) self-assembled structures with Camellia oleifera saponin, b) self-assembled structures with Soapnut saponin, c) aggregated multi-particles of Camellia oleifera saponin, and d) aggregated multi-particles of Soapnut saponin

The molecules are arranged by themselves to form a Fern-like crystal structure. These mixed particles demonstrate the self-assembled structure's inherent physical properties and corporate characteristics. According to [Wei et al. \(2019\)](#), the formation of self-assembled structures occurs when the solution contains sufficient particles and molecules that tend to attach, which are held together by van der Waals forces and electrostatic interactions to form complex structures. In addition, the saponin molecules encapsulate individual NGF particles and construct interdigitated bilayers around them ([Pal & Mandal, 2020](#)). Based on the region of examination and the distribution of particles, various morphologies were observed from the same solution. [Figure 6.17c](#) presented aggregated multi-particles as irregular rounded dark spots. The presence of nanoparticles and salt affects the bulk morphology into a Fern-like structure ([Figure 6.17d](#)).

Saponin is an amphiphilic molecule with a hydrophobic tail and hydrophilic polar heads groups. The presence of salt and nanoparticles reduced the CMC of saponin and led to the saponin aggregation (micelles) being more easily formed. Micelles formed by saponin are small structures (10-11.5nm) with a hydrophilic surface and a hydrophobic inside. In solution the hydrophilic heads of saponin connect to form a spherical shell at the exterior, and parts of hydrophobic NGF can be enclosed within micellar interiors ([Harikrishnan et al., 2017](#)). On the other hand, the bilayer structures formed by saponin-coated-NGF particles further enhance the ligand-ligand interdigitation between particles. Following that, delicate balancing of interparticle interactions such as hydrogen bonding, ionic bonding, Van der Waals interactions, hydration forces, electrostatic forces, and steric force between saponin and NGF particles in the presence of salt ionization leads to the self-assembly and crystallization behavior ([Shaban et al., 2017](#); [Wei et al., 2019](#)). Consequently, the highly ordered and densely-packed array of self-assembly particles formed a Fern-like structure. In general, these self-assembled Fern-like structures formed by highly ordered active multi-particles provide several advantages: 1) it integrates diverse functions of additives to form the new multi-particles with collective properties; 2) the Fern-like structure empowers the low salinity green surfactant nanofluid to have higher stability and compatibility,

especially facing the harsh reservoir conditions; 3) the property of self-assembly enhance the surface and interfacial activity; 4) the Fern-like structure and self-assembly behavior can contribute a better dispersion ability and stability of surface-active agents (saponin) on oil/water interface, and thereby induce the IFT reduction.

6.4 Conclusion

In this chapter, a series of tests were conducted to evaluate the IFT reduction in the presence of the green surfactants (Soapnut saponin and *Camellia oleifera* saponin), nanoparticle (NGF), and salts (NaCl and CaCl_2). Furthermore, TEM was applied to observe the bonding and interactions among the additives. The following conclusions were then drawn:

- 1) Increasing the saponin concentration reduces the IFT, which cause by the rapid diffusion of saponin molecules in solution, and the saponin monomers adsorbed on the oil-aqueous interface by hydrogen bonding. However, the IFT of saponins showed a slight rise when the concentration exceeds their optimum point (Soapnut saponin is 4.5wt% and *Camellia oleifera* saponin is 4wt%), which is mainly induced by the natural coagulants and impurities.
- 2) Anionic surfactant (*Camellia oleifera* saponin) was achieved a lower IFT value than the nonionic surfactant (Soapnut saponin), which induced by the heavier lateral electrostatic interactions of *Camellia oleifera* saponin drive the active saponin further adsorbed at the oil/aqueous interface.
- 3) When the additional NGF was added to the saponin solution, the IFT was further reduced compared to the results achieved by pure saponin. The mechanisms of electrostatic interactions and adsorption behavior contribute to IFT decreasing along with the concentration of NGF until it reaches its optimum point. Additionally, the lowest IFT achieved in the presence of NGF and saponin was 3.24mN/m and 2.97mN/m. The optimum concentration for NGF was 0.003wt%. However, the IFT increased for both saponins when the concentration of NGF was above 0.003wt%. It is mainly caused by the excess NGF occupying the interface space, thereby fewer saponin molecules

adsorbed. Also, it aggravates aggregation and enhances the electrostatic interaction between saponin and NGF particles, causing the IFT to increase.

- 4) For the combination of saponin and salt, NaCl or CaCl₂ decreases the IFT until the concentration reaches its optimum salinity, which could be linked to the salting-in effect, electrokinetic repulsion, double-layer screening effect, and migration of oil components. When the salinity passes 3500ppm, the IFT increases due to the enhanced electrostatic repulsion force restraining saponin from further dissolving into water.
- 5) Divalent salt CaCl₂ had a more negative influence than monovalent salt NaCl on the mechanism of salting-in/salting-out, variation of dissolution rate, and ion activity (ion valence, ionic charge, and ion radius), which could be related to the molecule radius). For Soapnut saponin, NaCl could further decrease IFT than CaCl₂ by 0.51mN/m. For Camellia oleifera saponin, this value increased to 0.57mN/m.
- 6) For the combination of saponin (Soapnut saponin or Camellia oleifera saponin), salt (NaCl or CaCl₂), and nanoparticles (NGF), the IFT decreases with an increase in the concentration of salt. The lowest IFT value was achieved at the optimum salinity (3500ppm) for NaCl and CaCl₂. In contrast to the pure saponin solution, the addition of nanoparticles and salts could reduce the IFT by around 33.7% further. The salting-in effect is mainly induced by repulsive Coulomb interactions between similarly charged particles and saponin adsorption. However, the IFT increased almost twofold when the salinity was above the threshold (3500ppm), just like in the previous tests. The two kinds of agglomeration significantly decrease the number of saponin molecules at the interface. On the other hand, parts of saponin-coated nanoparticles start to accumulate, precipitate and form a nano-saponin layer adjacent to the interface, preventing the saponin molecules from accessing it. As a result, the IFT increased almost double with the range between 2.29mN/m to 2.37mN/m.
- 7) The optimum salinity for both NaCl and CaCl₂ was 3500ppm. The ideal concentration for NGF was 0.003wt%. For Soapnut saponin and Camellia

oleifera saponin, the finest concentration was 4.5wt% and 4wt%, respectively.

- 8) TEM was used to examine the morphological properties and microstructure of a low salinity green surfactant nanofluid. It demonstrates that a series of crystallization processes occurred, and the molecules self-organize to form a Fern-like crystal structure. In salt ionization, a precise balancing of interparticle interactions such as hydrogen bonding, ionic bonding, Van der Waals interactions, hydration forces, electrostatic forces, and steric force between saponin and NGF particles leads to self-assembly and crystallization behavior.

Chapter 7: Wettability Study in Low Salinity Green Surfactant Nanofluid EOR Solutions

7.1 Introduction

Apart from implementing formation evaluation, the wettability condition of reservoir rock and its impact on rock-fluid characteristics cannot be neglected. Crude oil is frequently trapped in the reservoir rock's small pores or presented as a thin layer on its surface. The effectiveness of several oil recovery methods (like water flooding, surfactant injection, and nanoparticle flooding) is frequently impeded by the oil-wet or intermediate-wet property of formation rock. Oil-wet formation considerably maintains the oil phase more in the dense rock matrix, and intermediate-wet formations exhibit a higher affinity towards water than oil ([S. R. Shadizadeh & Amirpour, 2017](#)). Formation rocks saturated with various liquids are a complicated system with continual interactions between fluid and rock. Wettability refers to a liquid's tendency to spread on a solid surface when it comes into contact with another immiscible liquid related to the fluid's interactions and fluids-solids adhesion ([Huibers et al., 2017](#)). Improving the rock's wettability from oil-wet or intermediate-wet to water-wet is critical to improving oil recovery. There have been numerous studies that have identified the combination of salt, nanoparticles, and surfactants as appropriate modifiers in wettability alteration, although the consistency of the performance, the mechanisms or multi-mechanism of wettability alteration, and multi-interaction between different formation rocks and tested solutions have not yet been fully explored ([Pichot et al., 2012](#); [Aminian & ZareNezhad, 2019a](#); [Kazemzadeh et al., 2019](#); [Rostami et al., 2019](#); [Mofrad & Saeedi Dehaghani, 2020](#)). Therefore, this chapter investigated the wettability alteration by the novel green EOR solutions that contain saponin, salt, and nanoparticles in Berea sandstone, Malaysia sandstone, and Mancos shale. Contact angle measurement was based on the droplet and bubble methods embedded in the drop shape analyzer. Surfactants were chosen from the two extracted saponins from Soapnut and Camellia oleifera. NGF was used as nanoparticles. Monovalent salt NaCl and divalent salt CaCl_2 were applied as salt. Furthermore, the optimum concentrations

and mixing ratio of various additives were investigated in this chapter. A series of sensitivity analysis comparisons were also included.

7.2 Methodology

7.2.1 Experimental Apparatus

Most of the experimental apparatus were the same as in Chapter 6. The wettability condition was measured by the contact angle of the oil droplets at the rock surface. DSA100B manufactured by Krüss GmbH was applied to determine the contact angle at ambient conditions. The glass box has two bracing pieces to support the core slice (3.2cm x 0.1cm), specifically designed to estimate the contact angle between oil droplets and rock surfaces. Both types of equipment are shown in Figure 7.1. ThermoFisher Scientific's Quattro-S ESEM was utilized to investigate the particle interaction of salt, saponin, nanoparticle, and rock before and after core slices were immersed in the designed solution. All employed equipment was well cleaned to ensure excellent precision and repeatability, particularly the needle tip, which was well-treated due to the oil's tendency to adhere to its outer surface. The Malaysia core was hand drilling by Shaw portable core drill that was manufactured and distributed by Shaw Tool of Yamhill, Oregon, USA (shown in Figure 7.2)

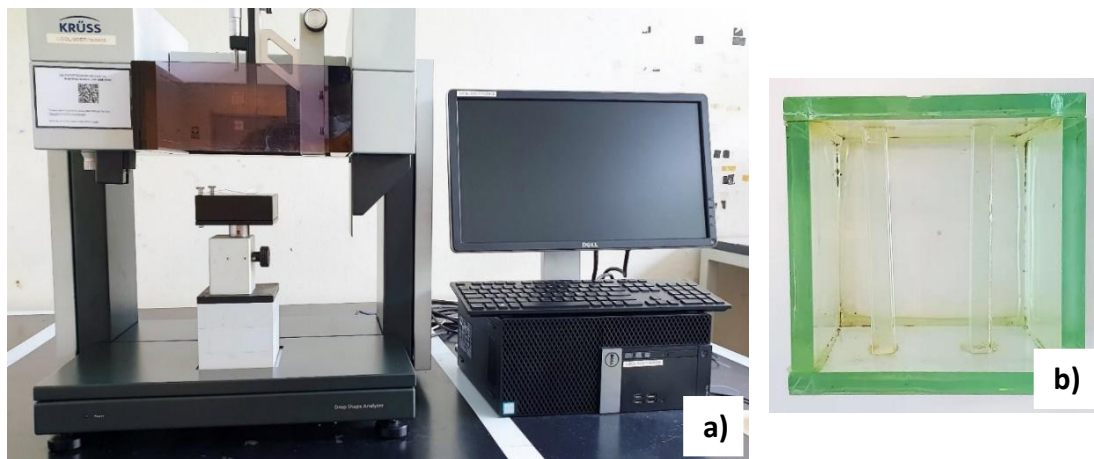


Figure 7.1: Contact angle measurement equipment. a) DSA-100B and b) Glass box for contact angle measurement



Figure 7.2: Shaw portable core drill

7.2.2 Experimental Materials

The materials prepared and experiments conducted were in accordance with Chapter 6. The Berea sandstone column (D: 3.8cm, L: 7.6cm), product ID SS-103, was purchased from Kocurek Industries (Hard Rock Division) from the upper Devonian formation with 80-120mD (KCl) permeability and 18-21% porosity. The Mancos outcrop shale core, with 3.8cm diameter and 7.6cm length, was purchased from Kocurek Industries (Hard Rock Division). The Malaysia sandstone cores (D: 3.2cm, L: 7cm) were coring at 2 meters depth from the Taman Awam outcrop by a shaw portable core drill (longitude 4°21'57.03"N, 113°58'45.37"E). Three formation cores are shown in [Figure 7.3](#). The mineralogy of those formation rocks also estimated by Energy Dispersive X-Ray Analysis (EDX) analysis with a TEM and summarized in [Table 7.1](#).



Figure 7.3: Formation cores used in wettability test. a) Berea sandstone core, b) Shale core, and c) Malaysia sandstone core

Table 7.1: The mineralogy of Berea sandstone, Mancos shale, and Malaysia sandstone

Berea sandstone	
Mineral	Concentration (wt%)
Quartz	86
Kaolinite	5
Feldspar	4
Chlorite	2
Calcite	2
Dolomite	1
Mancos shale	
Mineral	Concentration (wt%)
Quartz	54
Total clay	15
Ankerite	10
Calcite	8
Potassium feldspar	5
Siderite	5
Plagioclase	3
Malaysia sandstone	
Mineral	Concentration (wt%)
Quartz	88
Kaolinite	6
Albite	4
Illite	1
Calcite	1

7.2.3 Test Fluids Preparation

The preparation of crude oil, pure saponin solution mixed solution was the same as in Chapter 6. All the solutions were freshly prepared to avoid agglomeration and contamination.

7.2.4 Formation Core Slices Cutting, Cleaning, and Aging

In order to determine the wettability condition of rocks to various fluids, each core sample was dry cut into several horizontal thin slices with 5mm thickness by Lortone TS8-C Lapidary Trim Saw. After that, each slice was then thoroughly sanded by a 15 μ m diamond flat lap manufactured by Hillquist Thin Section Grinder. The final polish was conducted manually with abrasive paper until all core slices possessed the same smooth surface as [Figure 7.4](#). After that, all polished core slices were sent to the Soxhlet extractor for the cleaning stage. Reagent grade acetone and methanol were used to remove dissolved organic matter or inorganic contaminants from the core slices, then dried in an oven with a maximum temperature of 75°C for 72 hours for moisture removal ([Nwidee, 2017](#)).

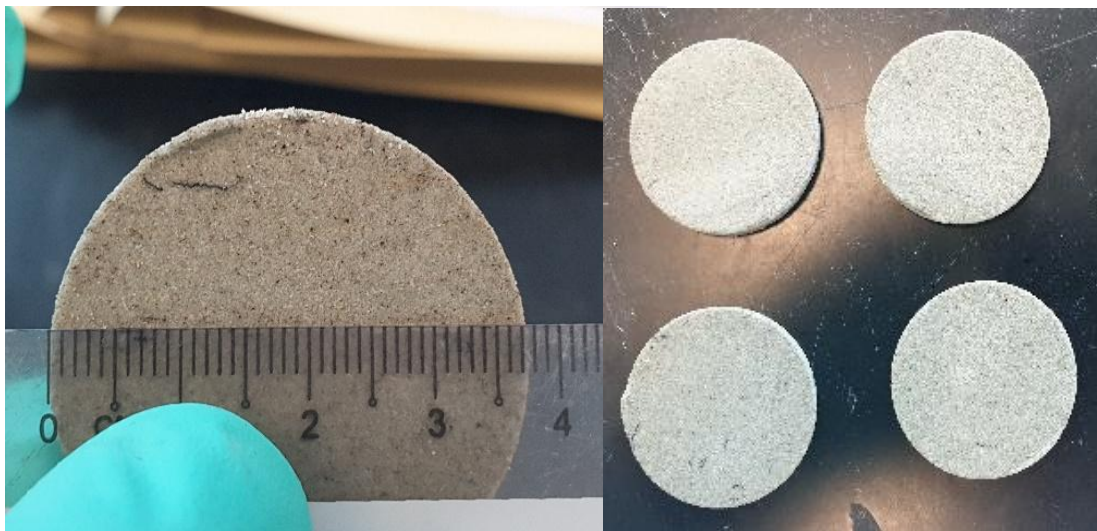


Figure 7.4: Core slice and polishing

All core slices were soaked in the formation water with 100,000 ppm NaCl at 75°C and 0.03 MPa within 48 hours when the drying stage was completed. After that, the slides were then transferred to the drying oven with full hot air ventilation at 75°C for 72 hours for the drying process. Then, 200ml of crude oil was poured

into a glass beaker, and all the core slices were evenly immersed in it. The beaker was covered with aluminum foil and placed in the drying oven at 75°C for 16 days before wettability measurements (Hu et al., 2016). The comparison of core slices before and after aging is shown in Figure 7.5.

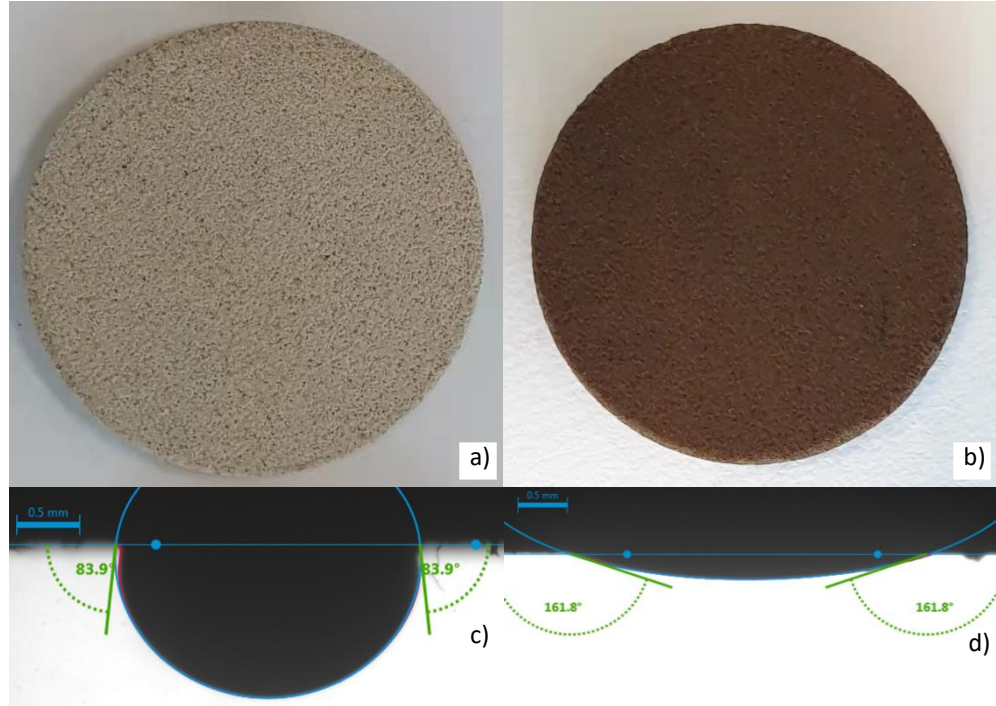


Figure 7.5: Berea sandstone core slice. a) before aging, b) after aging, c) contact angle before aging: 83.9°, d) contact angle after aging: 161.8°

7.2.5 Contact Angle Measurements (Wettability)

Contact angle measurement is a widely used technique for assessing surface wettability characterization. DSA-100B (with an accuracy of $\pm 0.1^\circ$) was used to measure the contact angle of an oil droplet on the core slices in the designed solution. The sessile drop/captive bubble method estimated the contact angle using drop shape analysis, and the measurement model was Young-Laplace (Okunade et al., 2021). The software automatically recorded the data every second, and the time was set to 30 minutes to ensure that the oil droplet reached equilibrium (Table 7.2). In order to measure the contact angle, the designed solution was filled in a glass box (5cm x 5cm x 5cm) that had a bracing piece (slice holder), and the aged core

slice was fully immersed in it. In the meantime, the crude oil was filled in a 3ml syringe with a 0.5mm J-shape stainless needle (manufactured by Fisher Scientific). After that, the J-shaped needle was completely immersed in the test fluid, and the tip of the needle was pointing upwards on the core slice surface from below (Xue et al., 2021). Then a drop of 5 μL crude oil was carefully dispensed from the needle and gently in contact with the rock surface.

The schematic image of contact angle measurement is shown in Figure 7.6. It is critical to make sure no air bubbles were floated on the rock surface. Three measurements were taken for each test, and the average value was reported. All the tests were performed at room temperature (20°C) and atmospheric pressure. It is worth noting that each core slice was used around 5-6 times, and the new oil droplet was dropped to a different spot of the slice at identical conditions for each test. During the wettability measurements, three different types of core slices were tested: Berea sandstone, Mancos shale, and Malay sandstone. All core slices do not account for the surface roughness and material heterogeneity. The mixing concentrations were the same as the values in Section 6.2.4.3.

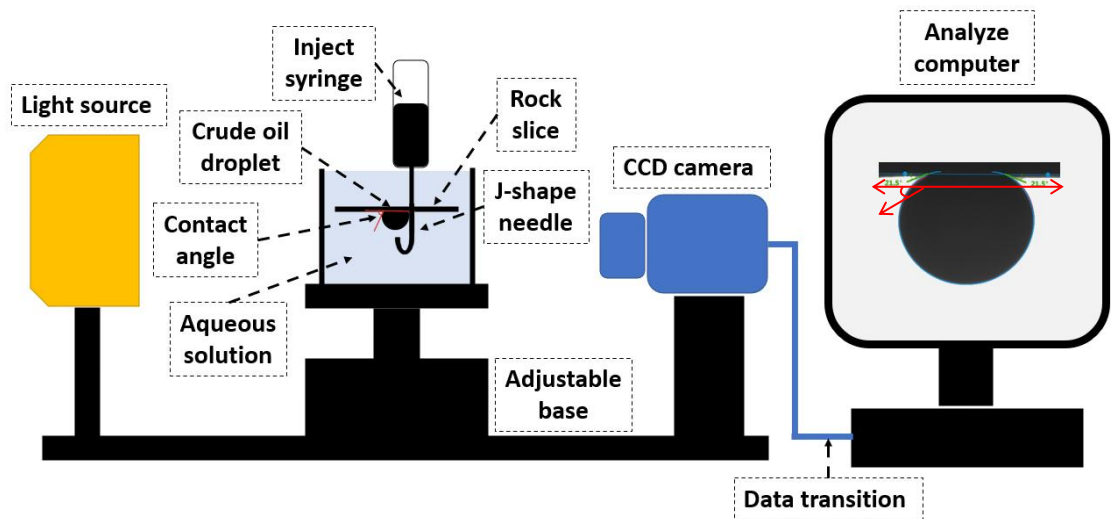
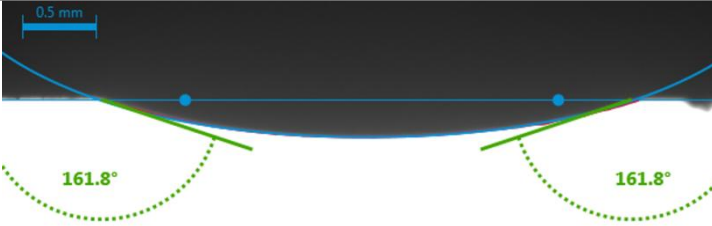
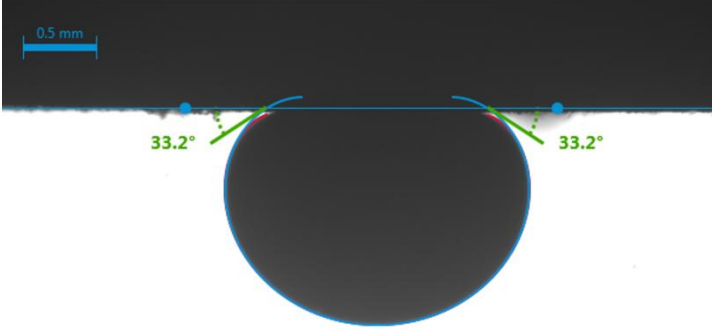
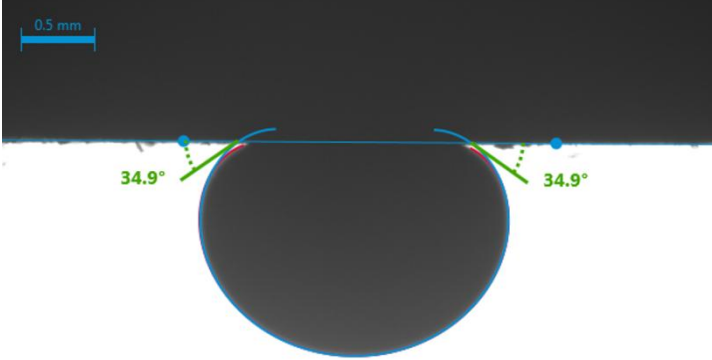


Figure 7.6: Schematic image of DSA-100B apparatus used to contact angle measurement

Table 7.2: Contact angle images for crude oil droplet on Mancos shale slice in the *Camellia oleifera* saponin solution

Concentration n (wt%)	Angle (degree)	Image
0	161.8	
4.5	33.2	
7	34.9	

7.2.6 SEM Characterization

As shown in [Figure 7.7](#), the Quattro ESEM (manufactured by ThermoFisher Scientific) was used to observe the particle interaction between salt, saponin, nanoparticle, and rock. The theoretical introduction of this technique has been presented in Chapter 4. The tested sample has been divided into two parts: the first part contained clean rock slices before wettability measurement (Berea sandstone, Mancos shale, and Malaysia sandstone), the second part was the slices after experienced wettability measurement (fully immersed in the designed solution). All slices were thoroughly dried in the oven with full hot air ventilation at 75°C for 72

hours, then separately stored in the blue cap bottle to avoid any contamination. A low vacuum mode - low vacuum detector (LVD) with 0.6x to 5000x magnification was used for SEM analysis. All test slices were left uncoated due to their electrical conductivity, which could have obliterated surface information concerning a failure cause (Zhao et al., 2021).



Figure 7.7: Quattro-S ESEM

The accelerating voltage for the electron beam was chosen between 7.50 and 10.00 kV (HV condition). The spot size was fixed between 2.0 and 3.0 microns. In order to provide a consistent image quality, double-sided carbon conductive tape was applied to the sample holder, and the core slice was distributed on top of the tape (Srivastava et al., 2020). The SEM image of the Berea sandstone core slice (before aging in crude oil) is shown in Figure 7.8.

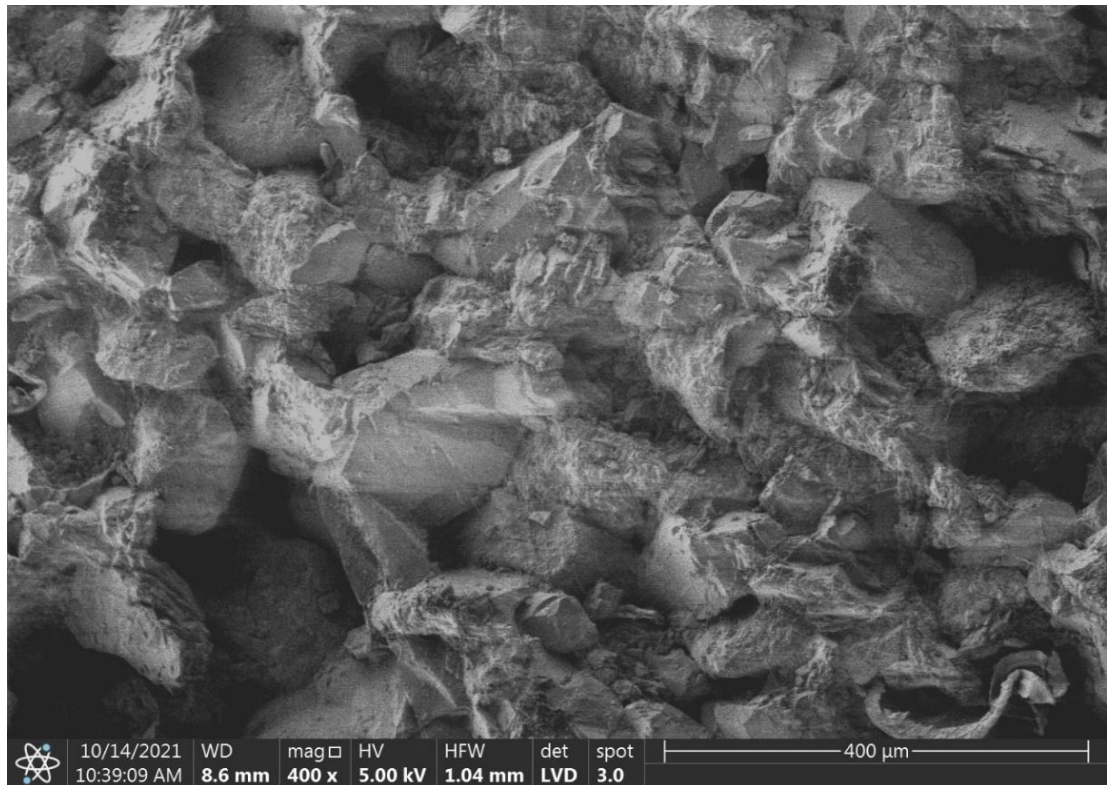


Figure 7.8: SEM image of Berea sandstone core slice (before aging in crude oil)

7.3 Results and Discussions

7.3.1 Three-phase Contact Angle Measurements

It is incontestable to recognize the significance of wettability and its effect on rock-fluid characteristics; however, it is also considered a complicated process that remains a challenge to understand fully. When it comes to oil recovery, the character of oil-wet or intermediate-wet of the formation rock frequently leads to poor results. On the contrary, a thin water film coating the rock surface in water-wet status is desired for effective oil transmissions and productivity (Huibers et al., 2017). Therefore, wettability alteration from oil-wet or intermediate-wet to water-wet is considered important in oil recovery. As a cheaper and more effective method, low salinity water flooding can generate positive capillary force and boost the microscopic sweep efficiency, improving the wetting condition. The fundamental mechanisms have been acknowledged as double-layer expansion, multi-ion exchange, salting-in effect, and pH increase (Katende & Sagala, 2019). In addition, nanoparticles have been demonstrated to be an inter-facially active and effective modifier of wettability by the mechanisms like wettability alteration, high

stability, disjoining pressure, IFT reduction, and Brownian motion (Olayiwola & Dejam, 2019). The surfactant has been considered an effective additive to improve the interface wettability condition by adsorption behavior (Peng & Nguyen, 2020). However, the application is always constrained by a high loss rate and micelle formation. Therefore, in this chapter, the study of wettability alteration in the presence of saponin, nanoparticles, and salt contributes to existing knowledge about fluid-rock interactions and provides new multi-mechanisms concepts.

In this study, the wettability estimations were systematically examined based on the concentration and exposure time of saponin (Soapnut saponin or *Camellia oleifera* saponin), nanoparticles (NGF), salt (NaCl or CaCl₂), and the combination among them. Furthermore, the synergistic effect (complicated interactions and multi-mechanisms) of combining low salinity water flooding, surfactant flooding, and nanoparticle flooding on the fluid-rock interface is also comprehensively addressed. In order to fulfill the economic achievements and avoid aggregation (clog oil-containing pores), the optimum concentrations of saponins, nanoparticles, and salts (generated at the lowest contact angle) were also estimated.

As shown in Table 7.3, the reference tests of contact angle (as a benchmark) were conducted when the variable additives were not added to the test solution. The first reference tests were initially tested on the clean aged rock slices, and the results indicate a strong oil-wet state for three different rock slices. Other reference tests were conducted under the optimum concentration of base additives prior to variable additives treatment.

Table 7.3: Reference values of contact angle under variable additives

Base Additives	Variable Additives	Solution Environment	Mancos Shale (degree)	Berea Sandstone (degree)	Malaysia sandstone (degree)
-	-	Ultra-pure water	161.8	143.15	152
Soapnut saponin	NGF	Soapnut saponin + NGF	37.7	24.3	21.2
Camellia oleifera saponin	NGF	Camellia oleifera saponin + NGF	33.17	22.8	19.9
Soapnut saponin	NaCl or CaCl ₂	Soapnut saponin + NaCl or CaCl ₂	37.7	24.3	21.2
Camellia oleifera saponin	NaCl or CaCl ₂	Camellia oleifera saponin + NaCl or CaCl ₂	33.17	22.8	19.9
Soapnut saponin NGF	NaCl or CaCl ₂	Soapnut saponin + NaCl or CaCl ₂ + NGF	28.93	18.81	16.54
Camellia oleifera saponin NGF	NaCl or CaCl ₂	Camellia oleifera saponin + NaCl or CaCl ₂ + NGF	24.75	16.27	14.86

7.3.1.1 Effect of Green Surfactants on Wettability Alteration

The effectiveness of saponins (Soapnut saponin and Camellia oleifera saponin) as wettability modifiers were established on the three different core slices of Mancos shale, Berea sandstone, and Malaysia sandstone. As the preliminary tests, various concentrations (0.1wt% to 7wt%) were applied to determine the optimum concentration that resulted in the lowest contact angle in the absence of other additives (nanoparticles and salts). As shown in [Figure 7.9a](#), the contact angles of all three different core slices significantly decreased along with the increasing saponin concentration until a particular concentration close to the CMC of saponin. The contact angle increased slightly along with the saponin concentration, and a water-wet status was achieved at last. Specifically, for Soapnut saponin, increasing concentration from 0wt% to 5wt% decreases the contact angle from 161.8° to 37.7°, slightly above the CMC of Soapnut saponin (4.5wt%). After increasing the

concentration to 6wt% and 7wt%, the contact angle demonstrated no significant change as it remained nearly similar with 37.7° and 38.2°, respectively. For Berea sandstone and Malaysia sandstone, the results show a similar trend as Mancos shale. The contact angle of Berea sandstone decreased from 143.15° to 24.34° at 5wt%, then slightly rose to 28.89° (6wt%) and 26.97° (7wt%). In Malaysia sandstone, the contact angle dropped from 152° to 21.2° at 6wt%, and then the angle maintained similar to 22.4° at 7wt%. According to [Figure 7.9b](#), the contact angle generated by *Camellia oleifera* saponin experienced a similar trend as Soapnut saponin. However, the angle was able to further decrease to 33.17° at 4.5wt% (Mancos shale), 22.8° at 4.5wt% (Berea sandstone), and 19.93° at 5wt% (Malaysia sandstone).

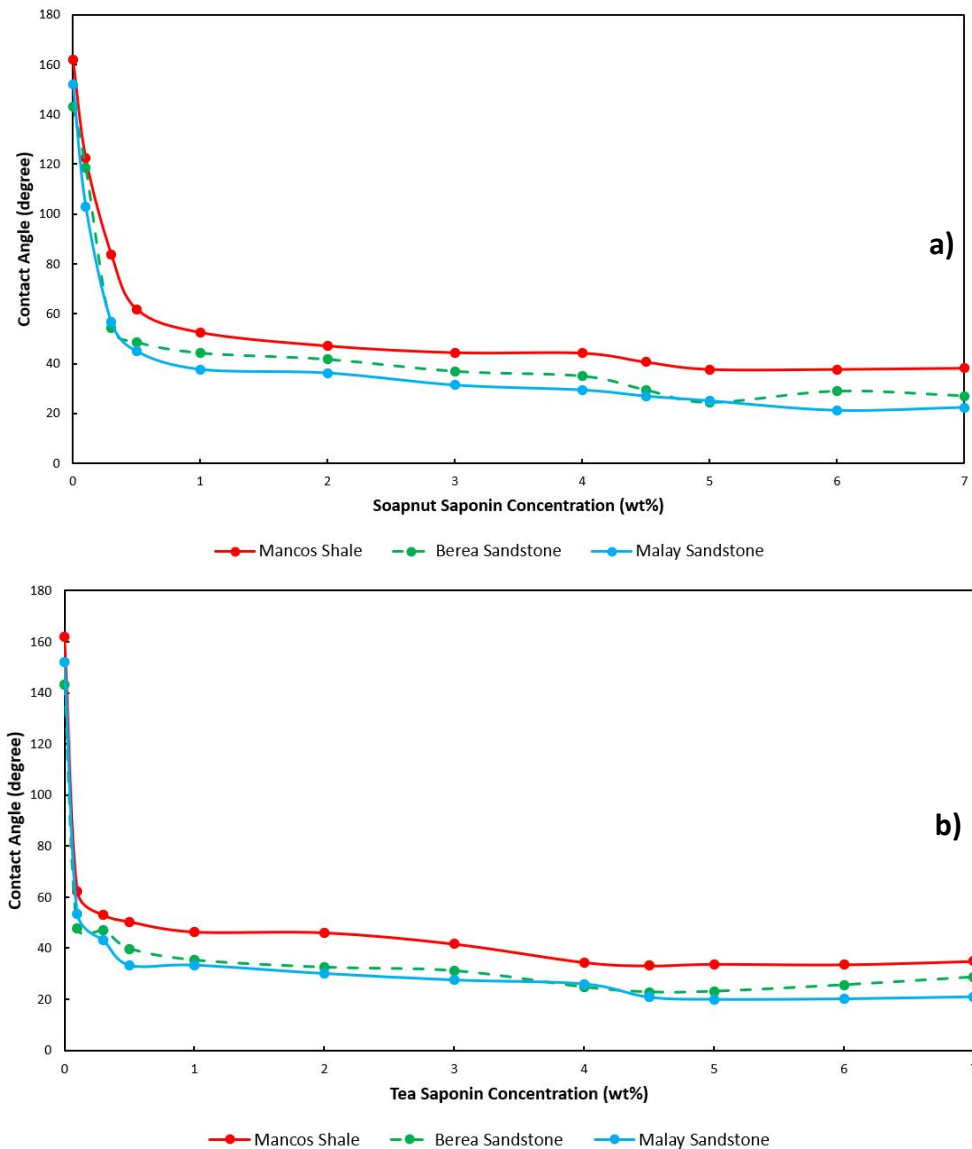


Figure 7.9: Contact angle of the various rock slices under increasing concentrations of a) Soapnut saponin, and b) *Camellia oleifera* saponin

Various factors influence wettability at the rock surface, including the characteristics of saponin, mineralogy of the formation rock, and crude oil compounds adsorbed on the rock surface. The wettability modification from strong oil-wet to water-wet implies the favorable adsorption behavior on the rock surface attributed to the Coulomb interactions and the same surface charge (Nourani et al., 2020). In order to further investigate the mechanisms of the wettability alteration by saponin, the zeta potential of both saponins was measured. As mentioned in Chapter 4, the Soapnut saponin was considered a nonionic surfactant, and *Camellia oleifera* saponin was considered an anionic surfactant (negative surface charge). The *Camellia oleifera* saponin molecules with a negatively surface charge absorb the positive basic components in crude oil from the rock surface through the electrostatic attraction force, forming ion pairing between the saponin molecules and the rock surface (Liu et al., 2022). Therefore, *Camellia oleifera* saponin was achieved a lower contact angle than Soapnut saponin. On the other hand, another explanation for the wettability alteration was the weakening in the adsorption of crude oil components onto rock surfaces by forming a layer (Kamal et al., 2017). Hydrophobic interaction between the hydrophobic part of oil components (adsorbed at rock surface) and the accumulated saponin molecules results in the disturbance of the overlying oil layer (Hou et al., 2015). Take Soapnut saponin as an example; the contact angle tests yielded the optimum concentrations of 5wt% and 6wt%, whereas 4.5wt% for the IFT in the absence of formation rocks. This demonstrates how the composition/mineralogy of the formation rocks affects the saponin's adsorption.

Although the increasing saponin concentration decreases the contact angle, the angle increases when the concentration exceeds its optimum points. For example, the angle raised from 22.8° at 4.5wt% (optimum concentration) to 28.66° at 7wt% when *Camellia oleifera* saponin was applied in Berea sandstone. Several reasons may be responsible for these abnormal phenomena: 1) the excessive saponin concentration causes micelle formation and more saponin adsorbed on the

rock surface, which leads to a mass loss of saponin and the decreased saponin concentration in solution, 2) the denser saponin monomers inhibit the spontaneous movement and relocation of saponin from the bulk solution to rock surfaces, 3) the natural coagulants and impurities contained in the saponin cause the formation of membranous to flocculate compounds at high concentration (Arabloo et al., 2016; Sajjad et al., 2019; Saxena et al., 2019). Therefore, the contact angle started to increase.

Overall, the lowest contact angle achieved by Soapnut saponin and *Camellia oleifera* saponin were summarized in Table 7.4.

Table 7.4: The optimum contact angle and related concentration achieved by saponins in various core slices

	Mancos shale (degree) (concentration)	Berea sandstone (degree) (concentration)	Malaysia sandstone (degree) (concentration)
Soapnut saponin	37.7 5wt%	24.34 5wt%	21.2 6wt%
Camellia oleifera saponin	33.17 4.5wt%	22.8 4.5wt%	19.93 5wt%

It was clearly shown that the *Camellia oleifera* saponin performs a superior wettability alteration than Soapnut saponin. The *Camellia oleifera* saponin molecules with a longer tail length possess a higher adsorption density and the ability to form the hydrophobic layer on rock surfaces than Soapnut saponin (Luan et al., 2020). Furthermore, the negative charged *Camellia oleifera* saponin could adsorb the positive basic components in crude oil from the rock surface by electrostatic attraction force (Khayati, 2020). On the other hand, the level of adsorption that occurred at *Camellia oleifera* saponin was less than the Soapnut saponin. Most sandstone formations and shale formations have a negatively charged surface (depending on mineralogy); the amount of adsorption on *Camellia oleifera* saponin was far less than the Soapnut saponin of the electrostatic repulsion forces on similarly charged particles (Lee & Lee, 2019, p. 2). Therefore, *Camellia oleifera* has more active saponin in solution to interact with the crude oil. The optimum injection concentration for Soapnut saponin was 5wt% for Mancos shale

and Berea sandstone and 6wt% for Malaysia sandstone. In terms of *Camellia oleifera* saponin, 4.5wt% (Mancos shale and Berea sandstone) and 5wt% (Malaysia sandstone) were selected as the appropriate injection concentration based on the contact angle measurements. It is worth noticing that the optimum concentration leading to the lowest contact angles was observed to be higher than the standard CMC point achieved in Chapter 4. For Soapnut saponin, the standard CMC was 4.6wt%, but the optimum concentration for contact angle was 5wt% and 6wt%. In terms of *Camellia oleifera* saponin, the standard CMC was 4wt%, while the optimum concentration of contact angle was 4.5wt% and 5wt%. This phenomenon can be explained by the adsorption behavior, in which negatively charged head groups of saponins were adsorbed on the positively charged clay edges included in the rock through electrostatic attraction force and hydrogen bonding (Kalam et al., 2021).

7.3.1.2 Effect of Green Surfactants and Nanoparticles' Interaction on Wettability Alteration

The application of nanoparticles (NGF) and saponins in oil recovery from conventional and unconventional formations requires a thorough understanding of their characters in wettability modification. Figure 7.10 demonstrates the addition of nanoparticles (NGF) to the saponin solution led to the variation in contact angles on the three core slides. It can be observed that the contact angle dropped steadily along with the concentration of NGF until the optimum point was reached. The standard value of contact angle can refer to in Table 7.3. Specifically, for Mancos shale, the contact angle decreased from 37.7° (0wt%) to 28.93° (0.003wt%) and 33.17° (0wt%) to 24.75° (0.003wt%) of Soapnut saponin and *Camellia oleifera* saponin, respectively. Berea sandstone and Malaysia sandstone show similar results: 1) the contact angle decreased from 24.3° at 0wt% to 16.27° at 0.003wt% in the presence of Soapnut saponin and dropped from 22.8° (0wt%) to 20.81° (0.004wt%) of *Camellia oleifera* saponin; 2) Malaysia sandstone experienced the lowest contact angle from 21.2° (0wt%) to 14.86° (0.004wt%) of Soapnut saponin, and 19.9° (0wt%) to 16.54° (0.0035wt%) of *Camellia oleifera* saponin. In general, all solutions with the additional NGF generated lower contact angles or stronger water-wet surfaces than

the pure saponin solutions, and the angle was further decreased by around 22.9% (depending on the type of saponin and formation rock).

With the steric hindrance effect and Van der Waals interaction, the synergistic complexes of NGF and saponin molecules lead to forming a durable and resilient barrier at the oil-water interface that prohibited Ostwald ripening, coalescence, and flocculation of the crude oil droplet, thereby modifying the surface wettability (Ali et al., 2018; Jin et al., 2018; Jha et al., 2019). Furthermore, NGF particles also acted as transportation to transfer the saponin molecules from bulk fluid to the oil/water interface. It decreases the number of saponins adsorbed on the rock surface and boosts the performance of saponins (Maestro et al., 2012).

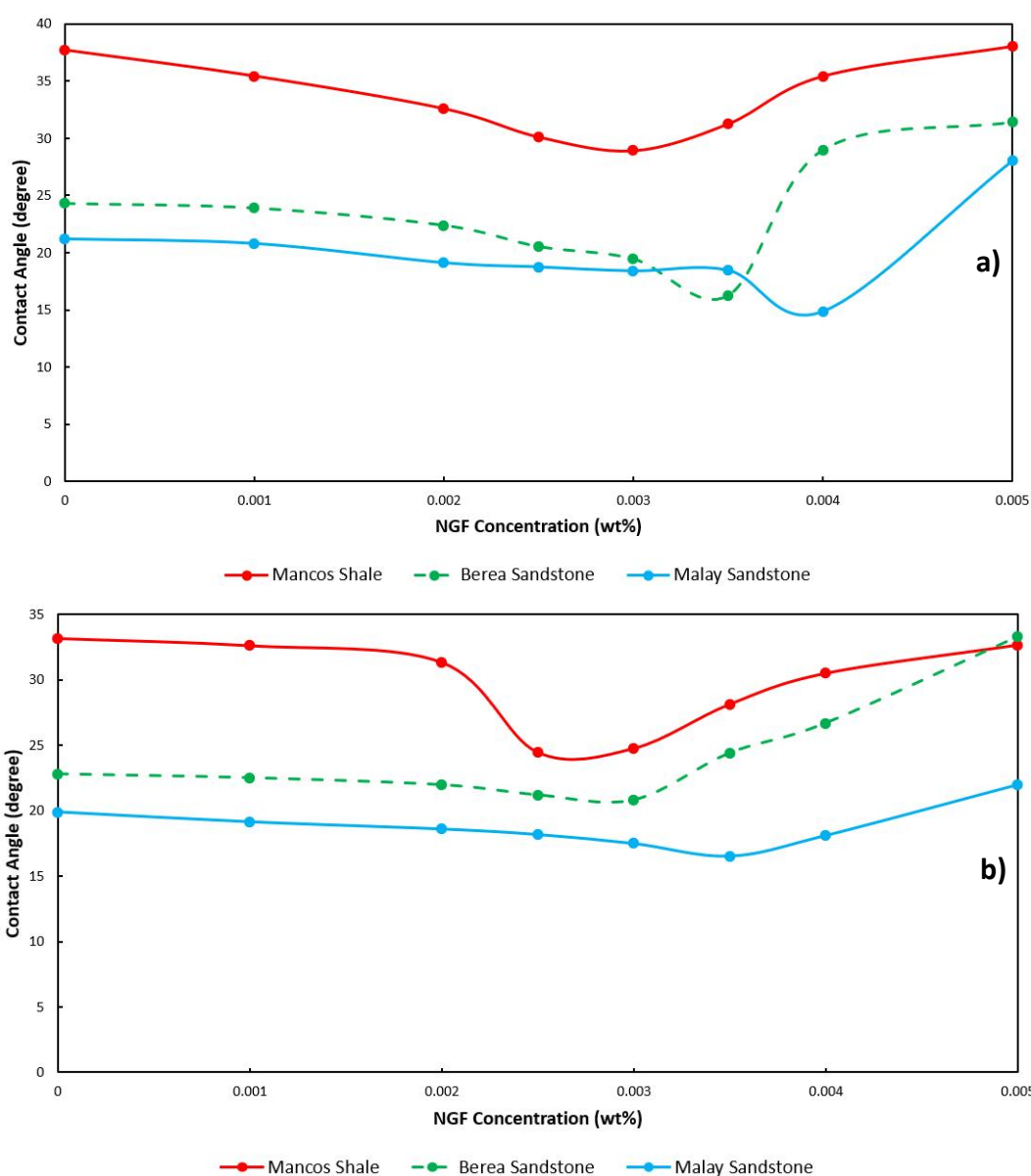


Figure 7.10: Contact angle of the various rock slices under increasing NGF concentration in a) Soapnut saponin solution and b) *Camellia oleifera* saponin solution

On the other hand, parts of NGF particles adsorbed on the rock surface by surface forces colloidal and hydrodynamic forces, which promoted the detachment of oil droplets from the rock surface, thereby modifying the wettability from oil-wet to water-wet (Soleimani & Dehaghani, 2016). Nanoparticles also can modify the surface wettability by altering the surface charge of pore walls, in which the energy barrier separates the fluid-rock interface is breached (Agi et al., 2018). With the size effect (extremely small size and high surface area to volume ratio), saponin molecules adsorb on the NGF surface and form monolayers (Sun et al., 2018). The saponin-coated NGF particles were distributed in the solution. The saponin monolayer is concentrated at the fluid/rock interface, and the NGF is scattered beneath the monolayer in the diffuse layer, which provides a stronger driving force for the saponin-coated NGF to move toward the interface (Zargartalebi et al., 2014). In addition, the electrostatic repulsion force between negative charged NGF particles and anionic saponin molecules enhanced the saponin diffusion to the interface. As a result, the contact angle further decreased.

However, the contact angle increases as the NGF concentration exceeds its optimum value. For Soapnut saponin, the contact angle increased from 28.93° (0wt%) to 38.01° (0.005wt%) at Mancos shale. Similar results occurred at Berea sandstone and Malaysia sandstone, in which the contact angle raised almost twofold. In terms of *Camellia oleifera* saponin, the increased intensity of contact angle on three core slices was approximately 41.7%.

The NGF particles tend to coagulate and aggregate at high concentrations, leading to pore throat blocking, fines migration, and surface wettability degradation (Sadatshojaei et al., 2019). Furthermore, more NGF particles were brought to the solution, and the distance between each particle was reduced. As a result, the attractive capillary force increased dramatically and became nearly uniform over the surface (Soleimani & Dehaghani, 2016). The high capillary force prevents oil droplets detach from rock pores, inhibiting the wettability alteration. High

nanoparticle concentration also induces more saponin adsorbed on its surface, decreasing the concentration of free saponin molecules in the solution (Roustaei & Bagherzadeh, 2015). It also enhances the more saponin-NGF complex formed and aggregated at the fluid/rock interface. With the extremely small size and high surface energy, the abundant NGF particles occupied much more rock surface area than saponin molecules (Zargartalebi et al., 2015; Olayiwola & Dejam, 2019). Therefore, less saponin is adsorbed at the fluid/rock interface and increased contact angle.

Overall, the optimum concentrations of NGF and lowest contact angles in Soapnut saponin were: 1) 0.003wt% and 28.93° in Mancos shale, 2) 0.0035wt% and 16.27° in Berea sandstone, 3) 0.004wt% and 14.86° in Malaysia sandstone. In terms of Camellia oleifera saponin, the optimum concentrations of NGF and lowest contact angles were summarized as 1) 0.003wt% and 24.75° in Mancos shale, 2) 0.003wt% and 20.81° in Berea sandstone, 3) 0.0035wt% and 16.54° in Malaysia sandstone.

7.3.1.3 Effect of Salt Type and Salinity on Wettability Alteration of Green Surfactant Solutions

The impact of salinity and the type of salt on the wettability of the Mancos shale, Berea sandstone, and Malaysia sandstone has been examined in this section. Two types of salt have been tested: monovalent salt NaCl and divalent salt CaCl₂. The contact angles were measured in the presence of saponins (Soapnut saponin and Camellia oleifera saponin) with increasing salinity from 0ppm to 40000ppm. According to Figure 7.11 and Figure 7.12, all 12 batch tests shows a similar trend. The contact angle decreases with increasing salinity until 3500ppm, whereas the contact angle increases approximately twofold when the salinity passes this threshold.

The finest result of 12 batch tests was shown in the Malaysia sandstone with 5wt% Camellia oleifera saponin and 3500ppm NaCl, in which a change in salinity from 0ppm to 3500ppm corresponded to a variation in contact angle from 19.93° to 14.51°. For Soapnut saponin, the lowest contact angle was also achieved in Malaysia

sandstone, even though the angle was slightly higher than *Camellia oleifera* saponin. It dropped from 21.2° (0ppm) to 15.98° (3500ppm), then increased to 31.18° (40000ppm). Therefore, it can be proved that low salinity brines improve the surface wettability of formation cores.

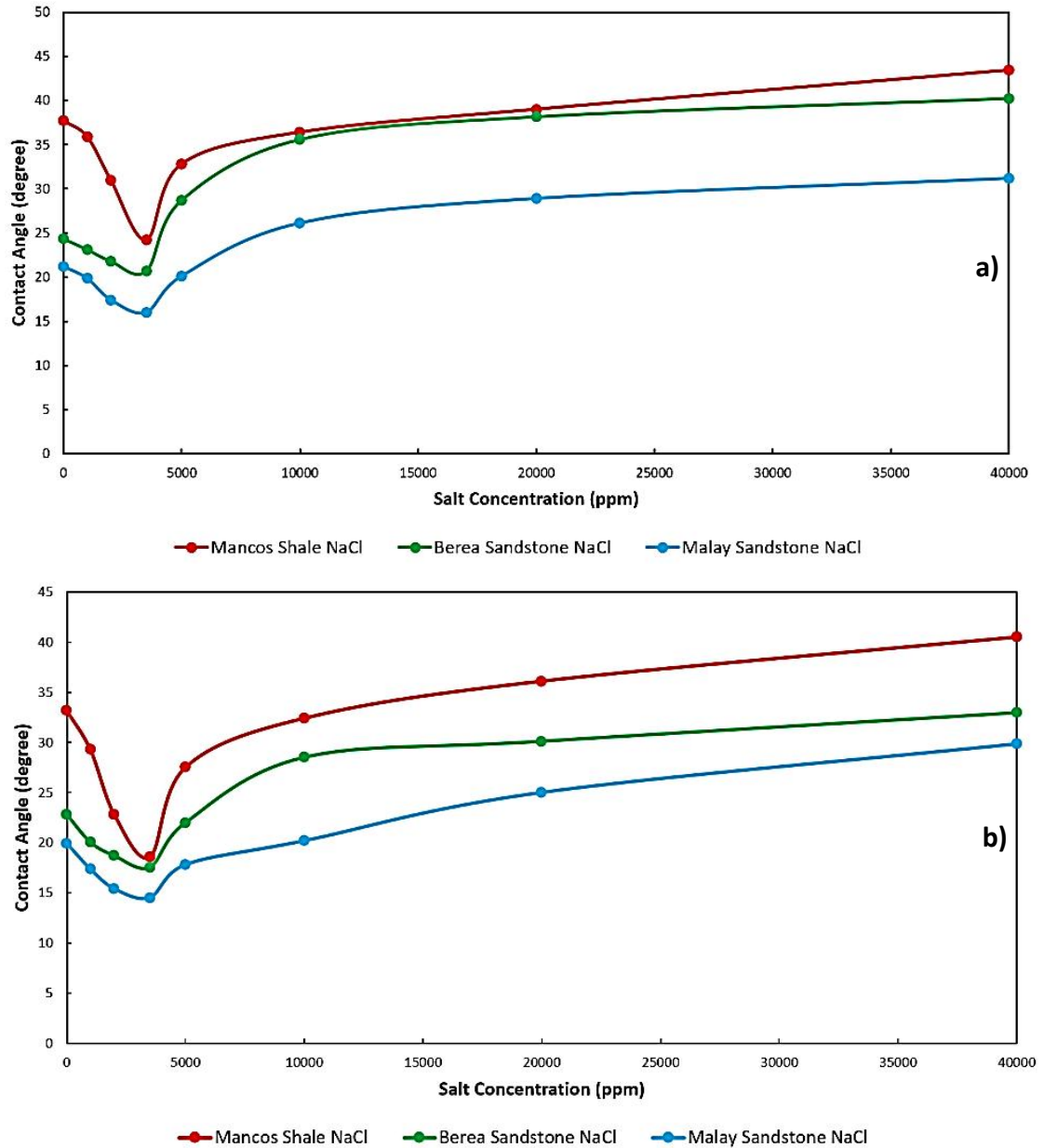


Figure 7.11: Contact angle of the various rock slices under increasing salinity of NaCl in a) Soapnut saponin solution and b) *Camellia oleifera* saponin solution

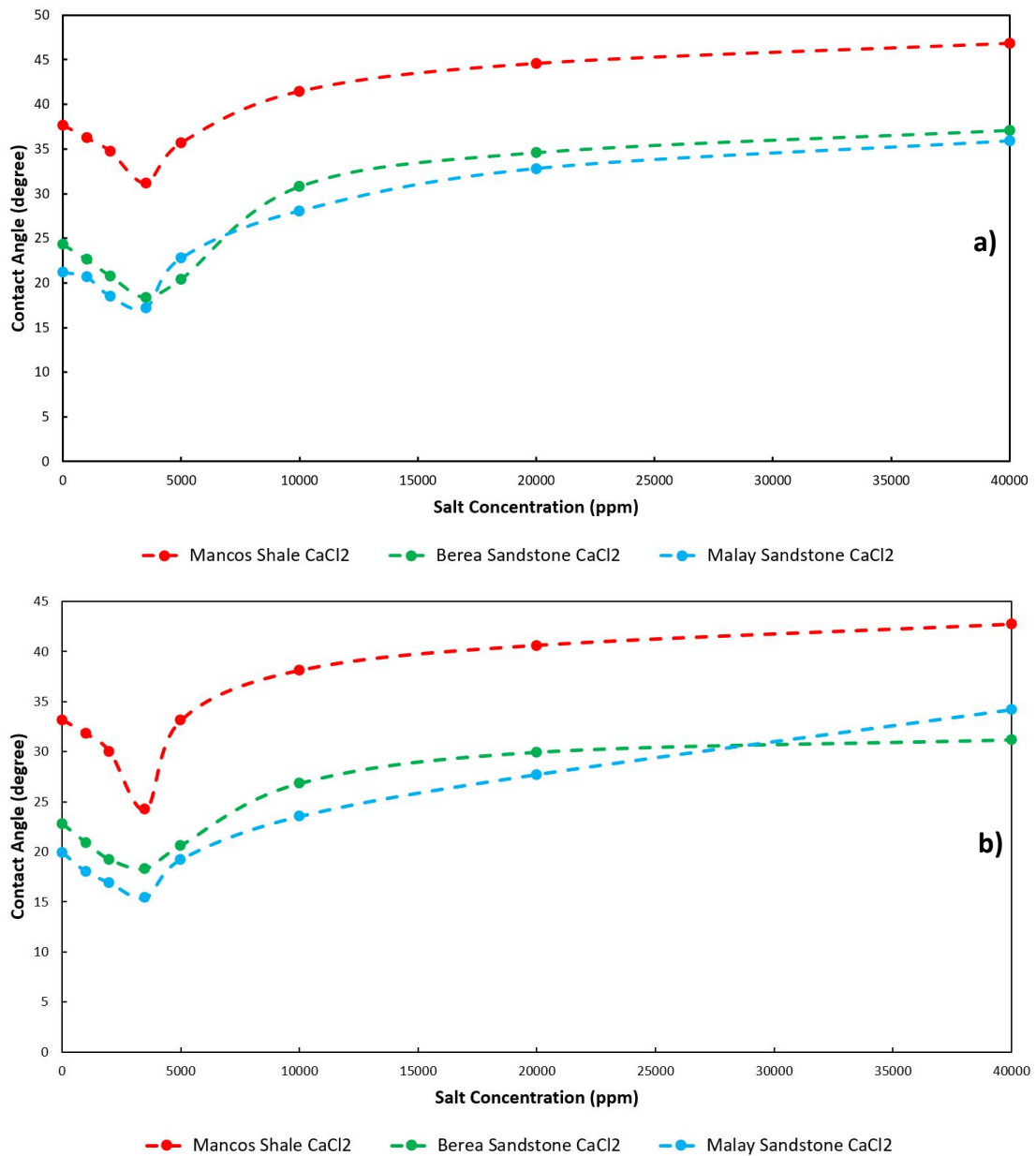


Figure 7.12: Contact angle of the various rock slices under increasing salinity of CaCl₂ in a) Soapnut saponin solution and b) Camellia oleifera saponin solution

Several mechanisms related to the synergistic effect and the individual characteristic contribute to the effective wettability alteration during the low salinity water combined with the saponins, such as capillary pressure, electrostatic interactions, ion-pairing, osmotic force, electrical double layer expansion, and spontaneous imbibition (Haagh et al., 2017; Ebrahim et al., 2019; S. Hosseini et al., 2020). Crude oil contained both acidic and basic components, the interactions with saponin and salt were dominated by electrostatic Coulomb force and ion-pairing

(Haagh et al., 2017). Specifically, the negatively charged saponin molecules form surfactant monolayers and adsorb on the surface of positive charged basic components by electrostatic attraction forces. The positive Na^+ and Ca^{2+} from brine adsorb the negative charged basic components on the rock surface through cation bridging and ligand bridging, forming the direct dative covalent bond (Shabib et al., 2015). Furthermore, the crude oil negatively charged carboxylic acid groups also interact with the brine's cations (Na^+ or Ca^{2+}) by a hydrogen bond. Thus, these interactions diminish the forces between rock formation and crude oil droplets, causing the wettability alteration with decreased contact angle. In the saponin-brine system, the saponin lowered the forces between fluids, while the cations of brine decreased the forces between rock and fluids (Mofrad & Saeedi Dehaghani, 2020). So the combination of salt with appropriate concentration and saponin was able to bring far superior results in wettability modification compared to the individual application of saponin. The lowest contact angle generated by pure *Camellia oleifera* saponin in Berea sandstone was 22.8° , while the angle was further reduced to 17.55° (NaCl) or 18.29° (CaCl_2) with additional low salinity brine. In the low salinity range, increasing salt concentration induced rising ionic strength in solution and enhanced the solubility of oil; thereby, the oil became easier to transfer into the water phase (Xie et al., 2019; Chávez et al., 2020). On the other hand, the presence of saponin can effectively prevent oil that was initially mobilized via low salinity brine from being re-trapped.

However, all 12 batch tests show that the contact angle raised almost twofold when the salinity increased from 3500ppm to 40000ppm; for example, the angle increased from 20.6° (3500ppm NaCl) to 40.22° (40000ppm NaCl) in the presence of Soapnut saponin on Berea sandstone. This could be attributed to the excess salt ions in the solution inhibiting the saponin adsorb on the rock surface, resulting in a shift in contact angle and wettability status (Al-Saedi et al., 2019). As mentioned before, the surface of both Berea sandstone and Malaysia sandstone were negatively charged, and the surface of Mancos shale was also partially negatively charged. Likewise, the average zeta-potential of Soapnut saponin and *Camellia oleifera* saponin were -6.35mV and -22.4mV, respectively. In contrast, the

ion of Na^+ and Ca^{2+} of brines were positively charged. The saponin molecules are adsorbed on rock surfaces mainly by van der Waals London dispersion attraction force; it also forms hydrogen bonds and covalent bonding with the mineral's hydroxyl groups by ion-pairing mechanism (Daghlian et al., 2016; S. Hosseini et al., 2020). As saline water that contains Na^+ or Ca^{2+} was injected into rock formations with saponin, the positive charged ion Na^+ or Ca^{2+} was firmly adsorbed on the negatively charged rock surface through electrostatic attraction force, forming a monolayer or double layer (Lashkarbolooki et al., 2017). The electrostatic attraction between cations Na^+ or Ca^{2+} and formation rock surface was substantially greater than the covalent bonding, hydrogen bonds, and van der Waals interactions between saponin and formation rock surface (Shabani & Zivar, 2020). Thereby, the majority of the area of rock surface was coated by Na^+ or Ca^{2+} rather than saponin molecules. Furthermore, the high salinity brine inhibits the saponin molecules from dissolving into the liquids phase because of increasing electrostatic double-layer forces and hydration repulsion forces. Salting-out is also considered one mechanism that induces a larger contact angle when the increasing salinity exceeds the threshold value, 3500ppm (Haagh et al., 2017). At very high ionic strength, the solubility of saponin molecules is reduced. It results in certain saponins aggregated together through hydrophobic and hydrophilic interactions, which may lead to the precipitation of saponin, thereby reducing the active saponin molecules at the fluid/rock interface (Hilner et al., 2015).

Figure 7.13 and Figure 7.14 show that the monovalent salt NaCl performs superior contact angle reduction than divalent salt CaCl_2 . Take Malaysia sandstone as an example (with Soapnut saponin); the angle achieved in NaCl was 15.98° at 3500ppm, whereas a higher value of 17.23° was obtained from CaCl_2 at the same salinity. Similar patterns were also observed in other tests.

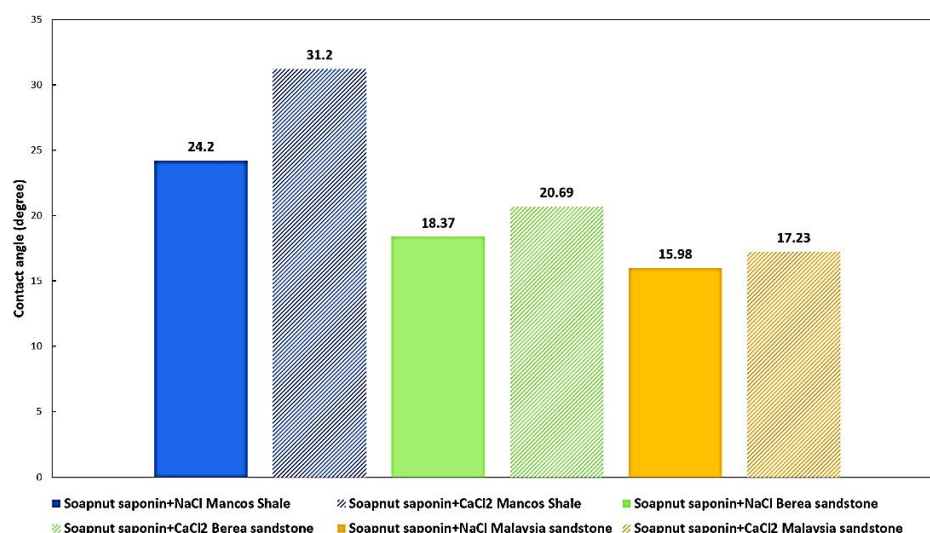


Figure 7.13: Contact angle of the various rock slices under 3500ppm salinity of NaCl and CaCl_2 in Soapnut saponin solution

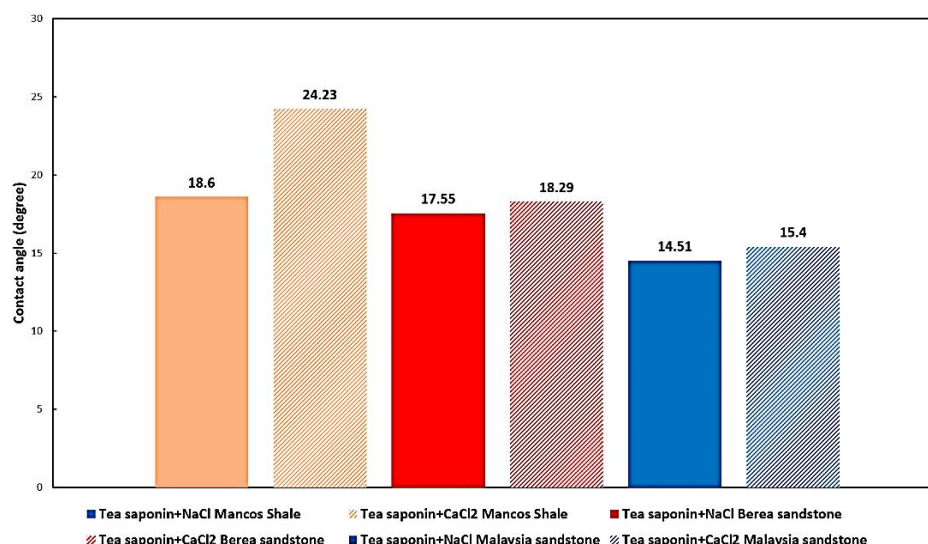


Figure 7.14: Contact angle of the various rock slices under 3500ppm salinity of NaCl and CaCl_2 in Camellia oleifera saponin solution

The NaCl reduces the contact angle by about 9.3% than CaCl_2 in the sandstone rock, and this value raised to 22.8% in the presence of Mancos shale. The salt NaCl is formed by spectator ion Na^+ ion and Cl^- and salt CaCl_2 is formed by ion Ca^{2+} and ion Cl^- . The mechanisms behind this behavior can be summarized as:

- 1) Monovalent cation Na^+ possesses lower ionic strength and more negative zeta potential than divalent cation Ca^{2+} , which makes Na^+ ions were more

effective detach carboxylic components of crude oil from the adsorbing rock surface (Kakati & Sangwai, 2018).

- 2) Monovalent ion Na^+ also has a higher reactivity value than divalent ion Ca^{2+} , which means more Na^+ would adsorb (occupied) on rock surface by forming a stronger bond. Thereby, the number of active saponin molecules adsorbed on the rock surface in NaCl would be less than in CaCl_2 . In terms of ionic charge, the divalent cation Ca^{2+} exhibits more electrostatic attraction forces than the monovalent cation Na^+ ; as a result, the aggregation tendency of saponin molecules (more micelles formed) is greater in CaCl_2 solution, resulting in higher contact angles (Kakati & Sangwai, 2018; H. Xu et al., 2019; Safari et al., 2022).

Overall, the optimum salinity of both salts NaCl and CaCl_2 was identified as 3500ppm. And the lowest contact angle in Soapnut saponin was shown in Malaysia sandstone with NaCl at 15.98° . In terms of Camellia oleifera saponin, the lowest contact angle was observed at Malay sandstone with NaCl at 14.51° . It was important to mention that Camellia oleifera saponin shows superior ability in contact angle reduction (wettability alteration) than Soapnut saponin, which is the lowest contact angle achieved by Camellia oleifera saponin was 14.51° while 15.98° for Soapnut saponin. The optimum ratio and its relative results are summarized in Table 7.5.

Table 7.5: The optimum salinity achieved by saponins in various core slices

	Mancos shale (degree) (salinity)	Berea sandstone (degree) (salinity)	Malaysia sandstone (degree) (salinity)
Soapnut saponin NaCl	24.2 3500ppm	18.37 3500ppm	15.98 3500ppm
Soapnut saponin CaCl_2	31.2 3500ppm	20.69 3500ppm	17.23 3500ppm
Camellia oleifera saponin NaCl	18.6 3500ppm	17.55 3500ppm	14.51 3500ppm
Camellia oleifera saponin CaCl_2	24.23 3500ppm	18.29 3500ppm	15.4 3500ppm

7.3.1.4 Effect of Salt Type and Salinity on Wettability Alteration of the Solution Contain Green Surfactants and Nanoparticles

Several experiments have been done in previous sections to demonstrate that salts or nanoparticles along with saponin can effectively result in wettability alteration (contact angle reduction). The additional additives combined with saponin surfactant successfully reduced the contact angle of oil droplets on the formation rock surfaces, thereby modifying the wettability from oil-wet to water-wet. However, there was still a lack of studies about combining salt, nanoparticles, and saponin on Mancos shale, Berea sandstone, and Malaysia sandstone. Furthermore, the optimum combination ratio and the mechanisms of fluid/fluid and fluid/rock interface interactions were still vague. Therefore, this section was going to provide an in-depth investigation of the synergic mechanisms behind the application of two kinds of salts (NaCl and CaCl₂) and nanoparticles (NGF) in combination with saponin solutions (Soapnut saponin or Camellia oleifera saponin) on wettability modifications. The contact angle fluctuations at increasing salinity (low and high) were also discussed. At last, the optimum salinity and additive's combination ratio were thoroughly highlighted in this section. For example, in the presence of Soapnut saponin, all tested solutions of two batches (NaCl and CaCl₂) on Mancos shale contained 5wt% Soapnut saponin and 0.003wt% NGF, and the corresponding benchmark (initiation) contact angle was 28.93°. The variable was the salinity with the concentration from 0ppm to 40000ppm and the salt types (NaCl and CaCl₂).

As shown in [Figure 7.15](#) and [Figure 7.16](#), the increasing salinity significantly decreased the contact angle until it reached 3500ppm. For Soapnut saponin, the angle dropped approximately 33%, and the lowest contact angle was achieved in Berea sandstone at 10.3° with 3500ppm NaCl, 5wt% Soapnut saponin, and 0.003wt% NGF. Camellia oleifera saponin's contact angle decreased around 27%, and the lowest angle showed on Malaysia sandstone at 10.02° with 3500ppm NaCl, 5wt% Camellia oleifera saponin, and 0.0035wt% NGF. In contrast to section 7.3.1.3, the additional nanoparticles can further reduce the contact angle by 33% for Soapnut saponin and 26% for Camellia oleifera saponin. At low salinity (<3500ppm) with a high surface-to-volume ratio and high surface energy, saponin molecules

adsorbed on the nanoparticle surface to form monolayers (Rezaei et al., 2021). Then the saponin monolayers concentrated at the fluid/rock interface, while the nanoparticles were diffusely scattered beneath the monolayer. This behavior provides a powerful driving force for the oil detachment from the rock surface, modifying the rock surface from oil-wet to water-wet (Olayiwola & Dejam, 2019). Furthermore, the additional NGF and salts also: 1) promote the saponin molecules dispersed more homogeneously in solution (weaken the agglomeration/coalescence behavior) by Coulomb interactions and Brownian motion, 2) push more free saponin towards fluid/rock interface by steric forces, electrostatic repulsion forces and electrical double layer expansion since particles possess same charges (Jha et al., 2019).

On the other hand, a more durable barrier at the oil-water interface was formed by the synergistic interactions of NGF, saponin molecules, and salt ions due to the steric hindrance effect and Van der Waals interaction (Divandari et al., 2020). This barrier prevented the coalescence of the crude oil droplet, resulting in an alteration in the surface wettability. The saponin-coated NGF particles are also adsorbed on the rock surface through surface forces colloidal and hydrodynamic forces which further enhance the wettability alteration process (Harikrishnan et al., 2017; Almahfood & Bai, 2018). Crude oil comprises acidic and basic components. The negative charged acidic part (carboxylic acid groups) interacts with cations (Na^+ and Ca^{2+}) from brines through hydrogen bonds, while the positive charged basic part interacts with saponin and saponin-coated NGF particles by electrostatic interactions and ion pairing (Khalafi et al., 2018; Sun et al., 2018). As a result of these interactions, the forces between the rock formation and crude oil droplets were reduced, leading to the altered wettability associated with a lower contact angle. On the other hand, the presence of Na^+ and Ca^{2+} ions increases the repulsive Coulomb interactions between similarly charged particles (including NGF coated with saponin) and causes additional saponin molecules to migrate to the fluid/rock interface (Jin et al., 2018; Olayiwola & Dejam, 2019). In addition, those cations adsorb the negatively charged rock surface through electrostatic attraction force, which effectively mitigates the number of saponin molecules and saponin-coated

NGF particles adsorbed on the rock surface (Zargartalebi et al., 2014). Hence, more free surface modification particles could transport to the fluid/rock interface and improve wettability (by reducing the contact angle).

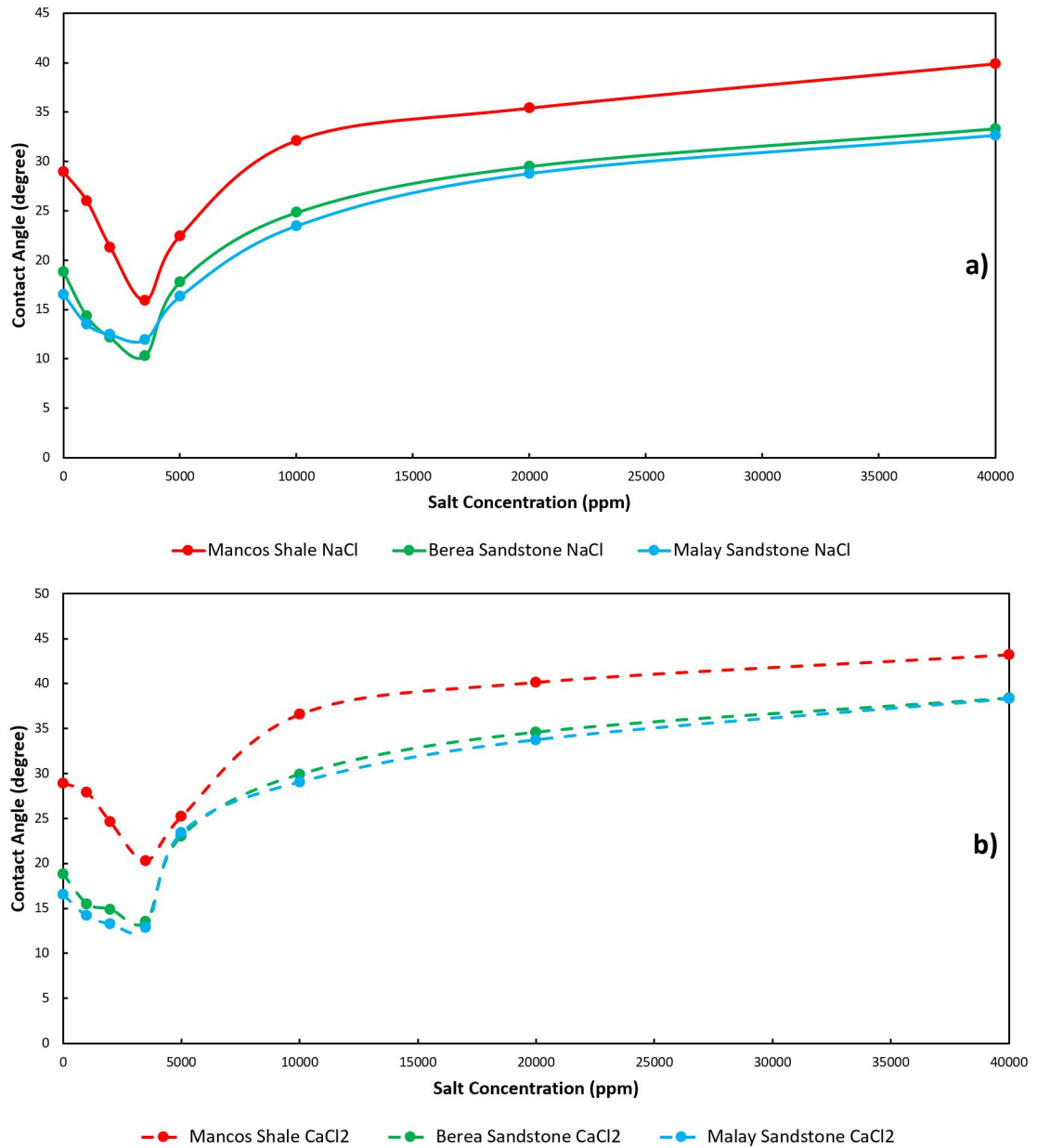


Figure 7.15: Contact angle of the various rock slices under increasing salinity. a) NaCl; and b) CaCl₂, respectively, in the solution containing Soapnut saponin and NGF

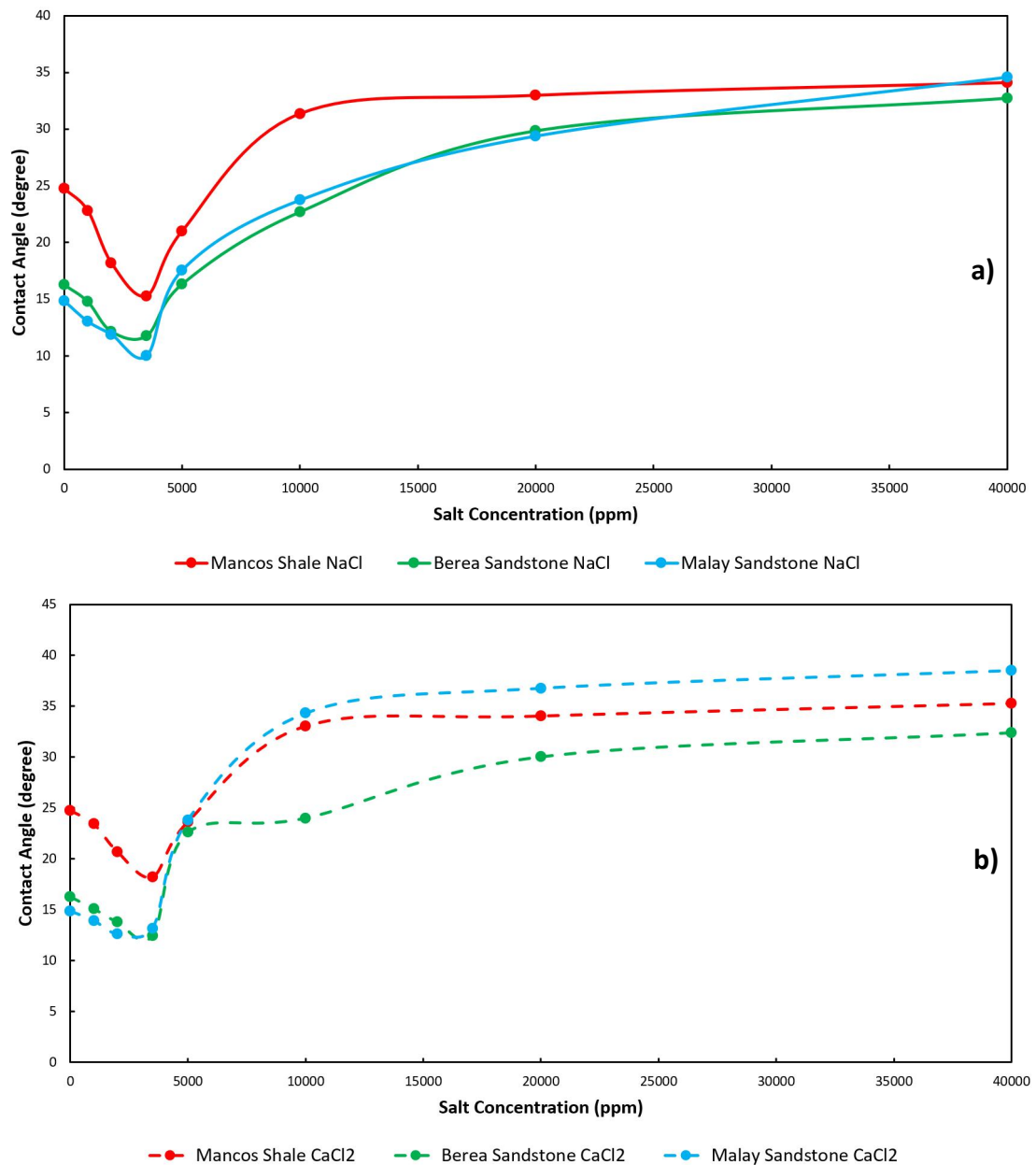


Figure 7.16: Contact angle of the various rock slices under increasing salinity of a) NaCl; and b) CaCl₂, respectively, in the solution containing *Camellia oleifera* saponin and NGF

After the salinity exceeds the limitation of 3500ppm, the contact angle increases and is achieved around twofold at 40000ppm. For Soapnut saponin, the largest variation range occurred at Berea sandstone with salt CaCl₂, in which the angle raised from 12.85° at 3500ppm to 38.3° at 40000ppm. *Camellia oleifera* saponin's angle increased from 13.15° (3500ppm) to 38.51° (40000ppm) on the Malaysia sandstone with salt CaCl₂. The results of contact angle at optimum salinity

and highest salinity were summarized in [Figure 7.17](#). A rise in the salinity increases the electrostatic repulsion force between particles, weakens the double layer expansion, and causes the hydration repulsion effect, preventing saponin from dispersing further into the fluid/rock interfaces ([Brady et al., 2015](#); [Al-Saedi et al., 2019](#)). Meanwhile, some adsorbed saponin molecules were forced away (detached) from the interfaces as the contact angle increased. At high salt concentrations, parts of saponin molecules interact with nanoparticles to form microemulsions, whereas some saponin molecules interact with salt ions to form cylindrical micelles ([Al-Saedi et al., 2019](#)). As a result, forming those two kinds of agglomeration decreased the number of free saponin molecules in the solution, thereby increasing the contact angle.

On the other hand, the high salinity also triggers 1) the CMC of saponins to decrease, thereby causing more micelles to form; 2) more saponin-coated nanoparticles accumulate and coalesce together ([Saxena et al., 2019](#)). Therefore, the solution's decreased overall concentration of active saponin molecules leads to a rising contact angle. The high concentration of cations Na^+ and Ca^{2+} also interact with saponin and nanoparticles to form a more dense barrier (saponin-surfactant nanoaggregate complex) to prevent the saponin molecules move toward fluid/rock interfaces ([Saxena et al., 2019](#)). According to [Figure 7.18](#), it was observed that the monovalent salt (NaCl) exhibits higher capabilities of contact angle reduction than the divalent salt (CaCl_2) in the solution containing both saponin and nanoparticles. Specifically, NaCl can further decrease the angle by around 22.2% and 18.6% more than CaCl_2 in the presence of Soapnut saponin and *Camellia oleifera* saponin, respectively. The mechanisms of this behavior were mainly caused by: 1) with the lower ionic strength and higher negative zeta potential, monovalent ion Na^+ can detach more carboxylic components of crude oil from the adsorbing rock surface than covalent ion Ca^{2+} , 2) the agglomeration of saponin-coated nanoparticles and the formation of saponin micelles more often occurred in the solution contain Ca^{2+} rather than Na^+ because the Na^+ possess less electrostatic attraction forces than Ca^{2+} , 3) the monovalent salt solution (NaCl) perform better in interact with crude

oil's acidic components than divalent salt solution (CaCl_2) (Arabloo et al., 2016; Chaalal et al., 2018, p. 201; Saxena et al., 2019).

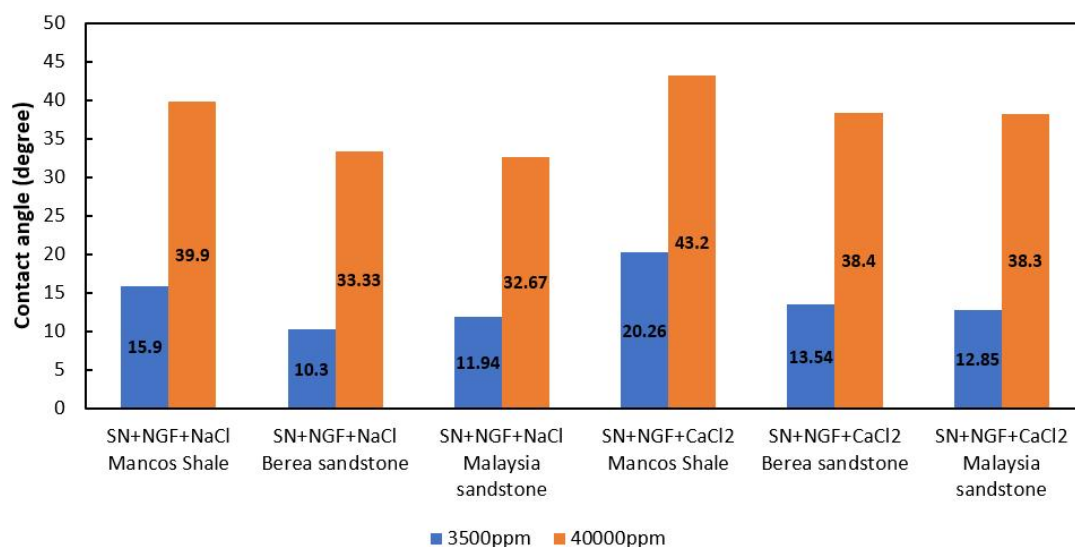


Figure 7.17: The difference between contact angles achieved by optimum salinity and highest salinity in Soapnut saponin

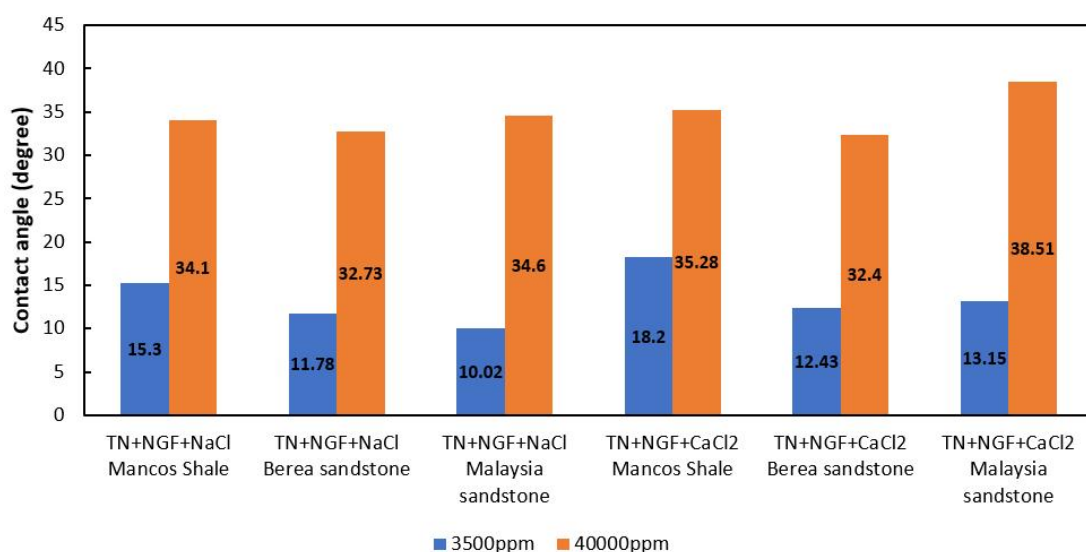


Figure 7.18: The difference between contact angles achieved by optimum salinity and highest salinity in Camellia oleifera saponin

Overall, 3500ppm was the optimum salinity for both salts (NaCl and CaCl_2) in low salinity NGF saponin fluid. For Soapnut saponin, the lowest contact angle achieved was 10.3° with 5wt% Soapnut saponin, 0.0035wt% NGF, and 3500ppm NaCl in Berea sandstone. Camellia oleifera saponin's lowest contact angle was

10.02° with 5wt% *Camellia oleifera* saponin, 0.0035wt% NGF, and 3500ppm NaCl in Malaysia sandstone. Like previous results, *Camellia oleifera* saponin performs superior wettability alteration than Soapnut saponin. And the application of NaCl also can be brought a lower contact angle than CaCl₂.

7.3.2 SEM Observation

In order to further analyze the variations of morphology and particles bonding that related to the mechanisms of wettability alteration, the core slices of Mancos shale, Berea sandstone, and Malaysia sandstone were characterized by the captured microphotographs of SEM (Figure 7.19). The tested samples were divided into two groups: the first group contained the clean core slices of Mancos shale, Berea sandstone, and Malaysia sandstone before aging with crude oil and immersed into low salinity NGF saponin fluid (Figures 7.19a, c, and e); the second group includes those core slides after aging with crude oil and immersed into low salinity NGF saponin fluid (Figures 7.19b, d, and f). The composition ratios of the low salinity NGF saponin fluid were summarized in Table 7.6.

The image of Mancos shale (Figure 7.19a) shows that the surface of core slices possesses a much less porous/more compact structure than Berea sandstone (Figure 7.19c) and Malaysia sandstone (Figure 7.19e) core slices. The morphology of Mancos shale in Figure 7.19a illustrates clay and quartz grains content. The morphology of both Berea sandstone and Malaysia sandstone in Figures 7.19c and 7.19e demonstrate the higher content of quartz grains. Furthermore, the high magnification photographs of the surface morphology demonstrate the presence of macropores, micropores, and fractures in Berea sandstone (Figure 7.19c) and Malaysia sandstone (Figure 7.19e).

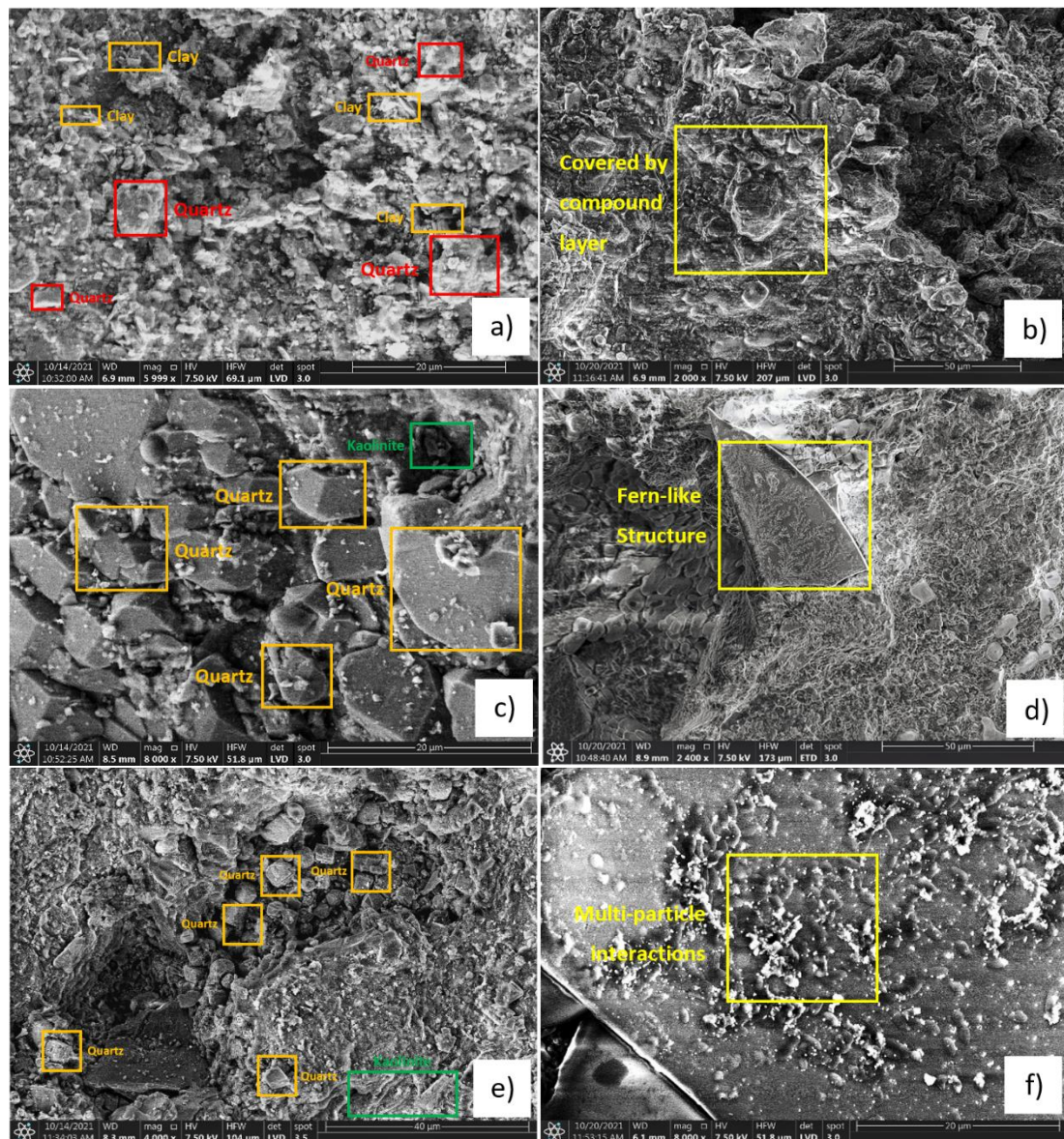


Figure 7. 19: SEM images of core slices before and after oil aging and immersed into low salinity NGF saponin fluid. a) Bancos shale core slice, b) Bancos shale core slice after oil aging and immersed into low salinity NGF saponin fluid, c) Berea sandstone core slice, d) Berea sandstone core slice after oil aging and immersed into low salinity NGF saponin fluid, and the Fern-like structure, e) Malaysia sandstone core slice, f) Malaysia sandstone core slice after oil aging and immersed into low salinity NGF saponin fluid, and the multi-particle interactions

Table 7.6: The composition ratios of the immersed low salinity NGF saponin fluid

Rock Type	Nanoparticles (NGF) Concentration (wt%)	Salt (NaCl) Concentration (ppm)	Saponin Concentration (wt%)
Mancos Shale	0.003	3500	5
Berea Sandstone	0.0035	3500	5
Malaysia Sandstone	0.004	3500	6

Specifically, Malaysia sandstone shows more pores than Berea sandstone and Mancos shale. Sandstone cracks were shaped differently than shale cracks. Because of the absence of striations and lack of direction in the particle arrangement, sandstone can be called isotropic in its whole. The components with similar atomic masses are spread equally across the sandstone. The white patches represent particles with bigger atomic masses placed randomly and are not orientated.

The rock surfaces significantly differ when the aged core slices are immersed in low salinity NGF saponin fluid. In contrast to [Figure 7.19a](#), it clearly showed that the surface of Mancos shale in [Figure 7.19b](#) is covered by a nanotextured layer (coating mechanism) that is constructed by the synergistic interactions of NGF particles, saponin molecules, and salt ions due to the steric hindrance effect, Van der Waals interaction, surface forces colloidal and hydrodynamic forces ([Srivastava et al., 2020](#); [Aljamhan et al., 2021](#); [Valenzuela et al., 2021](#)). This phenomenon was consistent with Berea sandstone ([Figure 7.19d](#)) and Malaysia sandstone ([Figure 7.19f](#)) core slices, confirming the mechanisms analyzed in previous sections. Moreover, the edges of the rock surface became more irregular, indicating that some crude oil components were detached from the rock pores. In terms of NGF particles and saponin-coated NGF particles, a portion of them adsorbed on the rock surface due to surface forces, colloidal forces, and hydrodynamic forces, promoting the separation of oil droplets from the rock surface and so changing the wettability from oil-wet to water-wet ([Olayiwola & Dejam, 2019](#); [Rezaei et al., 2021](#)). The

roughness of the rock surface also improved from scaly to smooth since the groups of the saponin-NaCl-NGF complex, in some cases, coalesce together to plug on some pores. Furthermore, the self-organized Fern-like crystal structure introduced in Chapter 6 can observe in [Figure 7.19d](#). It is considered crystallization behavior and formed by a highly-ordered and densely-packed array of self-assembly particles. [Figure 7.19f](#) shows the multi-particle interactions on the rock surface. Under the interactions such as hydrogen bonding, ionic bonding, Van der Waals interactions, hydration forces, electrostatic forces, and steric force, saponins, NGF particles, and saponin-coated NGF particles interact and are attached to each other ([Pichot et al., 2012](#); [Sun et al., 2018](#); [Abbas et al., 2020](#); [Belhaj et al., 2020](#)). It contributes to a better dispersion ability and stability of low salinity NGF saponin fluid on formation rocks.

7.4 Conclusion

Formation rock wettability modified by the fluid is a common method applied in many lab and field operations. However, there is a lack of understanding in the influence of green surfactants (saponins), saline water, salt type, nanoparticles, and the combination of multiple additives on rock surfaces' wetting status; the issue of whether oil-wet formation can be improved to water-wet is critical in EOR process since it is well established that oil production from water-wet formations is significantly higher than production from oil-wet formations. It has been previously noted that the use of nanoparticles in combination with surfactants and low salinity water can be beneficial; however, most published studies concentrate on IFT at the liquid-liquid interface. As part of this research, the wetting tendency of mixes of saponins, saline water, nanoparticles, and the combination of multiple additives at the fluid-rock interface was thoroughly studied. Optimum concentrations and several mechanisms have been addressed in this section. The following findings were reached as a result:

- 1) The contact angles of all three core slices reduced dramatically as the saponin concentration increased, up to a point around the saponin CMC. Following that, the contact angle increased slightly along with the excessive

saponin concentration, and a water-wet status was achieved at last. [Table 7.4](#) summarises the contact angles attained by Soapnut saponin and *Camellia oleifera* saponin. Unequivocally demonstrated that *Camellia oleifera* saponin alters wettability more effectively than Soapnut saponin. The lowest contact angle was achieved by 5wt% *Camellia oleifera* saponin at 19.93° on Malaysia sandstone.

- 2) Unequivocally demonstrated that anionic surfactant (*Camellia oleifera* saponin) alters wettability more effectively than nonionic surfactant (Soapnut saponin). It was mainly caused by the negatively surface-charged *Camellia oleifera* saponin absorbing the positive basic components in crude oil from the rock surface through the electrostatic attraction force, forming ion pairing between the saponin molecules and the rock surface. Furthermore, the level of surfactant adsorption also less occurred in *Camellia oleifera* saponin because of the electrostatic repulsion forces between the similarly charged particles.
- 3) In terms of the combination of saponins and nanoparticles (NGF), the contact angle dropped steadily along with the concentration of NGF until the optimum point was reached. Furthermore, all solutions containing added NGF had lower contact angles or a stronger water-wet surface than pure saponin solutions, and the angle was further reduced to around 22.9%. After that, the contact angle increases as the NGF concentration exceeds its optimum value. The optimum concentration for NGF nanoparticles in Soapnut saponin was: 1) 0.003wt% in Mancos shale, 2) 0.0035wt% in Berea sandstone, 3) 0.004wt% in Malaysia sandstone. For *Camellia oleifera* saponin, the NGF nanoparticles' optimum concentration was: 1) 0.003wt% in Mancos shale, 2) 0.003wt% in Berea sandstone, 3) 0.0035wt% in Malaysia sandstone. Specifically, the lowest contact angle was 14.86° achieved by Soapnut saponin with 0.004wt% NGF on Malaysia sandstone.
- 4) In terms of the combination of saponins and salts, the contact angle decreases with increasing salinity until 3500ppm. For Soapnut saponin, the lowest contact angle was achieved in Malaysia sandstone which dropped

from 21.2° (0ppm) to 15.98° (3500ppm). *Camellia oleifera* saponin's lowest contact angle also occurred in Malaysia sandstone, which dropped from 19.93° (0ppm) to 14.51° (3500ppm). After that, the contact angle increases approximately twofold when the salinity passes the 3500ppm threshold. Take NaCl as an example; the angle increased from 20.6° (3500ppm) to 40.22° (40000ppm) in the presence of Soapnut saponin on Berea sandstone. Additionally, the monovalent salt NaCl reduces contact angles more effectively than the divalent salt CaCl₂. The angle obtained in NaCl was 15.98° at 3500ppm, whereas the angle obtained in CaCl₂ was 17.23° at the same salinity. Other experiments revealed similar results. The optimal salinity for both NaCl and CaCl₂ was determined to be 3500ppm. *Camellia oleifera* saponin outperforms Soapnut saponin in terms of contact angle decrease (wettability alteration), with the lowest contact angle reached by *Camellia oleifera* saponin being 14.51°, compared to 15.98° for Soapnut saponin.

- 5) The combination of saponins, salts, and nanoparticles demonstrated exceptional potential as a novel type of EOR agent since the fluid system significantly improved the wetting status on all three core slices. The presence of low concentration salt ions and nanoparticles significantly affected the saponin behavior, altering the fluid's properties while boosting the saponin performance. For Soapnut saponin, the angle decreased by approximately 33%, and the lowest contact angle was achieved in Berea sandstone at 10.3° with 3500ppm NaCl, 5wt% Soapnut saponin, and 0.003wt% NGF. *Camellia oleifera* saponin's contact angle dropped around 27%, and the lowest angle showed on Malaysia sandstone at 10.02° with 3500ppm NaCl, 5wt% *Camellia oleifera* saponin, and 0.0035wt% NGF. Moreover, in contrast to the solution containing saponin and salt, the additional nanoparticles can further reduce the contact angle by 33% for Soapnut saponin and 26% for *Camellia oleifera* saponin. When the salinity exceeds the 3500ppm limit, the contact angle grows and nearly doubles at 40000ppm. The highest variable range for Soapnut saponin happened on

Berea sandstone with CaCl_2 , where the angle increased from 12.85° at 3500ppm to 38.3° at 40000ppm. *Camellia oleifera* saponin occurred on the Malaysian sandstone with CaCl_2 , which increased the angle from 13.15° (3500ppm) to 38.51° (40000ppm). The optimal salinity for both salts (NaCl and CaCl_2) was determined to be 3500ppm in low salinity NGF saponin fluid. *Camellia oleifera* saponin outperforms Soapnut saponin in terms of wettability modification. Additionally, NaCl can be used to achieve a lower contact angle than CaCl_2 .

Chapter 8: Conclusions and Recommendations

Conclusions and recommendations are included in this chapter. The conclusion summarises the findings from each chapter, and recommendations are made for the additional work of future studies.

8.1 Conclusions

This project is designed to develop a high-performance low salinity green surfactant nanofluid to enhance the oil recovery from mature reservoirs, which exhibits the following characteristics: 1) good wettability alteration and IFT reduction, 2) good stability under high-temperature conditions, 3) environmentally friendly behavior, and 4) economic efficiency. All objectives have been accomplished, especially two new green surfactants (Soapnut saponin and *Camellia oleifera* saponin) successfully extracted, characterized, and evaluated from Soapnut and *Camellia oleifera* as new green EOR additives (Chapters 3 and 4). Furthermore, the foamability and foam stability tests under 1) the different concentrations of saponins; 2) the variation of salinity; 3) the influence of temperature; 4) the fluid system contained nanoparticles, salt, or both; 5) the crude oil-foam interaction were investigated (Chapter 5). IFT (Chapter 6) and wettability (Chapter 7) are considered two of the most important secondary and enhanced oil recovery parameters since they can recover the residual oil by complicated oil-liquid or oil-liquid-rock interactions. Both chapters included batch experiments and mechanism analysis. The batch experiments were performed to determine the IFT reduction or wettability variation in the presence of 1) formation rock type, saponin concentration, salinity, salt categories, nanoparticle concentration, and the mixture of additives. The mechanism analysis was addressed in-depth expositions of all possible multi-particle interactions (both physical and chemical aspects) that contributed to IFT reduction and wettability alteration. It is worth noticing that the IFT was tested in a two-phase system (oil-liquid), and the wettability was examined under a three-phase system (oil-liquid-rock) on Mancos shale, Berea sandstone, and Malaysia sandstone. The following is the summary of the findings from this project.

8.1.1 Characterization of Soapnut Saponin and *Camellia oleifera* saponin

The average density of the extracted green surfactants is 0.89957 g/cm³ and 0.92567 g/cm³ for Soapnut saponin and *Camellia oleifera* saponin, respectively. As the concentration of surfactants increases, the pH of soapnut and *Camellia oleifera* saponins drops. The average pH of Soapnut saponin was 4.50, while *Camellia oleifera* saponin has a pH of 5.17. Both extracted saponins were classified as natural surfactants with low acidity. Both Saponin extracts possess excellent solubility and conductivity. The CMC point of Soapnut saponin was estimated at 4.6wt%. For *Camellia oleifera* saponin, the CMC point was located at 4wt%. The conductivity of saponin solutions increases as a function of temperature but ceases to increase above 80°C due to self-agglomeration. As a result, 80°C can be considered the maximum temperature for the saponin solution, particularly at large concentrations. The CMC points increased with temperature due to the monomers–micelles imbalance, reaching from 4.6wt% to 6.9 wt% (Soapnut saponin) at 100°C. The average particle size of Soapnut saponin and *Camellia oleifera* saponin was around 103.4nm and 123.6nm, respectively. For Soapnut saponin, the average polydispersity index (width of the overall distribution) was 0.576, while *Camellia oleifera* saponin was 0.586. Soapnut saponin has a zeta-potential of -6.35 mV and is classified as a nonionic surfactant due to its proximity to 0 mV. The zeta-potential of *Camellia oleifera* saponin was -22.4mV, indicating that it is an anionic surfactant. The results of TGA analysis are classified into three stages: 1) Between 100 °C and 150°C, the Soapnut saponin lost approximately 6.2% of its weight, while the *Camellia oleifera* saponin lost approximately 19.83%; 2) Between 150°C and 450°C, the Soapnut saponin lost approximately 20.24% of its weight, while the *Camellia oleifera* saponin lost approximately 19.8e%; and 3) Between 450°C and 900°C, the Soapnut saponin lost approximately 8.43% of its weight, while the *Camellia oleifera* saponin lost approximately 7.99%. It is worth mentioning that both surfactants degraded at 450°C. Therefore, Soapnut saponin and *Camellia oleifera* saponin show good thermal stability under reservoir conditions. The TEM images demonstrated that most saponin particles (Soapnut saponin and *Camellia oleifera* saponin) had a homogeneous spherical structure devoid of sharp edges.

Additionally, it was discovered that most of the spherical shape particles formed aggregates, resulting in complex formations. UV-Vis confirmed the saponins' authenticity. The results indicate that most Soapnut saponin compounds have a significant absorption peak between 200nm and 350nm, with the greatest absorption peak (max) found at 200nm. The absorption peak for *Camellia oleifera* saponin was detected between 200-380 nm. The maximum absorption peaks are 215nm, 270nm, and 350nm. The FTIR analysis confirmed the presence of functional groups in Soapnut and *Camellia oleifera* saponins. Specifically, the hydroxyl group (-OH) was identified at 3312cm^{-1} ; the absorbance of aliphatic carbon-hydrogen (C-H) was observed at 2923cm^{-1} ; the symmetric deformation vibration peak and the antisymmetric deformation vibration peak -CH- were identified at 1378 and 1239cm^{-1} ; the carboxylic acid or ester (C=O) was identified at 1728cm^{-1} ; and the peak at 1619cm^{-1} was most likely Absorptions of oligosaccharide linkages to sapogenins, notably C-O-C, were found in the 1029cm^{-1} region.

8.1.2 Salinity Effect, Foamability, Foam Stability, and Bubble Structure

Conductivity increases with an increasing salt concentration in solutions containing only salt (NaCl). On the other hand, when both salt and nanoparticles were added to the solution, the conductivity increased only up to 18000ppm salinity. Conductivity significantly rises with saponin concentration in a solution containing NaCl, NGF, and extracted saponins. These findings may be explained by the presence of active ions in the solutions, which alter their conductivity. When the solution contained just Soapnut saponin or *Camellia oleifera* saponin, the height of the foam increased linearly with the saponin concentration until it reached its CMC point of 4.6wt% (Soapnut saponin) and 4wt% (*Camellia oleifera* saponin). The foam column increased from 16mm at 0.1wt% to 83mm at 8wt% (Soapnut saponin) and 18.2mm at 0.1wt% to 90mm at 8wt% (*Camellia oleifera* saponin). However, the solution with a higher concentration experienced a faster foam structural collapse. The foam generated by Soapnut saponin was able to last 57 hours (2.8mm) at 0.5wt%, whereas it was reduced to 10 hours (0.9mm) when the concentration was

raised to 7wt%. The longest foam stability occurred from 0.1wt% to 0.3wt% concentration, which could maintain its foam structure for 56 hours.

On the other hand, the shortest period of foam structure was observed for the saponin with 8wt% concentration, which maintained its foam structure for only 19 hours. The average size of the foam bubble rose linearly with increasing saponins concentration up to the CMC point. When Soapnut saponin concentration was increased from 0.1wt% to 8wt%, the average bubble diameter grew from 18.9 μ m to 48.3 μ m. The average bubble size formed by *Camellia oleifera* saponin is somewhat greater than that generated by Soapnut saponin. It demonstrates a rise from 20.0 μ m at 0.1wt% to 50.13 μ m at 8wt%.

When the temperature increases to 85°C, both saponins' foam height improves significantly (roughly twofold). At low saponin concentration (0.1wt%), foam height increased from 16mm at room temperature (25°C) to 30mm at 85°C for Soapnut saponin. At the CMC point (4wt%), the foam height increased almost double from 81mm at 25°C to 157mm at 85°C for *Camellia oleifera* saponin. On the other hand, the stability of the foam decreased from 57 hours to 16 hours (Soapnut saponin), and *Camellia oleifera* saponin reduced from 61 hours to 24 hours when the temperature increased from 25°C to 85°C. For the solutions containing only nanoparticles (NGF), the foam length of both saponins increased along with the NGF concentration until it reached the threshold (0.003wt%). For Soapnut saponin, it raised from 27.1mm (0.001wt%) to 28mm (0.003wt%), then decreased to 26.8mm (0.005wt%). Similar results also happened in *Camellia oleifera* saponin, in which the foam length started to increase from 29.5mm at 0.001wt% to 30.6mm at 0.003wt%, then decreased to 29.3mm at 0.005wt%. Compared to tests using only pure saponins, the addition of NGF increased roughly 2mm foam length. Additionally, it successfully increased the foam's stability from 57 to 80 hours. For both saponins, the optimal concentration of NGF was 0.003wt%.

With the presence of saponins and nanoparticles (NGF), the foam height increases along with the concentration of salt (NaCl) until it exceeds the limitation (for Soapnut saponin is 60000ppm and *Camellia oleifera* saponin is 80000ppm). For Soapnut saponin, foam's length nearly doubled when the salinity reached

20000ppm (28mm to 47mm). *Camellia oleifera* saponin also had comparable results, increasing the foam length from 30.6mm to 50mm as salinity increased from 0 to 20000ppm. Soapnut saponin produced the longest foam length of 47mm at 20000ppm salinity. *Camellia oleifera* saponin generated a 50mm foam length (highest) at 20000ppm salinity. Based on the results, 20000ppm salinity was the optimum salt concentration for both saponins. The presence of crude oil accelerates the foam collapse/reduces the foam stability, and merely affects foamability. For Soapnut saponin containing 5000ppm salinity, the foam length of "solution without oil" remained stable for 39 hours at 1.3mm, whereas "solution with oil" only remained stable for 29 hours at 1.1mm. Similar to the results obtained with *Camellia oleifera* saponin, the "solution without oil" exhibited the longest foam stability at 51 hours (0.2mm).

8.1.3 Investigation of IFT Reduction by Combined Low Salinity Green Surfactant Nanofluid and TEM Observation

The IFT values experienced a rapid decrease and concentration for the solution only containing saponins. For Soapnut saponin, the IFT was initially changed from 17.8mN/m at 0wt% to 6.82mN/m at 1wt% with a sharp decrease, followed by a gentle fluctuation of 6.3mN/m at 7wt%. For *Camellia oleifera* saponin, the IFT variation path was similar to Soapnut saponin. It reduced from 17.8mN/m to 5.72mN/m at 1wt%, then fluctuated to 4.1mN/m at 7wt%, which shows a better ability at IFT reduction. The lowest IFT value was 3.8mN/m with 4.5wt% for Soapnut saponin and 3.72mN/m with 4wt% for *Camellia oleifera* saponin. However, the IFT experienced a small rise from 4.3mN/m (5wt%) to 6.3mN/m (7wt%) for Soapnut saponin and 3.85mN/m (4.5wt%) to 4.1mN/m (7wt%) for *Camellia oleifera* saponin when the concentration exceeds its optimum point.

For the solution contain saponins and nanoparticles (variable), the IFT variation with NGF concentration can be divided into two stages: 1) A gentle decrease of IFT observed from 0.001wt% at 3.71mN/m to 0.003wt% at 3.24mN/m (Soapnut saponin), and 3.67mN/m (0.001wt%) to 2.97mN/m (0.003wt%) for *Camellia oleifera* saponin. 2) The IFT starts to increase after passing the 0.003wt%.

For Soapnut saponin, the IFT rise from 3.24mN/m at 0.003wt% to 5.38mN/m at 0.005wt%. For *Camellia oleifera* saponin, the IFT increased from 2.97mN/m at 0.003wt% to 4.12mN/m at 0.005wt%. In general, 0.003wt% of NGF is the optimum concentration for both saponins, and the minimum IFT values were 3.24mN/m (Soapnut saponin) and 2.97mN/m (*Camellia oleifera* saponin). Furthermore, compared with the solution only containing saponin, 0.003wt% NGF can further reduce the IFT by approximately 0.56mN/m (Soapnut saponin) and 0.75mN/m for *Camellia oleifera* saponin.

For the solution containing saponins and salts (variable), the contact angle decreases along with the salinity until it reaches the limitation (3500ppm). For Soapnut saponin, the IFT decreased from 3.73mN/m at 1000ppm to 2.91mN/m at 3500ppm (NaCl). In the presence of CaCl_2 , the IFT dropped from 3.75mN/m at 1000ppm to 3.42mN/m at 3500ppm. In terms of *Camellia oleifera* saponin, the IFT was diminished from 3.67mN/m at 1000ppm to 2.7mN/m at 3500ppm (NaCl) and 3.59mN/m at 1000ppm to 3.27mN/m at 3500ppm (CaCl_2). The lowest results achieved by *Camellia oleifera* saponin was 2.7mN/m at 3500ppm salinity (NaCl), and Soapnut saponin was 2.91mN/m at 3500ppm salinity (NaCl). However, the IFT increased when the salinity exceeded 3500ppm. For Soapnut saponin, the IFT increased to 5.78mN/m and 6.15mN/m at 40000ppm for NaCl and CaCl_2 , respectively. For *Camellia oleifera* saponin, the final IFT reached 5.41mN/m for NaCl and 5.56mN/m for CaCl_2 at 40000ppm. In term of IFT reduction ability, the monovalent salt (NaCl) deliver better results than divalent salt (CaCl_2). For Soapnut saponin, NaCl could further decrease IFT than CaCl_2 by 0.51mN/m. For *Camellia oleifera* saponin, this value increased to 0.57mN/m.

For the solution containing saponins, nanoparticles, and salts (variable), the IFT decreases with an increase in salinity, and it reaches the lowest value at the optimum salinity (3500ppm). After passing this threshold, the IFT increased almost twofold. The saponin, NGF, and salt presented lower IFT results than in previous tests. The optimum combination concentration was: 4.5wt% Soapnut saponin or 4wt% *Camellia oleifera* saponin + 0.003wt% NGF + 3500ppm NaCl or CaCl_2 . Like the previous tests, the IFT increased almost twofold when the salinity was above the

threshold (3500ppm), and monovalent salt (NaCl) has superior IFT reduction capabilities when compared to the divalent salt (CaCl_2). In general, 3500ppm was the optimal salinity, and the lowest IFT, 2.14mN/m, was presented by combining 4wt% *Camellia oleifera* saponin, 0.003wt% NGF, and 3500ppm NaCl.

According to the TEM images, crystallization processes occurred, and the molecules self-organized to form a Fern-like crystal structure. In salt ionization, a precise balancing of interparticle interactions such as hydrogen bonding, ionic bonding, Van der Waals interactions, hydration forces, electrostatic forces, and steric force between saponin and NGF particles leads to self-assembly and crystallization behavior.

8.1.4 Investigation of Wettability Alteration by Combined Low Salinity Green Surfactant Nanofluid and SEM Observation

In the presence of only pure saponins, the contact angles of all three different core slices significantly decreased along with the increasing saponin concentration until the optimum concentration was reached. For Soapnut saponin, it was 5wt% for Mancos shale and Berea sandstone and 6wt% for Malaysia sandstone. For *Camellia oleifera* saponin, 4.5wt% (Mancos shale and Berea sandstone) and 5wt% (Malaysia sandstone) were selected as the appropriate injection concentration based on the contact angle measurements. Then the contact angle experienced a slight rise after boosting the concentration to 6wt% and 7wt%. For Soapnut saponin, the lowest contact angle was observed in Malaysia sandstone at 21.2° with 6wt%. *Camellia oleifera* saponin's lowest contact angle was observed in Malaysia sandstone at 19.93° with 5wt%. It was clearly shown that the *Camellia oleifera* saponin performs a superior wettability alteration than Soapnut saponin.

In the presence of solution contain nanoparticles (variable) and saponins. The contact angle dropped steadily along with the concentration of NGF until the optimum point was reached. It can summarise as 1) 0.003wt% and 28.93° in Mancos shale, 2) 0.0035wt% and 16.27° in Berea sandstone, 3) 0.004wt% and 14.86° in Malaysia sandstone. In terms of *Camellia oleifera* saponin, the optimum concentrations of NGF and lowest contact angles were summarized as 1) 0.003wt%

and 24.75° in Mancos shale, 2) 0.003wt% and 20.81° in Berea sandstone, 3) 0.0035wt% and 16.54° in Malaysia sandstone. In contrast to the pure saponin solution, the contact angle further decreased by around 22.9% with the additional NGF. However, the contact angle increases as the NGF concentration exceeds its optimum value. For Soapnut saponin, the contact angle increased from 28.93° (0wt%) to 38.01° (0.005wt%) at Mancos shale. Similar results occurred at Berea sandstone and Malaysia sandstone, in which the contact angle raised almost twofold. In terms of *Camellia oleifera* saponin, the increased intensity of contact angle on three core slices was approximately 41.7%.

In the presence of solution containing salts (variable) and saponins, the contact angle decreases with increasing salinity until 3500ppm, whereas the contact angle increases approximately twofold when the salinity increases from 3500ppm to 40000ppm. The lowest contact angle generated by pure *Camellia oleifera* saponin in Berea sandstone was 22.8°, while the angle was further reduced to 17.55° (NaCl) or 18.29° (CaCl₂) with additional low salinity brine. The lowest contact angle in Soapnut saponin was shown in Malaysia sandstone with NaCl at 15.98°. The optimum salinity of both salts NaCl and CaCl₂ was identified as 3500ppm. *Camellia oleifera* saponin shows superior ability in contact angle reduction (wettability alteration) than Soapnut saponin.

In the presence of a solution containing saponins, nanoparticles, and salts (variable), the increasing salinity significantly decreased the contact angle until it reached 3500ppm. For Soapnut saponin, the angle dropped approximately 33%, and the lowest contact angle was achieved in Berea sandstone at 10.3° with 3500ppm NaCl, 5wt% Soapnut saponin, and 0.003wt% NGF. *Camellia oleifera* saponin's contact angle decreased around 27%, and the lowest angle showed on Malaysia sandstone at 10.02° with 3500ppm NaCl, 5wt% *Camellia oleifera* saponin, and 0.0035wt% NGF. Moreover, the additional nanoparticles can further reduce the contact angle by 33% for Soapnut saponin and 26% for *Camellia oleifera* saponin. However, after the salinity exceeds the limitation of 3500ppm, the contact angle increases and is achieved around twofold at 40000ppm. In general, 3500ppm was the optimum salinity for both salts (NaCl and CaCl₂) in low salinity NGF saponin fluid.

For Soapnut saponin, the lowest contact angle achieved was 10.3° with 5wt% Soapnut saponin, 0.0035wt% NGF, and 3500ppm NaCl in Berea sandstone. Camellia oleifera saponin's lowest contact angle was 10.02° with 5wt% Camellia oleifera saponin, 0.0035wt% NGF, and 3500ppm NaCl in Malaysia sandstone.

After immersing the clean formation rocks into the low salinity NGF saponin fluid, the SEM images clearly show the more irregular edges of the rock surface. Furthermore, the roughness of the rock surface also improved from scaly to smooth, which is mostly covered by a nanotextured layer constructed by the synergistic interactions of NGF particles, saponin molecules, and salt ions. It is worth noting that the self-organized Fern-like crystal structure can be observed on the rock surfaces, which leads to a better dispersion ability and stability of low salinity NGF saponin fluid on formation rocks.

8.1.5 Related Mechanisms Fundamental Explanations

As mentioned in Chapter 1, investigating the multi-mechanisms between new green surfactants, nanoparticles, salt, rock formation, and oil droplets was one of the major objectives of this project. The fundamental explanations of all the related mechanisms are summarized below.

Foamability and foam stability

Pure saponin: the foamability increases along with the concentration until it reaches the CMC point. The formation of the micelles mainly contributes to it. For foam stability, it was clearly shown that the height of foam declined as time went by. The rising saponin concentration also enhanced the impact of graviton force on foam drainage resulting in continuous liquid drainage from the space between bubbles breaking the liquid films, thereby decreasing the stability of the foam ([Almobarky et al., 2018](#), [Petkova et al., 2021](#)).

Saponin and nanoparticle: the additional NGF can enhance the foam stability but only slightly increase the foamability. With the high surface energy, nanoparticles can effectively adsorb and aggregate at bubble films, thereby raising the maximum capillary pressure and particle detachment energy before foam break ([Shojaei et al., 2021](#)). Also, the extremely small size enables nanoparticles easily penetrate the

liquid film and arrange themselves as a monolayer of bridging particles. It also can prevent gas diffusion in the foam column and protect the foam film from thinning ([Z. Xu et al., 2020](#)).

Saponin and salt: foamability and foam stability increase along with the salt concentration until it reaches the 20000ppm threshold. The increasing salt concentration improves the foam structure from thermodynamically unstable to stable ([Majeed et al., 2020](#)). The bulk solution produced smaller and stronger bubbles due to the reduced double-layer force. The additional salt also reduces the solubility in the solution, thus decreasing the hydrophobic interaction between water and saponin molecules and increasing the foam stability by slowing the bubble coalescence rate ([Obisesan et al., 2021](#)).

Saponin and crude oil: the presence of oil significantly decreases the foam stability. It destabilizes the foam and causes a shorter lifespan of foam films ([Hadian et al., 2020](#)). Specifically, the crude oil unstable the foam thermodynamics by thinning the foam film ([L. Zhang et al., 2019](#)). Furthermore, with the gravity drainage, the accumulated crude oil droplets were drained through the borders and formulated an extra oil phase at the air/water interface, resulting in a faster bubble coalescence rate, thereby reducing the foam stability ([Lin et al., 2021](#)).

IFT reduction

Both IFT values experienced a rapid decrease with a small amount of saponin initially, then remained gentle declined until they reached the CMC point. The sharp decrease at the beginning was the rapid diffusion of saponin molecules in solution and the saponin monomers adsorbed on the oil-liquid interface by hydrogen bonding. More saponin molecules concentrate at the interface and aggregate to form micelles when the saponin concentration increases ([Kamal et al., 2017](#); [Peng and Nguyen, 2020](#)). Thereby, the IFT variation becomes soft. That is why the IFT normally stops decreasing after passing the CMC point. The additional salt and nanoparticles decrease and the concentration until they reach the limitation. The contribution mechanisms were summarized: with the high surface-to-volume ratio and high surface energy of NGF, saponin molecules tend to adsorb on the surface to form monolayers ([Rezaei et al., 2021](#)). It drove more saponins to move to the

oil/liquid interface and decrease the IFT. The electrostatic repulsion force between NGF particles and saponin enhanced the saponin diffuse in solution ([Moslemizadeh et al., 2021](#)).

On the other hand, when salt was added to the solution with low concentration, the counterions of salt screen electrostatic repulsion of saponin's polar head groups; Consequently, saponin molecules got even closer to each other and arranged a more compact layer at the oil/water interface ([Vatanparast et al., 2018](#)). Furthermore, a certain amount of saponin molecules and NGF were pushed to the interface due to the Brownian motion and electrostatic repulsion forces between similarly charged saponin head groups and NGF ([Harikrishnan et al., 2017](#)). As a result, the IFT decreased. However, saponins coated NGF aggregated together and induced the IFT increase when the NGF and salt concentration exceeded the limit. Furthermore, the formation of microemulsions and cylindrical micelles (two agglomerates) under the high salt concentration environment significantly decreases the number of saponin molecules at the interface ([Olayiwola & Dejam, 2019](#)). Thereby, the IFT increase along with the concentration.

Wettability alteration

The contact angles of all three different core slices significantly decreased along with the increasing saponin concentration until close to the CMC point. These saponin molecules with a negatively surface charge absorb the positive basic components in crude oil from the rock surface through the electrostatic attraction force, forming ion pairing between the saponin molecules and the rock surface, then weakening in the adsorption of crude oil components onto rock surfaces by forming a layer ([Nourani et al., 2020](#)). Hydrophobic interaction between the hydrophobic part of oil components (adsorbed at rock surface) and the accumulated saponin molecules results in the disturbance of the overlying oil layer. In terms of additional salt and nanoparticles, the contact angle could reduce further. The major mechanisms contributing further to contact angle reduction with additional nanoparticles and salt were: the interactions between NGF and saponin molecules, which lead to forming a durable and resilient barrier at the oil-water interface that prevents the flocculation of a crude oil droplet, thereby modifying the

surface wettability (Kamal et al., 2017). Furthermore, NGF particles also acted as transportation to transfer more saponin molecules from bulk fluid to the oil/water interface. With the extremely small size and high surface energy, NGF particles adsorbed on the rock surface, which promoted the detachment of oil droplets from the rock surface (Jha et al., 2019). The positive ions from the salt adsorb the negatively charged components on the rock surface through cation bridging, forming the direct covalent bond (Rezaei et al., 2021). Furthermore, the crude oil's negatively charged carboxylic acid groups also interact with the positive ions by a hydrogen bond. Therefore, these interactions reduce the forces between rock formation and crude oil droplets, causing wettability alteration with decreased contact angle (Divandari et al., 2020).

8.2 Recommendations

In this Ph.D. thesis, two green surfactants have been successfully extracted from Soapnut and *Camellia oleifera*, and the properties and performance of each additive (including saponins, NaCl or CaCl₂, NGF, and the combination of them) have been extensively investigated in foamability, foam stability, IFT reduction, and wettability alteration. Based on this thesis's findings and the difficulties experienced throughout the experimental work, some recommendations for future work are given:

(1) Core flooding

This thesis has shown that the new green surfactants and the low salinity saponin NGF fluids can perform excellently in IFT reduction and wettability alteration. In future studies, core flooding is suggested to examine the optimal development strategy for oil recovery and evaluate the effects of green saponins or the novel low salinity saponins NGF fluids in reservoir conditions. The objectives may include the determination of relative permeability, saturation variation, formation damage triggered by the fluid injection, or fluid-rock interactions. The test environment can be set at either room temperature with low confining pressure or HTHP condition. The test rocks are recommended to use Mancos shale, Berea sandstone, and Malaysia sandstone. The injection fluids are suggested to follow the sequences

shown above, which are: 1) pure saponins, 2) saponins and NGF nanoparticles (variable), 3) saponins and salts (variable), 4) saponins, NGF nanoparticles, and salts (variable). A series of measurements such as FTIR, UV-Vis, conductivity, and nuclear magnetic resonance (NMR) suggest to applied the fluids before and after core flooding. It is worth noting that all the injection fluids need to be freshly prepared and completely homogenized before injection.

The experiment started with measuring the core length and diameter, followed by core cleaning and aging, which can be referred to in Chapter 7. All cores need to initially flood with Oil to obtain the effective oil permeability (k_o) at irreducible water saturation. After pressure stabilization, the permeability will be determined using Darcy's law. The purpose is to displace oil with fresh oil and achieve equilibrium in the flooding system. The cores are suggested to be linked to a 30 bar confining pressure and 20 bar backpressure. All core flooding batches are suggested to start with the high salinity water injection. When no considerable amount of oil is produced, the injection stops. The core flooding is proceeded with a tertiary mode injection of low salinity brine (LS), followed by 0.5 PV of low salinity saponin (LSS), 2 PV of low salinity nanoparticle (LSN), and lastly, a chase water injection of 3 PV of low salinity brine. Consistent injection rates of 0.1mL/min are suggested to use. A computer will measure and record the pressure drop across the core. A camera will monitor the effluent collection and record the amount of waste produced over time. A 250ml measuring cylinder collects the volumetric production profiles of all flood phases. At last, the effective water permeability will be determined with LS brine at decreasing injection rates (0.1, 0.08, 0.06, and 0.04 - mL/min), and the endpoint relative permeability also will be calculated. The core sample will be put back in the oven for 48 hours at 75°C for 72 hours for the next core flooding test.

(2) Surfactant lost study

The retention of surfactants (saponins in this case) caused by adsorption, precipitation, degradation, and phase trapping is a major restraining factor that influences the cost-effectiveness of surfactant-based EOR flooding. Furthermore, the high adsorption of surfactants on porous media can fail flooding by interfering

with the surfactants' ability to IFT reduction and wettability alteration. Generally, the adsorption threshold for carbonate reservoirs at elevated temperatures was 1.0 mg/m².

Adsorption of a surfactant is the sum of the effects of hydrogen bonding, lateral associative interactions, electrostatic interactions, chemical interactions (covalent bonding), solvation, and desolvation. The driving forces can be modified by the physicochemical properties of fluids, surfactants, and adsorbents. Small changes in surfactant composition and concentration, temperature, pH, salinity, and the additional nanoparticles can result in considerable changes in adsorption density. Although adsorption and degradation behavior is inevitable, they can be minimized by mixing saponins, salt, and nanoparticles with a proper ratio. On the other hand, precipitation and phase trapping can be prevented by selecting the appropriate additives combination. During the EOR flooding project, surfactants can account for up to half or even more of the entire project cost. Therefore, from an economic standpoint, mitigating the surfactant lost from adsorption, precipitation, degradation, and phase trapping and learning about the factors that influence the surfactant lost and the related mechanisms are necessary for future studies. Techniques such as UV-Vis, conductivity measurement, high-performance liquid chromatography (HPLC), and total organic carbon analysis (TOC) are applicable to investigate surfactant loss. It should be mindful that all injectable fluids must be freshly prepared and thoroughly homogenized before injection. And all core samples need to be thoroughly ground into a fine powder then sieved through 28-10 mesh. After that, the fixed amount of rock powder mix with fluids then put in the shaker bath for 24th to reach maximum adsorption balance. Next, the mixture of samples will be put on the centrifuge; the clear upper solvent will use for analysis.

(3) Purity test

The purity test can accomplish by Electron Impact Ionization (EI) method on gas chromatography-mass spectrometry (GC-MS). The operating condition is as follows: fused silica capillary column (RTS-5MS) with a diameter of 30cm and length of 0.25mm. Oven: Initial temperature 70°C for 1 minutes, ramp 6°C/min to 180°C, hold 5 minutes, ramp 5°C/min to 280°C, hold 20 minutes, Injector temperature=220°C,

samples inject by splitting with the split ratio 10, helium carrier gas at constant pressure 90KPa, SolventDelay=1.59min, Transfer Temperature=280°C, Source Temperature=290°C, Scan: 50 to 600Da, Column 30.0m × 250µm.

The samples are analyzed using GC-MS in the following manner: the carrier gas flow rate is adjusted to achieve repeatable retention duration and to minimize detector dirt. The sample is then injected using a tiny syringe into the column via a heated injection portion that vaporizes the sample. The column's lengthy tube is densely packed with solid particles. A thin film of a high boiling liquid is applied uniformly to the solid support (the stationary phase). The samples are then partitioned into mobile and stationary phases and sorted into their constituents. The carrier gas and sample component exited the column and passed through a detector. The device measures the concentration of each component and creates an electrical signal. A detector is used to receive the signal.

Reference

- Abbas, A. H., Moslemizadeh, A., Wan Sulaiman, W. R., Jaafar, M. Z., & Agi, A. (2020). An insight into a di-chain surfactant adsorption onto sandstone minerals under different salinity-temperature conditions: Chemical EOR applications. *Chemical Engineering Research and Design*, 153, 657–665. <https://doi.org/10.1016/j.cherd.2019.11.021>
- Adiukwu, P. C., Bonsu, M., Okon-Ben, I., Peprah, P., Mensah-Kane, P., Jato, J., & Nambatya, G. (2017). Ultraviolet spectroscopic evaluation of bioactive saponin fraction from the aqueous extract of *Vernonia amygdalina* [Esteraceae] leaf. *International Journal of Biological and Chemical Sciences*, 11(4), 1893. <https://doi.org/10.4314/ijbcs.v11i4.38>
- Afolabi, R. O. (2019). Enhanced oil recovery for emergent energy demand: Challenges and prospects for a nanotechnology paradigm shift. *International Nano Letters*, 9(1), 1–15. <https://doi.org/10.1007/s40089-018-0248-0>
- Agi, A., Junin, R., & Gbadamosi, A. (2018). Mechanism governing nanoparticle flow behaviour in porous media: Insight for enhanced oil recovery applications. *International Nano Letters*, 8(2), 49–77. <https://doi.org/10.1007/s40089-018-0237-3>
- Agista, M., Guo, K., & Yu, Z. (2018). A State-of-the-Art Review of Nanoparticles Application in Petroleum with a Focus on Enhanced Oil Recovery. *Applied Sciences*, 8(6), 871. <https://doi.org/10.3390/app8060871>
- Ahmadi, M. A., Arabsahebi, Y., Shadizadeh, S. R., & Shokrollahzadeh Behbahani, S. (2014). Preliminary evaluation of mulberry leaf-derived surfactant on interfacial tension in an oil-aqueous system: EOR application. *Fuel*, 117, 749–755. <https://doi.org/10.1016/j.fuel.2013.08.081>
- Ahmadi, M. A., & Shadizadeh, S. R. (2012). Adsorption of Novel Nonionic Surfactant and Particles Mixture in Carbonates: Enhanced Oil Recovery Implication. *Energy & Fuels*, 26(8), 4655–4663. <https://doi.org/10.1021/ef300154h>
- Ahmadi, M. A., & Shadizadeh, S. R. (2013). Induced effect of adding nano silica on adsorption of a natural surfactant onto sandstone rock: Experimental and theoretical study. *Journal of Petroleum Science and Engineering*, 112, 239–247. <https://doi.org/10.1016/j.petrol.2013.11.010>
- Ahmadi, M. A., & Shadizadeh, S. R. (2015). Experimental investigation of a natural surfactant adsorption on shale-sandstone reservoir rocks: Static and dynamic conditions. *Fuel*, 159, 15–26. <https://doi.org/10.1016/j.fuel.2015.06.035>
- Ahmadi, M. A., & Shadizadeh, S. R. (2018). Spotlight on the New Natural Surfactant Flooding in Carbonate Rock Samples in Low Salinity Condition. *Scientific Reports*, 8(1), 10985. <https://doi.org/10.1038/s41598-018-29321-w>
- Ahmadi, M. A., Zendehboudi, S., Shafiei, A., & James, L. (2012). Nonionic Surfactant for Enhanced Oil Recovery from Carbonates: Adsorption Kinetics and Equilibrium. *Industrial & Engineering Chemistry Research*, 51(29), 9894–9905. <https://doi.org/10.1021/ie300269c>

- Ahmadi, M., & Chen, Z. (2020). Challenges and future of chemical assisted heavy oil recovery processes. *Advances in Colloid and Interface Science*, 275, 102081. <https://doi.org/10.1016/j.cis.2019.102081>
- Ahmed, A., Saaid, I. M., Ahmed, A. A., Pilus, R. M., & Baig, M. K. (2019). Evaluating the potential of surface-modified silica nanoparticles using internal olefin sulfonate for enhanced oil recovery. *Petroleum Science*. <https://doi.org/10.1007/s12182-019-00404-1>
- Ahmed, T. (2009). *Working Guide to Reservoir Rock Properties and Fluid Flow*. Elsevier Science & Technology. <http://ebookcentral.proquest.com/lib/curtin/detail.action?docID=566684>
- Ahmed, T. (2010). Part 2—Fundamentals of Rock Properties. In T. Ahmed (Ed.), *Working Guide to Reservoir Rock Properties and Fluid Flow* (pp. 31–115). Gulf Professional Publishing. <https://doi.org/10.1016/B978-1-85617-825-9.00002-8>
- Ahmed, T., & Ahmed Phd Pe, T. (2010). *Reservoir Engineering Handbook*. Elsevier Science & Technology. <http://ebookcentral.proquest.com/lib/curtin/detail.action?docID=648740>
- Akbar, M. I., Agenet, N., Kamp, A. M., & Gosselin, O. R. (2018). Evaluation and Optimisation of Smart Water Injection for Fractured Reservoir. *SPE Europec Featured at 80th EAGE Conference and Exhibition*. SPE Europec featured at 80th EAGE Conference and Exhibition, Copenhagen, Denmark. <https://doi.org/10.2118/190854-MS>
- Aksulu, H., Håmsø, D., Strand, S., Puntervold, T., & Austad, T. (2012). Evaluation of Low-Salinity Enhanced Oil Recovery Effects in Sandstone: Effects of the Temperature and pH Gradient. *Energy & Fuels*, 26(6), 3497–3503. <https://doi.org/10.1021/ef300162n>
- Al Maskari, N. S., Xie, Q., & Saeedi, A. (2019). Role of Basal-Charged Clays in Low Salinity Effect in Sandstone Reservoirs: Adhesion Force on Muscovite using Atomic Force Microscope. *Energy & Fuels*, 33(2), 756–764. <https://doi.org/10.1021/acs.energyfuels.8b03452>
- Alagic, E., Spildo, K., Skauge, A., & Solbakken, J. (2011). Effect of crude oil ageing on low salinity and low salinity surfactant flooding. *Journal of Petroleum Science and Engineering*, 78(2), 220–227. <https://doi.org/10.1016/j.petrol.2011.06.021>
- Alhuraishawy, A. K., Bai, B., Wei, M., & Al-Bazzaz, W. H. (2018). New Insights of Low Salinity Water Flooding in Low Permeability-Low Porosity Clay Rich Sandstone Reservoir. *SPE International Heavy Oil Conference and Exhibition*. SPE International Heavy Oil Conference and Exhibition, Kuwait City, Kuwait. <https://doi.org/10.2118/193744-MS>
- Ali, J. A., Kolo, K., Manshad, A. K., & Mohammadi, A. H. (2018). Recent advances in application of nanotechnology in chemical enhanced oil recovery: Effects of nanoparticles on wettability alteration, interfacial tension reduction, and flooding. *Egyptian Journal of Petroleum*, 27(4), 1371–1383. <https://doi.org/10.1016/j.ejpe.2018.09.006>
- Aljamhan, A. S., Alrefeai, M. H., Alhabdan, A., Alhusseini, S. A., Farooq, I., Vohra, F., Naseem, M., & Alkhudhairy, F. (2021). Influence of ER-CR-YSGG Laser and Photodynamic Therapy on the Dentin Bond Integrity of Nano-

- Hydroxyapatite Containing Resin Dentin Adhesive: SEM-EDX, Micro-Raman, Micro-Tensile, and FTIR Evaluation. *Polymers*, 13(12), 1903. <https://doi.org/10.3390/polym13121903>
- Almahfood, M., & Bai, B. (2018). The synergistic effects of nanoparticle-surfactant nanofluids in EOR applications. *Journal of Petroleum Science and Engineering*, 171, 196–210. <https://doi.org/10.1016/j.petrol.2018.07.030>
- Almao, P. P. (2012). In situ upgrading of bitumen and heavy oils via nanocatalysis. *The Canadian Journal of Chemical Engineering*, 90(2), 320–329. <https://doi.org/10.1002/cjce.21646>
- Almobarky, M., AlYousef, Z., & Schechter, D. (2018). Enhancing the Foam Stability Using Surfactants Mixtures. *SPE Kingdom of Saudi Arabia Annual Technical Symposium and Exhibition*. SPE Kingdom of Saudi Arabia Annual Technical Symposium and Exhibition, Dammam, Saudi Arabia. <https://doi.org/10.2118/192449-MS>
- Almubarak, M., AlYousef, Z., Almajid, M., Almubarak, T., & Ng, J. H. (2020). Enhancing Foam Stability Through a Combination of Surfactant and Nanoparticles. *Day 1 Mon, November 09, 2020*, D012S116R090. <https://doi.org/10.2118/202790-MS>
- Almutairi, M. S., & Ali, M. (2015). Direct detection of saponins in crude extracts of soapnuts by FTIR. *Natural Product Research*, 29(13), 1271–1275. <https://doi.org/10.1080/14786419.2014.992345>
- Alnarabiji, M. S., & Husein, M. M. (2020). Application of bare nanoparticle-based nanofluids in enhanced oil recovery. *Fuel*, 267, 117262. <https://doi.org/10.1016/j.fuel.2020.117262>
- Alonso, G. (2020). Assessing salt-surfactant synergistic effects on interfacial tension from molecular dynamics simulations. *Journal of Molecular Liquids*, 11.
- Alsaba, M. T., Al Dushaishi, M. F., & Abbas, A. K. (2020). A comprehensive review of nanoparticles applications in the oil and gas industry. *Journal of Petroleum Exploration and Production Technology*. <https://doi.org/10.1007/s13202-019-00825-z>
- Al-Saedi, H. N., Alhuraishawy, A. K., Flori, R., & Brady, P. V. (2019). Sequential injection mode of high-salinity/low-salinity water in sandstone reservoirs: Oil recovery and surface reactivity tests. *Journal of Petroleum Exploration and Production Technology*, 9(1), 261–270. <https://doi.org/10.1007/s13202-018-0466-z>
- Al-Saedi, H. N., Qubian, A., Al-Bazzaz, W., & Flori, R. (2020, January 13). *Experimental Study of Low Salinity Water Flooding: The Effect of Polar Organic Components in Low-Permeable Sandstone Reservoir*. International Petroleum Technology Conference. <https://doi.org/10.2523/IPTC-19740-MS>
- Al-Samhan, M., Jasim, F., Al-Attar, F., & AL-Fadhli, J. (2020). Prospect of Using Nano Particles in Compatible Water for EOR Application. In H. Okada & S. N. Atluri (Eds.), *Computational and Experimental Simulations in Engineering* (pp. 557–565). Springer International Publishing. https://doi.org/10.1007/978-3-030-27053-7_48
- Al-Sarihi, A., Zeinijahromi, A., Genolet, L., Behr, A., Kowollik, P., & Bedrikovetsky, P. (2018). Fines Migration as an EOR Method During Low Salinity Waterflooding. *SPE Asia Pacific Oil and Gas Conference and Exhibition*. SPE

- Asia Pacific Oil and Gas Conference and Exhibition, Brisbane, Australia. <https://doi.org/10.2118/192070-MS>
- Al-Shalabi, E. W., & Sepehrnoori, K. (2016). A comprehensive review of low salinity/engineered water injections and their applications in sandstone and carbonate rocks. *Journal of Petroleum Science and Engineering*, 139, 137–161. <https://doi.org/10.1016/j.petrol.2015.11.027>
- AlYousef, Z., & Schechter, D. (2019, October 13). *The Synergy of Surfactant and Nanoparticles: Towards Enhancing Foam Stability*. SPE Kuwait Oil & Gas Show and Conference. <https://doi.org/10.2118/198190-MS>
- Amani, P., Karakashev, S. I., Grozev, N. A., Simeonova, S. S., Miller, R., Rudolph, V., & Firouzi, M. (2021). Effect of selected monovalent salts on surfactant stabilized foams. *Advances in Colloid and Interface Science*, 295, 102490. <https://doi.org/10.1016/j.cis.2021.102490>
- Aminian, A., & ZareNezhad, B. (2019a). Wettability alteration in carbonate and sandstone rocks due to low salinity surfactant flooding. *Journal of Molecular Liquids*, 275, 265–280. <https://doi.org/10.1016/j.molliq.2018.11.080>
- Aminian, A., & ZareNezhad, B. (2019b). Oil-detachment from the calcium carbonate surfaces via the actions of surfactant, nanoparticle and low salinity brine: An insight from molecular dynamic simulation. *Chemical Engineering Science*, 202, 373–382. <https://doi.org/10.1016/j.ces.2019.03.031>
- Arabloo, M., Ghazanfari, M. H., & Rashtchian, D. (2015). Spotlight on kinetic and equilibrium adsorption of a new surfactant onto sandstone minerals: A comparative study. *Journal of the Taiwan Institute of Chemical Engineers*, 50, 12–23. <https://doi.org/10.1016/j.jtice.2014.12.012>
- Arabloo, M., Ghazanfari, M. H., & Rashtchian, D. (2016). Wettability modification, interfacial tension and adsorption characteristics of a new surfactant: Implications for enhanced oil recovery. *Fuel*, 185, 199–210. <https://doi.org/10.1016/j.fuel.2016.06.088>
- Austad, T. (2013). Water-Based EOR in Carbonates and Sandstones. In *Enhanced Oil Recovery Field Case Studies* (pp. 301–335). Elsevier. <https://doi.org/10.1016/B978-0-12-386545-8.00013-0>
- Austad, T., RezaeiDoust, A., & Puntervold, T. (2010). Chemical Mechanism of Low Salinity Water Flooding in Sandstone Reservoirs. *Society of Petroleum Engineers*, 17.
- Avendano, C., Lee, S., Escalera, G., & Colvin, V. (2012). Magnetic Characterization of Nanoparticles Designed for Use As Contrast Agents for Downhole Measurements. *Society of Petroleum Engineers - SPE International Oilfield Nanotechnology Conference 2012*. <https://doi.org/10.2118/157123-MS>
- Ayatollahi, S., & Zerafat, M. M. (2012, January 1). *Nanotechnology-Assisted EOR Techniques: New Solutions to Old Challenges*. SPE International Oilfield Nanotechnology Conference and Exhibition. <https://doi.org/10.2118/157094-MS>
- Ayirala, S. C., Boqmi, A., Alghamdi, A., & AlSofi, A. (2019). Dilute surfactants for wettability alteration and enhanced oil recovery in carbonates. *Journal of Molecular Liquids*, 285, 707–715. <https://doi.org/10.1016/j.molliq.2019.04.146>

- Ayirala, S. C., & Yousef, A. A. (2014). Injection Water Chemistry Requirement Guidelines for IOR/EOR. *SPE Improved Oil Recovery Symposium*. SPE Improved Oil Recovery Symposium, Tulsa, Oklahoma, USA. <https://doi.org/10.2118/169048-MS>
- Ayoub, M., Mohyaldinn, M. E., Mahmood, S. M., Aqsha, A., Jufar, S. R., Farrukh, S., Inayat, F., & Shamsuddin, M. R. (2019). A comparative study of dynamic adsorption of anionic synthetic and nanocellulose-based surfactant in Malaysian reservoir. *Journal of Petroleum Exploration and Production Technology*. <https://doi.org/10.1007/s13202-019-00743-0>
- Azam, M. R., Tan, I. M., Ismail, L., Mushtaq, M., Nadeem, M., & Sagir, M. (2013). Static adsorption of anionic surfactant onto crushed Berea sandstone. *Journal of Petroleum Exploration and Production Technology*, 3(3), 195–201. <https://doi.org/10.1007/s13202-013-0057-y>
- Aziz, U. A., Adnan, N., Sohri, M. Z. R., Mohshim, D. F., Idris, A. K., & Azman, M. A. (2019). Characterization of Anionic–Nonionic Surfactant Mixtures for Enhanced Oil Recovery. *Journal of Solution Chemistry*, 48(11–12), 1617–1637. <https://doi.org/10.1007/s10953-019-00902-1>
- Azwanida NN. (2015). A Review on the Extraction Methods Use in Medicinal Plants, Principle, Strength and Limitation. *Medicinal & Aromatic Plants*, 04(03). <https://doi.org/10.4172/2167-0412.1000196>
- Bachari, Z., Isari, A. A., Mahmoudi, H., Moradi, S., & Mahvelati, E. H. (2019). Application of Natural Surfactants for Enhanced Oil Recovery – Critical Review. *IOP Conference Series: Earth and Environmental Science*, 221, 012039. <https://doi.org/10.1088/1755-1315/221/1/012039>
- Bai, W., Kong, L., & Guo, A. (2013). Effects of physical properties on electrical conductivity of compacted lateritic soil. *Journal of Rock Mechanics and Geotechnical Engineering*, 5(5), 406–411. <https://doi.org/10.1016/j.jrmge.2013.07.003>
- Basu, A., Basu, S., Bandyopadhyay, S., & Chowdhury, R. (2015). Optimization of evaporative extraction of natural emulsifier cum surfactant from Sapindus mukorossi—Characterization and cost analysis. *Industrial Crops and Products*, 77, 920–931. <https://doi.org/10.1016/j.indcrop.2015.10.006>
- Balakrishnan, S., Varughese, S., & Deshpande, A. (2006). Micellar Characterisation of Saponin from Sapindus Mukorossi. *Tenside Surfactants Detergents*, 43, 262–268. <https://doi.org/10.3139/113.100315>
- Barati-Harooni, A., Najafi-Marghmaleki, A., Tatar, A., & Mohammadi, A. H. (2016). Experimental and modeling studies on adsorption of a nonionic surfactant on sandstone minerals in enhanced oil recovery process with surfactant flooding. *Journal of Molecular Liquids*, 220, 1022–1032. <https://doi.org/10.1016/j.molliq.2016.04.090>
- Bayat, A. E., Junin, R., Shamshirband, S., & Chong, W. T. (2015). Transport and retention of engineered Al₂O₃, TiO₂, and SiO₂ nanoparticles through various sedimentary rocks. *Scientific Reports*, 5, 14264. <https://doi.org/10.1038/srep14264>
- Behera, M. R., Varade, S. R., Ghosh, P., Paul, P., & Negi, A. S. (2014). Foaming in Micellar Solutions: Effects of Surfactant, Salt, and Oil Concentrations.

- Industrial & Engineering Chemistry Research*, 53(48), 18497–18507. <https://doi.org/10.1021/ie503591v>
- Belhaj, A. F., Elraies, K. A., Mahmood, S. M., Zulkifli, N. N., Akbari, S., & Hussien, O. S. (2020). The effect of surfactant concentration, salinity, temperature, and pH on surfactant adsorption for chemical enhanced oil recovery: A review. *Journal of Petroleum Exploration and Production Technology*, 10(1), 125–137. <https://doi.org/10.1007/s13202-019-0685-y>
- Beneventi, D., Carre, B., & Gandini, A. (2001). Role of surfactant structure on surface and foaming properties. *Colloids and Surfaces A: Physicochemical and Engineering Aspects*, 189(1–3), 65–73. [https://doi.org/10.1016/S0927-7757\(01\)00602-1](https://doi.org/10.1016/S0927-7757(01)00602-1)
- Bernard, G. G. (1967). *Effect of Floodwater Salinity on Recovery of Oil from Cores Containing Clays*. 8.
- Borkowski, M., & Zawala, J. (2021). Influence of Temperature on Rising Bubble Dynamics in Water and n-pentanol Solutions. *Minerals*, 11(10), 1067. <https://doi.org/10.3390/min11101067>
- Brady, P. V., Morrow, N. R., Fogden, A., Deniz, V., Loahardjo, N., & Winoto. (2015). Electrostatics and the Low Salinity Effect in Sandstone Reservoirs. *Energy & Fuels*, 29(2), 666–677. <https://doi.org/10.1021/ef502474a>
- Budhathoki, M., Barnee, S. H. R., Shiau, B.-J., & Harwell, J. H. (2016). Improved oil recovery by reducing surfactant adsorption with polyelectrolyte in high saline brine. *Colloids and Surfaces A: Physicochemical and Engineering Aspects*, 498, 66–73. <https://doi.org/10.1016/j.colsurfa.2016.03.012>
- CDC. (2018, March 28). *Comparative effects of surfactants*. Centers for Disease Control and Prevention. <https://www.cdc.gov/index.htm>
- Chaalal, O., Mohamed, H., & Lwisa, E. (2018). Green water flooding of fractured and heterogeneous oil reservoirs at high salinity and high temperature. *Advanced Materials Proceedings*, 6.
- Chakravarty, K. H., Fosbøl, P. L., & Thomsen, K. (2015a). Importance of Fines in Smart Water Enhanced Oil Recovery (SmW-EOR) for Chalk Outcrops. *EUROPEC 2015*. EUROPEC 2015, Madrid, Spain. <https://doi.org/10.2118/174334-MS>
- Chakravarty, K. H., Fosbøl, P. L., & Thomsen, K. (2015b). Interactions of Fines with Base Fractions of Oil and its Implication in Smart Water Flooding. *EUROPEC 2015*. EUROPEC 2015, Madrid, Spain. <https://doi.org/10.2118/174335-MS>
- Chavan, M., Dandekar, A., Patil, S., & Khataniar, S. (2019). Low-salinity-based enhanced oil recovery literature review and associated screening criteria. *Petroleum Science*, 16(6), 1344–1360. <https://doi.org/10.1007/s12182-019-0325-7>
- Chávez-Miyauch, T. E., Lu, Y., & Firoozabadi, A. (2020). Low salinity water injection in Berea sandstone: Effect of wettability, interface elasticity, and acid and base functionalities. *Fuel*, 263, 116572. <https://doi.org/10.1016/j.fuel.2019.116572>
- Chen, Y., Wang, B., Chen, J., Wang, X., Wang, R., Peng, S., Chen, L., Ma, L., & Luo, J. (2015). Identification of Rubisco rbcL and rbcS in *Camellia oleifera* and their potential as molecular markers for selection of high tea oil cultivars. *Frontiers in Plant Science*, 06. <https://doi.org/10.3389/fpls.2015.00189>

- Chen, Y., Xie, Q., & Saeedi, A. (2019). Role of ion exchange, surface complexation, and albite dissolution in low salinity water flooding in sandstone. *Journal of Petroleum Science and Engineering*, 176, 126–131. <https://doi.org/10.1016/j.petrol.2019.01.019>
- Chengara, A., Nikolov, A. D., Wasan, D. T., Trokhymchuk, A., & Henderson, D. (2004). Spreading of nanofluids driven by the structural disjoining pressure gradient. *Journal of Colloid and Interface Science*, 280(1), 192–201. <https://doi.org/10.1016/j.jcis.2004.07.005>
- Chemat, F., Abert-Vian, M., Fabiano-Tixier, A. S., Strube, J., Uhlenbrock, L., Gunjevic, V., & Cravotto, G. (2019). Green extraction of natural products. Origins, current status, and future challenges. *TrAC Trends in Analytical Chemistry*, 118, 248–263. <https://doi.org/10.1016/j.trac.2019.05.037>
- Chhetri, A. B., Watts, K. C., Rahman, M. S., & Islam, M. R. (2009). Soapnut Extract as a Natural Surfactant for Enhanced Oil Recovery. *Energy Sources, Part A: Recovery, Utilization, and Environmental Effects*, 31(20), 1893–1903. <https://doi.org/10.1080/15567030802462622>
- Cissokho, M., Boussour, S., Cordier, P., Bertin, H., & Hamon, G. (2010). *Low Salinity Oil Recovery on Clayey Sandstone: Experimental Study*. 9.
- Cosgrove, T., & Cosgrove, P. T. (2010). *Colloid Science: Principles, Methods and Applications*. John Wiley & Sons, Incorporated. <http://ebookcentral.proquest.com/lib/curtin/detail.action?docID=487733>
- Daghlian Sofla, S. J., Sharifi, M., & Hemmati Sarapardeh, A. (2016). Toward mechanistic understanding of natural surfactant flooding in enhanced oil recovery processes: The role of salinity, surfactant concentration and rock type. *Journal of Molecular Liquids*, 222, 632–639. <https://doi.org/10.1016/j.molliq.2016.07.086>
- Dehaghani, A. H. S., & Daneshfar, R. (2019). How much would silica nanoparticles enhance the performance of low-salinity water flooding? *Petroleum Science*, 16(3), 591–605. <https://doi.org/10.1007/s12182-019-0304-z>
- Denney, D. (2011). Nanosized Particles for Enhanced Oil Recovery. *Journal of Petroleum Technology*, 63(01), 54–56. <https://doi.org/10.2118/0111-0054-JPT>
- Derkani, M., Fletcher, A., Abdallah, W., Sauerer, B., Anderson, J., & Zhang, Z. (2018). Low Salinity Waterflooding in Carbonate Reservoirs: Review of Interfacial Mechanisms. *Colloids and Interfaces*, 2(2), 20. <https://doi.org/10.3390/colloids2020020>
- Deymeh, H., Shadizadeh, S. R., & Motafakkerfard, R. (2012). Experimental investigation of *Seidlitzia rosmarinus* effect on oil–water interfacial tension: Usable for chemical enhanced oil recovery. *Scientia Iranica*, 19(6), 1661–1664. <https://doi.org/10.1016/j.scient.2012.04.020>
- Ding, H., & Rahman, S. (2017). Experimental and theoretical study of wettability alteration during low salinity water flooding-an state of the art review. *Colloids and Surfaces A: Physicochemical and Engineering Aspects*, 520, 622–639. <https://doi.org/10.1016/j.colsurfa.2017.02.006>
- Divandari, H., Hemmati-Sarapardeh, A., Schaffie, M., & Ranjbar, M. (2020). Integrating functionalized magnetite nanoparticles with low salinity water

- and surfactant solution: Interfacial tension study. *Fuel*, 281, 118641. <https://doi.org/10.1016/j.fuel.2020.118641>
- Donath, A., Kantzas, A., & Bryant, S. (2019). Opportunities for Particles and Particle Suspensions to Experience Enhanced Transport in Porous Media: A Review. *Transport in Porous Media*, 128(2), 459–509. <https://doi.org/10.1007/s11242-019-01256-4>
- Du, M., Huang, S., Zhang, J., Wang, J., Hu, L., & Jiang, J. (2014). Isolation of total saponins from *Sapindus mukorossi* Gaertn. *Open Journal of Forestry*, 04(01), 24–27. <https://doi.org/10.4236/ojf.2014.41004>
- Ebaga-Ololo, J., & Chon, B. H. (2018). Experimental investigation of the influence of salinity gradient on low-concentration surfactant flooding in Berea sandstone. *Journal of Industrial and Engineering Chemistry*, 68, 355–363. <https://doi.org/10.1016/j.jiec.2018.08.007>
- Ebrahim, T., Mohsen, V. S., Mahdi, S. M., Esmaeel, K. T., & Saeb, A. (2019). Performance of low-salinity water flooding for enhanced oil recovery improved by SiO₂ nanoparticles. *Petroleum Science*, 16(2), 357–365. <https://doi.org/10.1007/s12182-018-0295-1>
- El Barky, A. R. (2020). Isolation, Characterization and the Biological Activity of Some Natural Components of Marine Sea Cucumber and Orange Peel. *Biomedical Journal of Scientific & Technical Research*, 27(2). <https://doi.org/10.26717/BJSTR.2020.27.004463>
- Elakneswaran, Y., Takeya, M., Ubaidah, A., Shimokawara, M., Okano, H., & Nawa, T. (2020, January 13). *Integrated Geochemical Modelling of Low Salinity Waterflooding for Enhanced Oil Recovery in Carbonate Reservoir*. International Petroleum Technology Conference. <https://doi.org/10.2523/IPTC-20250-MS>
- Esfandyari Bayat, A., Junin, R., Samsuri, A., Piroozian, A., & Hokmabadi, M. (2014). Impact of Metal Oxide Nanoparticles on Enhanced Oil Recovery from Limestone Media at Several Temperatures. *Energy & Fuels*, 28(10), 6255–6266. <https://doi.org/10.1021/ef5013616>
- Esmaeili, S., & Maaref, S. (2019). Investigating the effect of transient flow behavior from HSW to LSW on oil recovery in low-salinity water flooding simulation. *Journal of Petroleum Exploration and Production Technology*, 9(2), 1495–1515. <https://doi.org/10.1007/s13202-018-0561-1>
- Farajzadeh, R., Krastev, R., Zithat, P.L.J. (2008). Foam films stabilized with alpha olefin sulfonate (AOS). *Colloids and Surfaces A: Physicochemical and Engineering Aspects*, 324, 35–40. <https://doi.org/10.1016/j.colsurfa.2008.03.024>
- Fan, Z., Deng, Z., Wang, T., Yang, W., & Wang, K. (2018). Synthesis of Natural Tea-Saponin-Based Succinic Acid Sulfonate as Anionic Foaming Agent. *Journal of Surfactants and Detergents*, 21(3), 303–312. <https://doi.org/10.1002/jsde.12027>
- Flaaten, A., Nguyen, Q. P., Pope, G. A., & Zhang, J. (2008, January 1). *A Systematic Laboratory Approach to Low-Cost, High-Performance Chemical Flooding*. SPE Symposium on Improved Oil Recovery. <https://doi.org/10.2118/113469-MS>
- Fredriksen, S. B., Rognmo, A. U., & Fernø, M. A. (2018). Pore-scale mechanisms during low salinity waterflooding: Oil mobilization by diffusion and osmosis.

- Journal of Petroleum Science and Engineering*, 163, 650–660. <https://doi.org/10.1016/j.petrol.2017.10.022>
- Gbadamosi, A. O., Junin, R., Manan, M. A., Agi, A., & Yusuff, A. S. (2019). An overview of chemical enhanced oil recovery: Recent advances and prospects. *International Nano Letters*, 9(3), 171–202. <https://doi.org/10.1007/s40089-019-0272-8>
- Giribabu, K., Reddy, M. L. N., & Ghosh, P. (2007). COALESCENCE OF AIR BUBBLES IN SURFACTANT SOLUTIONS: ROLE OF SALTS CONTAINING MONO-, DI-, AND TRIVALENT IONS. *Chemical Engineering Communications*, 195(3), 336–351. <https://doi.org/10.1080/00986440701555316>
- Green, D. W., Hirasaki, G. J., & Pope, G. A. (2010). *Surfactant Flooding*. Society of Petroleum Engineers. <http://ebookcentral.proquest.com/lib/curtin/detail.action?docID=3405005>
- Green, D. W. & Willhite, G. P. (2018). *Enhanced Oil Recovery, Second Edition*. <https://store.spe.org/Enhanced-Oil-Recovery-Second-Edition-P1076.aspx>
- Gundewadi, G., Sarkar, D. J., Rudra, S. G., & Singh, D. (2018). Preparation of basil oil nanoemulsion using Sapindus mukorossi pericarp extract: Physico-chemical properties and antifungal activity against food spoilage pathogens. *Industrial Crops and Products*, 125, 95–104. <https://doi.org/10.1016/j.indcrop.2018.08.076>
- Guru, S., Bajpai, A. K., & Amritphale, S. S. (2020). Influence of nature of surfactant and precursor salt anion on the microwave assisted synthesis of barium carbonate nanoparticles. *Materials Chemistry and Physics*, 241, 122377. <https://doi.org/10.1016/j.matchemphys.2019.122377>
- Gundewadi, G., Sarkar, D. J., Rudra, S. G., & Singh, D. (2018). Preparation of basil oil nanoemulsion using Sapindus mukorossi pericarp extract: Physico-chemical properties and antifungal activity against food spoilage pathogens. *Industrial Crops and Products*, 125, 95–104. <https://doi.org/10.1016/j.indcrop.2018.08.076>
- Guzmán, E., Llamas, S., Fernández-Peña, L., Leónforte, F., Baghdadli, N., Cazeneuve, C., Ortega, F., Rubio, R. G., & Luengo, G. S. (2020). Effect of a natural amphoteric surfactant in the bulk and adsorption behavior of polyelectrolyte-surfactant mixtures. *Colloids and Surfaces A: Physicochemical and Engineering Aspects*, 585, 124178. <https://doi.org/10.1016/j.colsurfa.2019.124178>
- Haagh, M. E. J., Siretanu, I., Duits, M. H. G., & Mugele, F. (2017). Salinity-Dependent Contact Angle Alteration in Oil/Brine/Silicate Systems: The Critical Role of Divalent Cations. *Langmuir*, 33(14), 3349–3357. <https://doi.org/10.1021/acs.langmuir.6b04470>
- Hadian Nasr, N., Mahmood, S. M., Akbari, S., & Hematpur, H. (2020). A comparison of foam stability at varying salinities and surfactant concentrations using bulk foam tests and sandpack flooding. *Journal of Petroleum Exploration and Production Technology*, 10(2), 271–282. <https://doi.org/10.1007/s13202-019-0707-9>
- Haghighi, O., Zargar, G., Khaksar Manshad, A., Ali, M., Takassi, M., Ali, J., & Keshavarz, A. (2020). Effect of Environment-Friendly Non-Ionic Surfactant on Interfacial Tension Reduction and Wettability Alteration; Implications for

- Enhanced Oil Recovery. *Energies*, 13(15), 3988. <https://doi.org/10.3390/en13153988>
- Harikrishnan, A. R., Dhar, P., Agnihotri, P. K., & Gedupudi, S. (2017). *Effects of interplay of nanoparticles, surfactants and base fluid on the interfacial tension of nanocolloids*. 31.
- Hashemi, R., Nassar, N. N., & Pereira Almaso, P. (2014). Nanoparticle technology for heavy oil in-situ upgrading and recovery enhancement: Opportunities and challenges. *Applied Energy*, 133, 374–387. <https://doi.org/10.1016/j.apenergy.2014.07.069>
- Hashemi, R., Nassar, N. N., & Pereira-Almaso, P. (2012). Transport Behavior of Multimetallic Ultradispersed Nanoparticles in an Oil-Sands-Packed Bed Column at a High Temperature and Pressure. *Energy & Fuels*, 26(3), 1645–1655. <https://doi.org/10.1021/ef201939f>
- He, K., Nguyen, C., Kothamasu, R., & Xu, L. (2015). Insights into Whether Low Salinity Brine Enhances Oil Production in Liquids-rich Shale Formations. *EUROPEC 2015*. EUROPEC 2015, Madrid, Spain. <https://doi.org/10.2118/174362-MS>
- Hendraningrat, L., Li, S., & Torsæter, O. (2013, July 2). *Enhancing Oil Recovery of Low-Permeability Berea Sandstone through Optimised Nanofluids Concentration*. SPE Enhanced Oil Recovery Conference. <https://doi.org/10.2118/165283-MS>
- Hendraningrat, L., & Torsæter, O. (2015). Metal oxide-based nanoparticles: Revealing their potential to enhance oil recovery in different wettability systems. *Applied Nanoscience*, 5(2), 181–199. <https://doi.org/10.1007/s13204-014-0305-6>
- Hiemenz, P. C., Rajagopalan, R., & Rajagopalan, R. (2016). *Principles of Colloid and Surface Chemistry, Revised and Expanded*. CRC Press. <https://doi.org/10.1201/9781315274287>
- Hilner, E., Andersson, M. P., Hassenkam, T., Matthiesen, J., Salino, P. A., & Stipp, S. L. S. (2015). The effect of ionic strength on oil adhesion in sandstone – the search for the low salinity mechanism. *Scientific Reports*, 5(1), 9933. <https://doi.org/10.1038/srep09933>
- Hlawacek, G., Ahmad, I., Smithers, M. A., & Kooij, E. S. (2013). To see or not to see: Imaging surfactant coated nano-particles using HIM and SEM. *Ultramicroscopy*, 135, 89–94. <https://doi.org/10.1016/j.ultramic.2013.07.010>
- Hosseini, E., Hajivand, F., & Yaghodous, A. (2018). Experimental investigation of EOR using low-salinity water and nanoparticles in one of southern oil fields in Iran. *Energy Sources, Part A: Recovery, Utilization, and Environmental Effects*, 40(16), 1974–1982. <https://doi.org/10.1080/15567036.2018.1486923>
- Hosseini, S., Sabet, M., Zeinolabedini Hezave, A., A. Ayoub, M., & Elraies, K. A. (2020). Effect of combination of cationic surfactant and salts on wettability alteration of carbonate rock. *Energy Sources, Part A: Recovery, Utilization, and Environmental Effects*, 1–17. <https://doi.org/10.1080/15567036.2020.1778141>
- Hosseinzade Khanamiri, H., Torsæter, O., & Stensen, J. Å. (2016). Effect of Calcium in Pore Scale Oil Trapping by Low-Salinity Water and Surfactant Enhanced Oil

- Recovery at Strongly Water-Wet Conditions: In Situ Imaging by X-ray Microtomography. *Energy & Fuels*, 30(10), 8114–8124. <https://doi.org/10.1021/acs.energyfuels.6b01236>
- Hou, B., Wang, Y., & Huang, Y. (2015). Mechanistic study of wettability alteration of oil-wet sandstone surface using different surfactants. *Applied Surface Science*, 330, 56–64. <https://doi.org/10.1016/j.apsusc.2014.12.185>
- Huibers, B. M. J., Pales, A. R., Bai, L., Li, C., Mu, L., Ladner, D., Daigle, H., & Darnault, C. J. G. (2017). Wettability alteration of sandstones by silica nanoparticle dispersions in light and heavy crude oil. *Journal of Nanoparticle Research*, 19(9), 323. <https://doi.org/10.1007/s11051-017-4011-7>
- Issaoui, R., & Ben Mansour, L. (2019). Experimental study of temperature effects on bubble characteristics and gas holdup in electroflotation column. *DESALINATION AND WATER TREATMENT*, 162, 186–192. <https://doi.org/10.5004/dwt.2019.24407>
- Jalal, T. S., & Bodger, P. (2009). National Energy Policies and the electricity sector in Malaysia. *2009 3rd International Conference on Energy and Environment (ICEE)*, 385–392. <https://doi.org/10.1109/ICEENVIRON.2009.5398618>
- Jalali, A., Mohsenatabar Firozjahi, A., & Shadizadeh, S. R. (2019). Experimental investigation on new derived natural surfactant: Wettability alteration, IFT reduction, and core flooding in oil wet carbonate reservoir. *Energy Sources, Part A: Recovery, Utilization, and Environmental Effects*, 1–11. <https://doi.org/10.1080/15567036.2019.1670285>
- Jalil, R. R., & Hussein, H. (2019). Influence of Nano Fluid on Interfacial Tension oil/water and Wettability Alteration of limestone. *IOP Conference Series: Materials Science and Engineering*, 518(6), 062004. <https://doi.org/10.1088/1757-899X/518/6/062004>
- Jassal, V., Shanker, U., Gahlot, S., Kaith, B. S., Kamaluddin, Iqbal, M. A., & Samuel, P. (2016). Sapindus mukorossi mediated green synthesis of some manganese oxide nanoparticles interaction with aromatic amines. *Applied Physics A*, 122(4), 271. <https://doi.org/10.1007/s00339-016-9777-4>
- Jauhari, S., Parekh, K., & Upadhyay, R. V. (2011, January 1). *Corrosion Inhibition Of Mild Steel In Acidic Media Using A Nanomagnetic Fluid As A Novel Corrosion Inhibitor*. CORROSION 2011.
- Jha, N. K., Iglauer, S., Barifcani, A., Sarmadivaleh, M., & Sangwai, J. S. (2019). Low-Salinity Surfactant Nanofluid Formulations for Wettability Alteration of Sandstone: Role of the SiO₂ Nanoparticle Concentration and Divalent Cation/SO₄²⁻ Ratio. *Energy & Fuels*, 33(2), 739–746. <https://doi.org/10.1021/acs.energyfuels.8b03406>
- Jiang, X., Liu, M., Li, X., Wang, L., Liang, S., & Guo, X. (2021). Effects of Surfactant and Hydrophobic Nanoparticles on the Crude Oil-Water Interfacial Tension. *Energies*, 14(19), 6234. <https://doi.org/10.3390/en14196234>
- Jin, J., Li, X., Geng, J., & Jing, D. (2018). Insights into the complex interaction between hydrophilic nanoparticles and ionic surfactants at the liquid/air interface. *Physical Chemistry Chemical Physics*, 20(22), 15223–15235. <https://doi.org/10.1039/C8CP01838C>
- Jones, S. A., Laskaris, G., Vincent-Bonnieu, S., Farajzadeh, R., & Rossen, W. R. (2016). Effect of surfactant concentration on foam: From coreflood experiments to

- implicit-texture foam-model parameters. *Journal of Industrial and Engineering Chemistry*, 37, 268–276. <https://doi.org/10.1016/j.jiec.2016.03.041>
- Ju, B., Fan, T., & Li, Z. (2012). Improving water injectivity and enhancing oil recovery by wettability control using nanopowders. *Journal of Petroleum Science and Engineering*, 86–87, 206–216. <https://doi.org/10.1016/j.petrol.2012.03.022>
- Jun, Y., Choi, J., & Cheon, J. (2007). Heterostructured magnetic nanoparticles: Their versatility and high performance capabilities. *Chemical Communications*, 12, 1203–1214. <https://doi.org/10.1039/B614735F>
- Kaczerewska, O., Martins, R., Figueiredo, J., Loureiro, S., & Tedim, J. (2020). Environmental behaviour and ecotoxicity of cationic surfactants towards marine organisms. *Journal of Hazardous Materials*, 392, 122299. <https://doi.org/10.1016/j.jhazmat.2020.122299>
- Kakati, A., & Sangwai, J. S. (2018). Wettability Alteration of Mineral Surface during Low-Salinity Water Flooding: Role of Salt Type, Pure Alkanes, and Model Oils Containing Polar Components. *Energy & Fuels*, 32(3), 3127–3137. <https://doi.org/10.1021/acs.energyfuels.7b03727>
- Kalam, S., Abu-Khamsin, S. A., Kamal, M. S., & Patil, S. (2021). Surfactant Adsorption Isotherms: A Review. *ACS Omega*, 6(48), 32342–32348. <https://doi.org/10.1021/acsomega.1c04661>
- Kamal, M. S., Hussein, I. A., & Sultan, A. S. (2017). Review on Surfactant Flooding: Phase Behavior, Retention, IFT, and Field Applications. *Energy & Fuels*, 31(8), 7701–7720. <https://doi.org/10.1021/acs.energyfuels.7b00353>
- Katende, A., & Sagala, F. (2019). A critical review of low salinity water flooding: Mechanism, laboratory and field application. *Journal of Molecular Liquids*, 278, 627–649. <https://doi.org/10.1016/j.molliq.2019.01.037>
- Kawale, D. (2012). *Influence of dynamic surface tension on foams: Application in gas well deliquification*. <https://doi.org/10.13140/RG.2.1.1539.2241>
- Kazemzadeh, Y., Shojaei, S., Riazi, M., & Sharifi, M. (2019). Review on application of nanoparticles for EOR purposes: A critical review of the opportunities and challenges. *Chinese Journal of Chemical Engineering*, 27(2), 237–246. <https://doi.org/10.1016/j.cjche.2018.05.022>
- Kedir, A. S., Solbakken, J. S., & Aarra, M. G. (2022). Foamability and stability of anionic surfactant-anionic polymer solutions: Influence of ionic strength, polymer concentration, and molecular weight. *Colloids and Surfaces A: Physicochemical and Engineering Aspects*, 632, 127801. <https://doi.org/10.1016/j.colsurfa.2021.127801>
- Khalafi, E., Hashemi, A., Zallaghi, M., & Kharrat, R. (2018). An Experimental Investigation of Nanoparticles Assisted Surfactant Flooding for Improving Oil Recovery in a Micromodel System. *Journal of Petroleum & Environmental Biotechnology*, 09(01). <https://doi.org/10.4172/2157-7463.1000355>
- Khayati, H. (2020). An experimental investigation on the use of saponin as a non-ionic surfactant for chemical enhanced oil recovery (EOR) in sandstone and carbonate oil reservoirs: IFT, wettability alteration, and oil recovery. *Chemical Engineering Research and Design*, 9.
- Khorram Ghahfarokhi, A., Dadashi, A., Daryasafar, A., & Moghadasi, J. (2015). Feasibility study of new natural leaf-derived surfactants on the IFT in an oil–

- aqueous system: Experimental investigation. *Journal of Petroleum Exploration and Production Technology*, 5(4), 375–382. <https://doi.org/10.1007/s13202-015-0158-x>
- Kia, S. F. (1987). Effect of Salt Composition on Clay Release in Berea Sandstones. *Society of Petroleum Engineers*, 10.
- Kia, S. F., Fogler, H. S., & Reed, M. G. (1987). Effect of pH on colloiddally induced fines migration. *Journal of Colloid and Interface Science*, 118(1), 158–168. [https://doi.org/10.1016/0021-9797\(87\)90444-9](https://doi.org/10.1016/0021-9797(87)90444-9)
- Köse, M. D., & Bayraktar, O. (2016). *Extraction of Saponins from Soapnut (Sapindus Mukorossi) and Their Antimicrobial Properties*. 2(5), 6.
- Kronberg, B., Holmberg, K., & Lindman, B. (2014). *Surface Chemistry of Surfactants and Polymers*. John Wiley & Sons, Incorporated. <http://ebookcentral.proquest.com/lib/curtin/detail.action?docID=1791862>
- Kumar, A., & Mandal, A. (2017). Synthesis and physiochemical characterization of zwitterionic surfactant for application in enhanced oil recovery. *Journal of Molecular Liquids*, 243, 61–71. <https://doi.org/10.1016/j.molliq.2017.08.032>
- Kumar, A., & Mandal, A. (2019). Critical investigation of zwitterionic surfactant for enhanced oil recovery from both sandstone and carbonate reservoirs: Adsorption, wettability alteration and imbibition studies. *Chemical Engineering Science*, 209, 115222. <https://doi.org/10.1016/j.ces.2019.115222>
- Kundu, P. K., Cohen, I. M., & Dowling, D. R. (2011). *Fluid Mechanics*. Elsevier Science & Technology. <http://ebookcentral.proquest.com/lib/curtin/detail.action?docID=802513>
- Lager, A., Webb, K. J., Black, C. J. J., Singleton, M., & Sorbie, K. S. (2008). *Low Salinity Oil Recovery—An Experimental Investigation*. 8.
- Lashkarbolooki, M., Ayatollahi, S., & Riazi, M. (2014). The Impacts of Aqueous Ions on Interfacial Tension and Wettability of an Asphaltenic–Acidic Crude Oil Reservoir during Smart Water Injection. *Journal of Chemical & Engineering Data*, 59(11), 3624–3634. <https://doi.org/10.1021/je500730e>
- Lashkarbolooki, M., Ayatollahi, S., & Riazi, M. (2017). Mechanistical study of effect of ions in smart water injection into carbonate oil reservoir. *Process Safety and Environmental Protection*, 105, 361–372. <https://doi.org/10.1016/j.psep.2016.11.022>
- Lee, J. H., & Lee, K. S. (2019). Geochemical evaluation of low salinity hot water injection to enhance heavy oil recovery from carbonate reservoirs. *Petroleum Science*, 16(2), 366–381. <https://doi.org/10.1007/s12182-018-0274-6>
- Lee, S. Y., Webb, K. J., Collins, I., Lager, A., Clarke, S., O’apos, Sullivan, M., Routh, A., & Wang, X. (2010, January 1). *Low Salinity Oil Recovery: Increasing Understanding of the Underlying Mechanisms*. SPE Improved Oil Recovery Symposium. <https://doi.org/10.2118/129722-MS>
- Lee, K. S., & Lee, J. H. (2019). Chapter 2—Mechanisms of Low-Salinity and Smart Waterflood. In K. S. Lee & J. H. Lee (Eds.), *Hybrid Enhanced Oil Recovery using Smart Waterflooding* (pp. 27–37). Gulf Professional Publishing. <https://doi.org/10.1016/B978-0-12-816776-2.00002-7>

- Li, K., Wang, D., & Jiang, S. (2018). Review on enhanced oil recovery by nanofluids. *Oil & Gas Science and Technology – Revue d'IFP Energies Nouvelles*, 73, 37. <https://doi.org/10.2516/ogst/2018025>
- Li, S., Hadia, N. J., Lau, H. C., Torsæter, O., Stubbs, L. P., & Ng, Q. H. (2018). Silica Nanoparticles Suspension for Enhanced Oil Recovery: Stability Behavior and Flow Visualization. *SPE Europec Featured at 80th EAGE Conference and Exhibition*. SPE Europec featured at 80th EAGE Conference and Exhibition, Copenhagen, Denmark. <https://doi.org/10.2118/190802-MS>
- Li, W., Nan, Y., You, Q., Xie, Q., & Jin, Z. (2020). Effects of salts and silica nanoparticles on oil-brine interfacial properties under hydrocarbon reservoir conditions: A molecular dynamics simulation study. *Journal of Molecular Liquids*, 305, 112860. <https://doi.org/10.1016/j.molliq.2020.112860>
- Liu, J., Zhong, L., Zewen, Y., Liu, Y., Meng, X., Zhang, W., Zhang, H., Yang, G., & Shaojie, W. (2022). High-efficiency emulsification anionic surfactant for enhancing heavy oil recovery. *Colloids and Surfaces A: Physicochemical and Engineering Aspects*, 642, 128654. <https://doi.org/10.1016/j.colsurfa.2022.128654>
- Liang, S., Fang, T., Xiong, W., Ding, B., Yan, Y., & Zhang, J. (2019). Oil detachment by modified nanoparticles: A molecular dynamics simulation study. *Computational Materials Science*, 170, 109177. <https://doi.org/10.1016/j.commatsci.2019.109177>
- Lin, F., Ng, J. K., Huang, Y., Huang, C., & Zeng, H. (2021). Formation and stability of oil-laden foam: Effect of surfactant and hydrocarbon solvent. *The Canadian Journal of Chemical Engineering*, 99(12), 2658–2669. <https://doi.org/10.1002/cjce.24148>
- Luan, F., Zeng, J., Yang, Y., He, X., Wang, B., Gao, Y., & Zeng, N. (2020). Recent advances in *Camellia oleifera* Abel: A review of nutritional constituents, biofunctional properties, and potential industrial applications. *Journal of Functional Foods*, 75, 104242. <https://doi.org/10.1016/j.jff.2020.104242>
- Luan, H., Gong, L., Yue, X., Nie, X., Chen, Q., Guan, D., Que, T., Liao, G., Su, X., & Feng, Y. (2019). Micellar Aggregation Behavior of Alkylaryl Sulfonate Surfactants for Enhanced Oil Recovery. *Molecules*, 24(23), 4325. <https://doi.org/10.3390/molecules24234325>
- Ma, H., Luo, M., & Dai, L. L. (2008). Influences of surfactant and nanoparticle assembly on effective interfacial tensions. *Physical Chemistry Chemical Physics*, 10(16), 2207. <https://doi.org/10.1039/b718427c>
- Maestro, A., Guzmán, E., Santini, E., Ravera, F., Liggieri, L., Ortega, F., & Rubio, R. G. (2012). Wettability of silicananoparticle–surfactant nanocomposite interfacial layers. *Soft Matter*, 8(3), 837–843. <https://doi.org/10.1039/C1SM06421E>
- Mahdavi, S. Z., Aalaie, J., Miri, T., Razavi, S. M. R., & Rahmani, M. R. (2017). Study of polyacrylamide-surfactant system on the water–oil interface properties and rheological properties for EOR. *Arabian Journal of Chemistry*, 10(8), 1136–1146. <https://doi.org/10.1016/j.arabjc.2016.05.006>
- Majeed, T., Sølling, T. I., & Kamal, M. S. (2020). Foamstability: The interplay between salt-, surfactant- and critical micelle concentration. *Journal of*

- Petroleum Science and Engineering*, 187, 106871. <https://doi.org/10.1016/j.petrol.2019.106871>
- Marčelja, S. (2006). Selective Coalescence of Bubbles in Simple Electrolytes. *The Journal of Physical Chemistry B*, 110(26), 13062–13067. <https://doi.org/10.1021/jp0610158>
- Marinova, K. G., Basheva, E. S., Nenova, B., Temelska, M., Mirarefi, A. Y., Campbell, B., & Ivanov, I. B. (2009). Physico-chemical factors controlling the foamability and foam stability of milk proteins: Sodium caseinate and whey protein concentrates. *Food Hydrocolloids*, 23(7), 1864–1876. <https://doi.org/10.1016/j.foodhyd.2009.03.003>
- Martin, J. C. (1959, January 1). *The Effects of Clay on the Displacement of Heavy Oil by Water*. Venezuelan Annual Meeting. <https://doi.org/10.2118/1411-G>
- Massarweh, O., & Abushaikha, A. S. (2020). The use of surfactants in enhanced oil recovery: A review of recent advances. *Energy Reports*, 6, 3150–3178. <https://doi.org/10.1016/j.egyr.2020.11.009>
- Mathiarasi, R., Mugesha kanna, C., & Partha, N. (2017). Transesterification of soap nut oil using novel catalyst. *Journal of Saudi Chemical Society*, 21(1), 11–17. <https://doi.org/10.1016/j.jscs.2013.07.006>
- Mcelfresh, P. M., Holcomb, D. L., & Ector, D. (2012). Application of Nanofluid Technology to Improve Recovery in Oil and Gas Wells. *SPE International Oilfield Nanotechnology Conference and Exhibition*. SPE International Oilfield Nanotechnology Conference and Exhibition, Noordwijk, The Netherlands. <https://doi.org/10.2118/154827-MS>
- McGuire, P. L., Chatham, J. R., Paskvan, F. K., Sommer, D. M., Carini, F. H., & Exploration, B. (2005). Low Salinity Oil Recovery: An exciting new EOR Opportunity for Alaska's North Slope. *Society of Petroleum Engineers*, 15.
- Mehana, M., & Fahes, M. M. (2018). Investigation of Double Layer Expansion in Low-Salinity Waterflooding: Molecular Simulation Study. *SPE Western Regional Meeting*. SPE Western Regional Meeting, Garden Grove, California, USA. <https://doi.org/10.2118/190106-MS>
- Mofrad, S. K., & Saeedi Dehaghani, A. H. (2020). An experimental investigation into enhancing oil recovery using smart water combined with anionic and cationic surfactants in carbonate reservoir. *Energy Reports*, 6, 543–549. <https://doi.org/10.1016/j.egyr.2020.02.034>
- Mohajeri, M., Reza Rasaei, M., & Hekmatzadeh, M. (2019). Experimental study on using SiO₂ nanoparticles along with surfactant in an EOR process in micromodel. *Petroleum Research*, 4(1), 59–70. <https://doi.org/10.1016/j.ptlrs.2018.09.001>
- Mohanty, S., & Mukherji, S. (2013). Surfactant aided biodegradation of NAPLs by Burkholderia multivorans: Comparison between Triton X-100 and rhamnolipid JBR-515. *Colloids and Surfaces B: Biointerfaces*, 102, 644–652. <https://doi.org/10.1016/j.colsurfb.2012.08.064>
- Mokhtari, R., Ayatollahi, S., & Fatemi, M. (2019). Experimental investigation of the influence of fluid-fluid interactions on oil recovery during low salinity water flooding. *Journal of Petroleum Science and Engineering*, 182, 106194. <https://doi.org/10.1016/j.petrol.2019.106194>

- Moradi, S., Isari, A. A., Bachari, Z., & Mahmoodi, H. (2019). Combination of a new natural surfactant and smart water injection for enhanced oil recovery in carbonate rock: Synergic impacts of active ions and natural surfactant concentration. *Journal of Petroleum Science and Engineering*, 176, 1–10. <https://doi.org/10.1016/j.petrol.2019.01.043>
- Morrow, L., Potter, D. K., & Barron, A. R. (2015). Detection of magnetic nanoparticles against proppant and shale reservoir rocks. *Journal of Experimental Nanoscience*, 10(13), 1028–1041. <https://doi.org/10.1080/17458080.2014.951412>
- Morrow, N., & Buckley, J. (2011). *Improved Oil Recovery by Low-Salinity Waterflooding*. 7.
- Moslemizadeh, A., Khayati, H., Madani, M., Ghasemi, M., Shahbazi, K., Zendehboudi, S., & Hashim Abbas, A. (2021). A Systematic Study to Assess Displacement Performance of a Naturally-Derived Surfactant in Flow Porous Systems. *Energies*, 14(24), 8310. <https://doi.org/10.3390/en14248310>
- Mousavi Moghadam, A., & Baghban Salehi, M. (2019). Enhancing hydrocarbon productivity via wettability alteration: A review on the application of nanoparticles. *Reviews in Chemical Engineering*, 35(4), 531–563. <https://doi.org/10.1515/revce-2017-0105>
- Muggeridge, A., Cockin, A., Webb, K., Frampton, H., Collins, I., Moulds, T., & Salino, P. (2014). Recovery rates, enhanced oil recovery and technological limits. *Philosophical Transactions. Series A, Mathematical, Physical, and Engineering Sciences*, 372(2006). <https://doi.org/10.1098/rsta.2012.0320>
- Muneesawang, P., & Sirisathitkul, C. (2015). Size Measurement of Nanoparticle Assembly Using Multilevel Segmented TEM Images. *Journal of Nanomaterials*, 2015, 1–8. <https://doi.org/10.1155/2015/790508>
- Muntaha, S.-T., & Khan, M. N. (2015). Natural surfactant extracted from *Sapindus mukurossi* as an eco-friendly alternate to synthetic surfactant – a dye surfactant interaction study. *Journal of Cleaner Production*, 93, 145–150. <https://doi.org/10.1016/j.jclepro.2015.01.023>
- Murugesan, S., Monteiro, O. R., & Khabashesku, V. N. (2016, May 2). Extending the Lifetime of Oil and Gas Equipment with Corrosion and Erosion-Resistant Ni-B-Nanodiamond Metal-Matrix-Nanocomposite Coatings. *Offshore Technology Conference*. <https://doi.org/10.4043/26934-MS>
- Mustan, F., Politova-Brinkova, N., Rossetti, D., Rayment, P., & Tcholakova, S. (2022)(a). Oil soluble surfactants as efficient foam stabilizers. *Colloids and Surfaces A: Physicochemical and Engineering Aspects*, 633, 127874. <https://doi.org/10.1016/j.colsurfa.2021.127874>
- Mustan, F., Politova-Brinkova, N., Vinarov, Z., Rossetti, D., Rayment, P., & Tcholakova, S. (2022)(b). Interplay between bulk aggregates, surface properties and foam stability of nonionic surfactants. *Advances in Colloid and Interface Science*, 302:102618. <https://doi.org/10.1016/j.cis.2022.102618>
- Nadia Ariani. (2018). Data analysis of low-salinity waterflooding to enhance the oil recovery in sandstone reservoirs. *Masters Theses*. 7752. https://scholarsmine.mst.edu/masters_theses/7752

- Nasralla, R. A., & Nasr-El-Din, H. A. (2014). Double-Layer Expansion: Is It a Primary Mechanism of Improved Oil Recovery by Low-Salinity Waterflooding? *SPE Reservoir Evaluation & Engineering* 17 (01): 49–59.
- Nassabeh, S. M. M., Davarpanah, A., & Bayrami, J. (2019). Simulation of low and high salinity water injection method to determine the optimum salinity. *Petroleum Research*, 4(4), 348–353. <https://doi.org/10.1016/j.ptlrs.2019.07.003>
- Negin, C., Ali, S., & Xie, Q. (2016). Application of nanotechnology for enhancing oil recovery – A review. *Petroleum*, 2(4), 324–333. <https://doi.org/10.1016/j.petlm.2016.10.002>
- Negin, C., Ali, S., & Xie, Q. (2017). Most common surfactants employed in chemical enhanced oil recovery. *Petroleum*, 3(2), 197–211. <https://doi.org/10.1016/j.petlm.2016.11.007>
- Nesměrák, K., & Němcová, I. (2006). Determination of Critical Micelle Concentration by Electrochemical Means. *Analytical Letters*, 39(6), 1023–1040. <https://doi.org/10.1080/00032710600620302>
- Neumann, A. W., David, R., Zuo, Y., & Zuo, Y. (2010). *Applied Surface Thermodynamics*. CRC Press LLC. <http://ebookcentral.proquest.com/lib/curtin/detail.action?docID=589921>
- Nikolov, A., Kondiparty, K., & Wasan, D. (2010). Nanoparticle Self-Structuring in a Nanofluid Film Spreading on a Solid Surface. *Langmuir*, 26(11), 7665–7670. <https://doi.org/10.1021/la100928t>
- Nikolov, A., Wu, P., & Wasan, D. (2019). Structure and stability of nanofluid films wetting solids: An overview. *Advances in Colloid and Interface Science*, 264, 1–10. <https://doi.org/10.1016/j.cis.2018.12.001>
- Nourani, M., Tichelkamp, T., Hosseinzade Khanamiri, H., Johansen, T., Karlsen Hov, I., Gawel, B., Torsæter, O., & Øye, G. (2020). Dynamic wettability alteration for combined low salinity brine injection and surfactant flooding on silica surface. *SN Applied Sciences*, 2(7), 1274. <https://doi.org/10.1007/s42452-020-3094-4>
- Nowrouzi, I., Mohammadi, A. H., & Manshad, A. K. (2020). Water-oil interfacial tension (IFT) reduction and wettability alteration in surfactant flooding process using extracted saponin from *Anabasis Setifera* plant. *Journal of Petroleum Science and Engineering*, 189, 106901. <https://doi.org/10.1016/j.petrol.2019.106901>
- Nwidee, L. N., Lebedev, M., Barifcani, A., Sarmadivaleh, M., & Iglaue, S. (2017). Wettability alteration of oil-wet limestone using surfactant-nanoparticle formulation. *Journal of Colloid and Interface Science*, 504, 334–345. <https://doi.org/10.1016/j.jcis.2017.04.078>
- Obisesan, O., Ahmed, R., & Amani, M. (2021). The Effect of Salt on Stability of Aqueous Foams. *Energies*, 14(2), 279. <https://doi.org/10.3390/en14020279>
- Oetjen, K., Bilke-Krause, C., Madani, M., & Willers, T. (2014). Temperature effect on foamability, foam stability, and foam structure of milk. *Colloids and Surfaces A: Physicochemical and Engineering Aspects*, 460, 280–285. <https://doi.org/10.1016/j.colsurfa.014.01.086>
- Okunade, O. A., Yekeen, N., Padmanabhan, E., Al-Yaseri, A., Idris, A. K., & Khan, J. A. (2021). Shale core wettability alteration, foam and emulsion stabilization by

- surfactant: Impact of surfactant concentration, rock surface roughness and nanoparticles. *Journal of Petroleum Science and Engineering*, 207, 109139. <https://doi.org/10.1016/j.petrol.2021.109139>
- Olayiwola, S. O., & Dejam, M. (2019). A comprehensive review on interaction of nanoparticles with low salinity water and surfactant for enhanced oil recovery in sandstone and carbonate reservoirs. *Fuel*, 241, 1045–1057. <https://doi.org/10.1016/j.fuel.2018.12.122>
- Osama Al, A. B. (2015). Foamability and Foam Stability of Several Surfactants Solutions: The Role of Screening and Flooding. *Journal of Petroleum & Environmental Biotechnology*, 06(04). <https://doi.org/10.4172/2157-7463.1000227>
- Pal, N., & Mandal, A. (2020). Enhanced oil recovery performance of gemini surfactant-stabilized nanoemulsions functionalized with partially hydrolyzed polymer/silica nanoparticles. *Chemical Engineering Science*, 226, 115887. <https://doi.org/10.1016/j.ces.2020.115887>
- Pal, N., Saxena, N., & Mandal, A. (2018). Studies on the physicochemical properties of synthesized tailor-made gemini surfactants for application in enhanced oil recovery. *Journal of Molecular Liquids*, 258, 211–224. <https://doi.org/10.1016/j.molliq.2018.03.037>
- Parhizkar, M., Edirisinghe, M., & Stride, E. (2015). The effect of surfactant type and concentration on the size and stability of microbubbles produced in a capillary embedded T-junction device. *RSC Advances*, 5(14), 10751–10762. <https://doi.org/10.1039/C4RA15167D>
- Park, S., Lee, E. S., & Sulaiman, W. R. W. (2015). Adsorption behaviors of surfactants for chemical flooding in enhanced oil recovery. *Journal of Industrial and Engineering Chemistry*, 21, 1239–1245. <https://doi.org/10.1016/j.jiec.2014.05.040>
- Park, S.-J., & Seo, M.-K. (2011). Chapter 1—Intermolecular Force. In S.-J. Park & M.-K. Seo (Eds.), *Interface Science and Technology* (Vol. 18, pp. 1–57). Elsevier. <https://doi.org/10.1016/B978-0-12-375049-5.00001-3>
- Pasdar, M., Kazemzadeh, E., Kamari, E., Ghazanfari, M. H., & Soleymani, M. (2018). Monitoring the role of polymer and surfactant concentrations on bubble size distribution in colloidal gas aphron based fluids. *Colloids and Surfaces A: Physicochemical and Engineering Aspects*, 556, 93–98. <https://doi.org/10.1016/j.colsurfa.2018.08.020>
- Pastrana-Martínez, L. M., Pereira, N., Lima, R., Faria, J. L., Gomes, H. T., & Silva, A. M. T. (2015). Degradation of diphenhydramine by photo-Fenton using magnetically recoverable iron oxide nanoparticles as catalyst. *Chemical Engineering Journal*, 261, 45–52. <https://doi.org/10.1016/j.cej.2014.04.117>
- Paul, B. K., Moulik, S. P., & Kunz, W. (2015). *Ionic Liquid-Based Surfactant Science: Formulation, Characterization, and Applications*. John Wiley & Sons, Incorporated. <http://ebookcentral.proquest.com/lib/curtin/detail.action?docID=4039276>
- Peng, M., & Nguyen, A. V. (2020). Adsorption of ionic surfactants at the air-water interface: The gap between theory and experiment. *Advances in Colloid and Interface Science*, 275, 102052. <https://doi.org/10.1016/j.cis.2019.102052>

- Peng, M., Yang, Y., Sha, M., Fang, J., Zhang, D., Pan, R., & Jiang, B. (2021). Surface activity, wetting and foaming properties of amine-oxidized nonionic fluorocarbon surfactant and hydrocarbon anionic surfactants mixtures at low concentrations. *Journal of Molecular Liquids*, 343, 117701. <https://doi.org/10.1016/j.molliq.2021.117701>
- Petkova, B., Tcholakova, S., Chenkova, M., Golemanov, K., Denkov, N., Thorley, D., & Stoyanov, S. (2020). Foamability of aqueous solutions: Role of surfactant type and concentration. *Advances in Colloid and Interface Science*, 276, 102084. <https://doi.org/10.1016/j.cis.2019.102084>
- Petkova, B., Tcholakova, S., & Denkov, N. (2021). Foamability of surfactant solutions: Interplay between adsorption and hydrodynamic conditions. *Colloids and Surfaces A: Physicochemical and Engineering Aspects*, 626, 127009. <https://doi.org/10.1016/j.colsurfa.2021.127009>
- Petronas Carigali Sdn Bhd Miri Crude Oil Terminal. (2021). *Crude Oil Component Analysis Report*. Petroliaam Nasional Berhad
- Pichot, R., Spyropoulos, F., & Norton, I. T. (2012). Competitive adsorption of surfactants and hydrophilic silica particles at the oil–water interface: Interfacial tension and contact angle studies. *Journal of Colloid and Interface Science*, 377(1), 396–405. <https://doi.org/10.1016/j.jcis.2012.01.065>
- Pooryousefy, E., Xie, Q., Chen, Y., Sari, A., & Saeedi, A. (2018). Drivers of low salinity effect in sandstone reservoirs. *Journal of Molecular Liquids*, 250, 396–403. <https://doi.org/10.1016/j.molliq.2017.11.170>
- Pordel Shahri, M., Shadizadeh, S. R., & Jamialahmadi, M. (2012a). Applicability Test of New Surfactant Produced from Zizyphus Spina-Christi Leaves for Enhanced Oil Recovery in Carbonate Reservoirs. *Journal of the Japan Petroleum Institute*, 55(1), 27–32. <https://doi.org/10.1627/jpi.55.27>
- Pordel Shahri, M., Shadizadeh, S. R., & Jamialahmadi, M. (2012b). A New Type of Surfactant for Enhanced Oil Recovery. *Petroleum Science and Technology*, 30(6), 585–593. <https://doi.org/10.1080/10916466.2010.489093>
- Pouryousefy, E., Xie, Q., & Saeedi, A. (2016). Effect of multi-component ions exchange on low salinity EOR: Coupled geochemical simulation study. *Petroleum*, 2(3), 215–224. <https://doi.org/10.1016/j.petlm.2016.05.004>
- Prodanovic, M., & Johnston, K. P. (2017). *Development of Nanoparticle-Stabilized Foams to Improve Performance of Water-less Hydraulic Fracturing* (DOE-UT--FE0013723, 1427303; p. DOE-UT--FE0013723, 1427303). <https://doi.org/10.2172/1427303>
- Qi, Z., Han, M., Chen, S., & Wang, J. (2022). Surfactant enhanced imbibition in carbonate reservoirs: Effect of IFT reduction and surfactant partitioning. *JCIS Open*, 5, 100045. <https://doi.org/10.1016/j.jciso.2022.100045>
- Qian, C., Telmadarreie, A., Dong, M., & Bryant, S. (2020). Synergistic Effect between Surfactant and Nanoparticles on the Stability of Foam in EOR Processes. *SPE Journal*. <https://doi.org/10.2118/195310-PA>
- Qiao, C., Johns, R., & Li, L. (2016). Understanding the Chemical Mechanisms for Low Salinity Waterflooding. *Society of Petroleum Engineers*, 12.
- Rahmani, A. R., Bryant, S. L., Huh, C., Ahmadian, M., Zhang, W., & Liu, Q. H. (2015, February 23). *Characterizing Reservoir Heterogeneities Using Magnetic*

- Nanoparticles*. SPE Reservoir Simulation Symposium. <https://doi.org/10.2118/173195-MS>
- Rahmati, M., Mashayekhi, M., Songolzadeh, R., & Daryasafar, A. (2015). Effect of Natural Leaf-derived Surfactants on Wettability Alteration and Interfacial Tension Reduction in Water-oil System: EOR Application. *Journal of the Japan Petroleum Institute*, 58(4), 245–251. <https://doi.org/10.1627/jpi.58.245>
- Ramezanzpour, M., & Siavashi, M. (2019). Application of SiO₂–water nanofluid to enhance oil recovery. *Journal of Thermal Analysis and Calorimetry*, 135(1), 565–580. <https://doi.org/10.1007/s10973-018-7156-4>
- Ramly N. F., N. F. R., Ashqar A., A. A., Bakeri F. A., F. A. M. B., Dahlan N. A., N. A. M. D., Ling R. P., L. R. P., James S. M., S. M. J., Yusuf M. H., M. H. M. Y., Jamaluddin J., J. J., & Karim M. A., M. A. A. K. (2020, January 13). *Chasing Behind Casing Opportunities in a Low Salinity Laminated Brown Reservoirs*. International Petroleum Technology Conference. <https://doi.org/10.2523/IPTC-19763-Abstract>
- Rattanaudom, P., Shiao, B.-J. B., Harwell, J. H., Suriyapraphadilok, U., & Charoensaeng, A. (2022). The study of ultralow interfacial tension SiO₂-surfactant foam for enhanced oil recovery. *Journal of Petroleum Science and Engineering*, 209, 109898. <https://doi.org/10.1016/j.petrol.2021.109898>
- Rezaei, A., Khodabakhshi, A., Esmaili, A., & Razavifar, M. (2021). Effects of initial wettability and different surfactant-silica nanoparticles flooding scenarios on oil-recovery from carbonate rocks. *Petroleum*, S2405656121000249. <https://doi.org/10.1016/j.petlm.2021.03.009>
- RezaeiDoust, A., Puntervold, T., & Austad, T. (2011). Chemical Verification of the EOR Mechanism by Using Low Saline/Smart Water in Sandstone. *Energy & Fuels*, 25(5), 2151–2162. <https://doi.org/10.1021/ef200215y>
- Rezvani, H., Panahpoori, D., Riazi, M., Parsaei, R., Tabaei, M., & Cortés, F. B. (2020). A novel foam formulation by Al₂O₃/SiO₂ nanoparticles for EOR applications: A mechanistic study. *Journal of Molecular Liquids*, 112730. <https://doi.org/10.1016/j.molliq.2020.112730>
- Richard Sauerheber & Bettina Heinz. (2016). Temperature Effects on Conductivity of Seawater and Physiologic Saline, Mechanism and Significance. *Chemical Sciences Journal*. <https://doi.org/10.4172/2150-3494.1000109>
- Rock, A., Hincapie, R. E., Hoffmann, E., & Ganzer, L. (2018). Tertiary Low Salinity Waterflooding LSWF in Sandstone Reservoirs: Mechanisms, Synergies and Potentials in EOR Applications. *SPE Europec Featured at 80th EAGE Conference and Exhibition*. SPE Europec featured at 80th EAGE Conference and Exhibition, Copenhagen, Denmark. <https://doi.org/10.2118/190807-MS>
- Rodríguez Pantoja, Y. F., Villaquirán Vargas, A. P., & Muñoz Navarro, S. F. (2020). Study of mechanisms responsible for foaming-agent loss in porous media at high-temperature conditions. *Revista Facultad de Ingeniería Universidad de Antioquia*. <https://doi.org/10.17533/udea.redin.20200700>
- Rostami, P., Mehraban, M. F., Sharifi, M., Dejam, M., & Ayatollahi, S. (2019). Effect of water salinity on oil/brine interfacial behaviour during low salinity waterflooding: A mechanistic study. *Petroleum*, 5(4), 367–374. <https://doi.org/10.1016/j.petlm.2019.03.005>

- Rostami, P., Sharifi, M., Aminshahidy, B., & Fahimpour, J. (2019). The effect of nanoparticles on wettability alteration for enhanced oil recovery: Micromodel experimental studies and CFD simulation. *Petroleum Science*, 16(4), 859–873. <https://doi.org/10.1007/s12182-019-0312-z>
- Roustaei, A., & Bagherzadeh, H. (2015). Experimental investigation of SiO₂ nanoparticles on enhanced oil recovery of carbonate reservoirs. *Journal of Petroleum Exploration and Production Technology*, 5(1), 27–33. <https://doi.org/10.1007/s13202-014-0120-3>
- Saad, R., Asmani, F., Saad, M., Hussain, M., Khan, J., Kaleemullah, M., Othman, N. B., Tofigh, A., & Yusuf, E. (2015). *A New Approach for Predicting Antioxidant Property of Herbal Extracts*. 7(1), 10.
- Sadatshojaei, E., Jamialahmadi, M., Esmaeilzadeh, F., Wood, D. A., & Ghazanfari, M. H. (2019). The impacts of silica nanoparticles coupled with low-salinity water on wettability and interfacial tension: Experiments on a carbonate core. *Journal of Dispersion Science and Technology*, 1–15. <https://doi.org/10.1080/01932691.2019.1614943>
- Safari, M., Jiun Jye, J. W., Rahimi, A., Gholami, R., Yisong, L., & Khur, W. S. (2022). Salinity adjustment to improve the efficiency of nano glass flakes (NGFs) in interfacial tension reduction. *Journal of Petroleum Science and Engineering*, 212, 109874. <https://doi.org/10.1016/j.petrol.2021.109874>
- Saha, R., Uppaluri, R. V. S., & Tiwari, P. (2017). Effect of mineralogy on the adsorption characteristics of surfactant—Reservoir rock system. *Colloids and Surfaces A: Physicochemical and Engineering Aspects*, 531, 121–132. <https://doi.org/10.1016/j.colsurfa.2017.07.039>
- Saien, J., & Bahrami, M. (2016). Understanding the effect of different size silica nanoparticles and SDS surfactant mixtures on interfacial tension of n-hexane–water. *Journal of Molecular Liquids*, 224, 158–164. <https://doi.org/10.1016/j.molliq.2016.09.112>
- Saien, J., & Fadaei, V. (2018). The study of interfacial tension of kerosene-water under influence of CTAB surfactant and different size silica nanoparticles. *Journal of Molecular Liquids*, 255, 439–446. <https://doi.org/10.1016/j.molliq.2018.01.120>
- Saikia, B. D., Mahadevan, J., & Rao, D. N. (2018). Exploring mechanisms for wettability alteration in low-salinity waterfloods in carbonate rocks. *Journal of Petroleum Science and Engineering*, 164, 595–602. <https://doi.org/10.1016/j.petrol.2017.12.056>
- Sajjad Rabbani, H., Osman, Y., Almaghrabi, I., Azizur Rahman, M., & Seers, T. (2019). The Control of Apparent Wettability on the Efficiency of Surfactant Flooding in Tight Carbonate Rocks. *Processes*, 7(10), 684. <https://doi.org/10.3390/pr7100684>
- Salem Ragab, A. M., & Hannora, A. E. (2015, October 11). *A Comparative Investigation of Nano Particle Effects for Improved Oil Recovery – Experimental Work*. SPE Kuwait Oil and Gas Show and Conference. <https://doi.org/10.2118/175395-MS>
- Samal, K., Das, C., & Mohanty, K. (2017). Eco-friendly biosurfactant saponin for the solubilization of cationic and anionic dyes in aqueous system. *Dyes and Pigments*, 140, 100–108. <https://doi.org/10.1016/j.dyepig.2017.01.031>

- Samanta, A., Ojha, K., Mandal, A., & Sarkar, A. (2013). *Extraction and Characterization of an Eco-Friendly Surfactant for Its Use in Enhanced Oil Recovery*. 3(1), 10.
- Sanaei, A., Tavassoli, S., & Sepehrnoori, K. (2019). Investigation of modified Water chemistry for improved oil recovery: Application of DLVO theory and surface complexation model. *Colloids and Surfaces A: Physicochemical and Engineering Aspects*, 574, 131–145. <https://doi.org/10.1016/j.colsurfa.2019.04.075>
- Sar, P., Ghosh, A., Scarso, A., & Saha, B. (2019). Surfactant for better tomorrow: Applied aspect of surfactant aggregates from laboratory to industry. *Research on Chemical Intermediates*, 45(12), 6021–6041. <https://doi.org/10.1007/s11164-019-04017-6>
- Sarmah, S., Gogoi, S. B., Xianfeng, F., & Baruah, A. A. (2020). Characterization and identification of the most appropriate nonionic surfactant for enhanced oil recovery. *Journal of Petroleum Exploration and Production Technology*, 10(1), 115–123. <https://doi.org/10.1007/s13202-019-0682-1>
- Saxena, N., Goswami, A., Dhodapkar, P. K., Nihalani, M. C., & Mandal, A. (2019). Bio-based surfactant for enhanced oil recovery: Interfacial properties, emulsification and rock-fluid interactions. *Journal of Petroleum Science and Engineering*, 176, 299–311. <https://doi.org/10.1016/j.petrol.2019.01.052>
- Saxena, N., Kumar, A., & Mandal, A. (2019). Adsorption analysis of natural anionic surfactant for enhanced oil recovery: The role of mineralogy, salinity, alkalinity and nanoparticles. *Journal of Petroleum Science and Engineering*, 173, 1264–1283. <https://doi.org/10.1016/j.petrol.2018.11.002>
- Saxena, N., Pal, N., Ojha, K., Dey, S., & Mandal, A. (2018). Synthesis, characterization, physical and thermodynamic properties of a novel anionic surfactant derived from *Sapindus laurifolius*. *RSC Advances*, 8(43), 24485–24499. <https://doi.org/10.1039/C8RA03888K>
- Saxena, N., Saxena, A., & Mandal, A. (2019). Synthesis, characterization and enhanced oil recovery potential analysis through simulation of a natural anionic surfactant. *Journal of Molecular Liquids*, 282, 545–556. <https://doi.org/10.1016/j.molliq.2019.03.056>
- Schmiedel, P., & Rybinski, W. von. (2007). Applied Theory of Surfactants. In *Chemistry and Technology of Surfactants* (pp. 46–90). John Wiley & Sons, Ltd. <https://doi.org/10.1002/9780470988596.ch3>
- Schmitt, C., Grassl, B., Lespes, G., Desbrières, J., Pellerin, V., Reynaud, S., Gigault, J., & Hackley, V. A. (2014). Saponins: A Renewable and Biodegradable Surfactant From Its Microwave-Assisted Extraction to the Synthesis of Monodisperse Lattices. *Biomacromolecules*, 15(3), 856–862. <https://doi.org/10.1021/bm401708m>
- Schramm, L. L. (Ed.). (1994). *Foams: Fundamentals and Applications in the Petroleum Industry* (Vol. 242). American Chemical Society. <https://doi.org/10.1021/ba-1994-0242>
- Schramm, L. L. (Ed.). (2000). *Surfactants: Fundamentals and applications in the petroleum industry*. Cambridge University Press.
- Sciau, P., Mirguet-Archambeau, C., Roucau, C., Chabanne, D., & Schvoerer, M. (2009). Double Nanoparticle Layer in a 12(th) Century Lustreware

- Decoration: Accident or Technological Mastery? *Journal of Nano Research*, 8, 133. <https://doi.org/10.4028/www.scientific.net/JNanoR.8.133>
- Serrano, E., Rus, G., & García-Martínez, J. (2009). Nanotechnology for sustainable energy. *Renewable and Sustainable Energy Reviews*, 13(9), 2373–2384. <https://doi.org/10.1016/j.rser.2009.06.003>
- Shaban, S. M., Aiad, I., El-Sukkary, M. M., Soliman, E. A., & El-Awady, M. Y. (2017). Synthesis of newly cationic surfactant based on dimethylaminopropyl amine and their silver nanoparticles: Characterization; surface activity and biological activity. *Chinese Chemical Letters*, 28(2), 264–273. <https://doi.org/10.1016/j.cclet.2016.09.010>
- Shabani, A., & Zivar, D. (2020). Detailed analysis of the brine-rock interactions during low salinity water injection by a coupled geochemical-transport model. *Chemical Geology*, 537, 119484. <https://doi.org/10.1016/j.chemgeo.2020.119484>
- Shabib-Asl, A., Ayoub, M. A., Saaid, I. M., & Valentim, P. P. J. (2015). Experimental Investigation into Effects of Crude Oil Acid and Base Number on Wettability Alteration by Using Different Low Salinity Water in Sandstone Rock. *Journal of the Japan Petroleum Institute*, 58(4), 228–236. <https://doi.org/10.1627/jpi.58.228>
- Shadizadeh, S. R., & Amirpour, M. (2017). Reservoir rock wettability alteration using different types of surfactants: Experimental assessment. *Energy Sources, Part A: Recovery, Utilization, and Environmental Effects*, 1–7. <https://doi.org/10.1080/15567036.2016.1217291>
- Shadizadeh, S. S., & Kharrat, R. (2015). Experimental investigation of Matricaria chamomilla extract effect on oil-water interfacial tension: Usable for chemical enhanced oil recovery. *Petroleum Science and Technology*, 33(8), 901–907. <https://doi.org/10.1080/10916466.2015.1020063>
- Shah, R. D. (2009, January 1). *Application of Nanoparticle Saturated Injectant Gases for EOR of Heavy Oils*. SPE Annual Technical Conference and Exhibition. <https://doi.org/10.2118/129539-STU>
- Shen, B., Yu, X., Jiang, W., Yuan, H., Zhao, M., Zhou, H., & Pan, Z. (2021). Green Conversion of Saponins to Diosgenin in an Alcoholysis System Catalyzed by Solid Acid Derived from Phosphorus Tailings. *ACS Omega*, 6(8), 5423–5435. <https://doi.org/10.1021/acsomega.0c05627>
- Sheng, J. J. (2015). Status of surfactant EOR technology. *Petroleum*, 1(2), 97–105. <https://doi.org/10.1016/j.petlm.2015.07.003>
- Sheng, Y., Peng, Y., Yan, C., Li, Y., Ma, L., Wang, Q., & Zhang, S. (2022). Influence of nanoparticles on rheological properties and foam properties of mixed solutions of fluorocarbon and hydrocarbon surfactants. *Powder Technology*, 398, 117067. <https://doi.org/10.1016/j.powtec.2021.117067>
- Shi, S., Belhaj, H., & Bera, A. (2018). Capillary pressure and relative permeability correlations for transition zones of carbonate reservoirs. *Journal of Petroleum Exploration and Production Technology*, 8(3), 767–784. <https://doi.org/10.1007/s13202-017-0384-5>
- Shojaei, M. J., Méheust, Y., Osman, A., Grassia, P., & Shokri, N. (2021). Combined effects of nanoparticles and surfactants upon foam stability. *Chemical*

- Simjoo, M., Rezaei, T., Andrianov, A., & Zitha, P. L. J. (2013). Foam stability in the presence of oil: Effect of surfactant concentration and oil type. *Colloids and Surfaces A: Physicochemical and Engineering Aspects*, 438, 148–158. <https://doi.org/10.1016/j.colsurfa.2013.05.062>
- Singh, R., & Mohanty, K. K. (2020). Study of Nanoparticle-Stabilized Foams in Harsh Reservoir Conditions. *Transport in Porous Media*, 131(1), 135–155. <https://doi.org/10.1007/s11242-018-1215-y>
- Skauge, A., Solbakken, J., Ormehaug, P. A., & Aarra, M. G. (2020). Foam Generation, Propagation and Stability in Porous Medium. *Transport in Porous Media*, 131(1), 5–21. <https://doi.org/10.1007/s11242-019-01250-w>
- Smith, D. J. (2015). Chapter 1. Characterization of Nanomaterials Using Transmission Electron Microscopy. In A. I. Kirkland & S. J. Haigh (Eds.), *Nanoscience & Nanotechnology Series* (2nd ed., pp. 1–29). Royal Society of Chemistry. <https://doi.org/10.1039/9781782621867-00001>
- Smutek, W., Zdarta, A., Łuczak, M., Krawczyk, P., Jesionowski, T., & Kaczorek, E. (2016). Sapindus saponins' impact on hydrocarbon biodegradation by bacteria strains after short- and long-term contact with pollutant. *Colloids and Surfaces B: Biointerfaces*, 142, 207–213. <https://doi.org/10.1016/j.colsurfb.2016.02.049>
- Sofla, S. J. D., James, L. A., & Zhang, Y. (2019). Understanding the behavior of H+-protected silica nanoparticles at the oil-water interface for enhanced oil recovery (EOR) applications. *Journal of Molecular Liquids*, 274, 98–114. <https://doi.org/10.1016/j.molliq.2018.09.049>
- Soleimani, H. M., & Dehaghani, A. H. S. (2016). *The effect of smart water and silica nanoparticles injection on wettability of limestone*. 9.
- Sposito, G. (2016). *The Chemistry of Soils* (Third Edition). Oxford University Press.
- Srivastava, N., Choudhary, M., Singhal, G., & Bhagyawant, S. S. (2020). SEM Studies of Saponin Silver Nanoparticles Isolated From Leaves of *Chenopodium album* L. for In Vitro Anti-acne Activity. *Proceedings of the National Academy of Sciences, India Section B: Biological Sciences*, 90(2), 333–341. <https://doi.org/10.1007/s40011-019-01100-1>
- Strambeanu, N., Demetrovici, L., Dragos, D., & Lungu, M. (2015). *Nanoparticles: Definition, Classification and General Physical Properties*. 3–8. https://doi.org/10.1007/978-3-319-11728-7_1
- Sun, X., Zhang, Y., Chen, G., & Gai, Z. (2017). Application of Nanoparticles in Enhanced Oil Recovery: A Critical Review of Recent Progress. *Energies*, 10(3), 345. <https://doi.org/10.3390/en10030345>
- Sun, X., Zhang, Y., Chen, G., Liu, T., Ren, D., Ma, J., Sheng, Y., & Karwani, S. (2018). Wettability of Hybrid Nanofluid-Treated Sandstone/Heavy Oil/Brine Systems: Implications for Enhanced Heavy Oil Recovery Potential. *Energy & Fuels*, 32(11), 11118–11135. <https://doi.org/10.1021/acs.energyfuels.8b01730>
- Tackie-Otoo, B. N., Ayoub Mohammed, M. A., Yekeen, N., & Negash, B. M. (2020). Alternative chemical agents for alkalis, surfactants and polymers for enhanced oil recovery: Research trend and prospects. *Journal of Petroleum*

- Science and Engineering*, 187, 106828. <https://doi.org/10.1016/j.petrol.2019.106828>
- Tadros, T. F. (2015). *Interfacial Phenomena and Colloid Stability: Basic Principles*. De Gruyter, Inc. <http://ebookcentral.proquest.com/lib/curtin/detail.action?docID=1867320>
- Tale, F., Kalantariasl, A., Shabani, A., Abbasi, S., Zohoorian, A. H., & Khomehchi, E. (2020). Experimental and simulation study of low salinity brine interactions with carbonate rocks. *Journal of Petroleum Science and Engineering*, 184, 106497. <https://doi.org/10.1016/j.petrol.2019.106497>
- Tang, G., & Morrow, N. R. (1999). *OIL RECOVERY BY WATERFLOODING AND IMBIBITION - INVADING BRINE CATION VALENCY AND SALINITY*. 12.
- Tang, G.-Q., & Morrow, N. R. (1999). *Influence of brine composition and fines migration on crude oil-brine-rock interactions and oil recovery*. 13.
- Thakore, V., Ren, F., Voytek, J., Xi, J., Wang, H., Wang, J.-A. J., & Polsky, Y. (2020). *High-Temperature Stability of Aqueous Foams as Potential Waterless Hydrofracking Fluid for Geothermal Reservoir Stimulation*. 10.
- Tiab, D., & Donaldson, E. C. (2011). *Petrophysics: Theory and Practice of Measuring Reservoir Rock and Fluid Transport Properties*. Elsevier Science & Technology. <http://ebookcentral.proquest.com/lib/curtin/detail.action?docID=858640>
- Tmáková, L., Sekretár, S., & Schmidt, Š. (2016). Plant-derived surfactants as an alternative to synthetic surfactants: Surface and antioxidant activities. *Chemical Papers*, 70(2), 188–196. <https://doi.org/10.1515/chempap-2015-0200>
- Tran, T., Gonzalez Perdomo, M. E., Haghighi, M., & Amrouch, K. (2022). Study of the synergistic effects between different surfactant types and silica nanoparticles on the stability of liquid foams at elevated temperature. *Fuel*, 315, 122818. <https://doi.org/10.1016/j.fuel.2021.122818>
- Ueno, M., Isokawa, N., Fueda, K., Nakahara, S., Teshima, H., Yamamoto, N., Yokoyama, H., Noritsugu, Y., Shibata, K., Miyagawa, K., Tanaka, S., Hirano, T., Fujito, A., Takashima, A., & Kanno, K. (2016). *Practical Chemistry of Long-Lasting Bubbles*.
- Valenzuela-Elgueta, J., Delgado, A. V., & Ahualli, S. (2021). Effect of cationic surfactant addition on the electrokinetics and stability of silica/kaolinite suspensions in copper hydrometallurgy conditions. *Minerals Engineering*, 169, 106958. <https://doi.org/10.1016/j.mineng.2021.106958>
- Vatanparast, H., Shahabi, F., Bahramian, A., Javadi, A., & Miller, R. (2018). The Role of Electrostatic Repulsion on Increasing Surface Activity of Anionic Surfactants in the Presence of Hydrophilic Silica Nanoparticles. *Scientific Reports*, 8(1), 7251. <https://doi.org/10.1038/s41598-018-25493-7>
- Vishnumolakala, N., Zhang, J., & Ismail, N. B. (2020). A Comprehensive Review of Enhanced Oil Recovery Projects in Canada and Recommendations for Planning Successful Future EOR projects. *Day 4 Thu, October 01, 2020*, D041S009R001. <https://doi.org/10.2118/199951-MS>
- Wan, L. S. C., & Poon, P. K. C. (1969). Effect of Salts on the Surface/Interfacial Tension and Critical Micelle Concentration of Surfactants. *Journal of Pharmaceutical Sciences*, 58(12), 1562–1567. <https://doi.org/10.1002/jps.2600581238>

- Wang, H., Guo, W., Zheng, C., Wang, D., & Zhan, H. (2017). Effect of Temperature on Foaming Ability and Foam Stability of Typical Surfactants Used for Foaming Agent. *Journal of Surfactants and Detergents*, 20(3), 615–622. <https://doi.org/10.1007/s11743-017-1953-9>
- Wang, Q. (2014). *NANOPARTICLES FOR APPLICATIONS IN DRUG DELIVERY*. <https://doi.org/10.13140/RG.2.1.3200.7203>
- Wang, Q., Puerto, M. C., Warudkar, S., Buehler, J., & Biswal, S. L. (2018). Recyclable amine-functionalized magnetic nanoparticles for efficient demulsification of crude oil-in-water emulsions. *Environmental Science: Water Research & Technology*, 4(10), 1553–1563. <https://doi.org/10.1039/C8EW00188J>
- Wasan, D., Nikolov, A., & Kondiparty, K. (2011). The wetting and spreading of nanofluids on solids: Role of the structural disjoining pressure. *Current Opinion in Colloid & Interface Science*, 16(4), 344–349. <https://doi.org/10.1016/j.cocis.2011.02.001>
- Wei, W., Bai, F., & Fan, H. (2019). Surfactant-Assisted Cooperative Self-Assembly of Nanoparticles into Active Nanostructures. *IScience*, 11, 272–293. <https://doi.org/10.1016/j.isci.2018.12.025>
- White, R. J., Luque, R., Budarin, V. L., Clark, J. H., & Macquarrie, D. J. (2009). Supported metal nanoparticles on porous materials. Methods and applications. *Chemical Society Reviews*, 38(2), 481–494. <https://doi.org/10.1039/b802654h>
- Wissocq, A., Beaucaire, C., & Latrille, C. (2018). Application of the multi-site ion exchanger model to the sorption of Sr and Cs on natural clayey sandstone. *Applied Geochemistry*, 93, 167–177. <https://doi.org/10.1016/j.apgeochem.2017.12.010>
- Xie, Q., Liu, F., Chen, Y., Yang, H., Saeedi, A., & Hossain, M. M. (2019). Effect of electrical double layer and ion exchange on low salinity EOR in a pH controlled system. *Journal of Petroleum Science and Engineering*, 174, 418–424. <https://doi.org/10.1016/j.petrol.2018.11.050>
- Xu, H., Li, P., Ma, K., Welbourn, R. J. L., Penfold, J., Thomas, R. K., Roberts, D. W., & Petkov, J. T. (2019). The role of competitive counterion adsorption on the electrolyte induced surface ordering in methyl ester sulfonate surfactants at the air-water interface. *Journal of Colloid and Interface Science*, 533, 154–160. <https://doi.org/10.1016/j.jcis.2018.08.061>
- Xu, Z., Li, B., Zhao, H., He, L., Liu, Z., Chen, D., Yang, H., & Li, Z. (2020). Investigation of the Effect of Nanoparticle-Stabilized Foam on EOR: Nitrogen Foam and Methane Foam. *ACS Omega*, 5(30), 19092–19103. <https://doi.org/10.1021/acsomega.0c02434>
- Xue, H., Dong, Z., Tian, S., Lu, S., An, C., Zhou, Y., Li, B., & Xin, X. (2021). Characteristics of Shale Wettability by Contact Angle and Its Influencing Factors: A Case Study in Songliao. *Frontiers in Earth Science*, 9, 736938. <https://doi.org/10.3389/feart.2021.736938>
- Yang, J., Li, J., Wang, M., Zheng, L., Peng, B., Zou, X., Yin, Y., & Deng, Z. (2021). A Tea Saponin-Carbohydrate-Protein Complex Could Be One Key Emulsifiable Compound in the Emulsion Formed during Aqueous Extraction of Camellia Oil. *European Journal of Lipid Science and Technology*, 123(10), 2000312. <https://doi.org/10.1002/ejlt.202000312>

- Yang, Y., Yuan, W., Hou, J., You, Z., Li, J., & Liu, Y. (2020). Stochastic and upscaled analytical modeling of fines migration in porous media induced by low-salinity water injection. *Applied Mathematics and Mechanics*, 41(3), 491–506. <https://doi.org/10.1007/s10483-020-2583-9>
- Yang, Y., Zhang, Q., Wang, T., & Yang, Y. (2013). Determination of the Critical Micelle Concentration of Sodium Dodecyl Sulphate in Aqueous Solution in the Presence of an Organic Additive of Acetonitrile by Conductometry and an Inorganic Additive of Phosphate by Fluorometry. *Asian Journal of Chemistry*, 25(12), 6657–6660. <https://doi.org/10.14233/ajchem.2013.14403>
- Yekeen, N., Padmanabhan, E., Idris, A. K., & Ibad, S. M. (2019). Surfactant adsorption behaviors onto shale from Malaysian formations: Influence of silicon dioxide nanoparticles, surfactant type, temperature, salinity and shale lithology. *Journal of Petroleum Science and Engineering*, 179, 841–854. <https://doi.org/10.1016/j.petrol.2019.04.096>
- Yisong, L., Gholami, R., Safari, M., Rahimi, A., & Siaw Khur, W. (2022). On surface interactions of environmental friendly surfactant/oil/rock/low salinity system: IFT, wettability, and foamability. *Journal of Petroleum Science and Engineering*, 208, 109370. <https://doi.org/10.1016/j.petrol.2021.109370>
- Yu, W., France, D. M., Routbort, J. L., & Choi, S. U. S. (2008). Review and Comparison of Nanofluid Thermal Conductivity and Heat Transfer Enhancements. *Heat Transfer Engineering*, 29(5), 432–460. <https://doi.org/10.1080/01457630701850851>
- Yuan, C., Li, Y., Li, Q., Jin, R., & Ren, L. (2018). Purification of Tea saponins and Evaluation of its Effect on Alcohol Dehydrogenase Activity. *Open Life Sciences*, 13(1), 56–63. <https://doi.org/10.1515/biol-2018-0008>
- Zaeri, M. R., Shahverdi, H., Hashemi, R., & Mohammadi, M. (2019). Impact of water saturation and cation concentrations on wettability alteration and oil recovery of carbonate rocks using low-salinity water. *Journal of Petroleum Exploration and Production Technology*, 9(2), 1185–1196. <https://doi.org/10.1007/s13202-018-0552-2>
- Zargartalebi, M., Barati, N., & Kharrat, R. (2014). Influences of hydrophilic and hydrophobic silica nanoparticles on anionic surfactant properties: Interfacial and adsorption behaviors. *Journal of Petroleum Science and Engineering*, 119, 36–43. <https://doi.org/10.1016/j.petrol.2014.04.010>
- Zargartalebi, M., Kharrat, R., & Barati, N. (2015). Enhancement of surfactant flooding performance by the use of silica nanoparticles. *Fuel*, 143, 21–27. <https://doi.org/10.1016/j.fuel.2014.11.040>
- Zendehboudi, S., Ahmadi, M. A., Rajabzadeh, A. R., Mahinpey, N., & Chatzis, I. (2013). Experimental study on adsorption of a new surfactant onto carbonate reservoir samples-application to EOR. *The Canadian Journal of Chemical Engineering*, 91(8), 1439–1449. <https://doi.org/10.1002/cjce.21806>
- Zhang, H., Nikolov, A., & Wasan, D. (2014). Enhanced Oil Recovery (EOR) Using Nanoparticle Dispersions: Underlying Mechanism and Imbibition Experiments. *Energy & Fuels*, 28(5), 3002–3009. <https://doi.org/10.1021/ef500272r>

- Zhang, J., & Qu, F. (2013). Methods for Analysis of Triterpenoid Saponins. In K. G. Ramawat & J.-M. Mérillon (Eds.), *Natural Products* (pp. 3311–3323). Springer Berlin Heidelberg. https://doi.org/10.1007/978-3-642-22144-6_180
- Zhang, J., Wang, D., & Olatunji, K. (2016, May 5). *Surfactant Adsorption Investigation in Ultra-Low Permeable Rocks*. SPE Low Perm Symposium. <https://doi.org/10.2118/180214-MS>
- Zhang, L., Xie, L., Cui, X., Chen, J., & Zeng, H. (2019). Intermolecular and surface forces at solid/oil/water/gas interfaces in petroleum production. *Journal of Colloid and Interface Science*, 537, 505–519. <https://doi.org/10.1016/j.jcis.2018.11.052>
- Zhang, R., & Somasundaran, P. (2006). Advances in adsorption of surfactants and their mixtures at solid/solution interfaces. *Advances in Colloid and Interface Science*, 123–126, 213–229. <https://doi.org/10.1016/j.cis.2006.07.004>
- Zhang, T., Davidson, A., Bryant, S. L., & Huh, C. (2010). Nanoparticle-Stabilized Emulsions for Applications in Enhanced Oil Recovery. *Society of Petroleum Engineers*, 18.
- Zhang, Y., & Morrow, N. R. (2006). Comparison of Secondary and Tertiary Recovery With Change in Injection Brine Composition for Crude Oil/Sandstone Combinations. *Society of Petroleum Engineers*, 14. <https://doi.org/10.2118/99757-MS>
- Zhang, Y., Xie, X., & Morrow, N. R. (2007). Waterflood Performance by Injection of Brine With Different Salinity For Reservoir Cores. *Society of Petroleum Engineers*, 12.
- Zhang, Z., Li, K., Tian, R., & Lu, C. (2019). Substrate-Assisted Visualization of Surfactant Micelles via Transmission Electron Microscopy. *Frontiers in Chemistry*, 7, 242. <https://doi.org/10.3389/fchem.2019.00242>
- Zhang, X.-F., Han, Y.-Y., Di, T.-M., Gao, L.-P., & Xia, T. (2021). Triterpene saponins from tea seed pomace (*Camellia oleifera* Abel) and their cytotoxic activity on MCF-7 cells in vitro. *Natural Product Research*, 35(16), 2730–2733. <https://doi.org/10.1080/14786419.2019.1656625>
- Zhao, B., Li, S., Lin, H., Cheng, Y., Kong, X., & Ding, Y. (2021). Experimental study on the influence of surfactants in compound solution on the wetting-agglomeration properties of coal dust. *Powder Technology*, S0032591021009074. <https://doi.org/10.1016/j.powtec.2021.10.026>